High performance of silicone rubber nanocomposites with improved physical properties

By

Nik Intan Nik Ismail

A doctoral thesis submitted in partial fulfilment of the requirements for the award of Doctor of Philosophy of Loughborough University

Project Supervisors: Prof. Mo Song

Dr. Ali Ansarifar

Aeronautical, Automotive, Chemical and Materials Engineering

ACKNOWLEDGEMENT

The completion of this thesis has been one of the most significant achievement of my PhD journey. On that note, I wish to express my deepest appreciation to Prof Mo Song and Dr. Ali Ansarifar as my project supervisors. Their kindest support, guidance and useful insights certainly has helped towards the establishment of this thesis. Secondly, to my beloved husband and son, who have provided continous moral support. Also, my parents and siblings for being so supportive throughout this journey. For all technical staffs in the department of Materials, Dr Zhaoxia Zhou, Dr. Keith Yendall, Dr David Grandy, Dr Jane Clarke, Mr. Andy Wooley, Mr. Ray Owens, Mr Shaun Fowler thank you for sharing the wealth of their knowledge with me. Last but not least, a special gratitude to my sponsor the Malaysian Rubber Board for sponsoring this research project and my colleques for their constant encouragement and support during my studies in the UK.

Thank you and may God bless all of you…

ABSTRACT

Highly extent exfoliated and intercalated silicone rubber (SR) nanocomposites based on natural montmorillonite (Cloisite Na^+) and organically modified montmorillonite (Cloisite 30B and Cloisite 20A) were successfully prepared by melt-mixing technique. As indicated by the X-ray diffraction (XRD) and transmission electron microscopy (TEM) analysis, intercalation and exfoliation of the clay particles in the nanocomposites was achieved at less than 8 parts per hundred (phr) rubber by weight, irrespective of the initial interlayer spacing of the nanoclay particles. Cloisite 30B was spontaneously transformed into exfoliated nanostructures during the vulcanisation stage as suggested by X-ray diffraction (XRD), fourier transforms infra-red spectroscopy (FTIR) and differential scanning calorimeter (DSC) results. Overall, the use of the nanoclays in silicone rubber improved the Young's modulus, tensile strength and elongation at break by more than 50% as compared to the neat SR. However, the Cloisite Na^+ yielded outstanding mechanical properties with low hysteresis at the same loading of the exfoliated Cloisite 30B and intercalated Cloisite 20A organoclays, even though the filler had a tendency to produce mixture intercalated/exfoliated nanostructures in the SR matrix. It was concluded that the tensile strength and Young's modulus in this particular rubber nanocomposite are dominated by the degree of crosslink density instead of filler dispersion. In addition, incorporation of the nanoclays in SR altered the wear mechanism of silicone rubber where addition of the fillers minimised the weight loss during abrasion testing, particularly at low filler loading (<6phr). Moreover, this study showed that the SR/C30B nanocomposite exhibited excellent heat resistance in comparison to the other two nanocomposites and neat SR as revealed by higher retention strength. The thermal stability of the rubber in air was strongly dependent on the clay morphology and increased in the following order: highly intercalated/exfoliated SR/Na^+MMT < highly intercalated SR/C20A < highly exfoliated SR/C30B. Furthermore, the performance of SR

nanocomposites containing precipitated silica (PS) / montmorillonite (MMT) hybrid fillers were investigated as a function of PS/MMT hybrid filler weight ratio. Interestingly, the stress–strain properties of the nanocomposites with the hybrid fillers showed a large improvement at high deformation in comparison with the properties of those nanocomposites containing the PS and MMT fillers. The resistance to ageing of SR/PS/MMT was improved by gradually adding amounts of PS filler into the PS/MMT hybrid filler system. Finally, the comparative study demonstrated that the SR containing precipitated silica (PS) / multiwall carbon nanotube (MWMT) hybrid filler significantly improved stiffness of the rubber but accompanied by a small improvement in the tensile strength and elongation at break with regard to the SR/PS/MMT. In spite of that, the inclusion of PS/MWNT gave adverse effects to the cure efficiency of the SR compounds which is a drawback from processing point of view.

TABLE OF CONTENTS

LIST OF FIGURES

LIST OF TABLES

Symbols and Abbreviations

SR	silicone rubber
PDMS	polydimethylsiloxane
LSR	liquid silicone rubber
MMT	montmorillonite
OMMT	organomodified montmorillonite clay
PS	precipitated silica
MWNT	multi wall carbon nanotube
PEO	poly(ethylene oxide)
TESPT	bis(3-triethoxysilylpropyl)tetrasulfide
QAS	quaternary ammonium salts
DCP	dicumyl peroxide
MT_2EtOH	bis-2-hydroxyetyl, quaternary ammonium
2M2HT	dimethyl, dehydrogenated tallow, quaternary ammonium
XRD	wide angle X-ray diffraction
TEM	transmission electron microscopy
FTIR	fourier transforms infra-red spectroscopy
DSC	differential scanning calorimeter
ODR	oscillating disc rheometer
FEGSEM	field emission electron gun scanning electron microscopy
TGA	thermogravimetric analysis
NR	natural rubber
EPDM	ethylene propylene diene monomer
SBR	styrene-butadiene-rubber
NBR	nitrile rubber
CEC	cation exchange capacity
GPA	giga pascal
nm	nanometer
OH	hydroxyl group
d	interlayer spacing
SAXS	small-angle X-ray diffraction
AFM	atomic force microscopy
λ	X-ray wavelength
θ	Angle
n	Integer
IIRCNs	isobutylene-isoprene rubber/clay nanocomposites

AP	atmospheric
MPa	mega pascal
ENR	epoxidized natural rubber
TEOS	hexamethyldisilazane
phr	parts per hundred rubber by weight
rpm	revolutions per minute
M_L	min torque
Ts_2	scorch time
M_H	max torque
T_{95}	cure time
ΔM	delta torque
h	length
mm	milimeter
μm	micrometer
m_0	mass of original test rubber
m_1	mass of tested rubber
T_{onset}	onset of degradation temperature
DTG	derivative of the residual weight % versus temperature
E	arrhenius activation energy
R	gas constant
β	heating rate
T	Temperature

CHAPTER 1: Introduction

1.1 Background of the research

The world's global consumption of silicones is expected to increase 6.2% per year through 2015 [1]. According to a recent market survey, silicone rubber has a wide potential to be a leading product in the silicones industry due to a rapid growth of modern industrial, construction and medical products [2]. Silicone rubber is a class of specialty rubber with properties that are suitable for an extensive range of applications. It maintains good resistance to radiation, ozone, and chemicals; has excellent electrical properties; and is physiologically inert [3].

Nevertheless, owing to its poor mechanical properties, filler reinforcement in silicone rubber has been continuously researched since its discovery in 1940s [4]. Fumed silica (SiO_2) is used frequently in most silicone rubber end products, as it offers excellent reinforcing ability to the rubber. Strong polymer-filler interactions resulting from physico-chemical interactions between silanol groups (Si-OH) on the silica surface and siloxane (Si-O-Si) in the silicone rubber backbone are responsible for the improvement in mechanical properties of silica-filled silicone rubber [3-5].

In nature, fumed silica appears as a very light white powder with the particle diameter range from 10 to 16 nm [3]. Though fumed silica is not listed as a carcinogen [6-7], some

clinical studies suggests that the fine dust of fumed silica, if it becomes airborne, could pose a potential inhalation risk, as well as causing skin irritation and other possible health problems [8]. Apart from that, fumed silica is categorised as a premium additive in rubber, since it is more expensive than other common fillers such as precipitated silica [3]. These limitations have encouraged researchers to investigate new reinforcing fillers for silicone rubber.

Recent concerns about sustainable technology have opened the door for mineral fillers for example nanoclay [9-16], layered double hydroxide [17] and nanokaolin [18, 19] to partially replace the use of conventional fillers, such as carbon black and silica, in the rubber industry. Sustainable technology requires a balance between financial, environmental and social considerations [20]. In line with current trends within the industry, the use of nanoclays or layered silicates has received much attention because it is cheaper, easily available and considered a low risk material [21].

Similar to layered silicates reinforced polymer nanocomposites [22], the term 'nanocomposite' is used to describe nanostructured reinforced rubber [23] and is defined as the composite material that is constructed of dispersed components at the nanometre scale. The nanofiller can be in the form of particle, fibre or layer materials that have at least one dimension in the 1 to 100 nanometre range [22]. According to some previous studies, layered silicate filler imparts outstanding mechanical properties [23-24], thermal [25] and barrier properties [26] to most rubber/clay nanocomposites, at very low loading (i.e. <10 wt %).

Even though many researchers have reported the advantages of layered silicates in rubber/clay nanocomposites [23-26], only a few have focussed on silicone rubber. Layered silicate such as montmorillonite (MMT) consists of a triple-layer sandwich structure; therefore its dispersion mechanism in rubber is different from silica that has a spherical shape. As reported in the literature [22-23] intercalation and exfoliation morphologies are used to

characterise the clay layer dispersion in polymer/clay nanocomposites. The latter morphology is more desirable due to its high surface area, which is important in rubber reinforcement. However, it is difficult to achieve fully exfoliated clay in the rubber matrix due to obstacles such as high molecular weight, disruption from curing process and frequent incompatibility with inorganic fillers [23, 24]. To date, the exfoliation mechanism of layered silicates in rubber compounds is not clear.

Previous studies have shown that solution blending and in-situ modification techniques are the preferred approach used in the preparation of silicone rubber/clay nanocomposites [27-29]. However, these methods are often more complex and therefore less practical for commercial manufacturing, particularly since they involve organic solvents. As a result, rubber manufacturers are very interested on simple, low cost, and 'green' processes. For that reason, the main focus of the present work is the development of high performance silicone rubber/clay nanocomposites via simple methods, such as melt-compounding. This technique has great practical relevance to current rubber processing processes. The melt-mixing is the most direct, environmentally-friendly, and cost-effective route for the preparation of nanocomposites, as no organic solvent is needed. As such it is necessary to understand the effects of nanoclay filler on the physical properties of melt-compounded silicone rubber nanocomposites. The term 'performance' in this project refers to the mechanical properties, heat resistance and thermal stability of the nanocomposite.

Recently, there has been much interest in developing hybrid reinforcement in rubber based on a combination of two different types of nanoparticles, or of nanoparticles with conventional fillers such as carbon black and multi wall carbon nanotube [30], layered double hydroxide/multiwalled carbon nanotube [31] and multi-walled carbon nanotube/graphene [32]. This is because the adverse effects of one nanofiller can be diluted by adding a secondary filler which can balance the properties of the filled rubber. More interestingly, hybrid fillers have been shown to give a synergy reinforcing effect to the rubber's properties and, at the same time, the benefits from the individual fillers were still

retained [30-32]. Therefore, in the latter part of this thesis, a new hybrid filler system based on 2D montmorillonite (MMT) filler and 3D precipitated silica (PS) has been used to reinforce silicone rubber.

MMT is belonging to smectite family which consists of stack parallel lamellae. It has layer thickness approximately 1 nm with lateral dimensions within a range of 150 to 200 nm [33]. Due to a nature of platy morphology, the filler provides large aspect ratio (ratio of length/thickness) which gives advantages of improving gas-barrier properties, swelling behaviour and thermal stability of rubber/clay nanocomposites [34]. Also, MMT exhibits greater reinforcing effect in rubber nanocomposites at low loading. This is the most distinguish character of MMT as reinforcing fillers. However, the use of the MMT with high loading always deteriorates the mechanical performance of the rubber nanocomposites [35].

In spite of fumed silica (FS), precipitated silica (PS) is another type of filler that used to reinforce silicone rubber. It exhibits good mechanical properties in silicone rubber compound even not as good as fumed silica. In view of the encouraging results reported for the synergistic effects of some hybrid filler systems [36–39], the utilisation of hybrid filler or blends of MMT and PS is expected to give benefits to the rubber since MMT and PS possess their own advantages. Both MMT and PS fillers are nonpetroleum based which are safe to handle and known to be environmentally-friendly materials. In addition, these fillers are relatively cheap compared with FS, thus it helps to reduce the current processing cost and increase the economic benefit to the rubber manufacturing industry.

1.2 Aim and objectives of the project

Overall aim of this study is to improve mechanical and thermal properties of silicone rubber compound using montmorillonite nanoclay. Therefore, a good understanding on fundamental and technology aspects are essential in order to gain benefits from the novel rubber based nanocomposites. Hence, the specific objectives of this study are summarised as follows:

1. To prepare and characterise silicone rubber/clay nanocomposites with different types of montmorillonite, via melt-compounding method.

2. To understand the exfoliation and intercalation of the montmorillonite mechanism in silicone rubber nanocomposites.

3. To understand the reinforcing ability (tensile strength, modulus, elongation at break, hardness, store energy density and hysteresis) of montmorillonite in silicone rubber.

4. To study the effect of exfoliation and intercalation nanostructures on ageing and thermal stability of rubber.

5. To develop new filler system in silicone rubber based on the combination between montmorillonite (MMT) and precipitated silica (PS) – referred to as PS/MMT hybrid filler.

1.3 Structure of the thesis

The thesis structure is divided by few sections which are research background, literature review, methodology, results & discussions and conclusions. It consists of eight chapters. The outline of thesis structure is presented in the diagram in Fig 1.1.

Chapter 1 explains the background of the research topic. In addition, the aim and objectives of the research as well as the thesis structure are presented in this chapter.

Chapter 2 covers relevant literature review of the research area. The first section of this chapter describes a general understanding about rubber/clay nanocomposite technology. In the second section, some fundamental studies regarding silicone rubber properties are discussed. The latter part of this chapter is focussed on the recent works of silicone rubber/clay nanocomposites where preparation technique, mechanical properties and thermal stability is reviewed.

Chapter 3 is experimental section which presents the details of the materials, formulations, processing, preparation of test samples, characterisations and testing of silicone rubber and silicone rubber nanocomposites.

Results and discussions of this research are divided into four chapters which are chapter 4, 5, 6 and 7. Chapter 4 presents the results and discussion on characterisation of silicone rubber/clay nanocomposites based on wide angle X-ray diffraction (XRD), transmission electron microscopy (TEM), fourier transforms infra-red spectroscopy (FTIR), differential scanning calorimeter (DSC) and oscillating disc rheometer (ODR).

Chapter 5 presents the results and discussion on mechanical properties of silicone rubber and its composites. The mechanical properties are evaluated based on tensile properties, hardness, store energy density, hysteresis and abrasion resistance.

Chapter 6 covers effect of clay morphology on heat resistance and thermal stability of the nanocomposite. The activation energy of the nanocomposite is also calculated based on Flynn-Wall-Ozawa method.

Chapter 7 presents results and discussions on hybrid reinforcement of silicone rubber based on montmorillonite (MMT) and precipitated silica (PS). Filler dispersion of SR reinforced PS/MMT hybrid filler is characterised based on XRD, TEM and FEGSEM. Reinforcing capability of the PS/MMT hybrid filler is measured based on tensile properties, hardness and hysteresis. The comparative study between a combination of PS/MMT and PS/multi wall carbon nanotube (MWNT) are also presented in this chapter. Some results on the cure characteristics, tensile testing and hardness of SR/PS/MWNT are discussed.

Finally, chapter 8 summarises the main conclusions from this research and some suggestions of potential works for future research are disclosed.

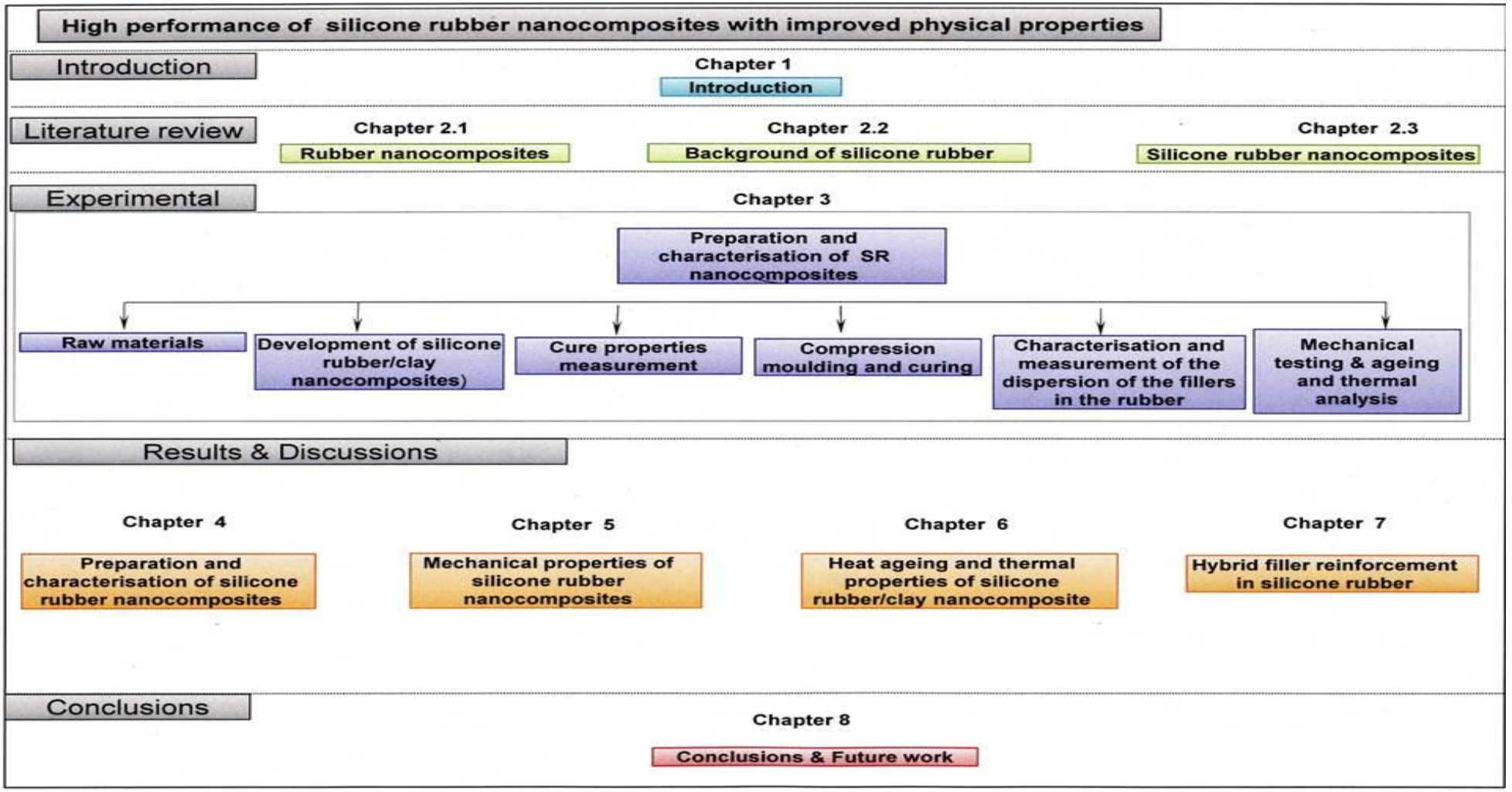

Fig. 1.1: The outline thesis structure

1.4 References

1. Freedoniagroup. *World Silicones 'Industry Study with Forecasts for 2015 & 2020 Study*'.http://www.freedoniagroup.com/brochure/27xx/2779smwe.pdf (accessed 1 Aug 2013).

2. Freedoniagroup. *Silicone. US Industry Study with Forecasts for 2018 & 2023.* http://www.freedoniagroup.com/DocumentDetails.aspx?ReferrerId=FG01&studyid=3138 (accessed 1 Apr 2014).

3. Sarkar A. Silicone rubber. In: White J, De SK and Naskar K (eds). *Rubber Technologist's Handbook.* Vol 2. United Kingdom, Smithers Rapra Technology Limited; 2009. 381 – 389.

4. Colas A, Curtis J. Silicone biomaterials: history and chemistry. In: *Biomaterials Science: An Introduction to Materials in Medicine*. 2nd ed. USA, Elsevier Academic Press; 2004. 80–85.

5. Orawan T, Rainer F, Mario S, Evonik D: *The last 100 years of fumed silica in rubber reinforcement.* http://www.thefreelibrary.com/ (accessed 1 Apr 2014).

6. Reuzel PG, Bruijntjes JP, Feron VJ, Woutersen RA. Subchronic inhalation toxicity of amorphous silicas and quartz dust in rats. *Food and Chemistry Toxicology* 1991; 29(5): 341-354.

7. McLaughlin JK. Chow WH. Levy LS. Amorphous silica: a review of health effects from inhalation exposure with particular reference to cancer. *Journal Toxicology. Environmental Health* 1997; 50(6): 553-566.

8. Merget R, Bauer T, Küpper HU, Philippou S, Bauer HD, Breitstadt R, Bruening T. Health hazards due to the inhalation of amorphous silica. *Archives of Toxicology* 2002; 75(11-12): 625-634.

9. Arroyo M, López-Manchado M, Herrero B. Organo-montmorillonite as substitute of carbon black in natural rubber compounds. *Polymer* 2003; 44(8): 2447–2453.

10. Li P, Wang L, Song G, Yin L, Qi F, Sun L. Characterization of High-performance Exfoliated Natural Rubber/Organoclay Nanocomposites. *Journal of Applied Polymer Science* 2008; 109(6): 3831-3838.

11. Lopez-Manchado M, Herrero B, Arroyo M. Preparation and characterization of organoclay nanocomposites based on natural rubber. *Polymer International* 2003; 52(7): 1070–1077.

12. Sun Y, Luo Y, Jia D. Preparation and Properties of Natural Rubber Nanocomposites with Solid-State Organomodified Montmorillonite. *Journal of Applied Polymer Science* 2008; 107(5): 2786–2792.

13. Ganguly A, Bhowmick AK, Li Y. Insights into Montmorillonite Nanoclay Based ex Situ Nanocomposites from SEBS and Modified SEBS by Small-Angle X-ray Scattering and Modulated DSC Studies. *Macromolecules* 2008; 41(16): 6246–6253.

14. He SJ, Wang YQ, Xi MM, Lin J, Xue Y, Zhang LQ. Prevention of oxide aging acceleration by nano-dispersed clay in styrene-butadiene rubber matrix. *Polymer Degradation Stability* 2013; 98(9): 1773–1779.

15. Schmidt DF, Clément F, Giannelis EP, On the Origins of Silicate Dispersion in Polysiloxane/Layered-Silicate Nanocomposites. *Advanced Functional Material* 2006; 16(3): 417–425.

16. Wang J, Chen Y, Jin Q. Organic Montmorillonite as a Substitute for Aerosilica in Addition-Type Liquid Silicone Rubber Systems. *Macromolecule Chemistry Phys*ics 2005; 206(24): 2512–2520.

17. Xiao S, Feng J, Zhu J, Wang X, Yi C, Su S. Preparation and characterization of lignin-layered double hydroxide/styrene-butadiene rubber composites. *Journal of Applied Polymer Science* 2013; 130(2): 1308-1312.

18. Liu Q, Zhang Y, Xu H. Properties of vulcanized rubber nanocomposites filled with nanokaolin and precipitated silica. *Applied Clay Science* 2008; 42(1-2): 232–236.

19. Preetha NK, Rani J. Nanokaolin clay as reinforcing filler in nitrile rubber. *International Journal of Scientific & Engineering Research* 2012; 3(3):1-9. http://www.ijser.org/onlineResearchPaperViewer.aspx.pdf (accessed 10 January 2014).

20. Sharma VP, Agarwal V, Umar S, Singh AK. Polymer Composites Sustainability: Environmental Perspective, Future Trends and. Minimization of Health Risk. *2nd International Conference on Environmental Science and Development (IPCBEE)*, Singapore; IACSIT Press; 2011.

21. Gao F, Nigmatullin R. Additional Information on the Health and safety of clay/polymer nanocompoistes- the size of clay particles and their comparison to the dust on street, In: Krzystof P (ed) *Modern Polymeric Materials for environmental applications; proceeding of 5TH International seminar*, 15-17 May 2013, Krakow, Poland; 2013.

22. Paul DR, Robeson LM. Polymer nanotechnology: Nanocomposites. *Polymer* 2008; 49(15): 3187–3204.

23. Sengupta R, Chakraborty S, Bandyopadhyay S, Dasgupta S, Mukhopadhyay R, Auddy K, Deuri AS, A Short Review on Rubber / Clay Nanocomposites With Emphasis on Mechanical Properties. *Polymer Engineering Science* 2007; 47: 1956-1974.

24. Stephen R, Thomas S. Nanocomposites: State of the Art, New Challenges and Opportunities, In: Thomas S, Stephen R (eds) *Rubber Nanocomposites: Preparation, Properties, and Applications*. Chichester, UK. John Wiley & Sons, Ltd; 2010. 1-19.

25. Duquesne S, Jama C, Le Bras M, Delobel R, Recourt P, Gloaguen J. Elaboration of EVA–nanoclay systems—characterization, thermal behaviour and fire performance. *Composites Science Technology 2003;* 63: 1141-1148.

26. Liang Y, Cao W, Li Z, Wang Y, Wu Y, Zhang L. A new strategy to improve the gas barrier property of isobutylene–isoprene rubber/clay nanocomposites. *Polymer Test*ing 2008; 27(3): 270–276.

27. Voulomenou A. Tarantili PA, Preparation, characterization, and property testing of condensation-type silicone/montmorillonite nanocomposites. *Journal of Applied Polymer Science* 2010; 118: 2521–2529.

28. Kaneko MLQA, Romero RB, Goncalves MC, Yoshida IVP, High molar mass silicone rubber reinforced with montmorillonite clay masterbatches: Morphology and mechanical properties. *European Polymer Journal* 2010; 46 (5): 881-890.

29. LeBaron CP, Wang Z. Pinnavaia TJ, Polymer-layered silicate nanocomposites: an overview. *Applied Clay Science* 1999; 15(1-2):11-29.

30. Ismail H, Ramly AF, Othman N. The Effect of Carbon Black/Multiwall Carbon Nanotube Hybrid Fillers on the Properties of Natural Rubber Nanocomposites. *Polymer Plastic Technology Eng*ineering 2011; 50 (7): 660 -666.

31. Pradhan B, Srivastava SK, Layered double hydroxide/multiwalled carbon nanotube hybrids as reinforcing filler in silicone rubber. *Composites Part A Applied Science Manufacturing* 2014; 56: 290-299.

32. Bratati P, Suneel KS. Synergistic effect of three dimensional multi-walled carbon nanotube/graphene nanofiller in enhancing the mechanical and thermal properties of high performance silicone rubber, *Article in press*. *Polymer International* (2013), doi: 10.1002/pi.4627. (Accessed 14 January 2014).

33. Garry WB, Clois EP. Thermodynamics and kinetics of polymer-clay Nano composites. In. *Fundamentals of Polymer/clay nanocomposites.* Cambridge, UK: University Press; 2011. 5-11

34. Pavlidou S, Papaspyrides CD. A review on polymer–layered silicate nanocomposites. *Proggress Polymer Science* 2008; 33(12): 1119-1198.

35. Jia C, Zhang LQ, Zhang H, Lu YL. Preparation, microstructure, and property of silicon rubber/organically modified montmorillonite nanocomposites and silicon rubber/OMMT/fumed silica ternary nanocomposites. *Polymer Composite* 2011; 32: 1245–1253.

36. Bokobza L, Rahmani M, Belin C, Bruneel JL, Bounia NE. Blends of carbon blacks and multiwall carbon nanotubes as reinforcing fillers for hydrocarbon rubbers. *Journal Polymer Science B Polymer Physics* 2008; 46: 1939–1951.

37. Qu L, Huang, G, Zhang P, Nie Y, Weng G, Wu J. Synergistic reinforcement of nanoclay and carbon black in natural rubber. *Polymer International* 2010; 59: 1397–1402.

38. Liu YB, Li L, Wang Q. Reinforcement of natural rubber with carbon black/nanoclay hybrid filler. *Plastic Rubber Composite* 2010; 39(8): 370 – 376.

39. Zhao G, Shi L, Zhang D, Feng X, Yuan S, Zhuo J. Synergistic effect of nanobarite and carbon black fillers in natural rubber matrix. *Materials Design* 2012; 35: 847-853.

CHAPTER 2: Literature review

2.1 Rubber/clay nanocomposites

The first commercial product based on exfoliated nylon-6/clay nanocomposites with improved physical and thermal properties was invented by Toyota Motors research group in the early 1990s [1-2]. This achievement opened up a new paradigm in nanotechnology research. Since then research in the polymer/clay nanocomposite field has expanded aggressively and substantial attention has been given to the use of nanoclay in thermoplastic and thermosetting polymers as well as in rubber matrices [1-7].

Rubber is an important class of polymer that has been widely used for a variety of applications, such as tyres, hoses, gaskets and medical products. The elastic behaviour of the polymer allows it to regain its original shape after being stretched or deformed. For example, pure silicone gum has elongation at break values ranging from 400 to about 600% [8]. Fillers are normally added to the rubber to reduce costs and to improve performance or failure properties, such as tensile strength, crack growth and abrasion resistance [5]. Relatively, only a limited numbers have been devoted to the incorporation of layered silicates in rubber matrices when compared to other common fillers such as carbon black and silica. This is because carbon black and silica fillers have dominated the filler reinforcement in rubber over the 50 years [5].

The past decade has produced an increasing amount of literature concerning synthesis, preparation and characterisation of rubber filled with nanoscale material such as nanoclay [6-7,

9-10]. Rubber/clay nanocomposites have been described based on three types of composites, as shown in the Fig. 2.1(a-c) [6]. The first is conventional composites (Fig. 2.1a) where non-swollen layered silicates are embedded in a polymer matrix. In this case, the size of clay interlayer spacing remains unchanged. The second is intercalated structure (Fig. 2.1b) when one or more polymer chains are inserted into the interlayer space to expand the inter layer spacing. Finally, exfoliated nanocomposite (Fig. 2.1c) is the most desired structure for polymer/clay nanocomposite, and is obtained by the separation of individual layers dispersed within the polymer matrix. The delamination of clay layers is usually due to the insertion of polymer chains into the clay galleries.

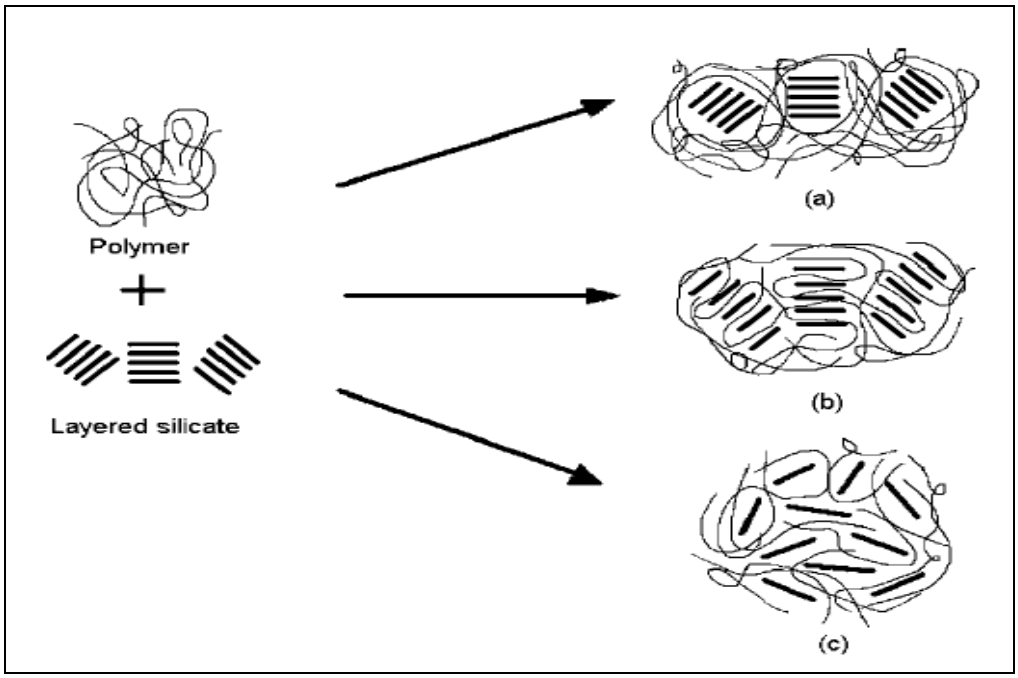

Fig. 2.1: Layered silicates in (a) conventional composites (b) intercalated nanocoposites and (c) exfoliated nanocomposites [6].

Nevertheless obtaining excellent clay dispersion in a rubber matrix is a key challenge in the preparation of rubber/clay nanocomposites. Therefore specific strategies, such as direct polymerisation and solution methods have been applied to create novel rubber products, using nanoclay as the reinforcing material in the rubber matrices. Melt-compounding has been recommended as the most promising technique for commercial manufacturing [6-10]. In addition, optimum clay loading level, type of curing system, mixing conditions, rubber grade,

preparation method and type of alkyl ammonium (clay modifier) used have been identified as the factors which influence the degree of clay dispersion in most common rubbers, such as natural rubber (NR), ethylene propylene diene monomer (EPDM), styrene-butadiene-rubber (SBR) and nitrile rubber (NBR) [6-10].

The reinforcement anisotropy and barrier properties in rubber nanocomposites attributed by exfoliated silicate layers with nanoscale thickness are the main topic discussed by other researchers [6-10]. It has been reported that fully exfoliated clay layers contributed to the high modulus, strength, and elongation-at-break of the nanocomposites [6]. In addition, exfoliated/intercalated nanoclays contribute positively to the thermal stability, increased flame retardancy, and improved barrier properties to gases and liquids of pure rubber [11-14].

2.1.1 Clays

Clays exist as a natural or synthetic mineral. They possess a layered structure with lateral dimensions approximately from 30nm to several micron metres and a layer thickness of about 1nm [3]. Phyllosilicates or 2:1 layered silicate clays, in particular smectite clays, have been highly investigated as reinforcing fillers in rubber due to their layered nanoparticles. These 2:1 phyllosilicates have a triple layer sandwich structure that consists of a central octahedral sheet dominated by alumina, bonded to two silicon tetrahedral sheets by oxygen atoms, which belong to both sheets as shown in Fig. 2.2 [3]. Unshared oxygen atoms are also present at the edges of layered silicates as part of a hydroxyl (OH) unit.

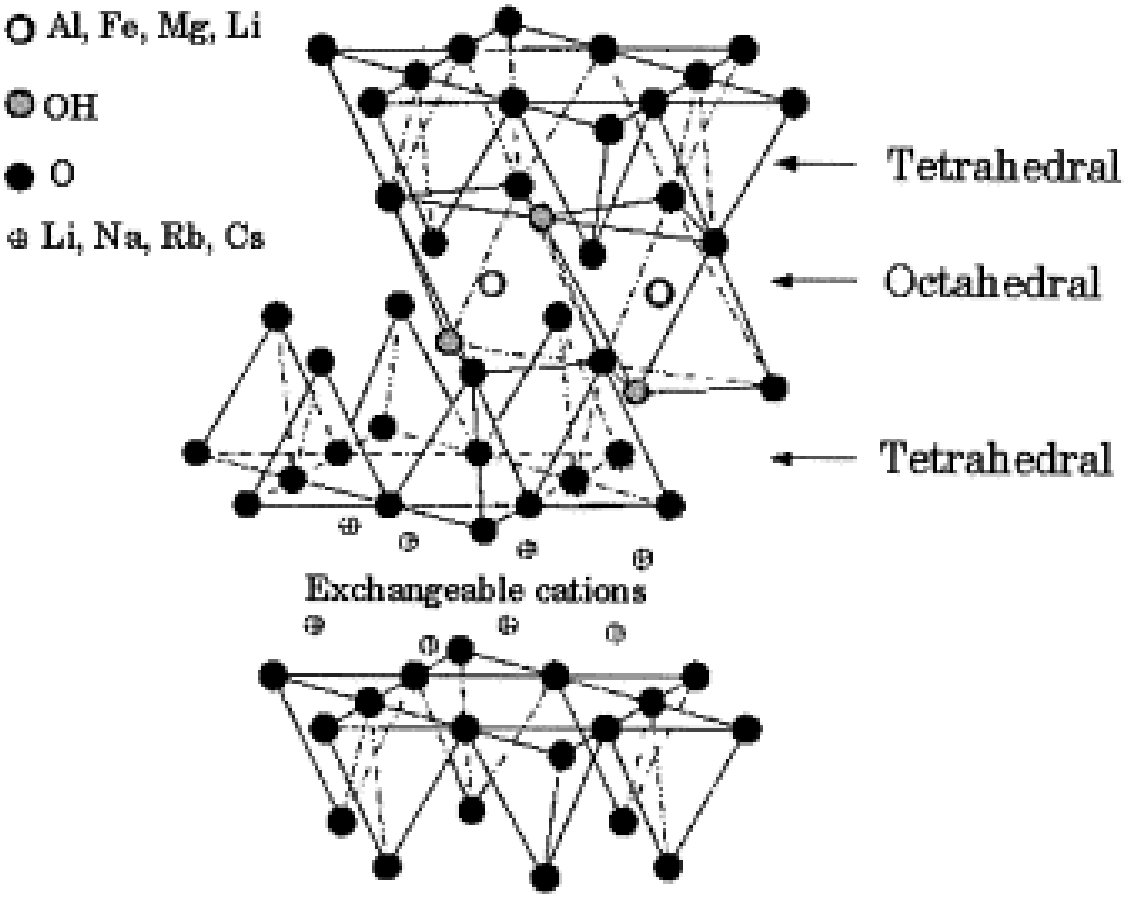

Fig. 2.2: The structure of 2:1 phyllosilicates [3]

Table 2.1: Chemical compositions of smectite type clays [3]

Smectites	Chemical formula
Montmorillonite	$M_x(Al_{4-x}Mg_x)Si_8O_{20}(OH)_4$
Hectorite	$M_x(Mg_{6-x}Li_X)Si_8O_{20}(OH)_4$
Saponite	$M_xMg_6(Si_{8-x}Al_X)O_{20}(OH)_4$

M: monovalent cation and x: degree of cations isomorphous substitution in octahedral sheets.

Montmorillonite (MMT), hectorite (HT) and saponite are examples of the smectite clay family. The chemical compositions of the fillers are listed in Table 2.1 [3]. Apart from that, mica, vermiculite and talc are the other minerals that fall under smectic type clays. These minerals can be differentiated mainly based on their structural filling, type of cation, and isomorphous substitution in the octahedral or tetrahedral layer [11]**.**

For example mica and MMT minerals have similar basic 2:1 crystal lattice structure. However, mica layers are difficult to exfoliate. In the case of mica, the silicon in tetrahedral sheet is substituted by aluminium where the negative surface charge is balanced by large cations such as potassium (K^+) [3]. The size of K^+ is fixed within the gap of Si/Al tetrahedral layer. Thus, the interlayer space in mica is strongly held by electrostatic attraction between the negatively charged tetrahedral layer and the K^+ ions. This strong interaction prevents mica from swelling [3].

Unlike mica, the MMT negative charge is balanced by metal cations (Na^+,Ca^{2+}, and Mg^{2+}) in the interlayer space. These ions are smaller than the size of tetrahedral layer therefore the layers are held with weak forces [1]. Also, MMT has larger cation exchange capacities which enable them to adsorb heavy metals and to be modified with quaternary salts including cationic surfactants [2]. This is a part of the reason why within the smectite clays group, MMT is preferred for the production of polymeric nanocomposites (PCN) due to its ability to expand the interlayer, thus easy to exfoliate.

2.1.2 Montmorilonite (MMT)

The unit cells of MMT are usually written as $[Al_{1.67}\, Mg_{0.33}\, (Na_{0.33})]\, Si_4O_{10}\, (OH)_2$. A typical MMT has 0.67 units of negative charge per unit cell. The negative charge is balanced by interlayer counter sodium or calcium ions. In addition, the cation exchange capacity (CEC) value indicates the capability of MMT to exchange ions. For MMT, the CEC ranges from 0.8 to 1.2 meq/g [15].

Generally, X-ray diffraction (XRD) patterns of hydrated MMT typically yields d_{001}= 1.2 – 1.4 nm basal spacing. The average dimensions of smectite clay platelets are about 1 nm thick, 150 nm wide and 500 nm long [15]. Thus, the aspect ratio of exfoliated mineral MMT is p=50 to 2000 and the specific surface area of MMT is 750 – 800 m^2/g. Finally, layered silicates have tensile modulus of ~ 175 GPa and tensile strength of ~ 1 GPa [15].

2.1.3 Organoclays (Intercalation by organic cations)

The layered structure of MMT is maintained by electrostatic and van der Waals forces. The cations present between the layers can be hydrated in aqueous solutions to increase the volume of interlayer space. This is known as clay swelling. Since pristine layered silicates (Na^+MMT) are naturally hydrophilic, they are usually modified with organic surfactant through ion-exchange reactions in order to improve compatibility with a polymer [16]. Fig. 2.3 demonstrates the scheme of the modification of clay layers by organic cations.

Theoretically an organic surfactant with a positive charge will proportionally balance the negative charge of the silicate layers, thus increasing the space between the layers. It then becomes possible for organic molecules to diffuse between the layers and eventually separate the clay layers further apart. At the same time the surface energy of the layered silicates is reduced by the presence of organic cations, increasing compatibility within the polymer matrix. Conclusively, two important things can be achieved from the surface modification; (1) increased basal spacing and (2) enhanced compatibility between the hydrophilic clay and the polymer.

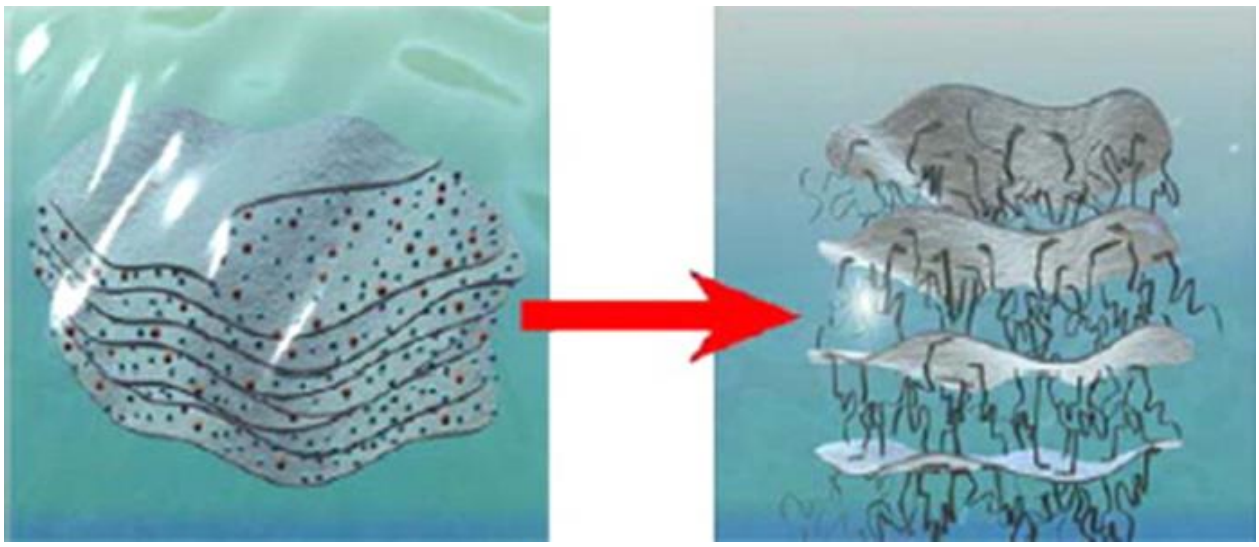

Fig. 2.3: Schematic picture of an ion-exchange reaction [3]

Most organo-modified MMT or orgnoclays can be found at a commercial grade for a relatively low price. Commercial organoclays such as Cloisite®, Nanomers and Nanofil have been used in a numerous studies to prepare polymer/clay nanocomposites [3] and are available in several types based on charge density, length of alkyl chain, and configurations of the organic modifiers inserted within the clay layers. All the parameters mentioned above control the respective basal spacing (d_{001}) in organoclays [15-17]. For example aliphatic salt was easier to intercalate into the clay galleries, due to the absence of steric effects in the aromatic rings [15], giving rise to a higher interlayer distance than aromatic salt. It was reported that intergallery spacing values of sodium MMT increased from 11.5 to 18.5 and 21.2 nm after modification with aromatic salt and aliphatic salt respectively [16].

In addition, the functionality of organic modifiers in alkyl surfactants determines the polarity of organoclays. Cloisite 30B, which contains hydroxyl group (OH) in alkyl ammonium chains, is an example of a polar organoclay. Cloisite 15A and Cloisite 20A, which have no polar functional group on the alkyl ammonium chain, are known as non-polar organoclays [17]. This measurement is important when selecting between an organoclay and a rubber.

2.1.4 Structure of rubber/clay nanocomposite (Intercalated and exfoliated)

In polymer/clay nanocomposites four types of layered silicate dispersion have been recognised. They have been identified as [1-3, 18]:

I. Conventional clay-filled composite with micron-sized aggregates of clay particles.
II. Nanocomposite with intercalated clay form where the interlayer spacing d_{001}< 8.8 nm.
III. Exfoliated nanocomposites with locally ordered structure where d_{001}>8.8 nm.
IV. Exfoliated nanocomposites with disordered structure where d_{001}>8.8nm.

A similar description is also applied to layered silicates nanostructures in a rubber matrix [6-7, 9-10]. Schematic illustrations of the rubber/clay nanocomposite morphology are shown in Fig. 2.4(a-d).

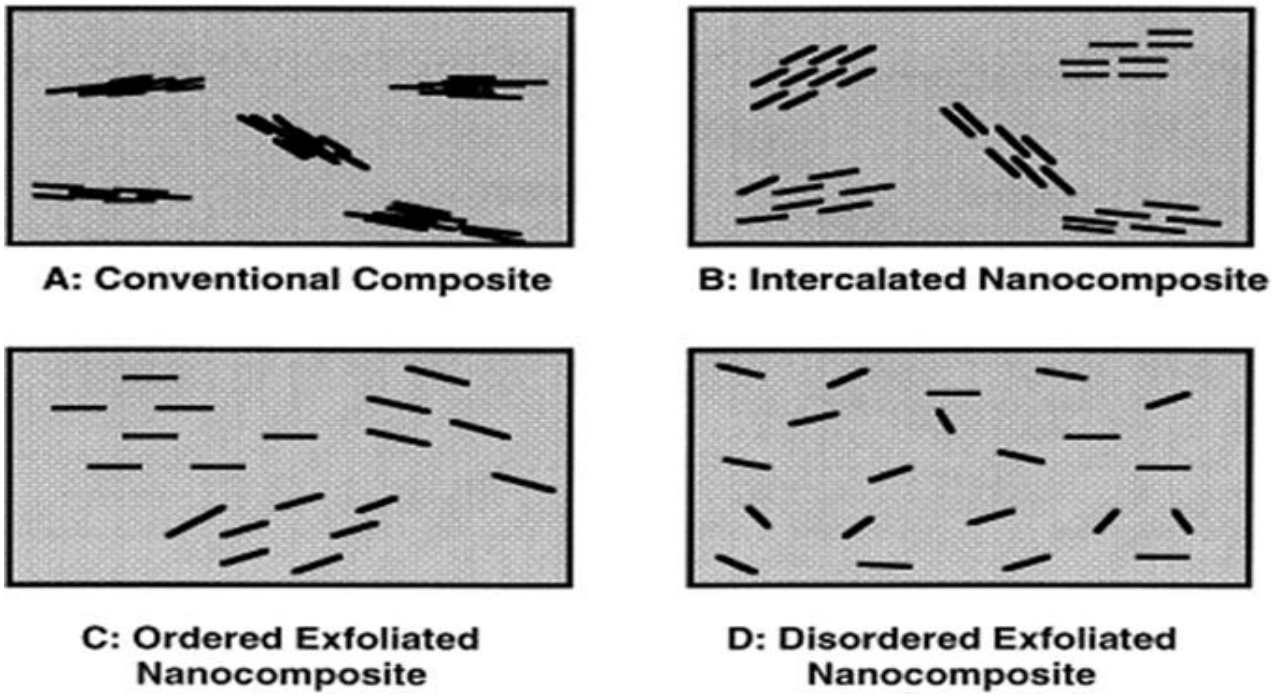

Fig. 2.4(a-d): Schematic illustration of (a) conventional (b) intercalated (c) ordered exfoliated (d) disordered exfoliated, polymer-nanocomposites [17].

2.1.5 Characterisations of nanoclay dispersion

The degree of clay dispersion in rubber/clay nanocomposites is commonly characterized by X-ray diffraction (XRD) and transmission electron microscopy (TEM) [6-7, 9-10]. Other than those techniques, optical microscopy, small-angle X-ray diffraction (SAXS) [19] and atomic force microscopy (AFM) are also viable ways to examine nanoclay dispersion [20]. Bound rubber measurements and in-situ testing of electrical conductance using a combination of field emission gun scanning electron microscopy (FEGSEM) with tensile devices [21] are examples of recent procedures developed to measure exfoliation in rubber. Additionally, a combination of XRD and TEM techniques is commonly used to confirm nanocomposite structure since those techniques are more easily available than other methods [1-4].

2.1.5.1 Wide-angle X-ray diffraction (WAXD)

Wide-angle X-ray diffraction (WAXD) appears as an ideal analytical method for characterizing polymer-clay nanocomposites, since the analysis is non-destructive, rapid, low cost and requires minimal sample preparation. Principally, the wavelength in XRD has the same order of size as the atomic dimensions of the clay's crystalline lattice. The yield peak at discrete angles is obtained when the X-ray constructively interferes with this and corresponds to the atomic spacing of the lattice by Bragg's Law (Equation 2.1) [22].

In this case, the basal spacing between the clay plates, also known as d-spacing, is derived from the peak position (d_{001}-reflection) in XRD diffractograms. The d value is measured according to the to the Bragg's law (Equation 2.1), where n is an integer, λ is the X-ray wavelength, d is the interlayer spacing, and θ is the angle of diffraction. In practice, 2theta is used rather than theta due to the geometry of the detector relative to the X-ray source [22].

$$\lambda n = 2d \sin \theta \qquad \text{Equation 2.1}$$

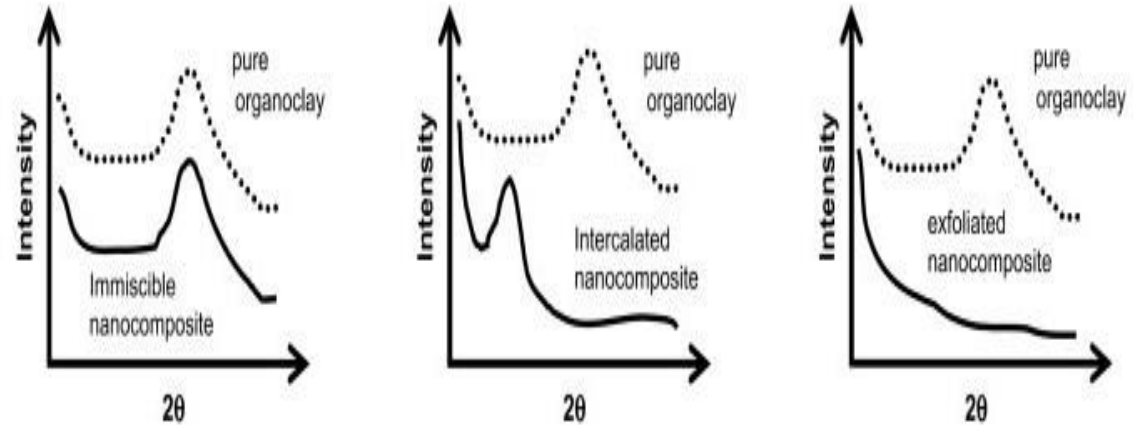

Fig. 2.5(a-c): Illustration of different state of dispersion of organoclays in polymer, corresponding to WAXD result [1].

Fig. 2.5(a-c) presents a typical XRD pattern of immiscible composite, intercalated nanocomposites and exfoliated nanocomposites For immiscible composite, characteristics of the original layered silicate basal reflections are unaffected, since no change occurs on the silicate lattice (Fig. 2.5a). Changes to the XRD, such as peak position, broadness, and intensity, are related to the measurement of d spacing according to Bragg's law equation. A shift of XRD peak to a lower diffraction angles - (2θ) angle (Fig. 2.5b) - corresponds to an increase of d spacing from the original value. The expansion of d spacing in the clay gallery is commonly due to intercalation of organic surfactant due to clay modification. The increase in *d* spacing or polymer intercalation between the clay layers is termed as intercalated nanocomposite.

In contrast, a flat diffraction pattern is associated with a delaminated or exfoliated structure of layered silicates, due to broad layer separation (Fig. 2.5c). As the spacing between separated layers exceed 8 nm in the case of an ordered exfoliated structure, the diffraction peak become undetectable [3]. However, invisible diffraction peaks also can be referred to as disordered tactoids, or a mixture of small clay tactoids moving toward exfoliation. Therefore, microscopy methods must be used to confirm exfoliation [22]

2.1.5.2 Transmission electron microscopy (TEM)

Transmission electron microscopy (TEM) is very useful since it can visualise clay dispersion in a rubber matrix. Normally results from XRD spectra are always supported by TEM imaging to further confirm the clay structure of a polymer matrix. Figure 2.6(a-c) presents an example of typical TEM images obtained from polymer/clay nanocomposites with different state organoclay dispersions [1].

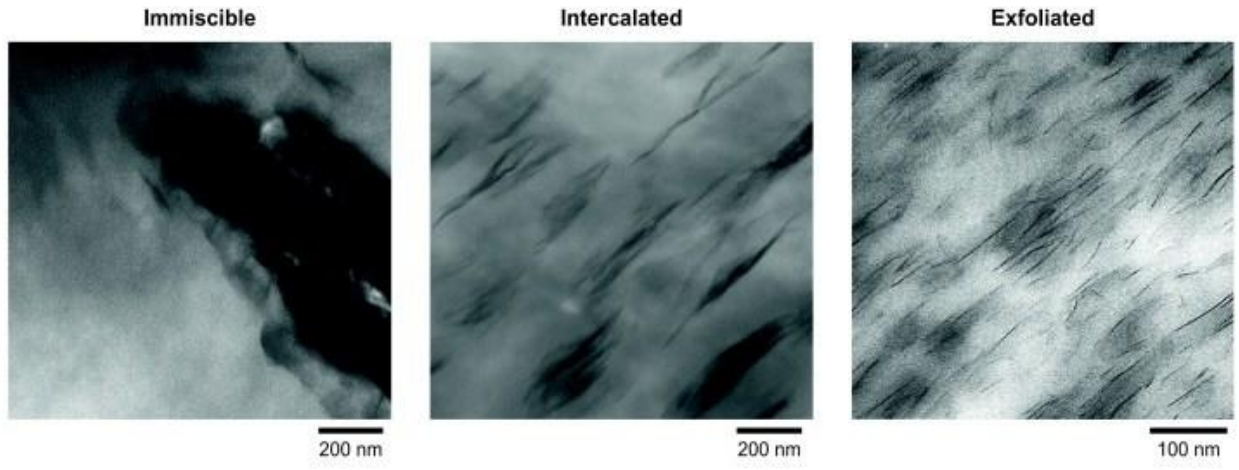

Fig. 2.6(a-c): TEM images of different state dispersions of organoclay in a polymer matrix [1].

For immiscible composites, the clay always exists as dark lines or multilayered bundles in the matrix, as shown in Fig. 2.6a. TEM imaging in Fig.2.6b shows incomplete exfoliated particles in a matrix that corresponds to intercalated nanocomposite. On the other hand, exfoliated clay in a polymer matrix can be seen as thin dark lines, indicating a single-clay layer (Fig. 2.6) [1]. TEM imaging provides direct evidence of clay dispersion. However to produce a clear TEM image, considerable skill and patience is essential. The main challenge in TEM analysis derives from issues of sample preparation. To obtain a thin section for a rubbery material is time-consuming and requires a well-experienced operator. For example, to prepare a thin section of silicone rubber at very low temperature (-150°C) is very difficult due to the nature of the polymer.

2.1.6 Preparation of rubber/clay nanocomposites

The motivation to achieve fully exfoliated clays in the rubber matrix is highlighted in most reports in the literature [6-7, 9-10]. Surface treatment of MMT clays and optimization of dispersing apparatus/equipment are the best strategies for achieving exfoliation in various types of rubber. Rubbers are usually available in solid (dry) and latex (solution) forms. Melt-intercalation [9, 24-27] and latex compounding [28, 29] are primarily used to prepare rubber/clay nanocomposites, although solution blending with the presence of solvent is also used [30].

2.1.6.1 Melt compounding

Melt compounding involves direct mixing between rubbers and compounding ingredients such as a curing agent, antioxidant, or filler under molten state, followed by vulcanisation. The mixing process is usually done in a shear device, such as mixers, open two-roll mills, and extruders. The concept of melt intercalation is described in Fig. 2.7 [1].

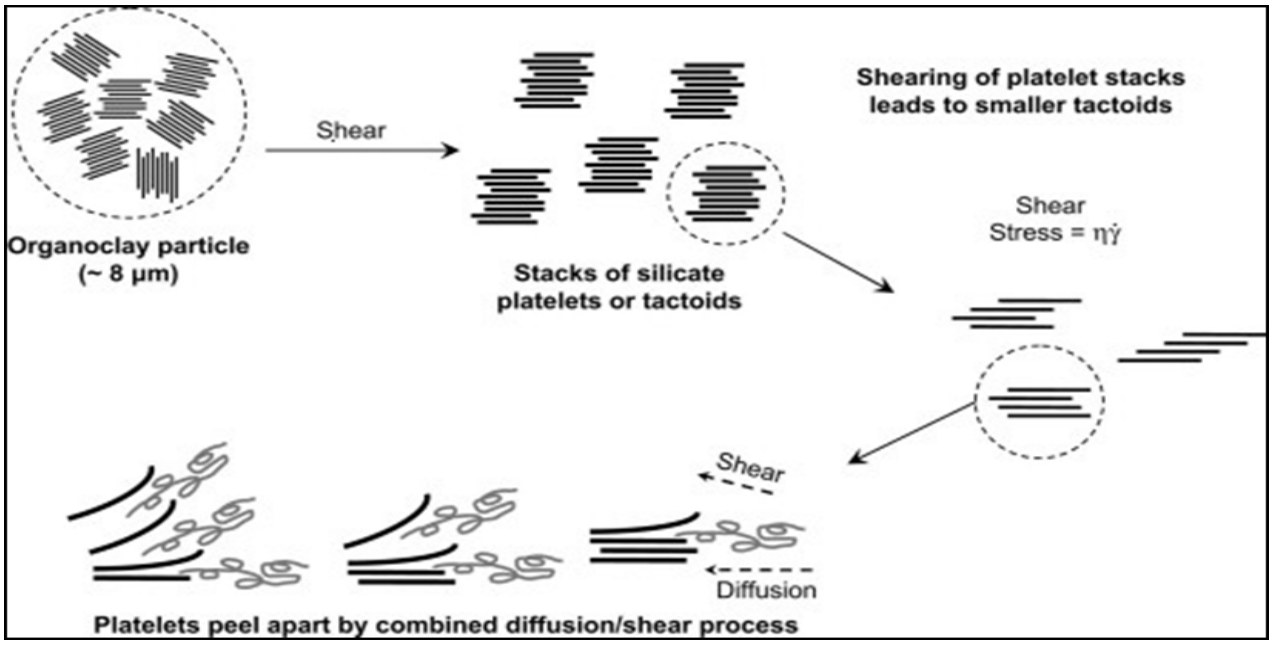

Fig.2.7: Mechanism of organoclay dispersion and exfoliation during melt processing [1]

At the initial stage, the particles of an organoclay powder consist of aggregates of tactoids, or stack of platelets about 8 μm in size. During melt mixing the aggregates break up into smaller particles under mechanical shear stress. However if the polymer and organoclay

have good thermodynamic affinity, the contact between polymer and organoclay can be increased by peeling the platelets one by one at a given mixing time [1].

The formation of exfoliated or intercalated clay in a rubber/clay nanocomposite using this route is also influenced by curing conditions, pressure, and temperature [9, 25]. Liang and co-workers [25] revealed that the intercalated structures of isobutylene-isoprene rubber/clay nanocomposites (IIRCNs) and their spatial distributions in the matrix were extensively altered by thermal treatment at atmospheric (AP) or higher pressure. When increasing the thermal treatment at AP the original intercalation was transformed to one with a smaller gallery height [25]. When extra pressure was applied, particularly beyond a critical point between 4.5 and 5.0 MPa, some intercalated silicates were assembled to form an intercalated-and-flocculated structure.

In addition, matching rubber and layered surfaces is important to allow the rubber chain to penetrate into the interlayer space and form either an intercalated or an exfoliated nanocomposite. A study carried out by Wu and co-workers [9] revealed that exfoliated nanocomposites with octadecylamine modified fluorohectorite were favoured for rubber with high polarity. It was reported that the degree of exfoliation increased in the following order EPDM < SBR < NR. This was because the polar or unsaturated rubber promoted better polymer-filler interactions between rubber and organoclay, facilitating the formation of exfoliated or intercalated nanocomposite. Also it has been proven that clay intercalation is kinetically easier in rubber compounds with a low molecular weight [9].

Some previous works have disclosed that the curing chemistry during vulcanisation is a major influence on the microstructure of rubber/clay nanocomposites [26,27]. For example, natural rubber (NR) molecules could intercalate into the inter gallery of organoclay during mixing at 100°C. However, the intercalated organoclay particles had a tendency to confine (re-aggregate) after the curing process [26]. A similar phenomenon was also observed in epoxidized natural rubber (ENR). Varghese and co-workers [27] suggested that a possible

reaction between intercalant and sulfuric curatives is responsible for the confinement of the organoclay in ENR.

2.1.6.2 Latex compounding

Latex compounding is one of the options available for making rubber/clay nanocomposites. The mixing and coagulation processes are illustrated in Fig. 2.8 [28]. Swollen clay is prepared by adding water to form clay slurry prior to mixing with latex, followed by coagulation.

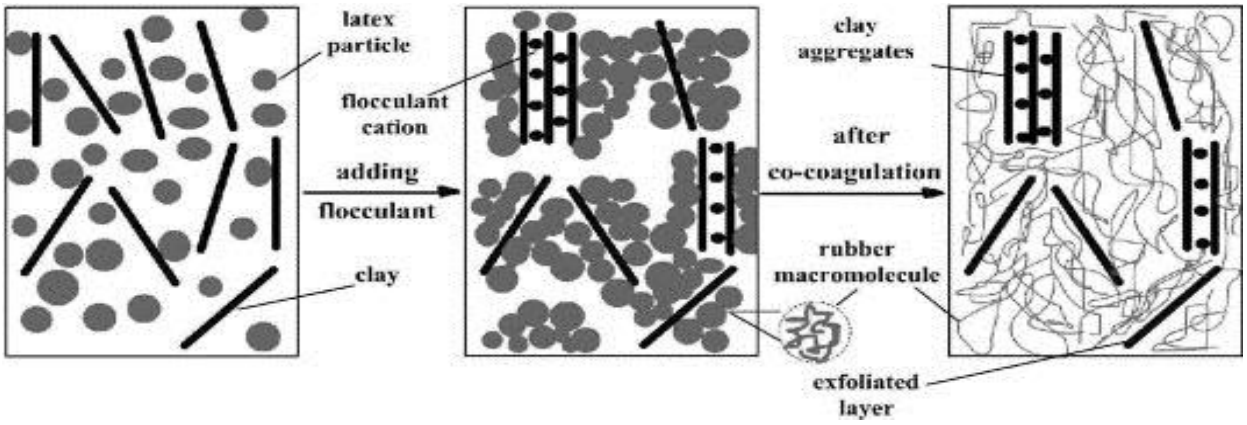

Fig. 2.8: Schematic illustration of the mixing and co-coagulating process [28]

Unlike melt-compounding, this method requires pristine clay, as it is easily dispersed in water due to hydration of Na^+ and K^+ [6]. A combination of XRD and TEM analysis showed that rubber/clay nanocomposite prepared by latex compounding always contains a mixture of exfoliated clay and non-exfoliated clay. This was attributed to the addition of flocculant during the coagulation process, disrupting the original intercalated structure. Some of the layered silicates are surrounded by agglomerated latex particles, causing re-aggregation [28]. However, obtaining a nanocompound with complete exfoliated particles, prepared by latex compounding, is highly possible as long as the mixing parameters (such as latex particle size and coagulation speed) are under control [29].

2.1.6.3 Solution blending

In solution blending organic solvent is needed as a medium to dissolve dry rubber, along with organoclay to prepare the rubber/clay nanocomposite [6]. The solvent is removed prior to vulcanization of the rubber. The level of intercalated and exfoliated clay dispersed in the rubber as a result of solution blending is promising [30].

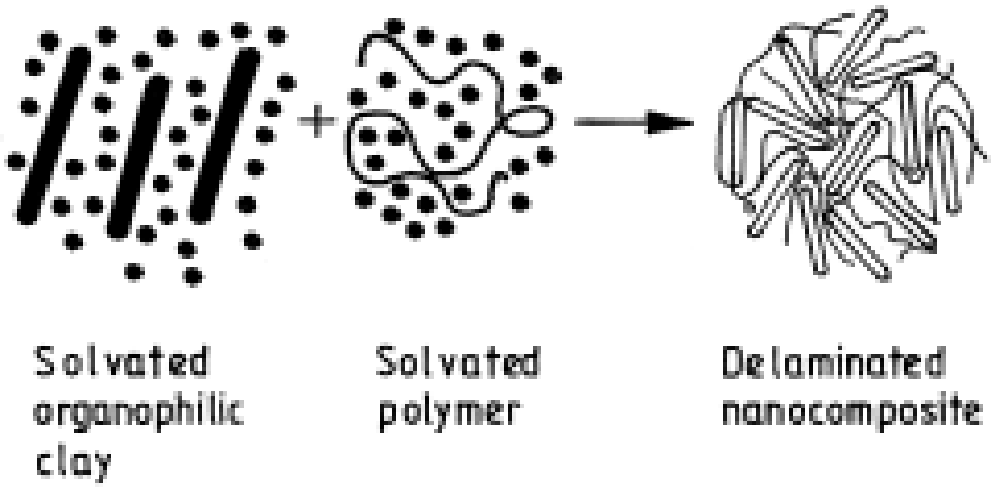

Fig. 2.9: A conceptual picture of the formation of nanocomposites through solution blending [30].

Pramanik and co-workers [29] prepared ethylene vinyl acetate rubber (45% vinyl acetate content, EVA-45) and organomodified clay (12Me-MMT) composites by solution blending. Dimethylacetamide was used as a medium to disperse the clay and mix the rubber. Scanning electron microscopy (SEM) and transmission electron microscopy (TEM) images proved that the EVA–clay nanocomposites containing 6 wt% of 12Me-MMT were dispersed in a range of 4 to 6 nm within the matrix. Based on the mechanical and dynamic mechanical results, they concluded that the nanocomposite of EVA-45 with organophilic clay (12Me-MMT) prepared by solution blending had superior performance over the conventional one.

2.2 Background of silicone rubber (SR)

2.2.1 Structure and chemistry of silicone rubber (SR).

Silicone rubber (SR) is a class of speciality elastomers which possess inorganic siloxane bonds (Si-O-Si) as their main backbone [31]. Polydimethylsiloxane (PDMS) $[(CH_3)2SiO]_n$, shown in Fig. 2.10, is a common unit of silicone rubber.

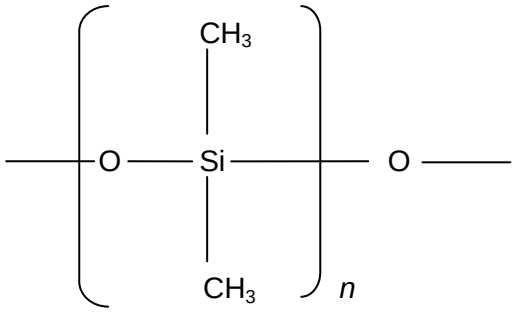

Fig. 2.10: Structure of polydimethylsiloxane (PDMS) [8]

Methyl (CH_3), as the basic organic group, usually exists in siloxane lateral chains. However, other substituent groups such as phenyl, vinyl or fluoro can be incorporated to replace methyl in order to impart different qualities of the rubber properties. For example, vinyl groups help to improve crosslink density in vulcanised silicone rubber, while fluoro groups are used to enhance oil and solvent resistance.

At commercial grades, silicone rubber is available in three different types. Room Temperature Vulcanised (RTV), High Consistency or Heat Cured Rubber (HCR), and Liquid Injection Moulding (LSR). They have distinct characteristics based on viscosity, molecular weight, processing, cure system and application. The silicone rubber used in this thesis is methyl vinyl silicone rubber (VMQ), categorised as a HCR silicone rubber. The molecular weight of HCR is usually within the range of 300,000 to 800, 000 g/mol and the average viscosity is approx. 20, 000 cm^2/s [8]. It is mainly used to produce O-rings, seals, boots, high voltage insulators, wire and cables.

2.2.2 Physical properties of silicone rubber (SR)

Si-O has higher bond strength (363 kJ/mol) than carbon bonds C-C (347 kJ/mol). This partially explains why silicone rubber is more stable than hydrocarbon polymer. In addition, the saturated backbone in silicone chains protects silicone rubber from oxidation and ozone attack, while many organic polymers possess unsaturated chains in their main structure. As such, silicone rubber provides excellent resistance to heat, chemical, ozone, and radiation, and possesses better electrical insulation compared to typical organic polymers. Silicone rubber is also able to withstand a wide temperature range (– 40°C to 150°C and above), giving it more versatile uses.

Despite its excellent thermal stability, a major drawback of a silicone rubber is its poor mechanical strength. The tensile strength of a crosslinked gum silicone rubber is about 0.35 MPa [31]. Weak intermolecular forces in siloxane chains provide only a low mechanical strength, due to longer Si-O bond length (2.34 Å). Table 2.2 summarises the siloxane characteristics that influence silicone rubber property [30].

Table 2.2: Siloxane characteristics [31]

Siloxane property	Effect on silicone rubber
High Si-C and Si-O bond strength (kJ/mol) Si-C = 363, Si-O = 451 and C-C = 347	Resistance to oxidative and chemical degradation
High association of CH_3 side groups	Low glass transition temperature. Hydrophobicity. Low surface energy.
High energy barrier to Si-O bond	Low glass transition temperature. Hydrophobicity. Very flexible. Low surface energy.

2.2.3 Silicone rubber compounding ingredients

A typical silicone rubber compound is a blend between rubber and other ingredients, such as reinforcing/extending filler, curing agents, process aids, and/or various additives (e.g., heat stabilisers or blowing agents for sponge and colours/pigments). Normally product performance requirements dictate initial selections of rubber formulation ingredients, and the materials used must be environmentally safe, meet occupational health standards, and be both processable and cost effective. Table 2.3 displays a typical formulation of a silicone rubber compound [31].

Table 2.3: A typical silicone rubber formulation [8]

Ingredients	Function	phr (part per hundred rubber)
Silicone rubber (s)	Polymer	100
Process aids (e.g. low molecular weight silicone fluid)	Aid mixing, modify viscosity, compatibilsers	0.25 to 2.0
Reinforcing filler (e.g. fumed or precipitated silica)	Reinforce mechanical and physical properties of elastomers such as hardness, tensile strength, modulus, abrasion resistance and tear strength.	2 to 50
Extending filler (e.g. quartz silica)	To replace a portion of elastomer in order to reduce cost	10 to 100
Stabilizers (e.g. phenothiazine, 4-tert butyl catechol)	antioxidant	0.5 to 2.0
Curing agent (e.g. peroxide, platinum)	Curing agent	0.75 to 1.5
Colour/pigments	Impart specific colouring	0.5 to 3.0

2.2.3.1 Crosslinking of silicone rubber

A linear silicone rubber gum is usually amorphous, rubbery and viscous at room temperature, and is usually crosslinked to obtain elastic properties. Curing of silicone rubber involves two mechanisms, radical reactions (peroxide) and/or addition reactions (platinum) [8].

Peroxide curing through free radical chemistry is an old technology used to crosslink silicones, especially HCR silicone rubber [8].

The free radical reaction involves decomposition of organic peroxide at elevated temperatures, generating polymer radicals. Their derivative radicals consumed during the reaction subsequently combine to form carbon-carbon bonds, along with by-products such as volatile organic acid. These volatile materials can be removed by exposing the compound to high temperature for an extended period (known as post-curing).

Platinum complexes are also employed to crosslink silicone rubber via addition reaction. The addition cure system produces no organic residue during the reaction, and therefore does not require post-curing treatment. In addition there is no handling of peroxide involved [32]. This provides an advantage for sterilized products where post-cure treatment can be avoided [33].

2.2.3.2 Free radical crosslinking of silicone rubber

The free radical crosslinking reaction transforms a linear silicone rubber chain into a three-dimensional network linked by covalent bonds between the macromolecular chains of the rubber. These covalent bonds are obtained by reaction between reactive sites. This crosslinking process is an exothermic reaction [33-36].

There are two types of organic peroxide used to crosslink silicone rubber, ‘vinyl’ specific peroxide and general purpose peroxide [8]. Dialkyl peroxide (e.g dicumyl peroxide (DCP)) is an example of vinyl specific group peroxide that can only be used to crosslink silicone rubber in the presence of some degree of vinyl. This is because the vinyl group lowers the activation energy, thus shortening the curing time [33].

DCP needs only short post cure treatment (sometimes none at all) since no acidic trace is produced during the crosslinking process. This is important for thermal stability, as no additional crosslinking is expected to occur at high temperature. It was reported that the best form of silicone rubber cured with DCP was obtained after press-curing [37]. However the

compound cured by DCP showed poor mechanical properties when aged at a temperature above 200°C [37].

On the other hand, general purpose peroxides can cure all kinds of silicone rubber compounds. Diacyl peroxides, such as benzoyl peroxide, fall under this category. This type of peroxide generates acidic decomposition, thus a long post cure treatment is needed for thick rubber profiles [31]. In this thesis DCP is chosen to crosslink silicone rubber, since it requires no post cure treatment after the crosslinking process. Fig.2.11 shows the DCP decomposition and free-radical crosslinking mechanism of vinyl-PDMS [33].

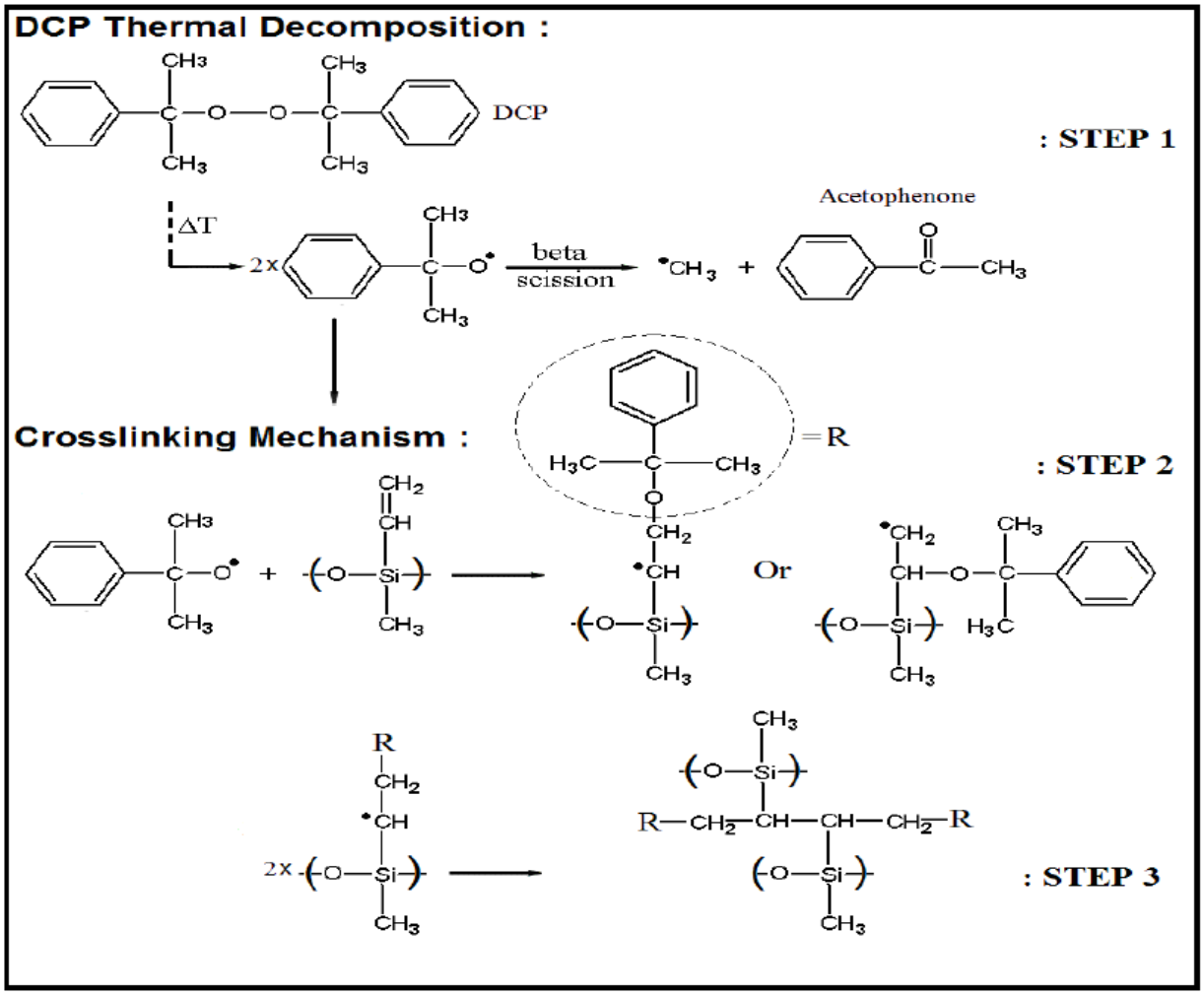

Fig. 2.11: DCP decomposition and free-radical crosslinking mechanism of vinyl-PDMS [33]

Three key steps involve in a crosslinking process of vinyl-PDMS by DCP as shown in Fig. 2.11. Firstly, the DCP decompose to form into two cumyloxy radicals via thermal decomposition (Step 1). The cumyloxy radicals react with the unsaturated pendant groups (vinyls) in the polymer chain to create polymer radicals (Step 2). The polymer radicals produced is unstable and reactive; hence the addition reaction is occurred among the polymer radicals to form a covalent carbon-carbon crosslink (Step 3) [33].

2.2.4 Fillers for silicone rubber

A major drawback of silicone rubber is its poor mechanical strength. The tensile strength of unfilled silicone rubber is about 0.35 MPa [8]. Thus, silicone rubber has always been reinforced with filler to improve its tensile strength, hardness, tear strength and abrasion resistance. The improved mechanical properties of the filled rubber are usually controlled by factors such as volume or weight fraction, shape and size of particles, as well as filler-filler and filler-matrix interaction [38].

At one time metal oxides were used to reinforce silicone rubber at the early stages of development [8]. However, the scenario changed when silica filler emerged in the early 1950 [39]. It was reported that silicone rubber filled with silica exhibited three times higher tensile strength when compared to silicone rubber filled with metal oxides [8]. Bokobza [40] investigated the reinforcement of a few different types of silicates fillers - colloidal silica, layered silicates and fiber clay (sepiolite). It was found that colloidal silica prepared by in-situ filling processes (where the mineral phase is generated by the sol–gel process) was the most effective with regard to layered silicates and sepiolite. Apart from that, there are few types of other filler that have been used to reinforce silicone rubber, usually for specific applications, such as titanium oxide (TiO_2), carbon nanotubes (CNT), polyhedral oligomeric silsesquioxanes (POSS), ferrite, iron and zeolite [41].

2.2.4.1 Silica filler

Silica is an active inorganic filler that is composed of siloxane and silanol (-OH) groups on its surface. Silica filler can be classified into three main groups based on the method of production and resultant properties. These are fumed silicas, precipitated silicas and aerogel silica. Until recently fumed silica has been exclusively employed in silicon rubber compounds due to its high surface area, ranging from 150 to 400 m^2/g. It is manufactured by the flame hydrolysis of silicon tetrachloride ($SiCl_4$) at high temperature. Hydrated amorphous silica (or precipitated silica) is also used to reinforce silicone rubber, though the reinforcing effect of precipitated silica is weaker than fumed silica. However, precipitated silica is less costly than fumed silica, thus it is beneficial from an economic stand point.

The characteristic structure of silica can be divided into agglomerates, aggregates and primary particles, as shown in Fig. 2.12. The size of the primary silica particle is between 5-45 nm and the typical dimensions of the silica aggregates are 100-500 nm [5]. The silica aggregates are formed by the reaction of primary particles, followed by dehydration. Within the aggregates nano-sized primary particles are linked together via siloxane bonds. The agglomerate of silica is typically in the dimension of 1-40 µm. This agglomerate of silica is formed by the agglomeration of silica aggregates by hydrogen bonding and van der Waals forces [5].

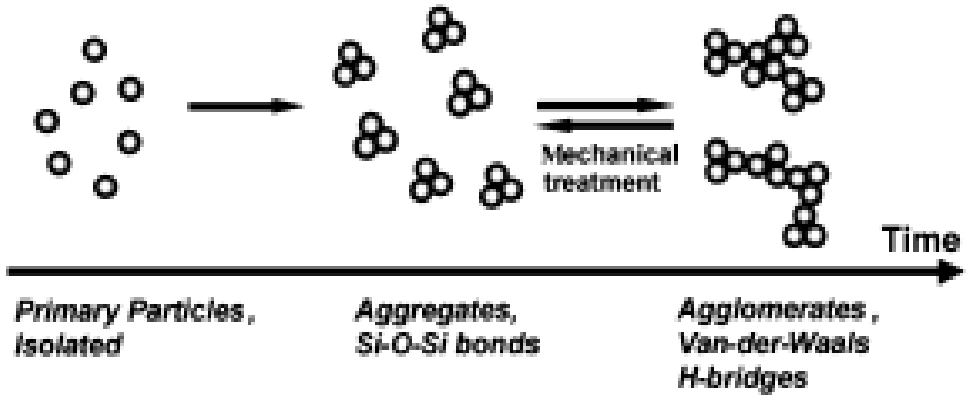

Fig. 2.12: Structure of silica: primary particles, aggregates and agglomerates [5]

The principal mechanical properties of silicone filled silica composites are controlled by the strength of filler-filler and filler-polymer interactions. This is because the applied mechanical force is transferred from the polymer, via the interface, to the filler. The level of potential interaction between polymer and filler is dependent on the particle size or related specific surface area (SSA) of the silica filler. In addition other factors, such as the particle surface chemistry and selection of polymer, also determine the strength of the filler-polymer interaction. Therefore increasing the potential interaction points by increasing the filler loading or SSA (with reduction of primary particle size) will enhance the mechanical properties of the rubber [43-45]. The greater reinforcement effect in fumed silica filled silicone rubber composites is attributed to strong physico-chemical interactions, which can be explained as follows [8]:

i these interactions may result in covalent chemical bonds resulting from condensation of silianols in siloxanes with silanols on the silica surface;

ii. hydrogen bonds between the silanols in the siloxane and on the silica surface;

iii. polar and/or Van der Waals forces through dipole-dipole interactions between the silica silanols and the polar Si-O-Si of the siloxane.

These physico-chemical interactions are always measured through bound rubber and swelling measurement [43]. The strength of polymer-filler interaction in silicone rubber compounds varies based on silica surface area and level of filler dispersion [43-45.]. It has been reported that rheological and mechanical properties of silicone rubber vulcanisates increase markedly with increasing surface area of fumed silica [44]. Remarkably the bound rubber and tensile strength reached a maximum (10.5 MPa) at a surface area between 170 and 250 m^2/g. However, the degree of filler dispersion, tear strength, and elongation-at-break were found to deteriorate [44].

Camenzinda and co-workers [45] observed that fumed silica under a grade name Aerosil 300, which had high surface area (e.g. Aerosil 300 ± 30 m^2g^{-1}), tended to agglomerate, reducing the Young's modulus of the rubber. On the other hand fumed silica (Aerosil 300 OX5O) which

had low surface area (40 ± 5 m^2g^{-1}) exhibited higher Young's modulus even at high filler loading, due less aggregation in the rubber matrix. A long mixing duration was recommended to obtain consistent and uniform agglomerate sizes in the composites.

Sun and Mark [46] revealed that the filler network of silica in silicone rubber was improved by precipitating silica directly into a swollen silicone rubber network after it was cured, or by incorporating silica prepared from a precursor such as partially hydrolysed hexamethyldisilazane (TEOS), containing some portions of polydimethylsiloxane (PDMS). Indeed, the in situ precipitation provides homogenise dispersion and are essentially unagglomerated (as demonstrated by electron microscopy); however such reaction is complicated, involving polymerization and branching [41]. A typical overall reaction involves hydrolysis of alkoxysilanes (organosilicates) to give silica, SiO_2 may be written as (1) where the $Si(OR)_4$ organometallic species is typically tetraethoxysilane (tetraethylorthosilicate, TEOS).

$$Si(OR)_4+2H_2O \rightarrow SiO_2+4ROH \quad (1)$$

In addition several studies have shown that silica modified by dimethylsiloxy [47] vinylethoxysilane [48] displays lowered surface activity of the silanol group on the silica surface and subsequently reduced agglomeration of filler in the silicone matrix.

2.3 Silicone rubber/clay nanocomposites

2.3.1 Preparation and characterisation of silicone rubber/clay nanocomposites

In early studies, Burnside and Giannelis [49] prepared silicone rubber-silicate nanocomposites with sonicated silicone rubber gum (molecular weight (MW; 18 000)) and modified montmorillonite mixture for 4 minutes at room temperature. Tetraethyl orthosilicate (TEOS) was added to the mixture to complete the crosslinking reaction, for 12 hours at ambient temperature. Fig. 2.13 presents a schematic illustration of nanocomposite synthesis. The process involved delamination of the layered silicates in the silicone matrix during the sonicating process, followed by crosslinking. The XRD results suggested that the delaminated or exfoliated

particles were homogeneously dispersed in the matrix. This conclusion was supported by the improvement in mechanical properties and dramatic decrease of solvent swelling [49].

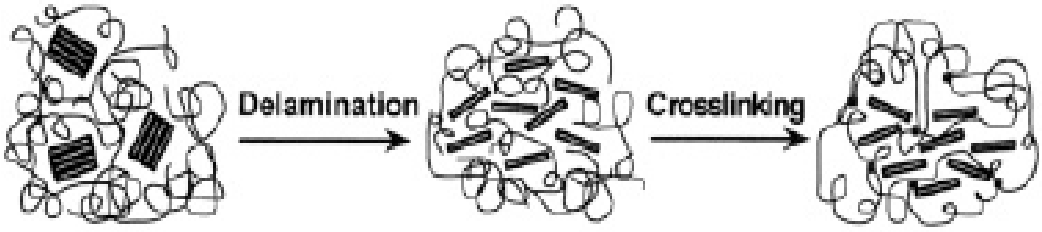

Fig. 2.13: Schematic illustration of nanocomposite synthesis [49]

Lebaron and Pinnavaia [50] examined the intercalation properties of a synthetic fluorohectorite in silicone rubber (Polydimethylsiloxane-PDMS) with molecular weights in the range of 400-4200. The intercalated nanocomposites were successfully prepared via in-situ mixing for 12 hours, with another 24 hours for curing (including post curing). Clay gallery expansion was increased by increasing the molecular weight of silicone rubber. In addition increased gallery heights in the silicone rubber-fluorohectorite system were also determined by the ratio of $-OSi(CH_3)_2-$ repeat units to terminal $-Si(CH_3)_2OH$ groups. It has been speculated that the silanol end groups of the polymer interact with the gallery surfaces, presumably through hydrogen bond formation, facilitating the intercalation of long-chain silicone rubber molecules (e.g., PDMS-4200). Fig. 2.14 exhibits the XRD patterns of intercalated silicone rubber-fluorohectorite nanocomposite at different molecular weights [50].

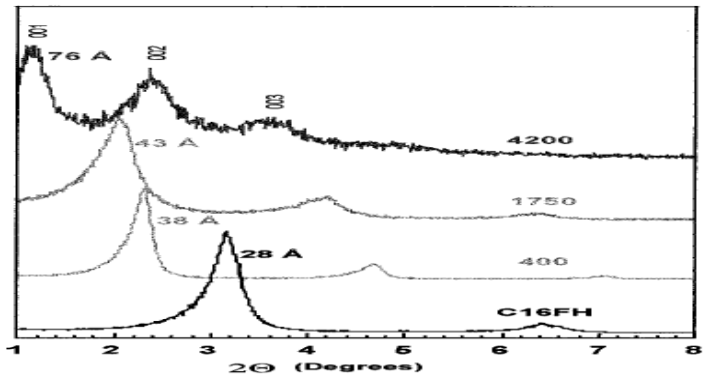

Fig. 2.14: X-ray diffraction of synthetic hexadecyltimethylammonium fluorochectorite, ($C_{16}FH$), initercalated by PDMS polymers with molecular weights of 400, 1750 and 4200. The pattern for initial organoclay in included for comparison [50].

Schmidt and co-workers [51] reported the effects of cationic modifier types on the compatibility with low-molecular-weight silanol-terminated silicone rubber. A variety of modifiers with different structures - length of tail surfactant and head groups in organically modified layered silicates were used in the study. In contrast to rubber/clay nanocomposites based on hydrocarbon chains, the silicone rubber backbone based on polydimethylsiloxane was generally incompatible with modified layered silicates. According to the report silicone required some level of functional grouping, either at the chain-ends or elsewhere in the polymer, to enhance compatibility with the filler and produce high levels of layered-silicate dispersion. A new epoxy/amine silicone rubber curing chemistry was employed to catalyse crosslinking in silicone rubber/clay nanocomposites, simultaneously improving clay dispersion. It was assumed that silicate modifiers containing OH or NH_2 groups reacted with the epoxy end-groups directly. However, the effects of the new curing system on the material's properties were not clear [51].

Silicone rubber/clay nanocomposite preparation using masterbatch techniques without any solvent assistance was first reported by Kaneko and co-workers [52]. The masterbatches were based on high molar mass (106 g mol^{-1}) silicone rubber gum and natural (MT), or organomodified (O-MT), montmorillonite clay with the addition of siloxane–polyether surfactant as a processing aid. The nanocomposites were also prepared using direct addition during compounding as a comparison. The XRD and TEM results suggested that the intercalated morphology in SR/OMT/mb, filled with 5 phr filler loading, was due to the lubricating effect of the polyether surfactant during preparation of the masterbatch. The TEM image in Fig. 2.15 shows some evidence of thin layers in a silicone matrix. However, in the case of nanocomposites prepared with direct addition no indication of delamination or intercalation was observed. The masterbatch technique has been recommended for high molar mass silicone rubber nanocomposite.

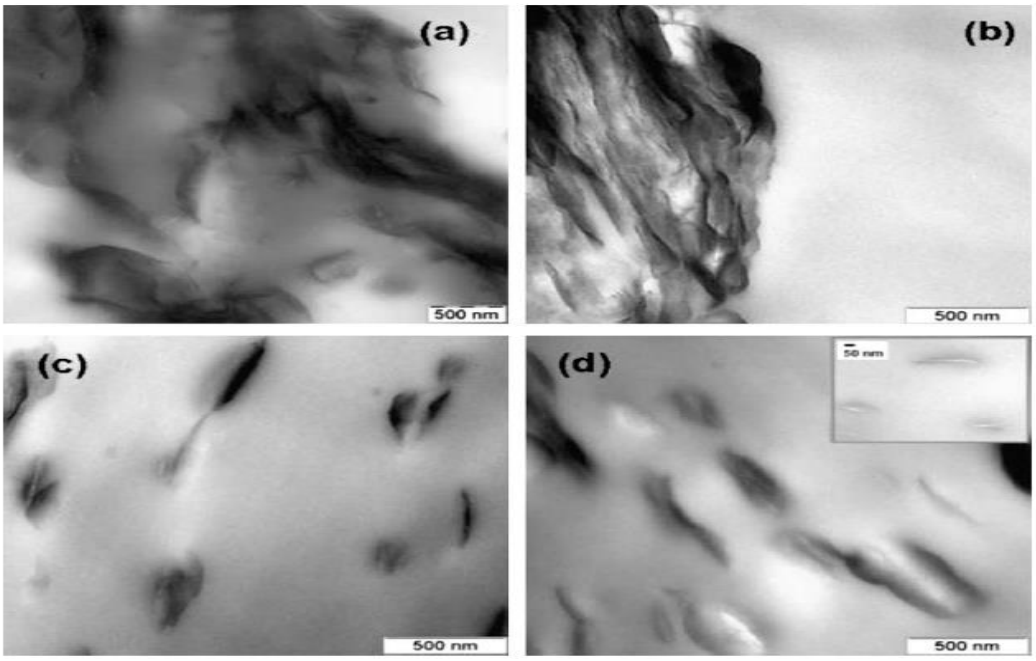

Fig. 2.15: TEM micrographs of (a),(b) PDMS/O-MT 5 phr composite; (c),(d) PDMS/O-MT/mb composite [52]

Simon and co-workers [53] produced grafted siloxane modified montmorillonite, enhancing its compatibility with siloxane chains in liquid silicone rubber (LSR). The siloxane modified montmorillonite was easily exfoliated in the LSR, contributing to a 20% reduction in water vapour permeation. However, no improvement in tensile strength was reported for this grade of silicone rubber [53]. Bhowmick and Roy [54] proposed an in situ polymerisation technique to produce a high dispersion of PDMS-sepiolite nanocomposite. Excellent clay dispersion and high interaction between clay and PDMS was observed in nanocomposites produced with this technique, compared to ex situ prepared nanocomposites. This produced significant enhancement in the mechanical and thermal properties of the rubber.

On the other hand, Kaneko and Yoshida [55] successfully prepared intercalated silicone rubber nanocomposite via melt-blending. The behaviour of unmodified montmorillonite (MT) and modified MMT (O-MT) in silicone rubber was compared in terms of dispersion, mechanical properties, thermal stability and solvent swelling. In contrast to most rubber/clay nanocomposite, intercalated nanocomposite was achieved with the addition of MMT, as proven by XRD results.

Fig. 2.16 shows the XRD patterns for the MT, MT/SR, O-MT and O-MT/SR composites. The increase in the basal space of MT was enhanced with clay content in SR up to 30 phr, as well as with crosslinking density. It was claimed that high clay loading facilitated intercalation of silicone molecules to the clay gallery. Interestingly, no such behaviour was seen in the SR filled with O-MT due to a lack of polarity in the filler, restricting SR intercalation into the clay gallery.

Subsequent studies emphasized the need to improve processability of the melt-mixed SR/clay nanocomposites [56]. According to the study, viscosity of silicone rubber improved with the addition of up to 40 phr filler loading of modified montmorillonite (OMMT). High viscosity facilitated the transfer of mechanical shear force to OMMT particles and resulted in better filler dispersion. Nevertheless, with increasing the clay loading the chances of the filler particles re-agglomerating were high, leading to poor mechanical properties [56].

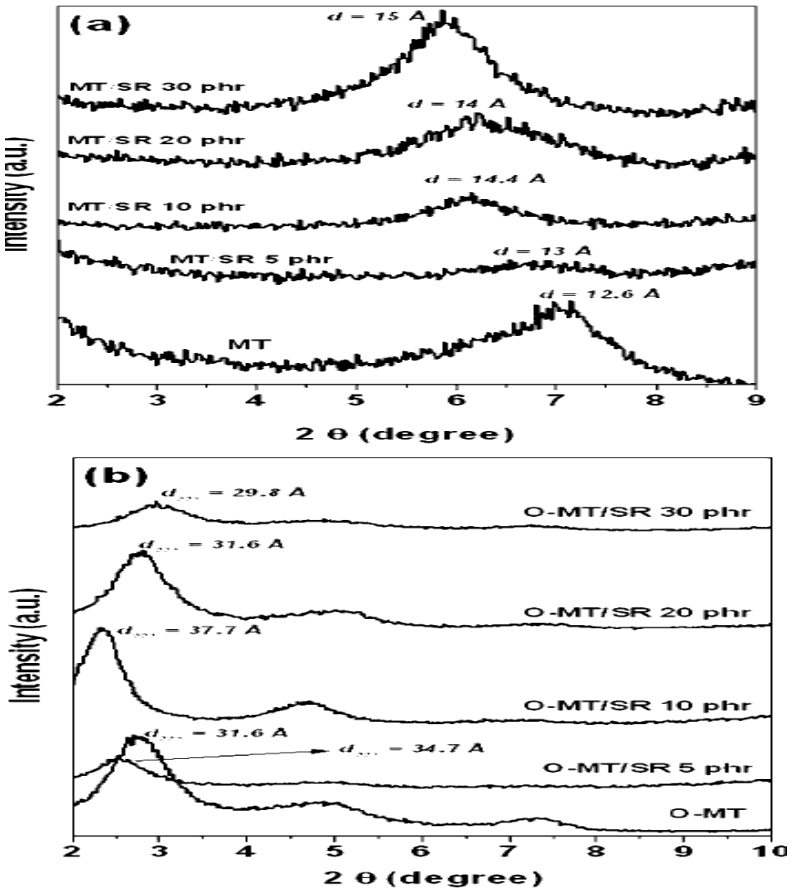

Fig. 2.16 (a-b): XRD patterns for the (a) MT and MT/SR and (b) O-MT and O-MT/SR composites [55].

2.3.2 Mechanical properties of silicone rubber/clay nanocomposites

Most silicone rubber/clay nanocomposites studies report tensile properties such as modulus, tensile strength, elongation-at-break as a function of clay content. Generally, a significant improvement in tensile strength and modulus of silicone rubber filled with nanoclay is achieved at low filler loadings below 5 phr [57, 58]. For example, the addition of 1 phr organomodified clay (OMMT) to liquid silicone rubber (LSR) resulted in a substantial enhancement in elongation-at-break and tensile strength, which was about 1.6 times higher than that of pure SR. The tensile strength and elongation-at-break of SR/OMMT-1 phr was almost identical to that of SR filled with 3 phr aerosilica. This improvement was attributed to good dispersion of exfoliated OMMT particles in the SR/OMMT nanocomposite (shown by wide-angle X-ray diffraction and transmission electron microscopy) [57]. However, above 1 phr of OMMT filler loading the properties became worse due to filler agglomeration.

Voulomenou and Tarantili [58] revealed that the incorporation of 2.5 or 3.5 phr of Cloisite 20A into hydroxyl-terminated silicone rubber moderately altered its mechanical properties. The tensile strength and modulus of elasticity of silicon rubber increased about 48% and 28% respectively, accompanied by an increase in the elongation-at-break strength, as shown in the Table 2.5. The improvement of mechanical strength and stiffness was attributed to the presence of exfoliated and intercalated particles in the OMMT of the silicone matrix and additional crosslinks [58].

Table 2.4: Tensile test results of the SR/Cloisite 20A composites [58]

MMT content in PDMS (phr)	Tensile strength (MPa)	Modulus of elasticity (MPa)	Strain at break (%)
0	0.338 ± 0.047	0.811 ± 0.057	85.29 ± 7.174
2	0.395 ± 0.016	0.825 ± 0.240	114.40 ± 8.150
3.5	0.368 ± 0.039	0.896 ± 0.181	95.80 ± 9.474
5	0.396 ± 0.054	0.854 ± 0.056	140.20 ± 10.700

Exceptions to this general trend have been reported. Some studies investigated the effect of high loaded silicone rubber composites (e.g 20 and 30 phr) [55]. Intercalated and immiscible silicone rubber composites contained high natural montmorillonite (MT) and modified montmorillonite (OMMT) respectively. MT promoted better reinforcement than O-MT, as shown by a major improvement in tensile strength and modulus. This was believed to be due to the high number of covalent bonds at the MT–PDMS interface. However, the elongation-at-break was dramatically reduced, even at low filler loading (5 phr). Fig. 2.17 shows the stress-strain of silicone rubber/clay composites as a function of clay content.

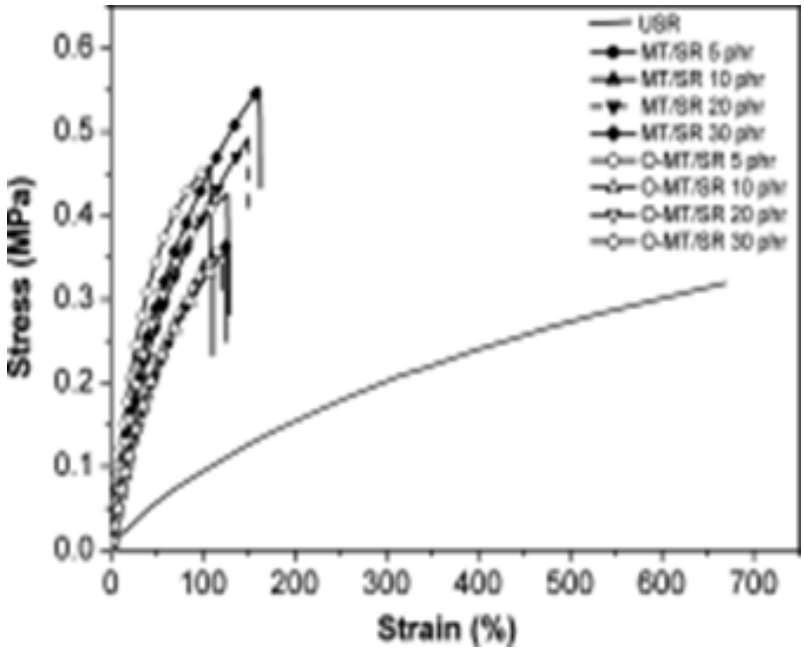

Fig. 2.17: Stress-strain curves for the unfilled silicone rubber and SR composites [55]

A similar finding was highlighted by Jia and co-workers [56]. The lack of interfacial adhesion between O-MT and SR contributed to low tensile strength, even when intercalated morphology was achieved in the nanocomposite. For example, the high loaded SR/O-MT nanocomposites filled with 40 phr O-MT exhibited 0.78 MPa of tensile strength which is only 0.51 MPa increase from the unfilled SR as shown by the stress-strain curve in Fig. 2.18.

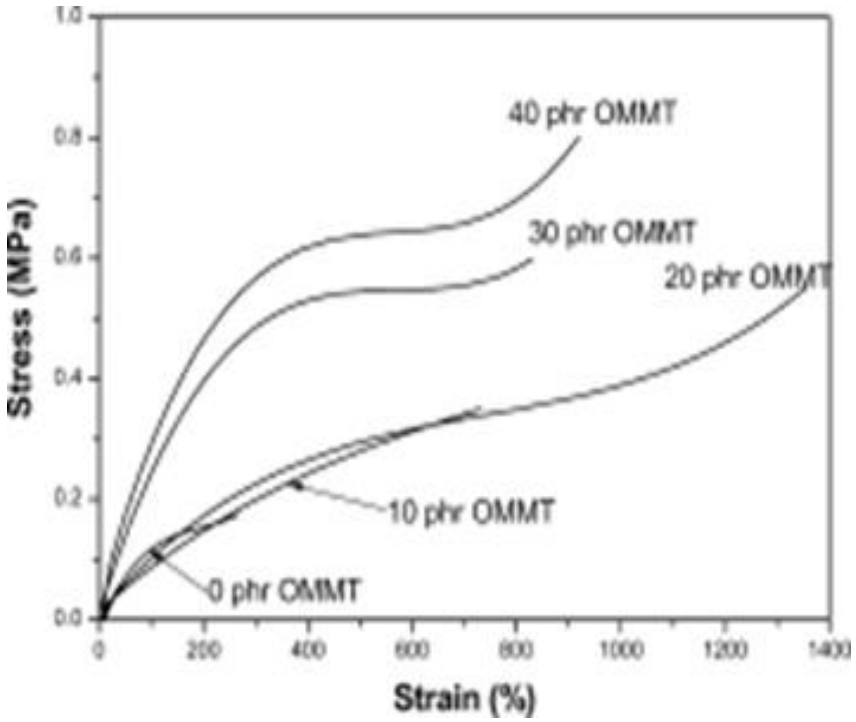

Fig. 2.18: The strain–stress curves of SiR/OMMT (I.44P) nanocomposites with different OMMT loadings. Zero phr represents the net cured SiR. [56]

Apart from the degree of exfoliation and clay content, there are other factors that influence the tensile properties of silicone rubber nanocomposites. Kaneko and co-workers [52] studied the effect of compounding procedures on the mechanical properties of silicone rubber nanocomposites. The tensile strength of SR/O-MT filled 5 phr filler loading prepared by masterbatch compounding and SR/O-MT filled with 30 phr filler loading prepared by direct addition was comparable. It was believed that filler dispersion contributed to greater reinforcement of SR/O-MT/mb even at lower filler concentrations. The inclusion of poly (ethylene oxide) (PEO) offered some benefits to the filler dispersion during masterbatch compounding preparation [52].

The first systematic study on the relationship between degree of silicate dispersion, equilibrium solvent uptake of a range of polysiloxane nanocomposites (based on treated and untreated montmorillonite), and fumed silica nanofiller silicate layers (and mechanical properties) was reported by Schmidt and Giannelis in 2010 [59]. In contrast to other rubber/clay nanocomposite systems, equilibrium solvent uptake and mechanical properties in silicone

rubber/clay nanocomposites was independent of dispersion state. The level of reinforcement in this system was dominated by interactions between siloxane bonds in the silicone rubber chains and silanols present at the edges of the montmorillonite layers. The report concluded that edge interactions play a more significant role than degree of exfoliation in silicone rubber/clay nanocomposites.

More recently, a novel approach was introduced to reinforce vinyl-terminated polydimethylsiloxane (PDMS) with functionalised nanoclays [60]. Two commercially available clays, sodium montmorillonite and Cloisite® 25A, were functionalized with bis(3-triethoxysilylpropyl)tetrasulfide (TESPT) to prepare Na^+MMTS_4 and $C25AS_4$, respectively. The Na^+MMTS_4 filler appeared as the most effective filler for the improvement of tensile properties and tear strength of silicone rubber. It was reported that modification by TESPT did not change the d spacing level in the clay gallery for both fillers, but it did reduce crosslink density of the filled rubber. It was concluded that the improvement in mechanical properties of silicone rubber/Na^+MMTS_4 nanocomposites was entirely due to strong interfacial interaction between filler and the rubber and was not caused by crosslink density.

2.3.3 Thermal properties of SR/clay nanocomposites

Following recent developments of SR/clay nanocomposites, there has been increasing concern about how clay affects thermal degradation and the stability of silicone rubber, particularly at high temperatures. Lewicki and co-workers [61] identified major changes in the physical and chemical structures of the polymer-filler network in some SR/Cloisite 6A nanocomposites after ageing the rubbers at 150ºC (for 504 h in moisture air and dry nitrogen). It was postulated that a major re-structuring of the polymer-filler network, involving aged chain scission, backbiting, and recombination, had taken place in the nanocomposites due to thermodynamic reformation, stabilizing the network. However, the mechanical properties of the aged nanocomposites were not measured in this study.

Kong and colleques [62] observed that the addition of modified montmorillonite (OMT) enhanced the thermal stability of SR/clay nanocomposites significantly. Thermogravimetric

analysis (TGA) showed that both onset degradation temperature $T_{0.1}$ (10% degradation occurs) and midpoint of degradation process, $T_{0.5}$ (50% degradation occurs) of the SR/Fe-MMT and SR/Na-MMT nanocomposites were higher compared to the neat SR (Table 2.5). In comparison, the SR/Fe-MMT nanocomposite had better thermal stability than SR/Na-MMT due to the action of iron (Fe^{3+}) as an antioxidant.

Table 2.5: TGA results of SR/clay nanocomposites and SR [62]

Contents	$T_{0.1}$ (ºC)	$T_{0.5}$ (ºC)	Residue at 700ºC (wt%)
Pure SR	415	488	0.3
1 % Fe-OMT	453	543	2.4
4 % Fe-OMT	462	556	6.0
7 % Fe-OMT	460	558	8.5
4 % Na-OMT	427	524	4.9

Thermal degradation characteristics obtained from the TGA tests on room temperature vulcanized (RTV) SR filled with natural (Na^+MMT), quaternary ammonium salts (QAS), modified MMT (OMMT), and hyperbranched QAS (HQAS) modified MMT (HOMMT), showed that rubber filled with 3 wt% HOMMT exhibited higher T_{onset} than its counterparts. This was due to uniform dispersion of filler particles and stronger rubber/filler interactions [63]. To some extent the rubber filled with Na^+MMT presented a higher center temperature of thermal degradation (T_{max}, the temperature at which weight loss is the fastest). In addition the yield residue of rubber with Na^+MMT (77.8%) was far higher than for ones filled with OMMT (51.5%) and HOMMT (53.2%) fillers. It was concluded that the higher ratio of inorganic silicate layers in the Na^+MMT filler improved the thermal stability of the rubber [63].

In another study, Lewicki and co-workers [64] observed the thermal degradation behavior of some SR/MMT nanocomposites. They noticed that the inclusion of Cloisite 6A (MMT modified with quarternary alkyl ammonium cations) significantly altered non-oxidative

degradation behaviour and modified the thermal degradation profile, resulting in a negative impact on the thermal stability of the rubber. It was subsequently concluded that at high temperatures, i.e. 400-500°C, the clay promoted radical cleavage reactions, as indicated by the formation of benzene and dimethylsiloxane (based on thermal vitalization analysis - TVA). The production of these by products was associated with the level of side radicals that contributed to the reduction of thermal stability. It was suggested that Cloisite 6A probably acted as a pro-degradant within the SR matrix due to the acid sites on the clay platelets, or via breakdown of the organic modifier. Interestingly at clay loadings above 2 wt% this phenomenon became less dominant. It was also observed that physical barrier properties improved when clay loading increased to 8 wt% [64].

2.3.4 Applications of silicone rubber/clay nanocomposites

The superior mechanical properties of silicone rubber/clay nanocomposites were achieved at low filler loading, resulting in favourable, lightweight produces. Due to the excellent thermal stability of the nanocomposite at high temperature with the T_{onset} ranges from 427 to 462°C [62], the potential applications of lightweight silicone rubber nanocomposites are seen in a broad range of products in the construction, automotive and aerospace industries, where they are used in lightweight insulators, cables in engine compartments and flame retardant flexible heaters.

2.4 Summary

In summary, solution and in-situ polymerisation techniques were mainly used to prepare silicone rubber/clay nanocomposites However, from the commercial manufacturing point of view, these techniques are less suitable for practical industrial applications since they involve complex processing and require the use of organic solvents.

Melt-blending is the most common way to produce rubber compounds in the rubber industry since it is simple and highly cost effective. Normally the mixing process will be done in two-roll mill or a mixer with high rotor speed, to produce high shear force followed by

compression moulding for shaping and curing. Unfortunately, it must be noted that only a few sources report the use of this technique to disperse clay particles in silicone rubber/clay nanocomposites [55--56]. In addition the exfoliation mechanism in melt-compounded silicone rubber is not yet clear.

In addition, most studies focus on tensile properties such as modulus, tensile strength, and elongation-at-break of silicone rubber/clay nanocomposites. The effect of nanoclays on the viscoelasticity and abrasion resistance of silicone rubber is rarely reported. On top of that there has been relatively little work done to measure the mechanical properties of SR/MMT nanocomposites after ageing at elevated temperatures, e.g. 200°C. Also, there has been little consensus on the effect of clay on the thermal stability of SR/clay nanocomposites. To the best of our knowledge none of the previous reports focussed on hybrid fillers reinforcement in silicone rubber nanocomposites when this project was created.

This work was carried out to investigate dispersion of different clays in silicone rubber using the melt-mixing technique. SR/clay nanocomposites were prepared and cured and then the interlayer spacing, *d*, of the clay particles in the rubber matrix was measured by X-ray diffraction spectroscopy. Effect of the filler loading on the processing and mechanical properties of the rubber vulcanisate was investigated. In addition, the formation of exfoliated and intercalated structures in the SR/clay nanocomposites was discussed and effect of the clays on the cure characteristics and mechanical properties of the rubbers was measured. For a better understanding of the reinforcing mechanism of the clays, fresh insight into the way intercalated and exfoliated morphologies change the mechanical properties, thermal stability of the rubber nanocomposites was also discussed. Finally, hybrid filler system based on MMT and precipitated silica was developed and the benefit of the hybrid reinforcement on the properties of SR was disclosed.

2.5 References

1. Paul DR, Robeson LM. Polymer nanotechnology: Nanocomposites. *Polymer* 2008; 49(15): 3187–3204

2. Ali O. Polymer/Clay Nano composites.In: Boreddy R (ed). *Advances in Diverse Industrial Applications of Nanocomposites. In Tech: 2011.*http://www.intechopen.com/books/advances in diverse industrial applications of Nano composites *(Accessed 21 Dec 2013).*

3. Pavlidou S, Papaspyrides CD. A review on polymer–layered silicate nanocomposites. *Progress Polymer Science* 2008; 33(12): 1119-1198.

4. Ray SS, Okamoto M. Polymer/layered silicate nanocomposites: a review from preparation to processing. *Progress Polymer Science* 2003; 28 (11): 1539–1641.

5. Donnet ED. Reinforcement of Elastomer by particulate fillers. In: James E, Mark BE, Frederick RE, (eds). *The Science and Technology of Rubber*. 3rd ed. United Kingdom: Elsevier Academic Press; 2005. 367-401.

6. Sengupta R, Chakraborty S, Bandyopadhyay S, Dasgupta S, Mukhopadhyay R, Auddy K, Deuri AS, A Short Review on Rubber / Clay Nanocomposites With Emphasis on Mechanical Properties. *Polymer Engineering Science* 2007; 47:1956-1974.

7. Jin KK, Kaishik P, Sridhar V. Role of different nanoparticles in elstomeric Nano composites. In: Mittal V, Kim JK, Pal K (eds). *Recent Advances in Elastomeric Nanocomposites: Advanced structured materials,* Verlag Berlin, Heidelberg: Springer; 2011.3-57.

8. Sarkar A, Silicone rubber. In: J. White, S.K. De and K.Naskar (eds). *Rubber Technologist's Handbook.* Vol 2. United Kingdom, Smithers Rapra Technology Limited; 2009.387 – 389.

9. Wu YP, Ma Y, Wang YQ, Zhang LQ. Effects of Characteristics of Rubber, Mixing and Vulcanization on the Structure and Properties of Rubber/Clay Nanocomposites by Melt Blending. *Macromolecule Material Engineering* 2004; 289(10): 890-894.

10. Gatos KG, Karger K, Rubber nanocomposites: preparation, properties and applications, In: Stephen R and Thomas S (eds), *Rubber nanocomposites: preparation, properties and applications*, John Wiley & Sons, Inc. New Jersey; 2010. 170-195.

11. Utracki LA, Clays, In: *Clay containing Polymeric nanocomposites*. Vol 1. United Kingdom, Rapra Technology; 2004; 80-84.

12. Wang S, Long C, Wang X, Li Q, and Qi Z. Synthesis and properties of silicone rubber/organomontmorillonite hybrid Nano composites. *Journal of Applied Polymer* Science 1998; 69(8):1557–1561.

13. Yang L, Hu Y, Lu H, Song L. Morphology, thermal, and mechanical properties of flame-retardant silicone rubber/montmorillonite nanocomposites. *Journal of Applied Polymer Science* 2006; 99(6):3275–3280.

14. Simon MW, Stafford KT, Duan LO, Nanoclay Reinforcement of Liquid Silicone Rubber. *Journal of inorganic and organometallic polymers* 2008; 18 (3), 364-373.

15. Labruyère C, Gorrasi G, Monteverde F, Alexandre M, Dubois P. Transport properties of organic vapours in silicone/clay nanocomposites. *Polymer* 2009; 50(15):3626–3637.

16. Avalos F, Ortiz JC, Zitzumbo R, López-Manchado MA, Verdejo R, Arroyo M. Effect of

montmorillonite intercalant structure on the cure parameters of natural rubber. *European Polymer Journal* 2008; 44(10): 3108-3115.

17. Tjong SC, Synthesis and structure –property Characteristics of clay-Polymer nanocompoistes In: Tjong SC (ed), *Nanocrystalline Materials: Their Synthesis –Structure –Property Relationships and Applications* (1st ed); United Kingdom; Elsevier 2006, 315-317.

18. Peter C. LeBaron, Zhen W, Thomas J. Pinnavaia, Polymer–layered silicate nanocomposites: an overview. *Applied Clay Science* 1999; 15(1-2): 11-29.

19. Bafna A, Beaucage G, Mirabella F, Mehta S, 3D Hierarchical orientation in polymer-clay nanocomposite films. *Polymer*, 2003; 44: 1103–1115.

20. Sadhu S, Bhowmick AK, Morphology study of rubber based nanocomposites by transmission electron microscopy and atomic force microscopy. *Journal Material Science* 2005; 40(7): 1633–1642.

21. Ali Z, Le HH, Ilisch S, Busse K, Radusch H. Nanoclay Exfoliation in Rubber Compounds Characterized by Online Measurements of Electrical Conductance. *Journal of Applied Polymer Science* 2009; 113: 667-677.

22. Beall G. Powell C, Analytical method utilized in nanocomposites. In: *Fundamentals of Polymer-Clay Nano composites*, United Kingdom: Cambridge University Press; 2011; 23-33

23. Giannelis EP, Krishnamoorti R, Manias E. Polymer-Silicate Nanocomposites: Model Systems for Confined Polymers and Polymer Brushes. *Advanced Polymer Science*, 1999, 138: 108-147.

24. Soares BG., Marlucy DO, Soraia Z. Nitrile rubber-based nanocomposites prepared by melt mixing: effect of the mixing parameters on mechanical, dynamic-mechanical and creep behavior. *Polímeros: Ciência e Tecnologia* 2010; 20(5): 371-376.

25. Liang YR, Ma J, Lu YL, Wu YP, Zhang LQ, Mai YW. Effects of heat and pressure on intercalation structures of isobutylene-isoprene rubber/clay nanocomposites. I. Prepared by melt blending. *Journal Polymer Science B Polymer Physic* 2005; 43: 2653–2664.

26. Lopez-Manchado M, Herrero B, Arroyo M. Preparation and characterization of organoclay nanocomposites based on natural rubber. *Polymer International* 2003; 52(7):1070–1077.

27. Varghese S, Karger-Kocsis J, Gatos KG. Melt compounded epoxidized natural rubber/layered silicate nanocomposites: structure-properties relationships. *Polymer* 2003; 44(14): 3977-3983

28. Wu YP, Wang YQ, Zhang HF, Wang YZ, Yu DS, Zhang LQ, Yang J. Rubber–pristine clay nanocomposites prepared by co-coagulating rubber latex and clay aqueous suspension. *Composite Science Technology* 2005; 65(7-8): 1195–202.

29. He SJ, Wang YQ, Wu YP, Wu XH, Lu YL, Zhang LQ. Preparation, structure, performance, industrialisation and application of advanced rubber/clay nanocomposites based on latex compounding method. *Plastics, Rubber and Composite* 2010; 39(1): 33-42.

30. Pramanik M, Srivastava, SK., Samantaray BK. Bhowmick AK. Rubber–clay nanocomposite by solution blending. *Journal of Applied Polymer Science* 2003; 87: 2216–2220.

31. Budden G. High Temperature Properties of Silicone Elastomers. *Journal Industrial Text*. 1998; 27(4):294–308.

32. Malczewski RM, Donald AJ, Schoenherr WJ, Peroxide or Platinum?Cure System Considerations for Silicone Tubing Applications, http://www.dowcorning.com/content/publishedlit/52-1077-01.pdf (accessed 1 Dec 2013)

33. Heiner J, Stenberg B, Persson M. Crosslinking of siloxane elastomers. *Polymer Testing* 2003; 22(3): 253–257.

34. Bork PG. Roush, CW. *Vulcanization of Elastomers*. Alliger, G. Sjothun, IJ (eds). New York: Reinhold publishing Corporation; 1964.

35. Warrick EL, Pierce OR, Polmanteer KE, Saam JC, Silicone Elastomer Developments. *Rubber Chemistry and Technology* 1979; 52(3): 437-525.

36. Skander M, Fundamental aspects of crosslinking control of PDMS rubber at high temperature using tempo nitroxide, PhD thesis, University Claude Bernard Lyon, France; 2011.

37. Thomas DK. The crosslinking of methylvinyl silicones with organic peroxides. *Polymer.* 1966; 7(5): 243–50.

38. Bokobza L, The Reinforcement of Elastomeric Networks by Fillers, *Macromolecule Material Engineering* 2004; 289 (7): 607–621.

39. Kraus G. *Reinforcement of elastomer*; Interscience Publishing: New York, 1965

40. Bokobza L. Elastomeric composites. I. Silicone composites. *Journal of Applied Polymer Science* 2004; 93(5): 2095–2104.

41. Paul DR, Mark JE. Fillers for polysiloxane ('silicone') elastomers. *Progress Polymer Science* 2010; 35(7): 893–901.

42. Orawan T, Rainer F, Mario S, Evonik D. The last 100 years of fumed silica in rubber reinforcement, The Free Library, http://www.thefreelibrary.com/The last 100 years of fumed silica in rubber reinforcement. (Accessed 1 Apr 2014).

43. Aranguren, MI, Mora E, and Macosko CW, Compounding fumed silicas:Bound rubber and final aggregate size. *Journal Colloid Interface Science* 1997; 195(2): 329–337.

44. Wang MJ, Morris MD, Kutsovsky Y. Effect of fumed silica surface area on silicone rubber reinforcement. *Kautsch. Gummi Kunstst*. 2008; 61:107-117.

45. Camenzind A, Schweizer T, Sztucki M, Pratsinis SE. Structure & strength of silica-PDMS nanocomposites. *Polymer* 2010; 51(8): 1796-1804.

46. Sun CC, Mark JE. Comparisons among the reinforcing effects provided by various silica-based fillers in a siloxane elastomer. *Polymer* 1989; 30:104-106.

47. Barthel H, Surface interactions of dimethylsiloxy group-modified fumed silica. *Colloids Surfaces A Physicochem. Engineering* 1995; 101(2–3): 217–226.

48. Jia L,Du Z, Zhang C, Li C, Li H. Reinforcement of polydimethylsiloxane through formation of inorganic–organic hybrid networks. *Polymer Engineering Science* 2008; 48: 74–79.

49. Burnside SD, Giannelis EP. Synthesis and Properties of New Poly(Dimethylsiloxane) nanocomposites. *Chemistry Material* 1995; 7: 1597-1600.

50. Lebaron PC, Pinnavaia TJ. Clay Nanolayer Reinforcement of a Silicone Elastomer. *Chemistry Material* 2011; 13: 3760–3765.

51. Schmidt DF, Clément F, Giannelis EP. On the Origins of Silicate Dispersion in Polysiloxane/Layered-Silicate Nanocomposites. *Advanced Functional Materials* 2006; 16: 417–425.

52. Kaneko MLQA, Romero RB, Goncalves MC, Yoshida IVP, High molar mass silicone rubber reinforced with montmorillonite clay masterbatches: Morphology and mechanical properties. *European Polymer Journal* 2010; 46 (5): 881-890.

53. Simon MW, Stafford KT. and Duan LO, Nanoclay Reinforcement of Liquid Silicone Rubber. *Journal Inorganic Organometalic Polymer materials* 2008; 18: 364-373.

54. Roy N, Bhowmick AK. Novel in situ polydimethylsiloxane-sepiolite Nano composites. Structure-property relationship. *Polymer* 2010: 51; 5172-5185.

55. Kaneko MLQA, Yoshida IVP. Effect of Natural and Organically Modified Montmorillonite Clays on the Properties of Polydimethylsiloxane Rubber. *Journal of Applied Polymer Science* 2008: 108; 2587-2596.

56. Jia C, Zhang LQ, Zhang H, Lu YL. Preparation, microstructure, and property of silicon rubber/organically modified montmorillonite nanocomposites and silicon rubber/OMMT/fumed silica ternary nanocomposites. *Polymer Composite* 2011; 32: 1245–1253.

57. Wang J, Chen Y, Jin Q. Organic Montmorillonite as a Substitute for Aerosilica in Addition-Type Liquid Silicone Rubber Systems. *Macromolecule Chemistry Physics* 2005; 206 (24): 2512–2520.

58. Voulomenou A. Tarantili PA. Preparation, characterization, and property testing of Condensation-type silicone/montmorillonite nanocomposites. *Journal of Applied Polymer Science* 2010; 118: 2521–2529.

59. Schmidt DF, Giannelis EP. Silicate Dispersion and Mechanical Reinforcement in Polysiloxane/Layered Silicate Nano composites. *Chemistry Material* 2010; 22(1): 167–174.

60. Kim ES, Shim JH, Jung SH, Joo JH, Yoon JS, Lee SH, Influence of clay modification on the reinforcement of vinyl-terminated polydimethylsiloxane networks. *Polymer International* 2010; 59(4): 479–485.

61. Lewicki JP, Liggat JJ, Pethrick RA, Patel M, Rhoney I. Investigating the ageing behavior of polysiloxane nanocomposites by degradative thermal analysis. *Polymer Degradation Stability*. 2008; 93 (1): 158 – 168.

62. Kong Q, Hu Y, Song L, Wang Y, Chen Z, Fan W. Influence of Fe-MMT on crosslinking and thermal degradation in silicone rubber/clay nanocomposites. *Polymer Advanced Technology* 2006; 17: 463–467.

63. Jincheng W, Wenli, H. Effect of organic modification on structure and properties of room-temperature vulcanized silicone rubber/montmorillonite nanocomposites. *Journal of Applied Polymer Science* 2013; 129: 1852–1860.

64. Lewicki JP, Liggat JJ, Patel M. The thermal degradation behaviour of polydimethylsiloxane/montmorillonite nanocomposites. *Polymer Degradation Stability* 2009: 94(9); 1548-1557.

CHAPTER 3: Experimental

3.1 Raw materials

3.1.1 Silicone rubber

The raw elastomer used was polydimethylsiloxane (PDMS) with 0.12 wt% vinyl content. It was a random copolymer in which some of the methyl groups were substituted with vinyl ones to produce vinyl dimethyl silicone rubber. The polymer was provided by Dow Corning Limited, UK under the trade name of Silastic (R) SGM-26 with a molecular weight of 300,000. Figure 3.1 shows (a) the molecular structure of the vinyl-PDMS and (b) the image of silicone rubber.

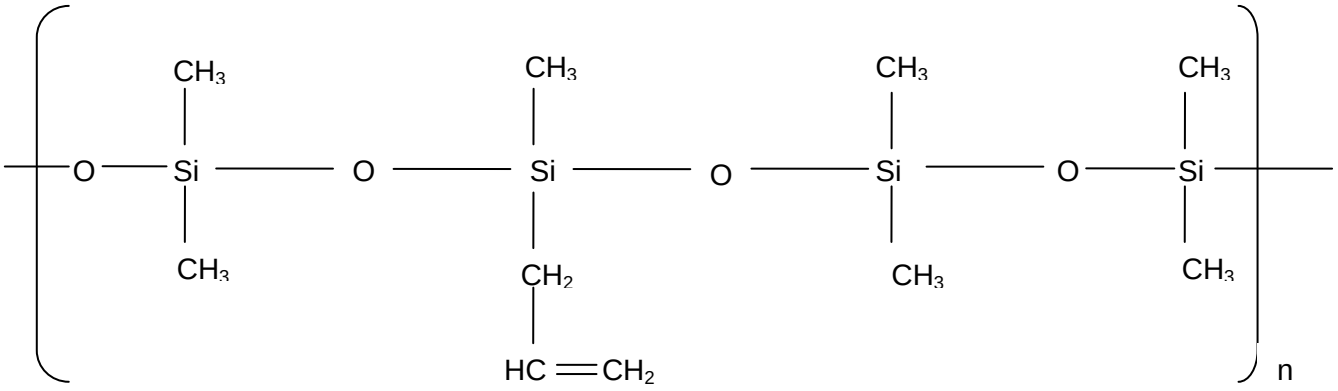

Fig.3.1a: Molecular structure of vinyl-polydimethylsiloxane [1]

Fig.3.1 (b): Photo of silicone rubber (Silastic (R) SGM-26).

3.1.2 Peroxide (curing agent)

A high purity (99%) dicumyl peroxide (DCP) or bis(α,α-dimethylbenzyl) was used as a vulcanizing agent (Fisher Scientific, UK). The chemical name of the peroxide was Bis(α,α-dimethylbenzyl) with the formula molecule of $C_{18}H_{22}O_2$. Figure 3.2 shows the molecular structure of the DCP.

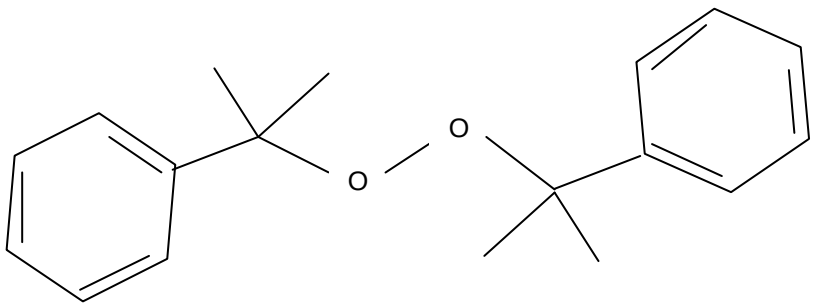

Fig. 3.2: Molecule structure of bis (α, α-dimethylbenzyl) peroxide [2]

3.1.3 Natural montmorillonite (Cloisite Na^+)

Natural montmorillonite, referred to as Cloisite Na^+ in this experiment, was supplied by Southern Clay Product, USA. The technical specification of this clay is given in Table 3.1.

Table 3.1: Typical physical properties of natural montmorillonite [3]

Properties	Details
Organic modifier	None
Modifier concentration	None
% moisture	4-9%
Dry particle size	90% less than 13 μm
Density	2.86 g/cc
X-ray data (d_{001})	11.7 Å

3.1.4 Organoclays (Cloisite 30B and Cloisite 20A)

Two types of commercial Cloisite 30B and Cloisite 20A organoclays were used. These were modified with different functional treatments namely methyl, tallow, bis-2-hydroxyetyl, quaternary ammonium (MT2EtOH), and dimethyl, dehydrogenated tallow, quaternary ammonium (2M2HT), respectively. Both modified clays were supplied by Southern Clay Product, USA. Physical properties of Cloisite 30B and Closite 20A organoclays are presented in Table 3.2.

Table 3.2: Typical physical properties of organoclays [3]

Physical properties	**Organoclays**	
	Cloisite 30B	**Cloisite 20A**
Modifier concentration	90 meq/100g/clay	95 meq/100g/clay
% moisture	< 2%	< 2%
Dry particle size	90% less than 13 μm	90% less than 13 μm
Density	1.98 g/cc	1.77 g/cc
X-ray data (d_{001})	18.5 Å	24.2 Å
Chemical structure of cationic surfactant	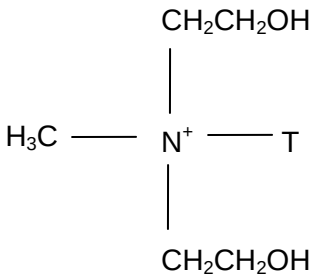	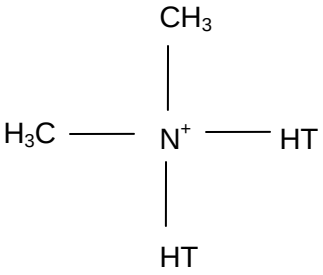
	MT2EtOH (T is Tallow ~ 65% C18; ~ 30% C16; ~ 5% C14)	2M2HT (HT is Hydrogenated Tallow ~ 65% C18; ~ 30% C16; ~ 5% C14)

3.1.5 Precipitated silica

Precipitated silica under trade name Ultrasil VN3 provided by Evonik Industries AG of Germany. Ultrasil VN3 has a 175 m^2/g surface area (measured by N_2 adsorption) and a 20-54 nm particle size [4].

3.1.6 Multi Wall Carbon Nanotube (MWNT)

Commercialised multi wall carbon nanotube (MWNT), with the following dimensions, where the length is about 50 μm and diameter approximately 8-15 nm was used. The

MWNTs was purchased from Chengdu Institute of Organic Chemistry, Chinese Academy of Sciences.

3.2 Development of silicone rubber/clay nanocomposites

Melt-mixing techniques were employed to prepare the silicone rubber/clay nanocomposites. The experimental producers involved in this thesis are summarised in Figure. 3.3.

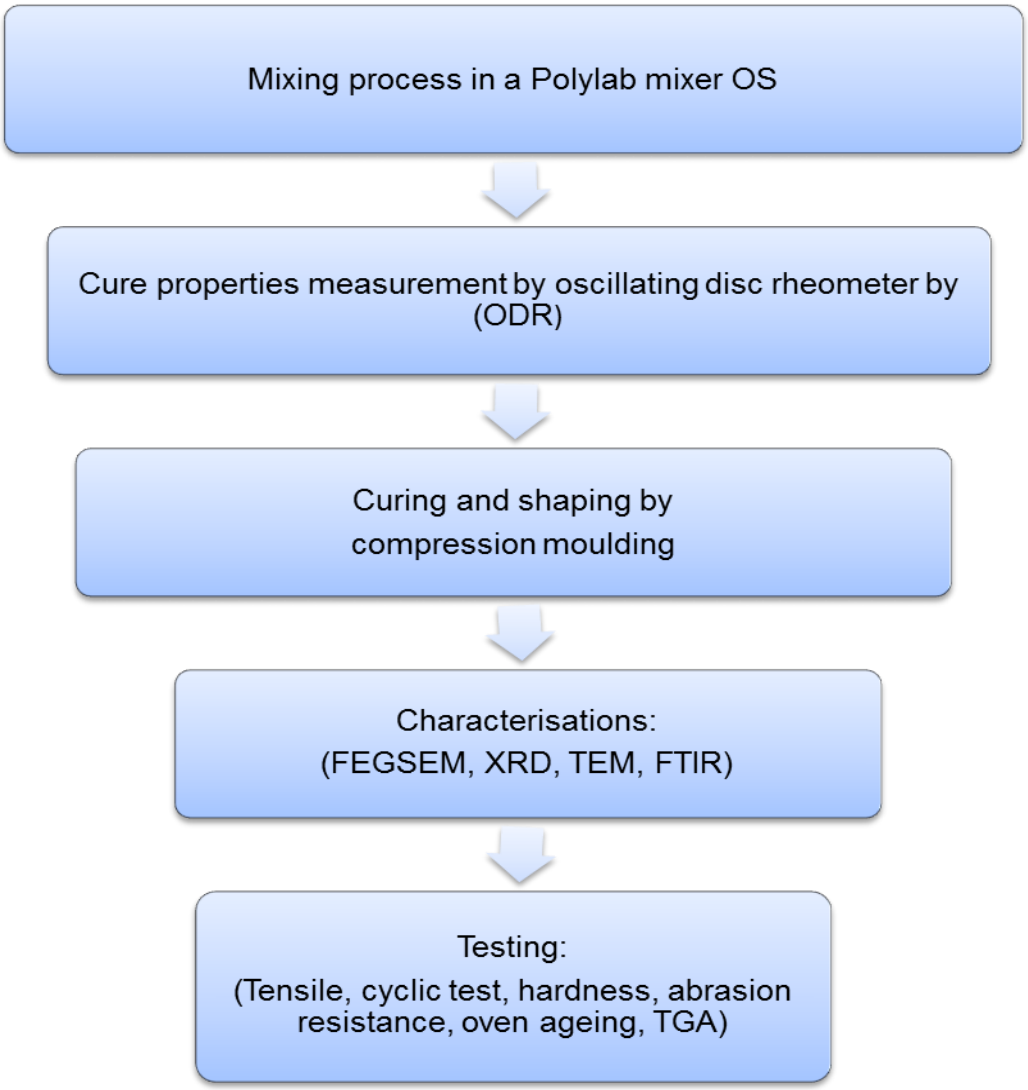

Fig. 3.3: Flow chart of experimental procedures

3.2.1 Mixing and processing of silicone rubber nanocomposites

The silicone rubber and all the compounding ingredients were mixed in a Polylab mixer OS (ThermoHAAKE, Germany) using counter-rotating Banbury rotors, as shown in Figs. 3.4(a-b). The unit was controlled by PolyLab OS software (Fig. 3.4 (c)), comprises elements, such as a torque rheometer, required to drive the measuring system (e.g. precise speed controller, temperature) and to monitor the torque (e.g. accurate torque sensor) during mixing.

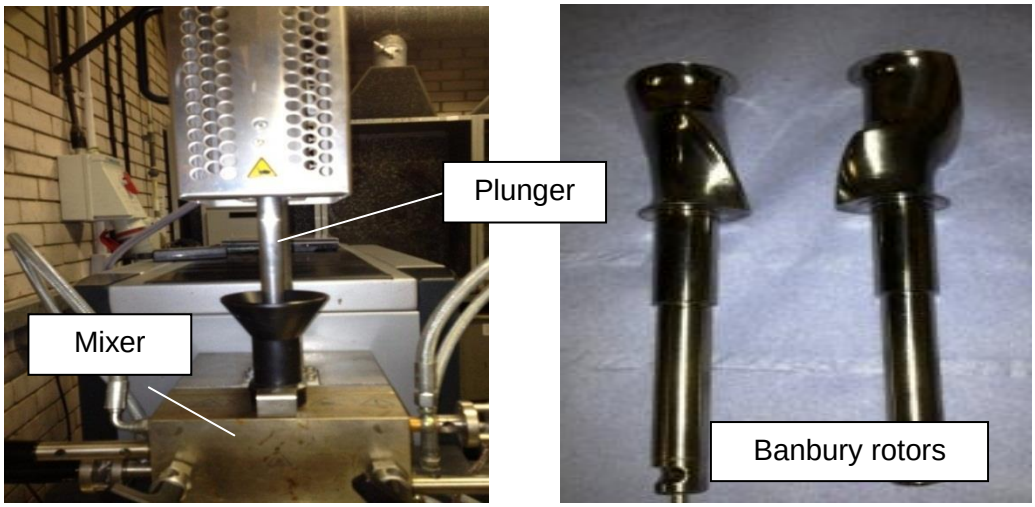

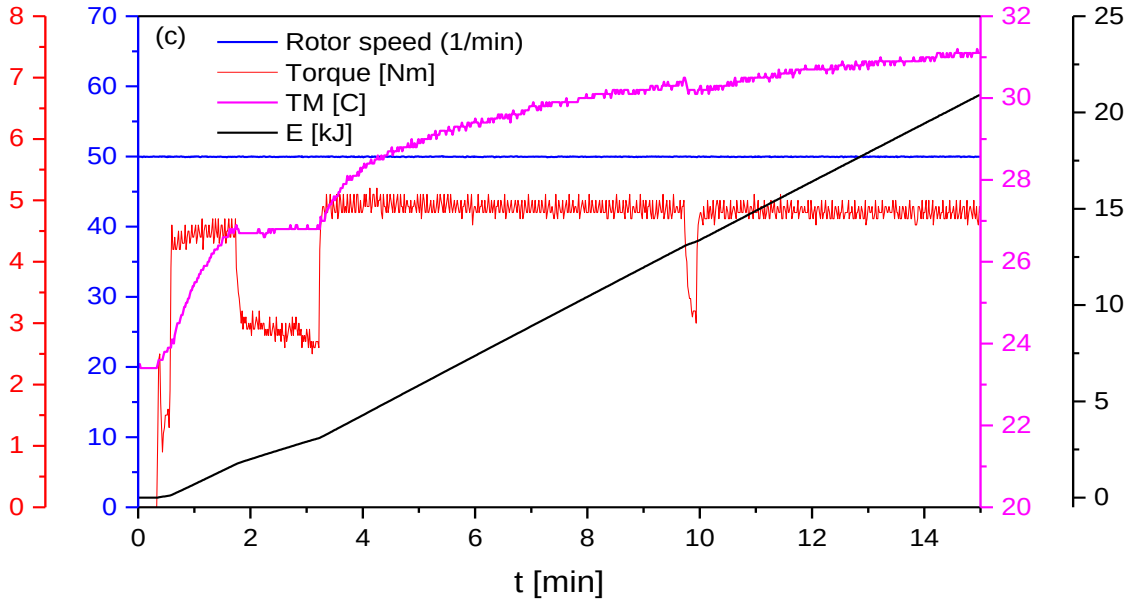

Figs. 3.4(a-c): Photos of (a) Polylab mixer OS (b) counter-rotating Banbury rotors and (c) Polylab OS software.

3.2.2 Preparation of silicone rubber/clay nanocomposites

Three rubber compounds were made. One was based on the natural clay and the other two based on the organoclays. An unfilled silicone rubber compound was also prepared as a control by mixing the raw rubber with peroxide**.** Table 3.3 presents the formulation for silicone rubber/clay nanocomposites. The temperature of the mixing chamber and the rotor speed were set at 20 °C and 50 r.p.m., The SR/MMT nanocomposites were prepared by mixing the raw rubber with the MMT fillers for 10 min after which peroxide was added and mixed for another 5 min with a mixing time of 15 minutes.

Table 3.3: Formulations of silicone rubber/clay nanocomposites

Formulation	**phr (part per hundred rubber by weight)**		
	1st series	**2nd series**	**3rd series**
Silicone rubber (SR)	100	100	100
Peroxide	0.3	0.3	0.3
Cloisite Na^+	4,6,8,10,12	0	0
Cloisite 30B	0	4,6,8,10,12	0
Cloisite 20A	0	0	4,6,8,10,12

3.2.3 Preparation of silicone rubber (SR) filled with PS/MMT hybrid fillers

Six SR nanocomposites were made with precipitated silica (PS) and MMT fillers. An unfilled rubber was also prepared as a control compound by mixing the raw rubber with 0.3 phr DCP. A previous investigation showed that 0.3 phr DCP was sufficient to fully cure the

SR [5] and this amount was subsequently used to make the rubber compounds for this study.

Before mixing, the clay was dried in a vacuum oven at 60^{o} C for 48 h to remove moisture. The SR and all the compounding ingredients were then mixed in a Polylab Haake Rheocord internal mixer (ThermoHAAKE, Germany), using counter-rotating Banbury rotors. The temperature of the mixing chamber and the rotor speed were set at 20°C and 50 r.p.m, and the total mixing time was 15 min. Table 3.4 presents formulation of SR/PS/MMT nanocomposites.

Table 3.4: Formulations of SR/PS/MMT nanocomposites

Compounds	**phr (part per hundred rubber by weight)**			
(filler weight ratio: PS:MMT)	**SR**	**Peroxide**	**MMT**	**PS**
Control SR	100	0.3	-	-
SR/MMT$_{(0.0)}$	100	0.3	6	-
SR/PS$_{(0.0)}$	100	0.3	-	6 and 10
SR/PS/MMT$_{(0.4)}$	100	0.3	6	2.5
SR/PS/MMT$_{(1.0)}$	100	0.3	6	6
SR/PS/MMT$_{(1.3)}$	100	0.3	6	7.5
SR/PS/MMT$_{(1.7)}$	100	0.3	6	10

SR:silicone rubber, MMT: montmorillonite, PS:precipitated silica

To make the control rubber, peroxide was added to the raw rubber and mixed for 15 min. The SR/PS and SR/MMT nanocomposites were prepared by mixing the raw rubber with the PS and MMT fillers for 10 min after which peroxide was added and mixed for another 5

min. The SR/PS/MMT nanocomposites were made by mixing the raw rubber with MMT for 5 min and then PS was incorporated in the rubber and mixed for an additional 5 min. Finally, peroxide was added and mixed for another 5 min.

3.2.4 Preparation of silicone rubber (SR) filled with PS/MWNT hybrid fillers

A similar mixing procedure in section 3.2.3 was used to prepare SR/PS/MWNT nanocomposites. The recipes for SR rubber filled with PS/MWNT hybrid fillers are presented in the Table 3.5.

Table 3.5: Formulations of SR/PS/MWNT nanocomposites

Compounds (filler weight ratio: PS:MWNT)	**phr (part per hundred rubber by weight)**			
	SR	**Peroxide**	**PS**	**MWNT**
Control SR	100	0.3	0	0
$SR/PS_{(0.0)}$	100	0.3	6	0
$SR/MWNT_{(0.0)}$	100	0.3	0	6
$SR/PS/MWNT_{(0.4)}$	100	0.3	2.5	6
$SR/PS/MWNT_{(1.0)}$	100	0.3	6.0	6
$SR/PS/MWNT_{(1.7)}$	100	0.3	10	6

* SR:silicone rubber, MWNT: multi wall carbon nanotube, PS:precipitated silica;

3.3 Cure properties measurement

An oscillating disc rheometer (ODR) (Monsanto, Swindon, UK) was used to measure the cure properties of the rubber compounds at 160 °C and an angular displacement of ± 3°

and test frequency of 1.7 Hz. About 6 grams of uncured sample was required for this testing. The test sample was placed on top of the heated rotor and the heated top die was immediately brought down towards the lower die to fill the cavity. At the end of the testing, the torque curve versus time was obtained. The value of scorch time (Ts_2), min torque (M_L) and max torque (M_H), cure time (T_{95}) were also shown on the computer. Figure 3.5 shows a typical rheometer graph and information obtained from the test.

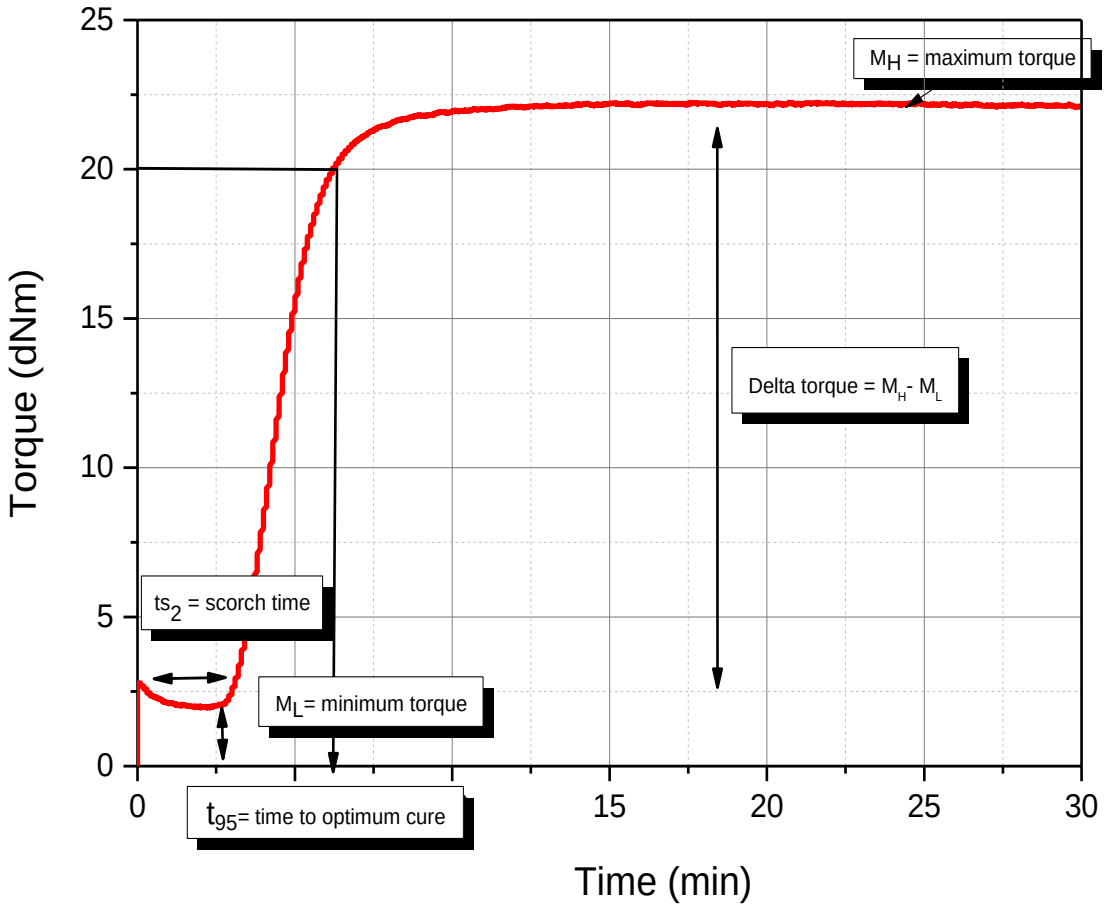

Fig. 3.5: A typical rheometer curves from ODR measurement

3.4 Compression moulding and curing

The rubber compounds were cured in a compression mould at 160 °C in a 40 ton hydraulic press (Bradley & Turton Ltd). To avoid anisotropy in the rubber sheets, the rubber

compound was placed in the centre of the mould to allow it to flow in all directions before curing. Pressure was fixed at 20 MPa and two types of moulds were employed for test sampling, particularly tensile testing and hardness. To prepare a cured tensile sheet, the uncured compound was moulded using a flat mould (150 mm x 150 mm x 2 mm). A thicker plate with a 6 cavity mould was used to cure small cylinder-shaped rubber (160 mm diameter x 90 mm thickness) for hardness measurement. The curing period of every sample was based on their individual cure time (t_{95}) measured from the ODR test. Figs. 3.6 (a-c) display a photo of hydraulic press and moulds for tensile slab and test pieces for hardness testing.

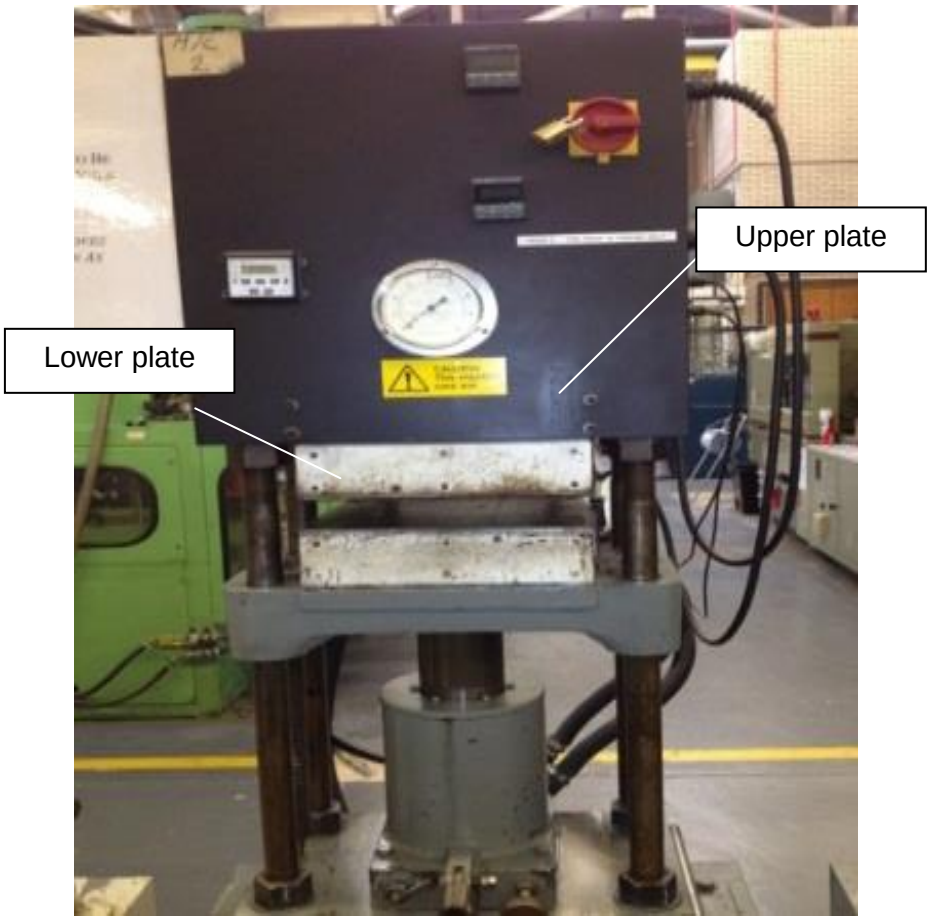

(a)

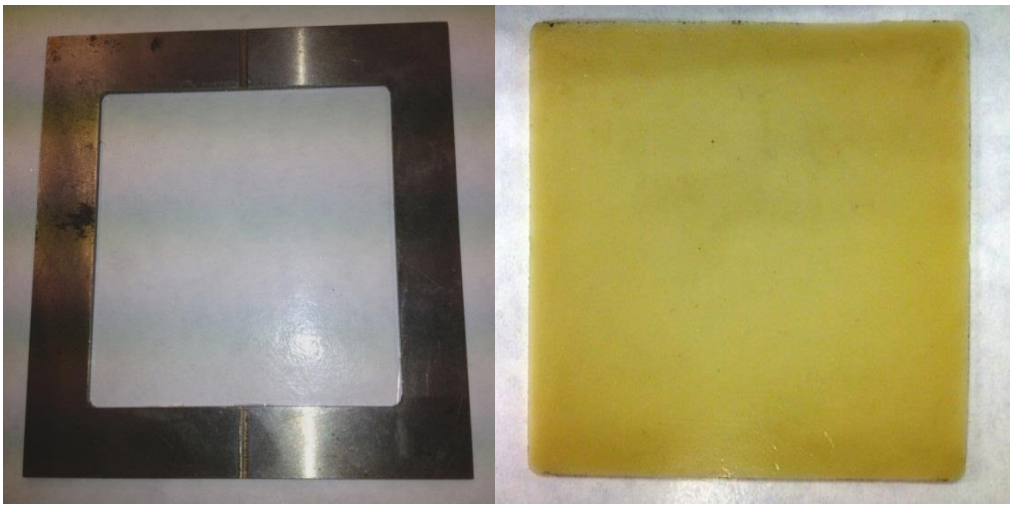

(b)

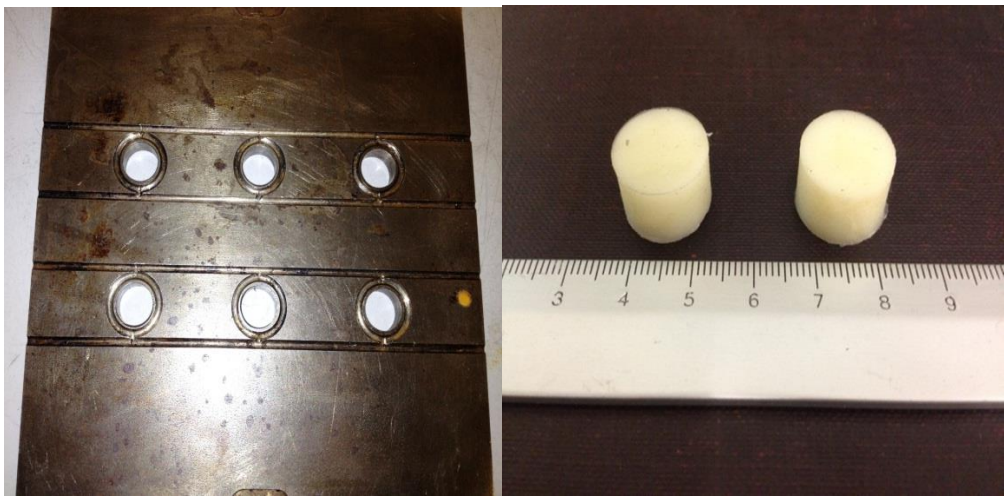

(c)

Figs. 3.6(a-c): Photos of (a) hydraulic press and (b) mould tensile slab and (c) mould test pieces for hardness.

3.5 Characterisation and measurement of the dispersion of the fillers in the rubber

3.5.1 Wide angle X-ray diffraction (XRD)

The X-ray diffraction (XRD) spectra of the layered silicates and clay-filled nanocomposites were produced on a Bruker D8 diffractometer (Bruker, Germany). The diffractometer was equipped with Cu Kα radiation (λ=0.15418 nm), 40 mA of current and 40kV of voltage. A minimum of 3g of dried clay powder was used to carry out the X-ray analysis of the mineral clays. A square flat sheet 30mm by 30mm in dimensions and 2mm thick of the cured compound was required for the X-ray analysis of the silicone rubber nanocomposites. The experiment was performed at a low angle in the range 2θ = 1-10º with the scan rate of 0.02º/second. In addition, the spacing between the structural layers of the silicates was measured according to the Bragg's law (Equation 3.1), where *n* is an integer, *λ* is the X-ray wavelength, *d* is the interlayer spacing, and *θ* is the angle of diffraction. Figure 3.7 displays a schematic drawing of XRD Bragg's law.

$$\lambda n = 2d \sin \theta \qquad \text{Equation 3.1}$$

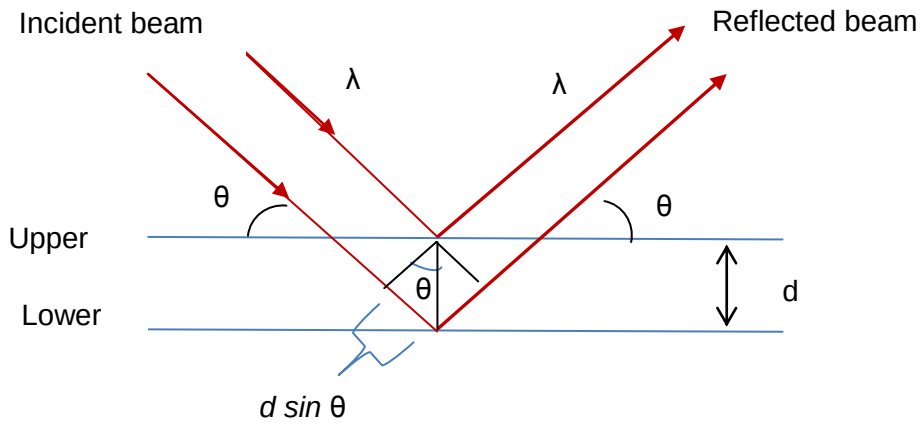

Fig. 3.7: Schematic drawing of XRD Bragg's law.

3.5.2 Transmission electron microscopy (TEM)

Dispersion of the clay particles in the rubber matrix was investigated by a transmission electron microscopy (TEM) model 2000FX (JEOL, Japan). Ultra-thin sections were prepared by cryo-ultramicrotomy model CR-X (RMC, USA). The sectioning process was carried out at –150ºC, using a diamond knife with a cutting edge of 45º. The cryo sections thickness was set at 100 nm. Sections of rubber were collected on a copper grid and examined with a TEM model 2000FX (JEOL, Japan). The operating voltage of the TEM was 80 kV.

3.5.3 Field Emission Gun Scanning Electron Microscope (FEGSEM)

Dispersion of fillers in the rubber was assessed by a Carl Zeis Leo 1530VP Field Emission Gun Scanning Electron Microscope (FEGSEM) (Carl Zeiss NTS GmbH, Oberkochen, Germany). Small pieces of the cured rubber were placed in liquid nitrogen for 3 min and then fractured to create two fresh surfaces. The samples, 65 mm^2 in area and 2 mm thick, were coated with gold and then examined and photographed in the FEGSEM. The average voltage used is 5.00 kV.

3.5.4 Differential scanning calorimeter (DSC)

The heat of fusion of SR/clay nanocomposites was obtained with a differential scanning calorimeter (DSC) model 2920 (TA Instrument, USA). About 10 mg of sample was used and placed into aluminium pan holder. The test was performed from 50 °C to 220 °C at a heating rate of 10 °C min^{-1} under nitrogen flow.

3.5.5 Fourier transforms infra-red spectroscopy (FTIR)

An Infrared (IR) spectrometer model FTIR-8400S (Shimadzu, Japan) was utilised to analyse surface chemistry of the rubber samples. Attenuated total reflectance (ATR) technique was also used as it was suitable for solid samples. The spectra were obtained in

the range 600-4000 cm^{-1} after 64 scans were completed. Exception for powder sample, a mixture of sample and potassium bromide (KBr) was prepared and pressed into a pellet form.

3.6 Mechanical testing

3.6.1 Tensile testing

The tensile stress and elongation-at-break of the nanocomposites were measured in uniaxial tension in a Lloyd testing machine LR50K (Hampshire, UK) with standard dumbbell test pieces (Type 1) at 24 °C and a cross-head speed of 100 mm/min according to BS903: Part A2;1995 [6]. The standard dumbbell test pieces (75 mm (l) x 25 mm (gauge length) x 3.6 mm (w)) as shown in Figure 3.8 were die-stamped from tensile slabs with thickness approximately 2.8 mm. Lloyd Nexygen 4.5.1 computer software was used to store and process the data. Five test pieces were tested for each compound and the median of the values was subsequently noted. Finally stress-strain curves were produced for each rubber sample to determine the Young's modulus, tensile strength and elongation at break.

Fig. 3.8: Dumbbell test pieces Type 1 [Test length: 25 ± 0.5 mm]

3.6.2 Store-energy-density at break.

The store-energy-density at break or toughness was calculated from the area under the stress-strain curve using the trapezium rule. Firstly, the area under stress-strain curve was divided into smaller intervals, each of which has length *h* (see diagram in Figure 3.9). Then the trapezium area was calculated based on the following calculation:

$$\int_b^a fx\,dx = \frac{1}{2}h\,[[y0 + yn] + 2\,(y1 + y2 + \cdots \ldots \ldots + yn - 1)]$$

$h = \frac{a-b}{n}$, where n is the number of strips

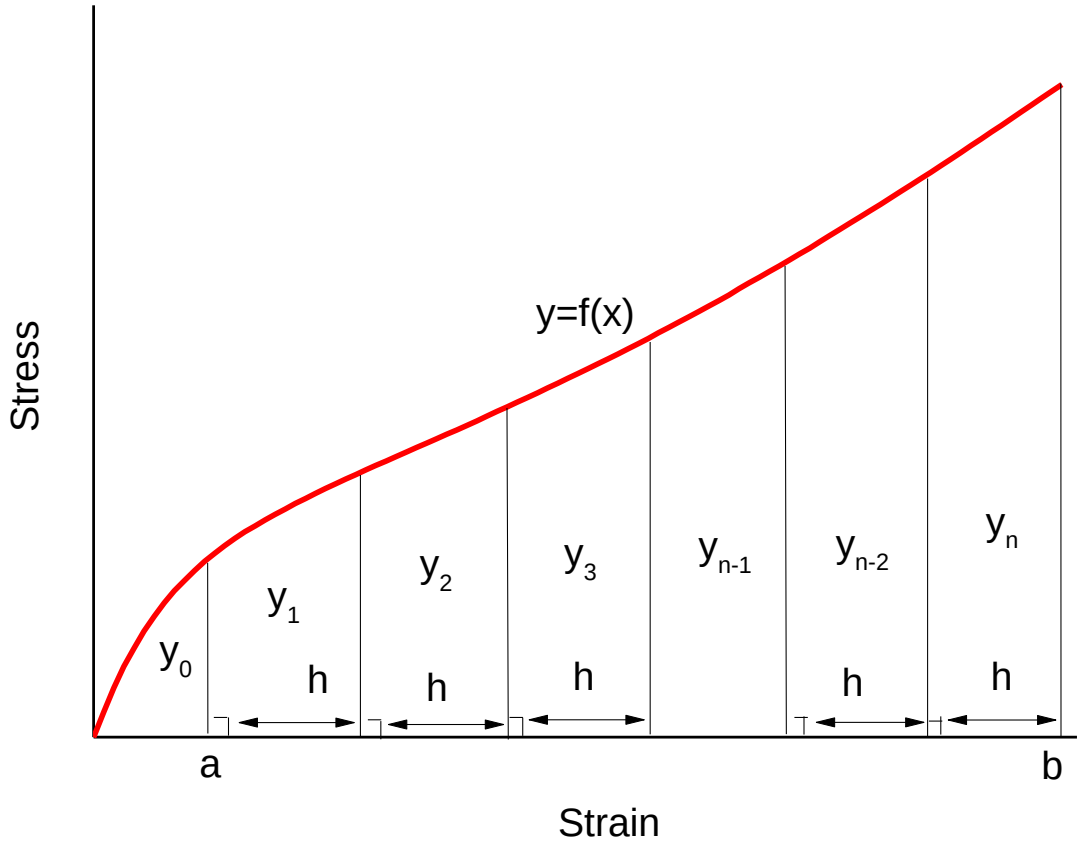

Fig. 3.9: Area under stress-strain curve with smaller intervals

3.6.3 Cyclic test

The tensile cyclic test was carried out for 10 cycles. In each test, 10 stress-strain curves were generated. The strain amplitude on the rubber samples was set at 100%, 200% and 400%, which corresponded to 25 mm, 50 mm and 100 mm extension of the gauge length. The energy dissipated in the rubber was calculated from the hysteresis loop, which was the area between the extension and retraction curves in each cycle (see diagram in Figure 3.10). The area under the curves was calculated based on trapezium rule as explained in the section 3.6.2.

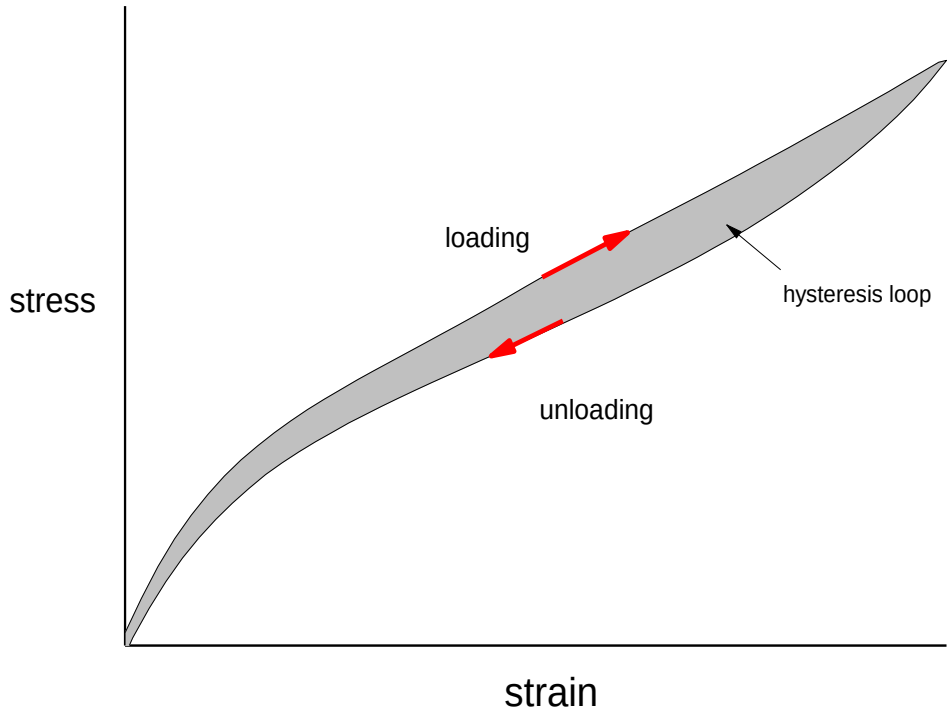

Fig. 3.10: Stress versus strain data for calculating the hysteresis loop

3.6.4 Hardness

The hardness was measured in a Shore A hardness tester (The Wallace Instrument, Surrey UK). The test was performed at 24 °C according to BS903: PartA26; 1995 [7]. Cylindrical samples with a thickness of 10 mm and diameter 15 mm (Fig. 3.6c) were moulded and cured. The cylindrical rubber test piece was then placed in the hardness tester

for 15s. The test measured the depth of an indentation in the rubber created by a given force. The measurement was made at three different positions of each sample and finally the median of the hardness values was noted.

Fig. 3.11: Shore hardness tester

3.6.5 Abrasion test

Abrasion testing was carried out following BS903-A9:1988 (method B) [7]. The test machine seen in Fig. 3.12a, consists of a laterally movable test piece holder and a rotatable cylinder, to which abrasive sheet was fixed. The standard abrasive sheet was made from aluminium oxide. The test piece was clamped in sample holder and compressed about 0.5 mm. The sample holder was travelled along the abrasive wheel which diameter is about 150 mm long and 25 mm thick so that the mounted sample has a sufficient contact with the abrasive wheel (Fig. 3.12b). The weight of the test piece was measured before and after test to determine the weight loss. The percentage of weight loss was recorded based on the following calculation:

$$\frac{m0 - m1}{m0} \times 100$$

m_0= mass of original test rubber (g)

m_1= mass of tested rubber (g)

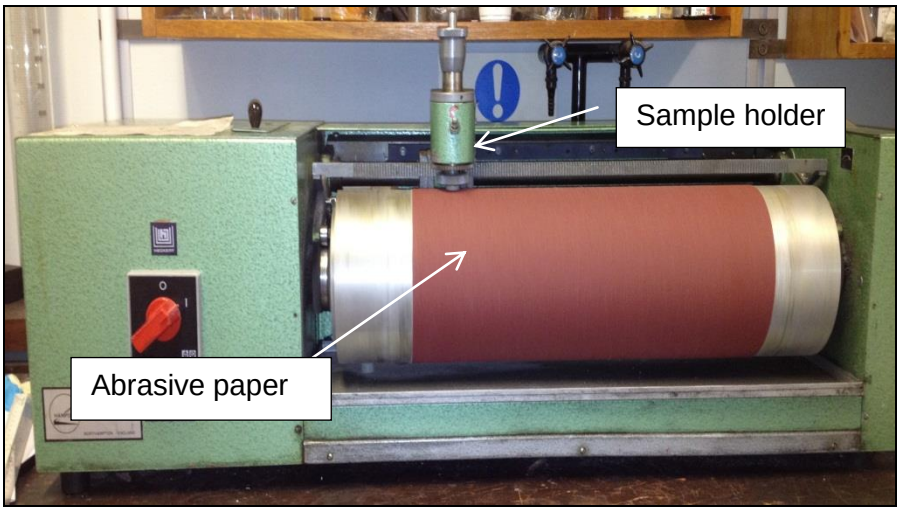

(a)

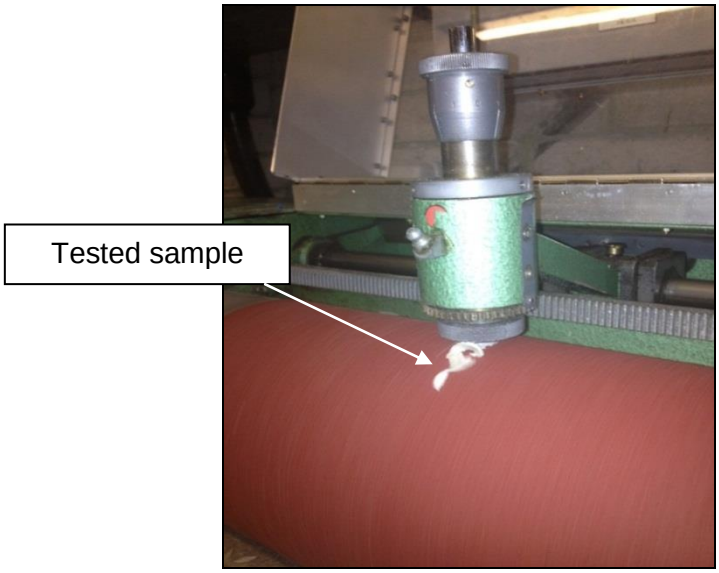

(b)

Fig 3.12 (a-b): (a) Abrasion machine and (b) tested sample with some debris

3.7 Ageing and thermal analysis

3.7.1 Oven Ageing

Accelerated ageing by heating in air was carried out according to the procedure described in BS 903-A19 [8]. The samples were aged in an oven at 200ºC for 10, 20, 24 and 30 h, respectively with no strain on them (Fig. 3.13). The tensile properties of the aged samples were then measured in uniaxial tension in a Lloyd testing machine LR50K (Hampshire, UK) with standard dumbbell test pieces at 24°C and a cross-head speed of 100 mm/min according to BS903: Part A2;1995. Five test pieces were tested for each rubber compound and the median of the values were subsequently noted. Finally, the results were expressed based on % retention ((aged ÷ unaged) × 100).

Fig. 3.13: Aged test sample in a cell-type oven with no strain

3.7.2 Thermogravimetric analysis (TGA)

Thermogravimetric analysis (TGA) was conducted with a model Q5000IR (TA Instruments, United Kingdom). The 12-15 mg specimens were heated from ambient temperature (23^{o}C) to 800°C with a linear heating rate of 10°C min^{-1}. The TGA analyses were performed in air and in nitrogen atmospheres at a flow rate of 60 mL min^{-1}. Details on thermal degradation such as onset of degradation temperature, (T_{onset}, the temperature at which mass loss is 5%), temperatures for 10% and 50% mass loss (T_{10} and T_{50}), and residue mass at 650°C were recorded.

In order to understand the depolymerisation mechanism of the neat SR and nanocomposites, DTG curves (derivative of the residual weight % versus temperature) in air and in nitrogen were also analysed. The DTG plots were prepared based on derivative of the mass change with respect to temperature (dm/dT) as a function of temperature. Thus, in a DTG plot, the peak height gives the rate of mass change at any temperature or the rate of degradation.

3.7.1 Kinetic analysis of the thermal degradation of the neat SR and nanocomposites

Activation energies against conversion levels in the range 1-20% during the thermal oxidative degradation of the neat SR and nanocomposites were determined using ASTM E1641-07 [6], which follows the well-known Flynn-Wall-Ozawa method [9]. A rapid TGA test of the studied materials was carried out based on three different heating rates, 5ºC min^{-1}, 10°C min^{-1} and 20 min^{-1}. The activation energy was then calculated using equation 3.2:

$$E = -\left(\frac{R}{b}\right) * \Delta(\log \beta)/\Delta\left(1/T\right) \qquad \text{Equation 3.2}$$

where E is Arrhenius activation energy (J/mol), R is gas constant (8.314 (J/mol.K), b is a constant (0.457/K) measured by Flynn and Wall [9], β is a heating rate (ºC/min) and finally, T is temperature at constant conversion.

3.8 References

1. Yael I, Jacques C, Jacques L. Photo-oxidation of polydimethylsiloxane oils:II –Effect of vinyl groups. *Polymer Degradation and Stability* 1992; 37: 201-208.

2. Skander M. *Fundamental aspects of crosslinking control of PDMS rubber at high temperature using tempo nitroxide*. PhD thesis. University Claude Bernard Lyon, France; 2011.

3. Southern clay. *Product bulletin Cloisite*. http://www.scprod.com/product_bulletins. (accessed on 9 June 2013).

4. Ansarifar A, Lim BY. Reinforcement of silicone rubber with precipitated amorphous white silicananofiller effect of silica aggregates on the rubber properties. *Journal of Rubber Research* 2006;9(3):140 -148.

5. British Standards Institution. BS 903-A19: Part A2. *Method for determination of tensile stress-strain properties.* London: BSI; 1995.

6. British Standards Institution. BS ISO-7619: Part 1*. Method for Determination of indentation hardness Part 1: Durometer method (Shore hardness): Rubber, vulcanized or thermoplastic.*London: BSI; 2010.

7. British Standards Institution. BS 903-A19*. Heat resistance and accelerated ageing tests*. London: BSI;1986.

8. American Standard Test Method. ASTM E1641-07*. Method for Decomposition Kinetics byThermogravimetry.* New York: ANSI; 2012.

9. Flynn, J H. and Wall, LA. A quick, direct method for the determination of activation energy from thermogravimetric data. *Journal Polymer Science B Polymer Letter* 1966; 4: 323-328.

CHAPTER 4: Preparation and characterisation of silicone rubber nanocomposite

4.1 Introduction

Several techniques such as in-situ polymerisation [1-2], solution blending [3-8] and melt-intercalation [9-12] are often highlighted in the literature about the preparation silicone rubber/clay nanocomposites, as these methods are capable of producing highly exfoliated clays. However the melt-intercalation/melt-mixing technique is the most relevant approach for the rubber blend applications since it requires the same tools used to prepare conventional filled rubber. In this thesis, a simple and versatile melt-mixing process using a small laboratory internal mixer was utilised to produce rubber/clay nanocomposites. It must be noted that while there are a few papers which report the use of the melt-mixing technique to disperse clay particles in silicone rubber/clay nanocomposite [9-12], to the best of our knowledge the fundamental process that contributes to the nanoclay dispersion in silicone rubber is not well understood. This work was carried out to investigate dispersion of different clays in silicone rubber using the melt-mixing technique.

In this chapter, the commercial clay powders were analysed using scanning electron microscopy (SEM), fourier transform infrared (FTIR) and x-ray diffraction (XRD). Then, the silicone rubber (SR)/clay nanocomposites were prepared based on natural montmorillonite (Na^+MMT) and organically modified montmorillonites (C30B and C20A). The SR/clay nanocomposites were prepared and cured, after which the interlayer *d* spacing of the clay

particles in the rubber matrix was measured by X-ray diffraction (XRD). From this the effect of the filler loading (from 0 phr to 12 phr) on clay dispersion in the silicone matrix was investigated.

Secondly, the dispersion state of SR/clay nanocomposites containing Na^+MMT, C30B and C20A respectively was compared at a fixed amount of filler loading (6 phr). In addition the formation of exfoliated and intercalated structures in the SR/clay nanocomposites was analysed based on XRD and transmission electron microscopy (TEM). For a better understanding on the exfoliation mechanism of the clays, the processing conditions affecting the formation of intercalated and exfoliated morphologies were also discussed. The results were supported by differential scanning calorimetry (DSC) and fourier transform infrared spectroscopy (FTIR) analysis. Finally, the effect of the clays on the cure characteristics of the rubber was also measured.

4.2 Materials characterisation

4.2.1 Scanning electron microscopy (SEM) analysis of the clay powder

The SEM micrographs of Na^+MMT, C20A and C30B clay powders are presented in Fig. 4.1(a-c). It can be observed that, the Na^+MMT, C30B and C20A appear in aggregates particles which have a wide variety form of structure. Most of the aggregates particles are a combination of flaky and rock shaped. In addition, some of the Na^+MMT particles have flat surface whereas some aggregates of C30B and C20A particles are highly entangled together. Overall, the average size of the aggregates particles is in the range from 5 to 28 µm.

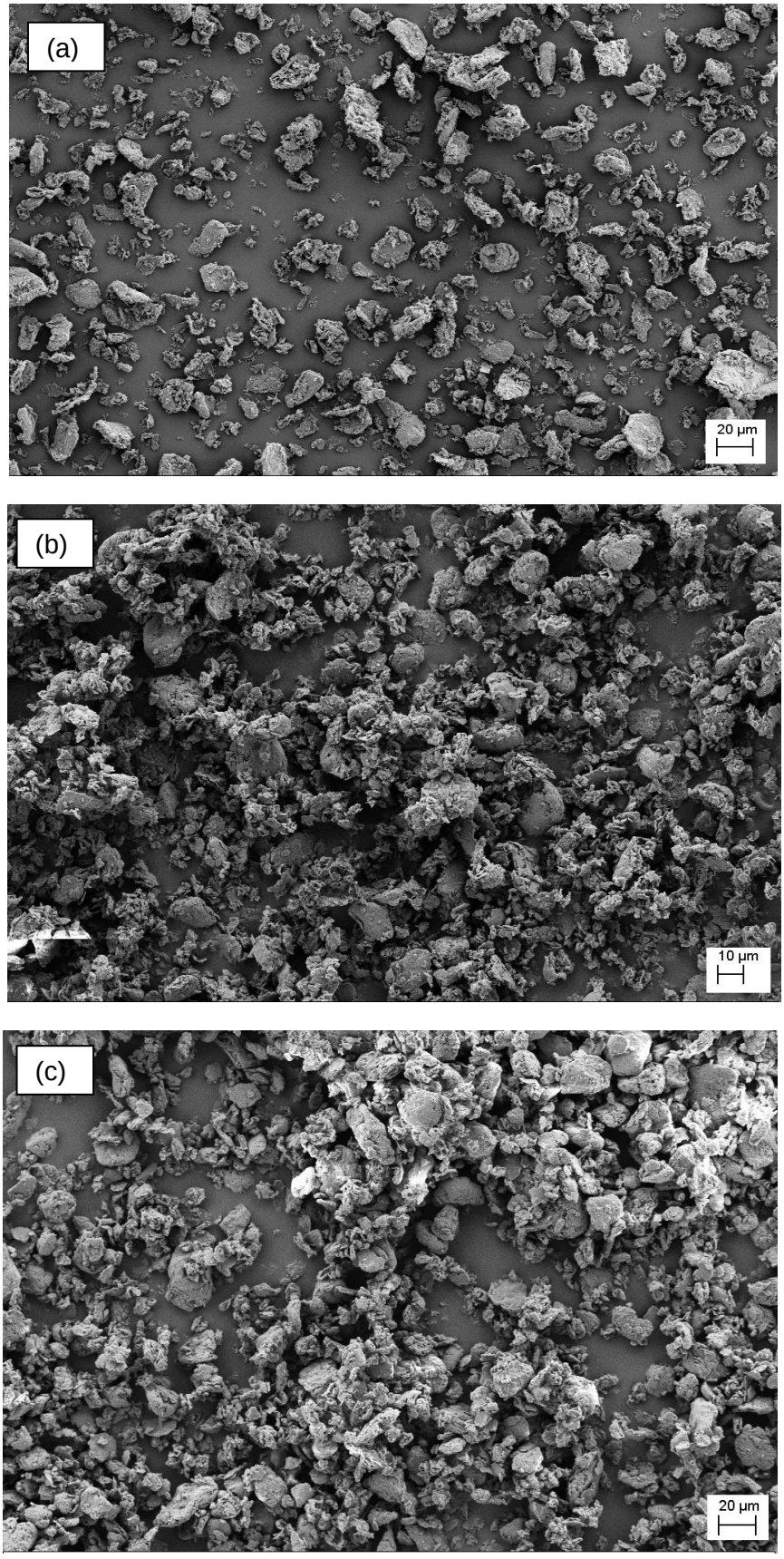

Fig. 4.1 (a-c): SEM micrographs of the clay powders (a) Na^{+}MMT, (b) C30B and (c) C20A.

4.2.2 Fourier transforms infrared spectroscopy (FTIR) analysis of the clay powder

Fig. 4.2(a-c) illustrates the FTIR spectrum of Na^+MMT, C30B and C20A clay powders. The peaks labelled as I, II, III and IV in the Fig.4.2a are represented the most distinguish peaks for the MMT identification as reported in the published literature [13]. Peak I and II indicates the presence of hydroxyl (OH) groups. The splitting peak at 3626 cm^{-1} and 3450 cm^{-1} is due to different absorption frequency that suggests the presence of O-H stretching for the silicate group and O-H stretching of water respectively. Peak III at 1640 cm^{-1} is related to O-H deformation of water [13]. In addition, the presence of the most intense peak labelled as peak IV at 1045 cm^{-1} is corresponded to the vibration of Si-O-Si from silicates [13].

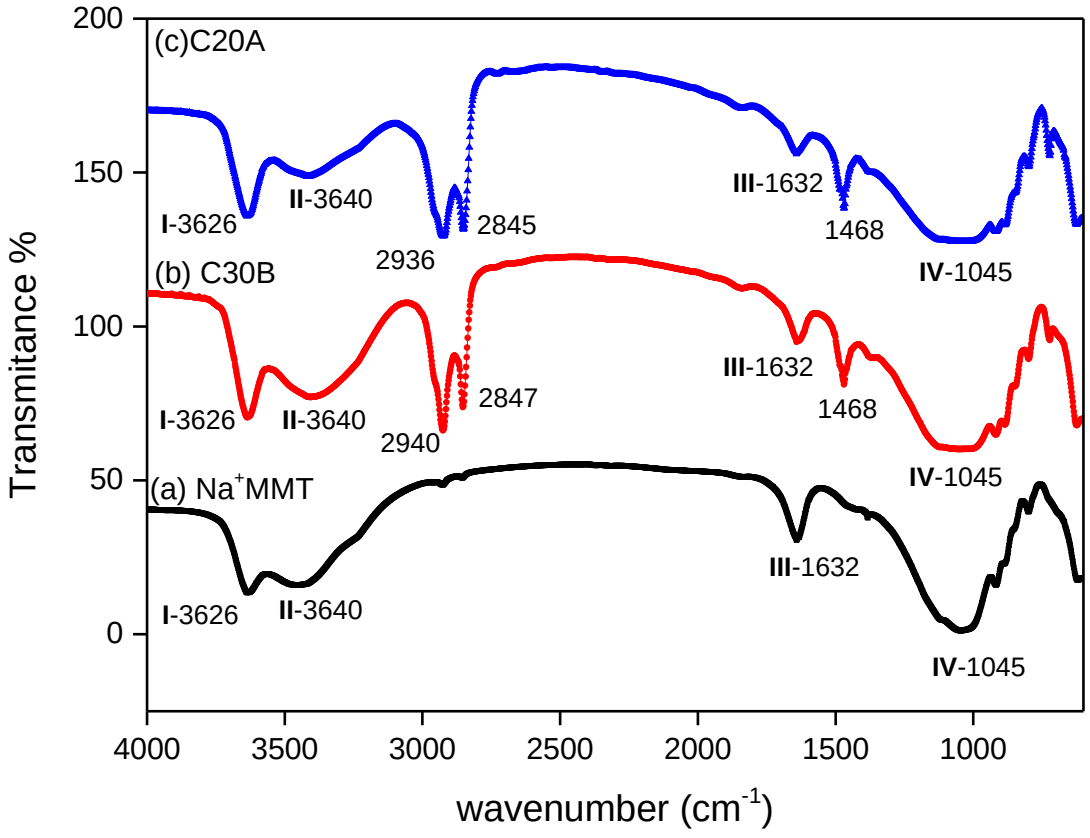

Fig. 4.2(a-c): FTIR spectrum of (a) Na^+MMT, (b) C30B and (c) C20A clay powders.

It can be observed that all the four prominent peaks that represent MMT structure labelled as I, II, II and IV also appear in the Fig. 4.2(b-c) that belongs to C30B and C20A

respectively. However, some additional peaks located at 2940, 2847 and 1468 cm^{-1} were observed in the Fig.4.2 (b) which were assigned for C-H vibrations of methylene groups (asymmetric stretching, symmetric stretching and bending respectively) [14]. A similar pattern can be seen in the Fig. 4.2c where the additional peaks appear at 2936, 2845 and 1468 cm^{-1} which was responsible for C-H vibration. Unlike Na^{+}MMT, there was no peak observed at the range from 2936 to 2847 cm^{-1}. Therefore it was confirmed that both C30B and C20A were modified by organic surfactant.

4.2.3 XRD analysis of the clay powder

XRD patterns of Na^{+}MMT, C30B and C20A are presented in Fig. 4.3. The interlayer spacing of the silicate layers, as shown in the graph, is derived from the peak position (d_{001}-reflection) in the XRD diffractograms according to Bragg's law (Equation 2.1). It can be seen that the clays show different values of *d* spacing. The basal spacing (d_{001}) of the Na^{+}MMT, C30B and C20A are 1.22 nm, 1.88 nm and 2.57 nm respectively. All the values are consistent with the information provided in the technical product bulletin [15].

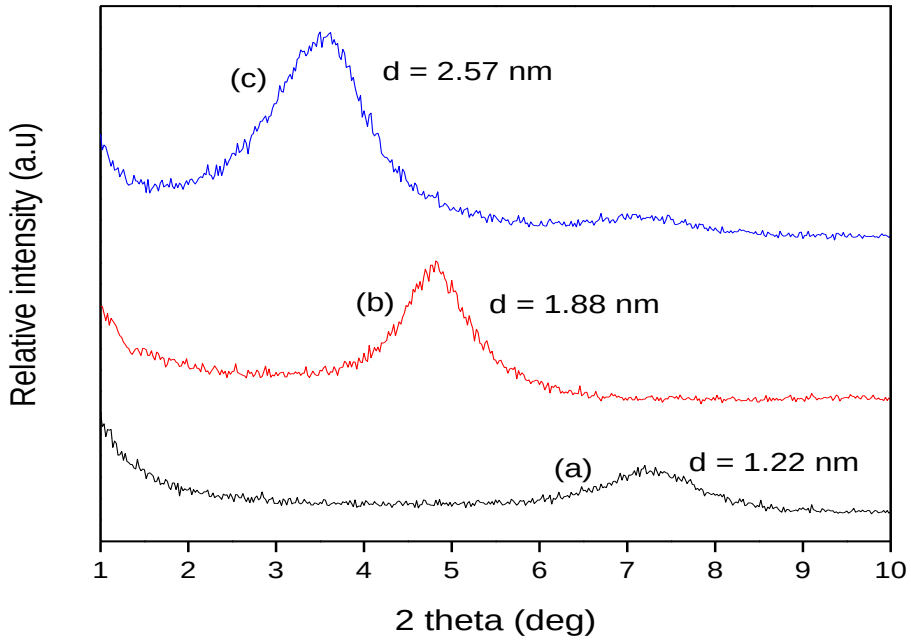

Fig. 4.3: X-ray diffraction pattern of (a) pristine MMT (Na^{+}MMT) and organoclays (b) C30B, (c) C20A.

As expected, both C30B and C20A organoclays have larger interlayer spacing compared to the unmodified Na^+MMT. This is because C30B and C20A are commercial organoclays that have been modified with organic modifier surfactant through cation exchange reactions. The modification is needed to expand the interlayer spacing of the silicate layers, and at the same time increase hydrophobicity of the silicate surface [17]. According to the product literature [18], C30B was modified with the organic surfactant methyl, tallow, bis-2-hydroxyetyl, quaternary ammonium (MT2EtOH). Therefore C30B is categorised as a polar organoclay, due to the presence of hydroxyl (OH) functional groups on the organic modifier. On the other hand, C20A is a nonpolar organoclay which has been modified with dimethyl, dehydrogenated tallow, quaternary ammonium (2M2HT) which consist two alkyl chains. The initial *d* spacing of the organoclays is determined by the density of the organic surfactant. In this case, C20A comprises a high content of organic modifier (95 meq/100g clay) as compared to the C30B (90 meq/100g clay), leading to higher inter gallery spacing.

4.3 Effect of the filler loading on the dispersion of montmorillonite (MMT) in the rubber

Fig. 4.4 shows the XRD patterns of Na^+MMT clay and the composites. Notably a broad peak was seen at the range of 2θ = 4.5 to 5.5° for the nanocomposites containing 4 and 6 phr. The position of the peaks shifted to a lower angle from the original position of the pure Na^+MMT (2θ = 7.2°), indicating formation of an intercalated structure. Based on the Bragg's law equation, the *d* spacing had increased from 1.22 nm to 1.77 nm. This suggested that the size of the *d* spacing had expanded approximately 0.55 nm. This expansion was due to the insertion of rubber chains into the spaces between the layers of the clay [17, 19]. However in this case the intensity of the intercalated peaks was very low. Thus it was believed that some of the clays were partially intercalated at 4 phr and 6 phr filler concentration. Presumably some of the delaminated NA^+MMT layers were presented in the rubber that contributed to the weak XRD signal.

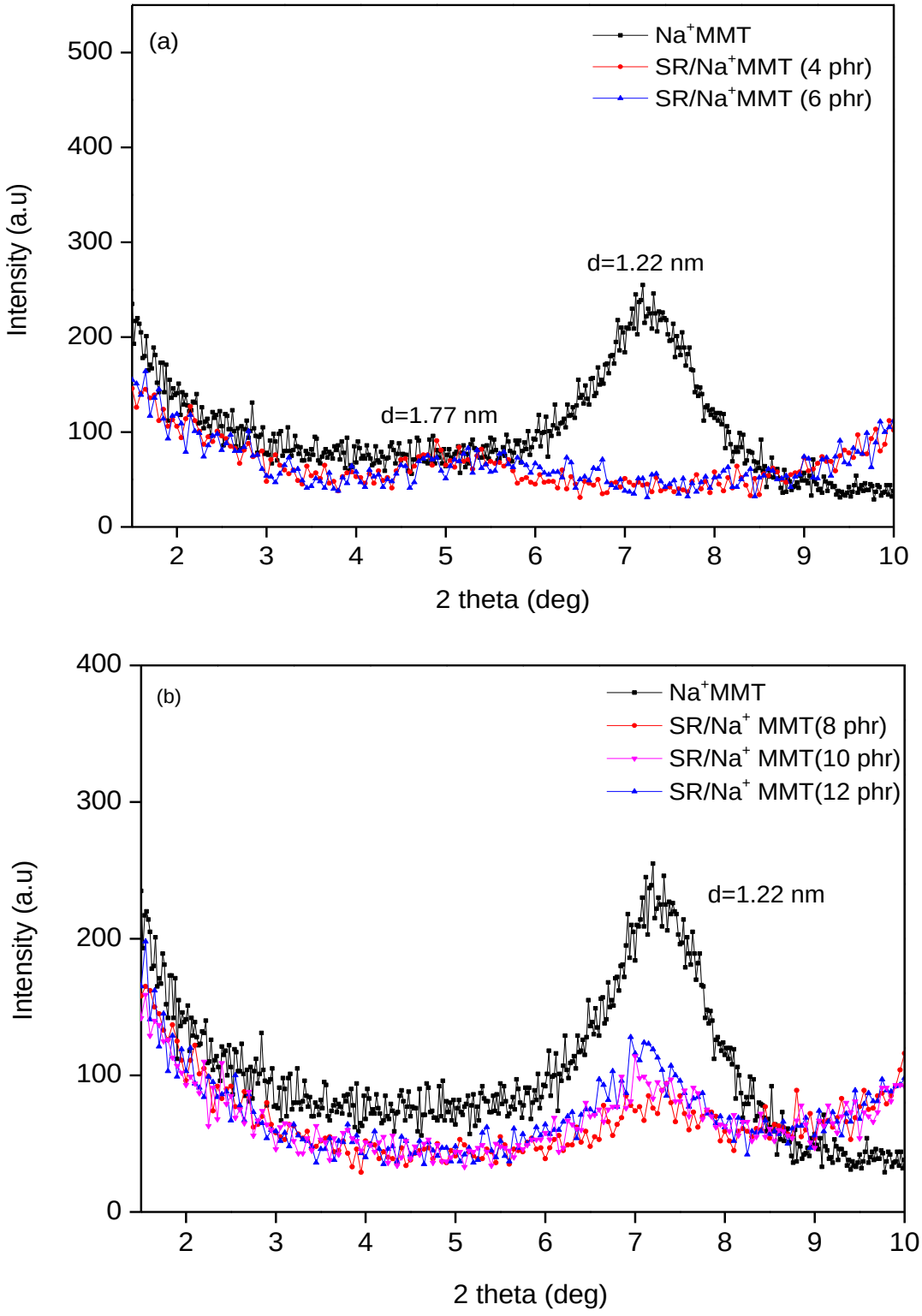

Fig. 4.4(a-b): XRD spectra for (a) SR/Na^+MMT nanocomposites filled with 4 and 6 phr (b) SR/Na^+MMT nanocomposites filled with 8, 10 and 12 phr.

In the case of the nanocomposites with high filler loading, (from 8 phr to 12 phr), the XRD peaks appeared at 2θ = 7.2° which was drawn at the same position of pure Na^+MMT clay as shown in Fig. 4.4b. As the XRD peak of the nanocomposite appears at the similar point as the original clay, it suggests the clay is dispersed in an aggregated form [19, 20]. As can be seen the XRD signal intensified as filler concentration reached 12 phr. It was believed that even when the large amount of filler was added the chance for the clay to exfoliate was low, since the clay particles had a high tendency to agglomerate.

Figs. 4.5(a-b) display a series of silicone rubber/clay nanocomposites containing C30B at different filler loadings, from 4 phr to 12 phr. No diffraction peak was observed for nanocomposites containing 4 and 6 phr of C30B (Fig. 4.5a), suggesting high extent of exfoliation had been achieved. As far intercalated/exfoliated structures are concerned, the undetectable XRD signal is because of the loss of the structure of stacked MMT layers, or alternatively due to the increase of basal spacing beyond that detectable by XRD [19].

In Fig. 4.5b when the loading of the clay exceeded 8 phr, 10 phr and 12 phr, broad reflection peaks were seen at similar positions as the pure C30B organoclay, corresponding to the micro-structured composite. From the results it can be deduced that a high extent of exfoliation was achieved at the very low filler loading of 4 and 6 phr, as suggested by the near absence of an XRD peak. Above this filler concentration, the clay dispersed in macro scale.

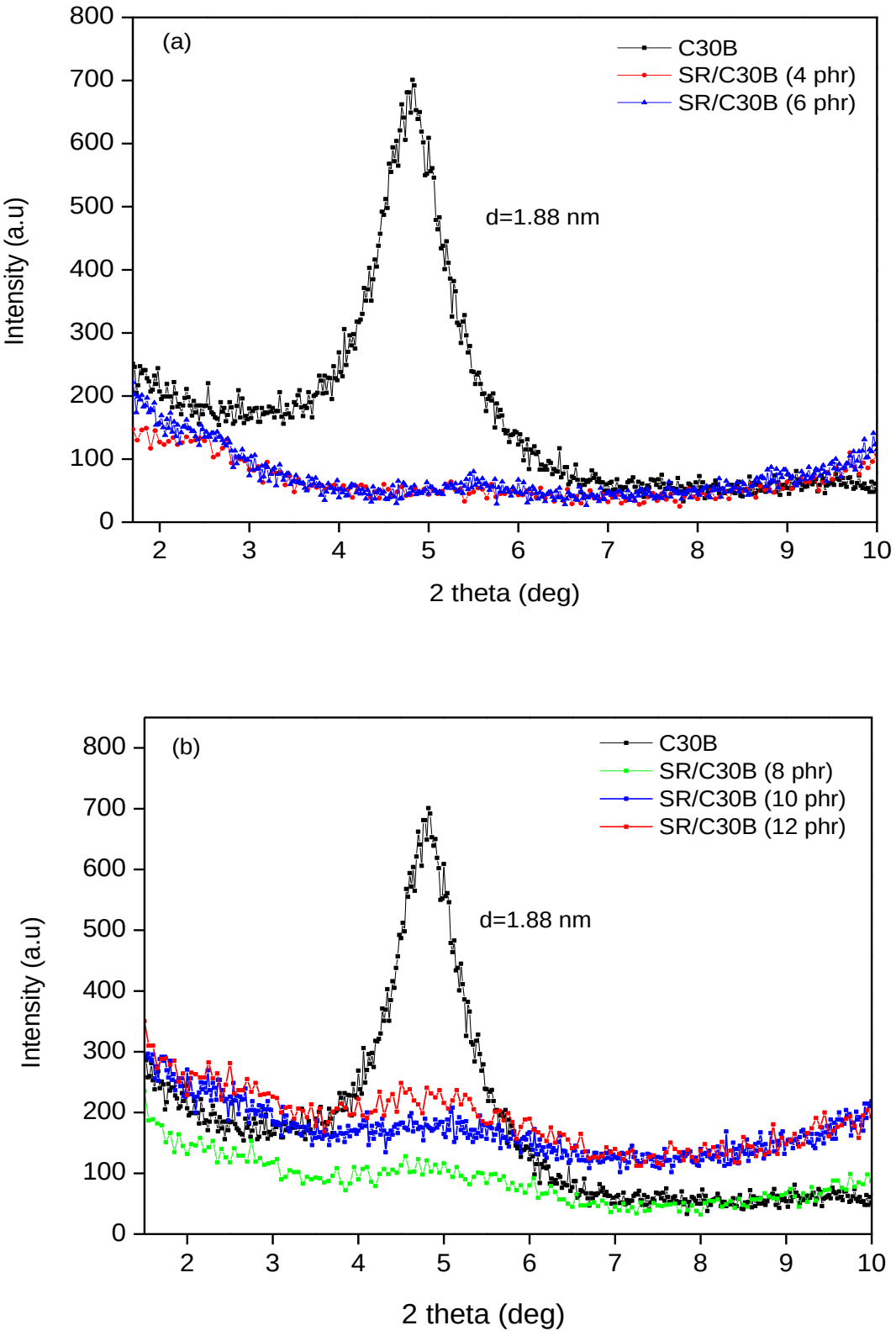

Fig. 4.5(a-b): XRD spectra for (a) SR/30B nanocomposites filled with 4 and 6 phr (b) SR/30B nanocomposites filled with 8, 10 and 12 phr.

A series of XRD spectra for the SR/C20A nanocomposites filled with different loadings are presented in Fig. 4.6(a-b). Evidently, the diffraction peaks of all the rubber nanocomposites containing up to 12 phr of the filler shifted towards the lower angle, in comparison with the original peak of the pure C20A organoclay. The peak shift indicated that the distance between the clay layers had stretched from its original size spacing. This suggested that the silicone rubber chain had diffused into the clay gallery that corresponded to intercalated nanocomposite.

Table 4.1 summarises the peak positions of the SR/C20A nanocomposites with different filler loadings and their *d* spacing values. It appears the expansion of interlayer spacing for SR/C20A nanocomposites depends on the clay concentration. The *d* spacing expanded by about 0.89 nm in the nanocomposites containing 4 phr and 6 phr of C20A. As the content reached 8 phr, the Δ *d* spacing started to decrease towards the initial value. The reduction of *d* spacing values can be clearly seen at 10 phr and 12 phr filler loading.

It was concluded that when a large amount of C20A was presented in the rubber matrix, the *d* spacing of the silicate layers tended to remain similar to its original size. This was because the dispersion was more limited at high levels of filler loading - some of the filler particles tended to aggregate or agglomerate, forming big structures in the rubber matrix. Therefore the possibility of rubber chains diffusing into the silicate layer spacing was significantly lower at high filler loadings. Compared at the lower filler loading, the chances for the particles to agglomerate was low, thus it helped the formation of high extent intercalated nanocomposite to achieve.

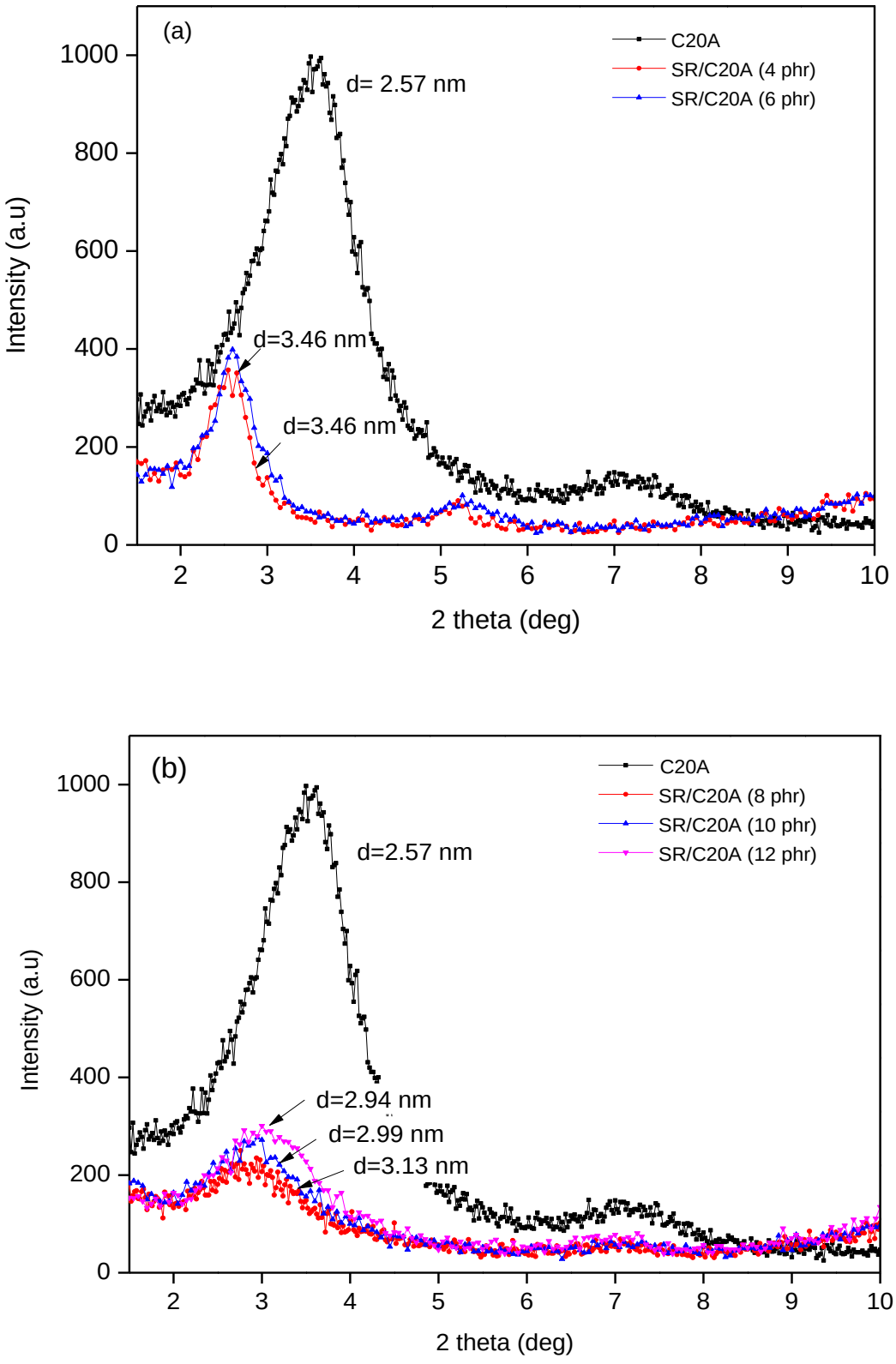

Fig. 4.6(a-b): XRD spectra for (a) SR/20A nanocomposites filled with 4 and 6 phr (b) SR/20A nanocomposites filled with 8, 10 and 12 phr.

Table 4.1: XRD data of C20A and SR/C20A nanocomposites

Samples	2θ	d (nm)	∆d (nm)
C20A	3.4	2.57	-
SR / C20A - 4phr	2.55	3.46	0.89
SR / C20A - 6phr	2.55	3.46	0.89
SR / C20A - 8 phr	2.82	3.13	0.56
SR / C20A - 10 phr	2.95	2.99	0.42
SR / C20A - 12 phr	3.00	2.94	0.37

From the XRD analysis shown above it emerged that the dispersion state of the filler in the SR/clay nanocomposites prepared via the melt mixing process was highly dependent on the level of the clay concentration, regardless of the initial *d* spacing of the clay's interlayers. On average, the high extent of exfoliation in the SR nanocomposites was achieved at very low loading of the clay filler, i.e. 4 phr to 6 phr. This result contradicted previous findings [9, 12]. Because of the low viscosity of SR, most researchers believed that melt intercalation would occur favourably at high loading of OMMT (organoclays) [9, 12]. According to some authors, increases in viscosity at high dosage of OMMT would provide effective shearing forces within the rubber to facilitate the intercalation of the SR chains into the interlayer spacing of OMMT. However, a significant improvement in the mechanical properties of the rubber vulcanisate was not achieved because of the formation of filler agglomerates in the rubber [9, 12].

4.4 A comparison of morphology and structure between pristine clay (Na^+MMT), and organoclays (C30B and C20A) in the SR matrix at constant filler loading (6 phr).

4.4.1 Wide angle X-ray diffraction analysis (XRD)

A comparison of morphology and structure was also made between the nanocomposites containing different type of clay (Na^+MMT, C30B and C20A). The XRD pattern of the nanocomposites was compared at the same amount of filler loading (i.e. 6phr) as demonstrated in Fig. 4.7 (remember that the nanocomposites containing 6 phr Na^+MMT showed a weak intercalated peak). This suggested that a small degree of intercalated clay nanoplatelets was present in the SR matrix.

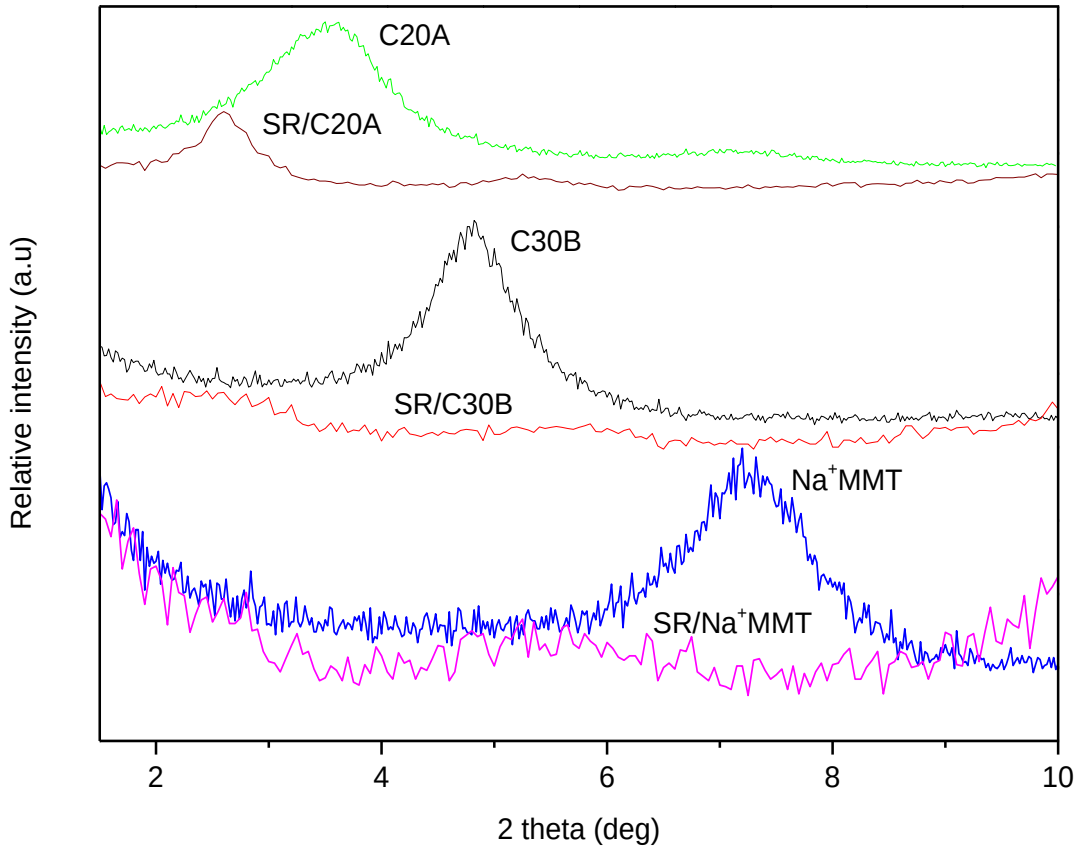

Fig. 4.7: XRD spectra of SR/Na^+MMT nanocomposites (6 phr), SR/C30B nanocomposites (6 phr) and SR/C20A nanocomposites (6 phr).

In Fig. 4.7, the near absence of XRD diffraction for SR/C30B nanocomposites indicated the existence of highly exfoliated clay. In contrast, C20A had dispersed in an intercalated state, as suggested by a remarkable shift of XRD peak towards the lower angle (Fig. 4.5) and an expanded *d* size increased by 0.89 nm (Table 4.1). A primary conclusion drawn from the XRD pattern suggested exfoliated nanocomposite was achieved with the addition of C30B at 6 phr filler loading. On the other hand, C20A organoclays and Na^+MMT exhibited intercalated structures. A further investigation of nanocomposite structure was carried out by microscopy analysis in the next section.

4.4.2 Transmission electron microscopy (TEM)

The filler morphology in the rubber matrix was further investigated at high magnifications, as shown in TEM micrographs (Fig. 4.8(a-c)). The fine and thick dark lines in these figures correspond to the cross-section of individual clay layers and a typical sandwich layer, respectively. In Fig. 4.8a, a number of intercalated Na^+MMT particles can be seen in the rubber matrix (shown by white arrows). In addition, on the same figure, it is evident that some filler particles approximately 8 nm thick are dispersed in the rubber matrix (shown by black arrows). Note that the XRD results in Fig.4.7 did not reveal spatial distribution of the platelets. Therefore, after considering the results in Figs.4.7 & 4.8a, it was concluded that the coexisting of exfoliated and intercalated clay structures were present in the rubber matrix.

Fig. 4.8b shows nanoscale dispersion of Cloisite 30B layers in the rubber matrix. Thin dark lines in the figure represent exfoliated platelets (shown by black arrows). In this case information obtained from XRD (Fig. 4.7) agreed with that from Fig. 4.8b. It was obvious that only a few thick dark lines, representing stacked layers, were present in the figure (as indicated with white arrows). Therefore it was concluded that high extent of exfoliation of Cloisite 30B clay particles were present in the rubber matrix.

Fig. 4.8a: TEM image for SR/Na^{+}MMT nanocomposite (6 phr)

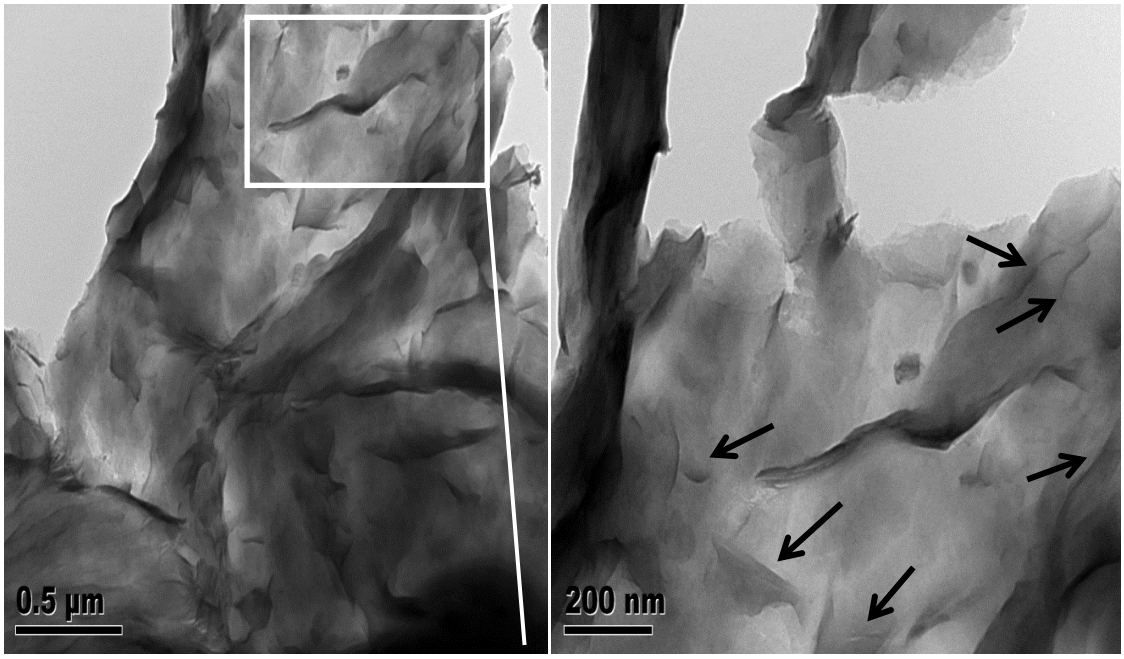

Fig. 4.8b: TEM image for SR/C30B nanocomposite (6 phr)

Fig. 4.8c shows dispersion of the clay in the SR/C20A nanocomposite. Intercalated Cloisite 20A can be seen clearly (indicated by the white arrows). The interlayer spacing has expanded due to diffusion of the rubber chains into the stacked layer [2]. This observation was confirmed in Fig. 4.8c. Surprisingly, high extent of exfoliation was achieved in SR/C30B nanocomposites despite having a smaller *d* spacing with regard to C20A. Remember that the C20A dispersed as intercalated state in the rubber matrix even though it had relatively larger *d* spacing than C30B. Therefore it was concluded that organoclay having a larger interlayer spacing was not sufficient to transform clay particles into individual platelets.

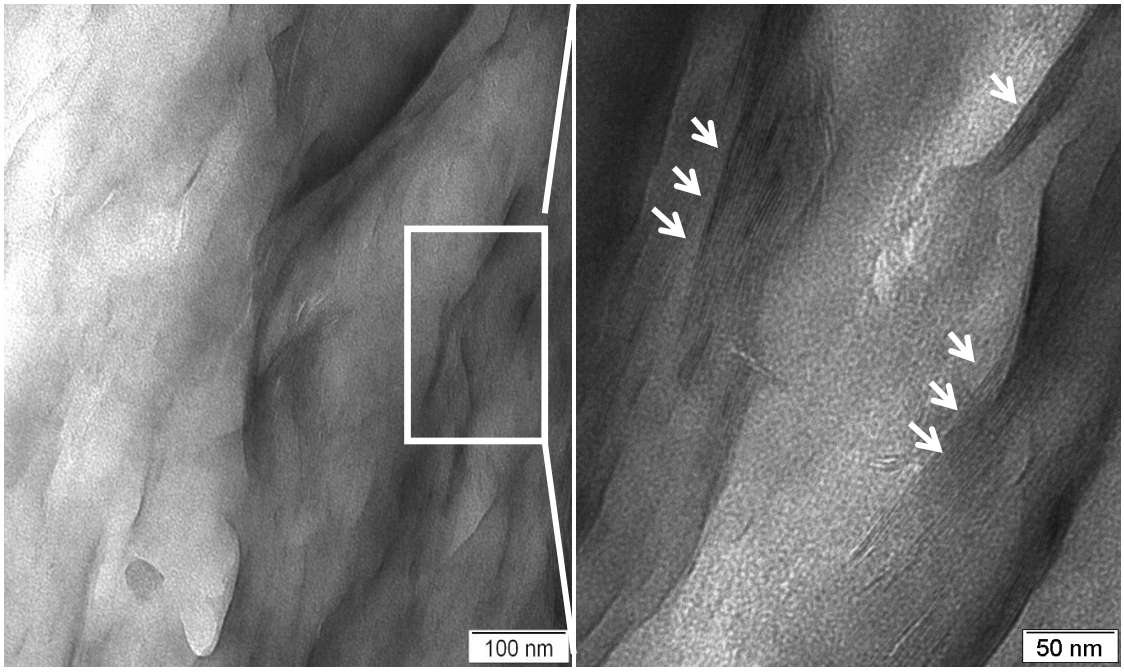

Fig. 4.8c: TEM image for SR/C20A nanocomposite (6 phr)

Note that C30B organoclay was modified with MT2EtOH containing hydroxyl groups, highlighting the role of chemical interaction in facilitating the exfoliation process, presumably through the formation of hydrogen bonding. It was feasible for the OH group in the C30B to interact within the siloxane segment (Si-O-Si) on silicone rubber to form hydrogen bonding. Such interaction presumably contributed to the collapsing of clay layers.

A comparable observation was also seen in the SR/Na^+MMT nanocomposite, which contained both intercalated/exfoliated morphology, though the unmodified Na^+MMT had the smallest *d* spacing. Since the pristine Na^+MMT was used without any organic modification the polar interaction between the OH group from the layer edges and silicone backbone also can be considered an accelerating exfoliation process. On the other hand, C20A lacked active surface groups because it was modified with the hydrogenated tallow (2M2HT). This prevented C20A from interacting favourably with the siloxane groups in the silicone rubber chains and consequently exfoliation of the clay particles did not occur. This finding is consistent with those of Vaulot and co-workers [12]. They proposed that a specific interaction between the reactive polymer end groups and the filler surface played an important role in the exfoliation of the filler. A schematic drawing of a proposed exfoliation mechanism of C30B platelets in silicone matrix is presented in Fig. 4.9.

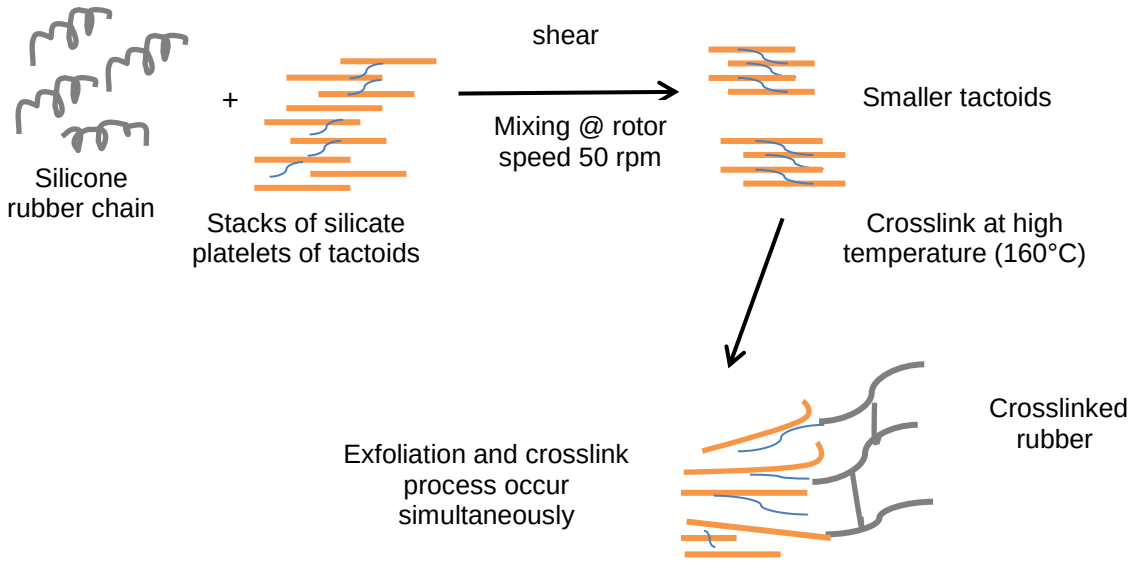

Fig. 4.9: Schematic of a proposed exfoliation mechanism of C30B platelets in silicone matrix.

4.5 ATR-FTIR studies

Fig.4.10a compares FTIR spectra of C30B, unfilled SR and high extent of exfoliation SR/C30B nanocomposite (6 phr). As can be seen, the intensity of OH absorption was more prominent for C30B compared to the nanocomposite and the neat SR. For C30B spectra, absorption band in the range of 3200 to 3600 cm^{-1} was due to -OH stretching from the hydroxyl group in bis-2-hydroxyetyl, quaternary ammonium organic modifier and the OH absorption from the edges of the clay layer. In addition, the C30B reveals absorption band at 1045 cm^{-1} deriving from stretching vibration of Si-O-Si from silicate which is important characteristic peak of C30B. However, there was no peak observed in that region for SR/C30B nanocomposite spectra. This was due to the low concentration of the C30B filler presented in the rubber matrix.

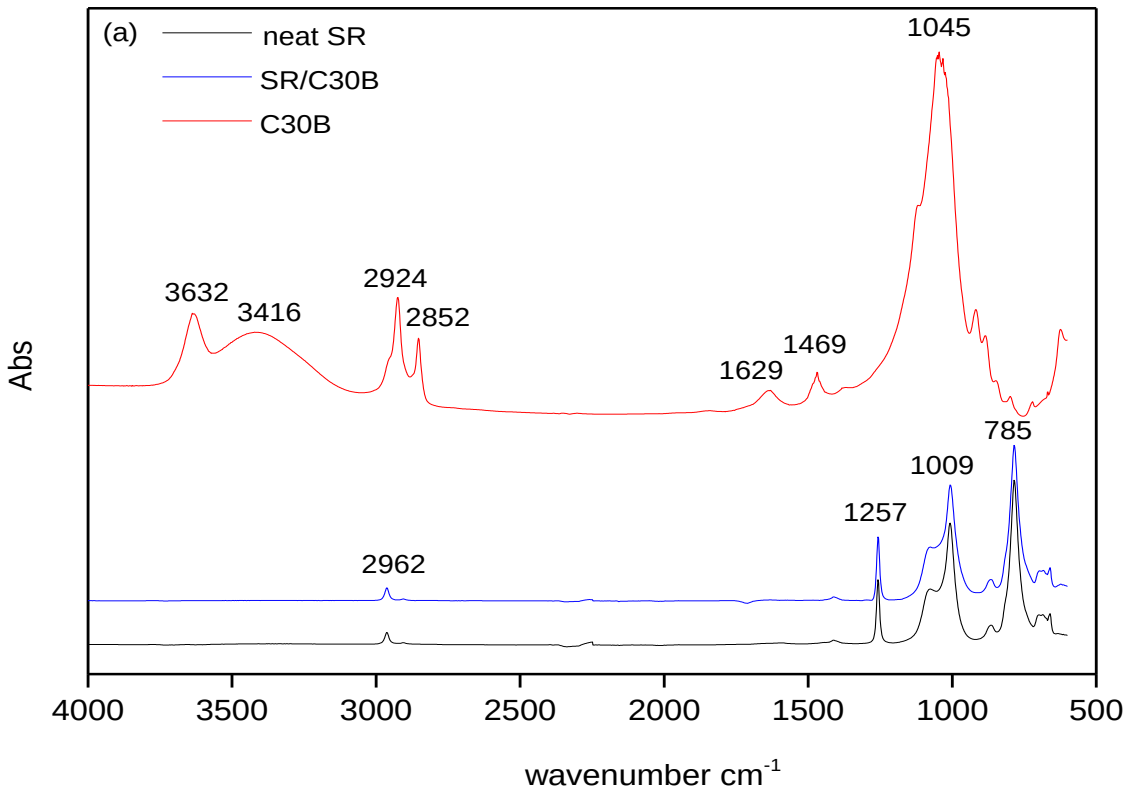

Fig. 4.10a: FTIR spectra of C30B, SR/C30B (6 phr) and neat SR.

FTIR spectra of C30B and SR/C30B nanocomposite were compared as illustrated in Fig. 4.10b. Only a broad shoulder peak was noticed for OH absorption of the SR/C30B

nanocomposite. The position of the OH band for the SR/C30B nanocomposite shows a marginal shift to the lower frequency, from 3416 cm^{-1} to 3392 cm^{-1}. This is most probably due to weakening of the OH bond as a result of H-bonding [2].

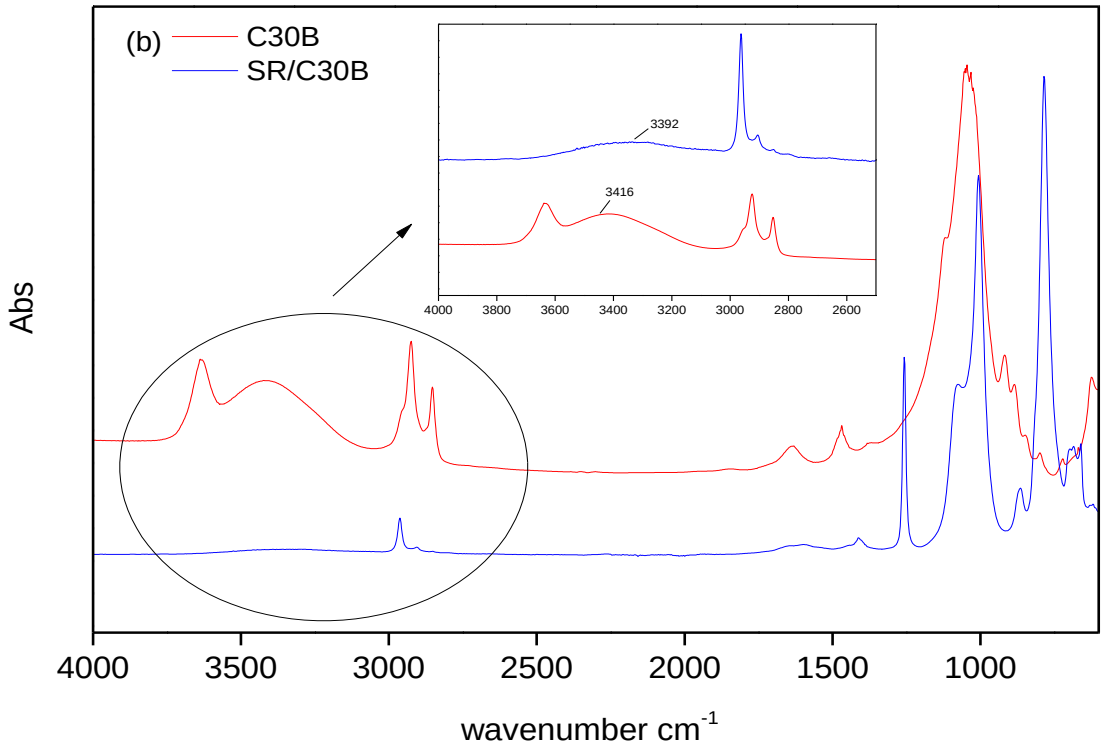

Fig. 4.10b: FTIR spectra of C30B and SR/C30B (6 phr).

On the other hand, it was found that IR absorption for SR/C30B nanocomposite was almost identical to the unfilled SR, as shown in Fig 4.10c The vinyl terminated polydimethylsiloxane (PDMS) silicone rubber exhibited the following main characteristics: a strong and sharp peak around 2962 cm^{-1}, corresponding to the CH stretching of CH_3. The CH_3 deformation also induced a sharp and strong absorption at the range of 1257 cm^{-1}, whereas the Si-O-Si backbone produced a broad band with two maxima at 1009 and 1078 cm^{-1}. A sharp peak at 785 cm^{-1} resulted from the stretching of Si-C. Nevertheless slight movements of the peak position from 1009 to 1006 and 1078 to 1074, corresponding to the Si-O-Si segment, were identified in magnified spectrum in Fig. 4.10c. A shift of Si-O-Si absorption towards the lower frequency is most probably due to the existence of hydrogen

bond interactions between the SR backbone and the C30B layers. A similar phenomenon has been reported previously [2, 19].

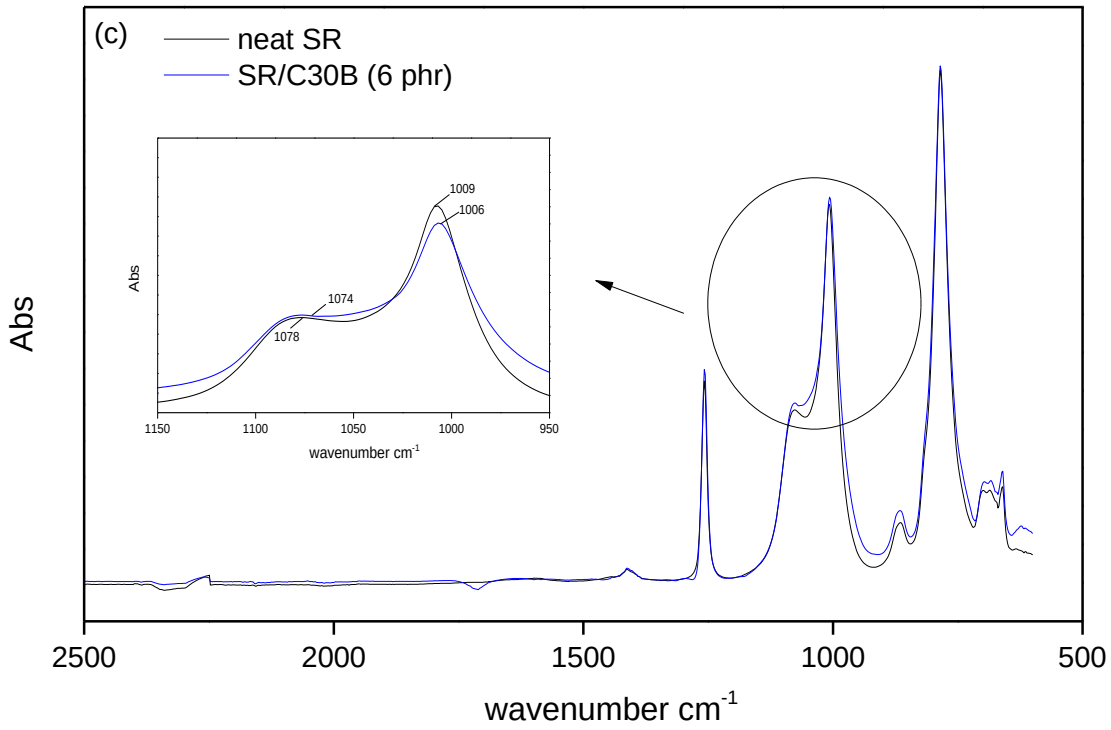

Fig. 4.10c: FTIR spectra of neat SR and SR/C30B (6 phr).

4.6 Dispersion mechanism of the clay particles in rubber matrix

4.6.1 Effect of mixing time on clay dispersion

As discussed above, the coexistence of intercalated/exfoliated SR/Na^+MMT nanocomposite, high extent exfoliated SR/C30B nanocomposite and intercalated SR/C20A nanocomposite were successfully achieved at 6 phr filler loading. Further investigation was carried out to determine the effect of mixing conditions on the ultimate structure of the clay layer in the rubber. Initially, we investigated the effects of the mixing time on the degree of exfoliation/intercalation in the rubber. Figs. 4.11(a-c) show the XRD patterns of the SR nanocomposites based on three different clays (i.e: Na^+MMT, C30B and C20A). The

samples were prepared at two different mixing times (i.e. 3 min and 15 min) and the ultimate structure of the nanocomposite was analysed after curing.

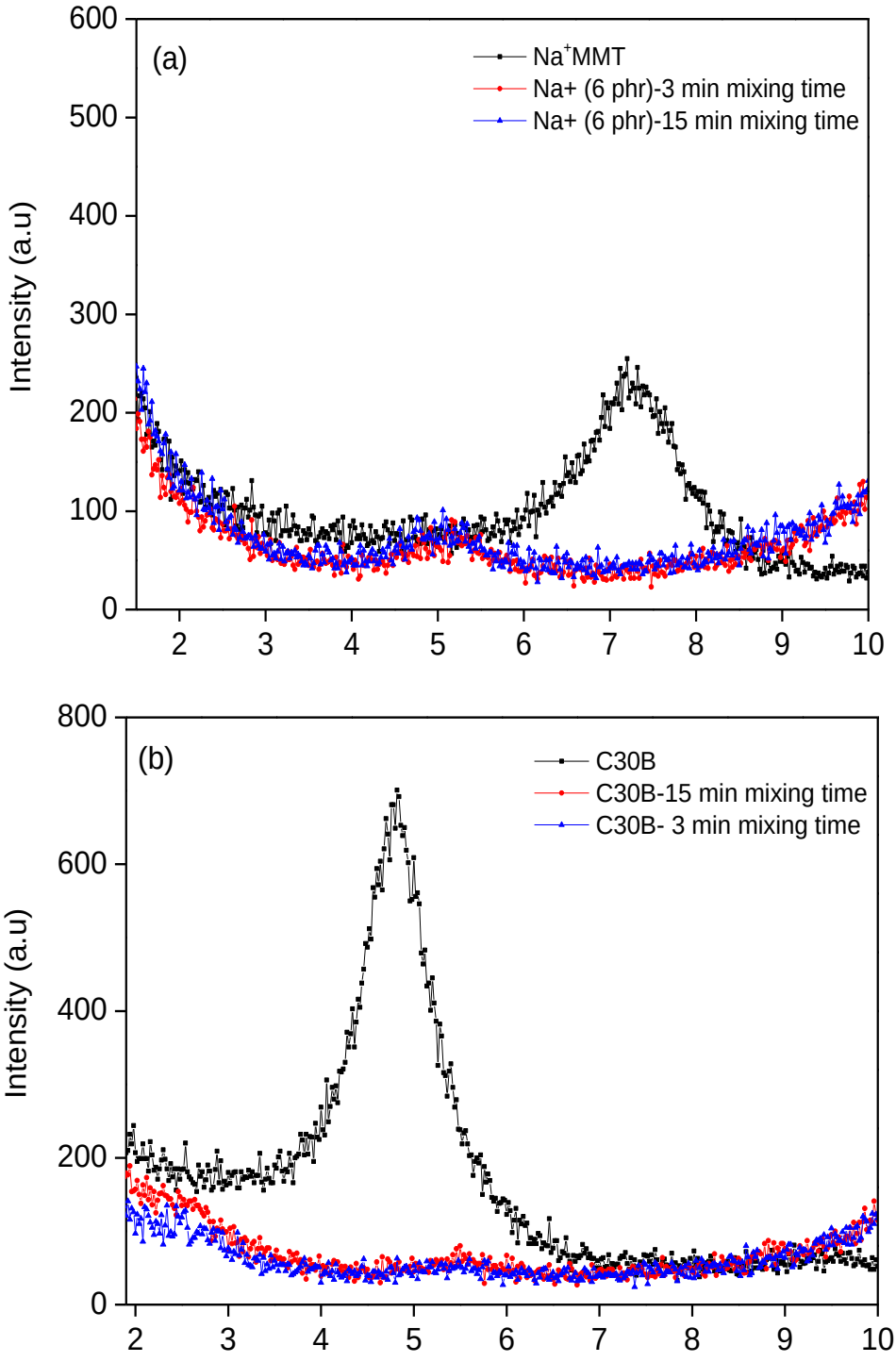

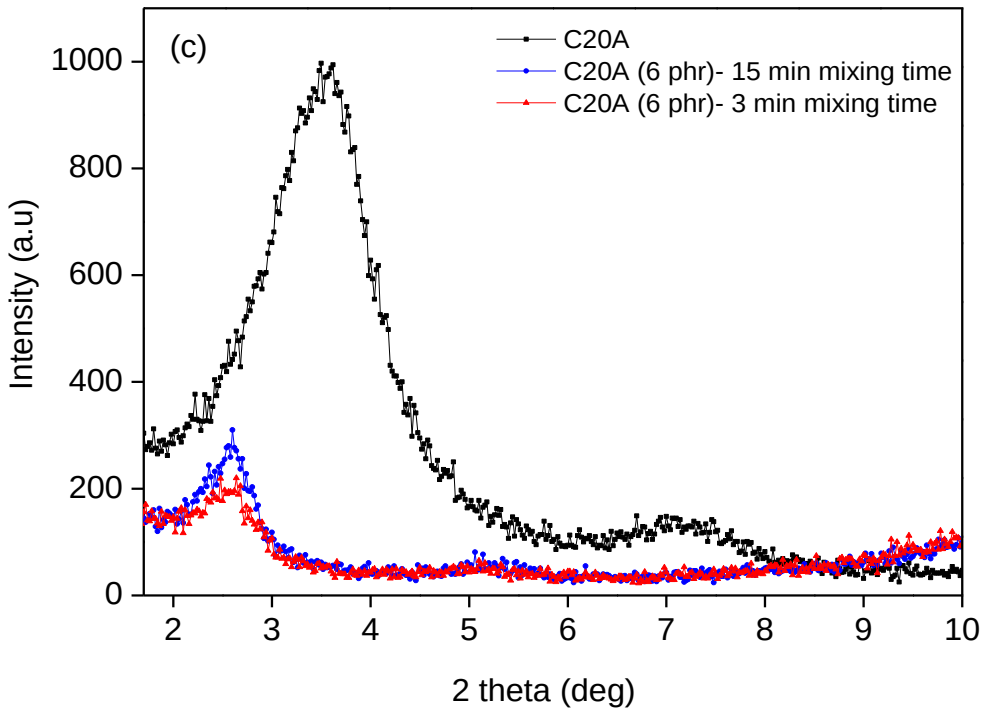

Fig. 4.11(a-c): XRD spectra of (a) Na^+MMT and SR/Na^+MMT(6 phr), (b) C30B and SR/C30B (6 phr) (c) C20A and SR/C20A (6 phr) prepared at 3 min and 15 min mixing time respectively.

In the case of SR/Na^+MMT a broad intercalated peak was seen for both samples (Fig. 4.11a) indicating the formation of an intercalated structure. This suggested no significant change in the ultimate nanocomposite structure, even when the sample was prepared under short mixing periods (3 min). A similar phenomenon was observed regarding SR/C30B and SR/C20A. In Fig. 4.11b, a similar pattern of XRD peaks was seen to that when the SR/C30B nanocomposites were prepared within 3 min mixing time and 15 min mixing time respectively.

The absence of any peaks on the spectra suggests that the C30B clay transformed to nanoplatelets. In the case of the SR/C20A a remarkable shift of XRD spectra towards a lower angle was observed for both mixing conditions, indicating the existence of an intercalated structure in the nanocomposites (Fig. 4.11c). From the investigation, it was

concluded that the degree of intercalation/exfoliation in the rubber was unaffected by increasing the mixing time. Nevertheless, a mixing time of 15 min was considered most appropriate when using the small laboratory internal mixer.

4.6.2 Effect of curing state on clay dispersion

Curing is the final stage in the processing of rubber nanocomposites. Thus it is important to investigate the effect of high temperature curing on the dispersion of the clays in the rubber. A comparison was made between SR/Na^+MMT before curing and SR/Na^+MMT after curing, as shown in Fig. 4.12a.

The SR/Na^+MMT before curing exhibited a noticeable peak at a similar position as the pure Na^+MMT at 2θ = 7.2º. This indicated that the clay structure remained as stacking layers before curing. However, after curing the structure of the clay changed dramatically. A peak appeared at a lower angle, from 2θ = 4.5° to 5.5°, on the XRD spectrum for the SR/Na^+MMT before curing (Fig. 4.12a) indicating the formation of an intercalated structure. These results suggest that the change of the clay structure from the stacked layer to intercalated state was a result of the curing process and not mixing time. A similar observation was seen in ethylene propylene diene rubber EPDM)/organoclay. It has been reported that the intercalated structure of EPDM/organoclay occurred as a result of the vulcanisation process [18].

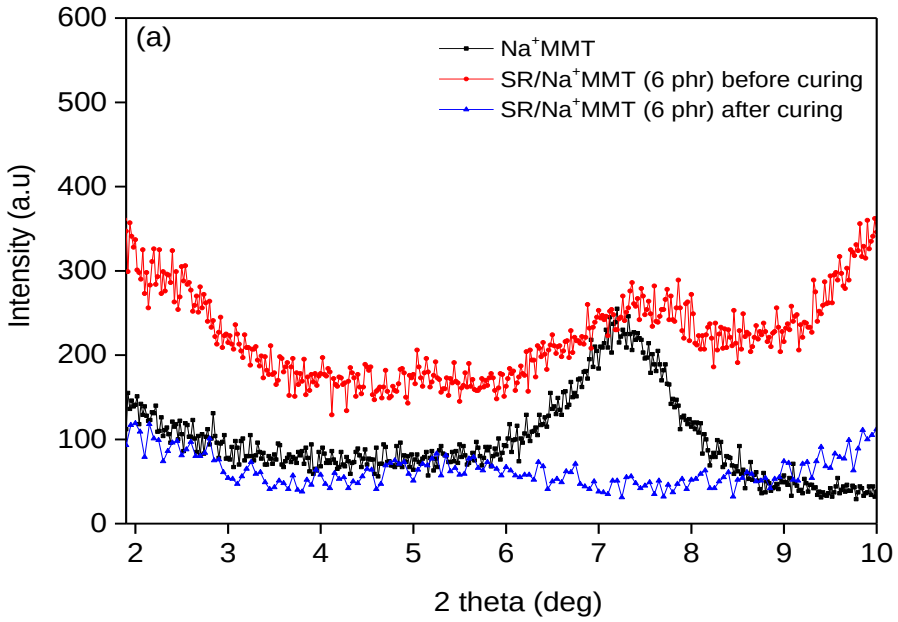

Fig. 4.12a: XRD spectra of (a) Na^+MMT and SR/Na^+MMT before and after curing respectively

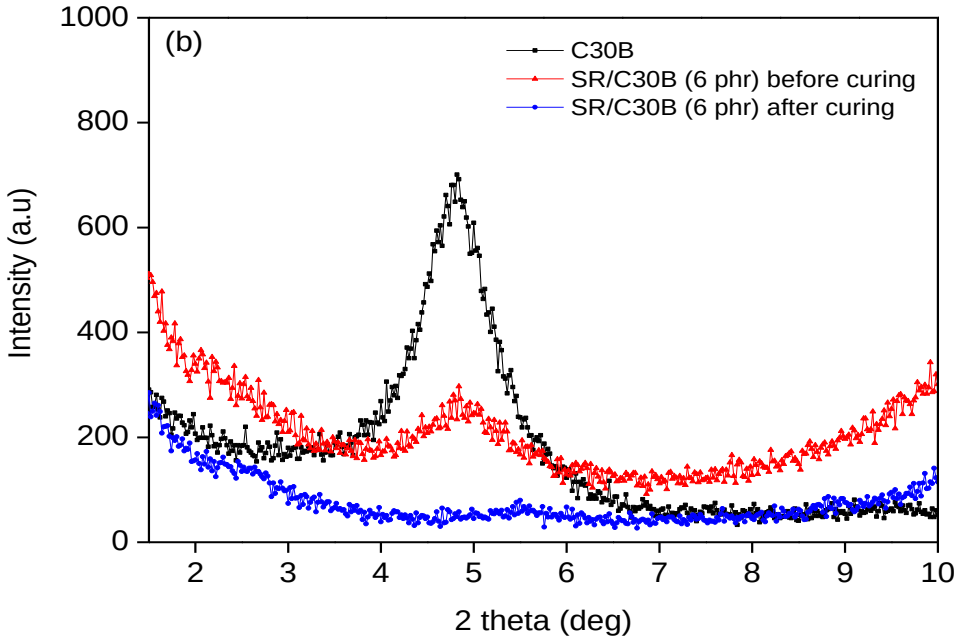

Fig. 4.12b: XRD spectra of (b) C30B and SR/C30B before and after curing respectively

A similar feature was also seen for the SR/C30B nanocomposite (Fig. 4.12b). Before curing, a peak was clearly observed on the XRD spectrum, roughly where a peak appeared

for the pure C30B. However, after curing there was no peak on the XRD spectrum of the nanocomposite, indicating high extent exfoliation of the clay particles in the rubber matrix. The results show exfoliation of the clay particles has taken place during the curing process.

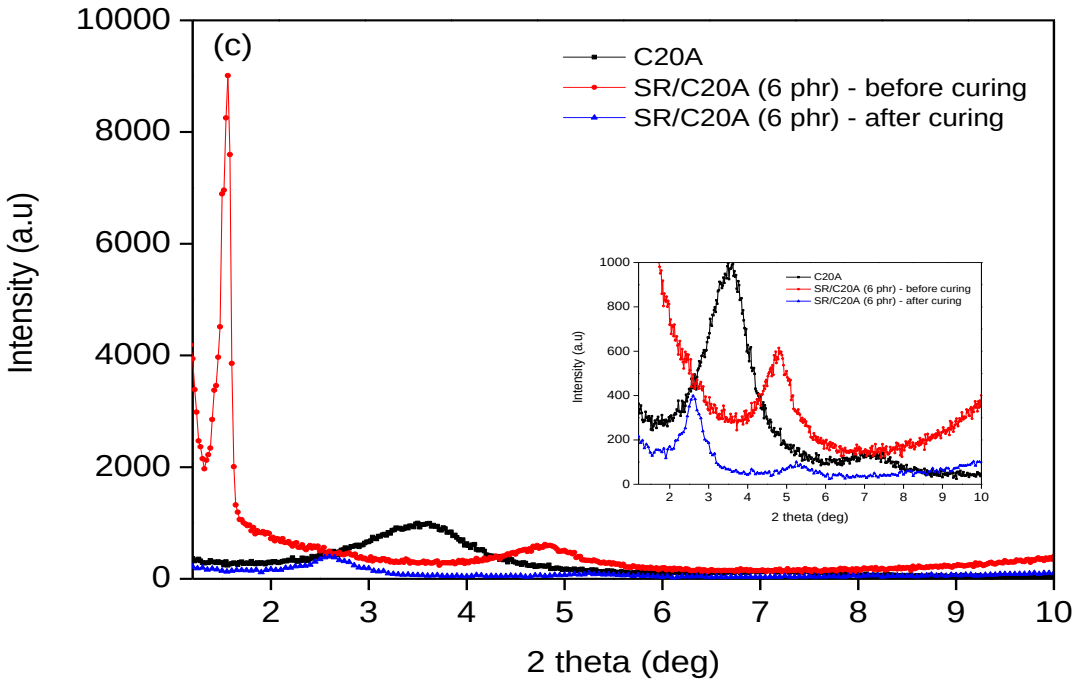

Fig. 4.12c: XRD spectra of (c) C20A and SR/C20A before and after curing respectively

The dispersion state of the clay in the SR/C20A nanocomposite (Fig.4.12c) was noticeably different from that seen in the SR/Na^+MMT and SR/C30B nanocomposites. Before curing a sharp XRD peak appeared at 2θ = 1.56°, corresponding to 5.66 nm *d* spacing. However for the original C20A clay the major peak appeared at 2θ = 3.42°, corresponding to 2.57 nm *d* spacing. The large difference between the *d* spacing of the clay particles, 3.09 nm, before curing suggested that the rubber chains had intercalated into the clay gallery under the shear forces present during mixing. However after curing the rubber, the XRD peak appeared at 2θ = 2.55°, corresponding to 3.46 nm *d* spacing - lower than the *d* spacing measured for the uncured rubber at 5.66 nm.

Clearly, there was a reduction of 2.2 nm in *d* spacing, indicating that the rubber chains were pulled out of the interlayer spacing during the curing process. However in spite of this

reduction, there was intercalation of the clay particles by the rubber chains in the SR/C20 nanocomposites. The full explanation of this phenomenon is not clear at the moment. It is possible to explain the effect of curing state on exfoliation/intercalation mechanism based on TEM image but the analysis was not carry out in this study.

4.6.3 Differential scanning calorimetry (DSC)

It was suggested that the transformation of clay layers into individual platelets could happen spontaneously during the curing process. Thus it is worthy to validate the exfoliation mechanism under thermal treatment by DSC analysis. Fig. 4.14 presents DSC traces of SR + C30B mixture, SR + peroxide mixture and SR/C30 cured compound.

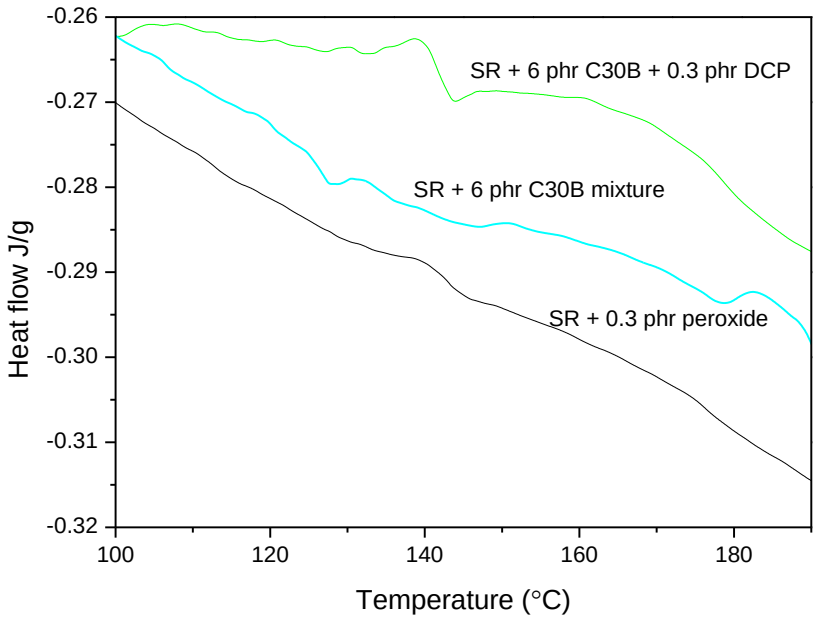

Fig. 4.13: DSC traces of SR + C30B mixture, SR + peroxide mixture and SR/C30 cured compound

This process is presented as an exothermic peak. The heat or energy involved in such a reaction could be determined by integrating the area of the calorimetric peak. Table 4.2 summarises the onset (T_0) and end set (T_e) of crosslink reaction temperature and the peak temperature, and the enthalpy of cure reaction obtained from the DSC analysis.

Table 4.2: DSC cure parameters of the SR+ C30B mixture, SR + peroxide and high extent of exfoliation SR/C30B nanocomposite

Compound	Temperature (°C)			Enthalpy of cure reaction (J/g)
	T_{onset}	T_p	T_e	
SR + C30B mixture	137	157	178	0.7
SR+ peroxide	147	156	165	3.5
High extent of exfoliation SR/C30B (SR + C30B + peroxide)	144	157	170	6.4

The SR/C30B (6 phr) containing exfoliated particles was selected for this analysis and the results were compared with the control (SR + peroxide) and the SR + C30B mixture. As Table 4.2 shows, the SR + C30B mixture produced about 0.7 J/g enthalpy value under the same thermal treatment. The amount of C30B in the SR + mixture was 6 phr, similar to that of the SR/C30B nanocomposite. Considering that no curing reaction occurred in the SR + C30B mixture the small enthalpy values generated from the uncured SR + C30B sample can be related to the favourable interaction between polymer chain and the filler.

For the control sample, amount for enthalpy value of cure reaction was 3.5 J/g. Since the volume of peroxide present in the SR/C30B nanocomposite was equivalent to the amount of peroxide in the control sample it was assumed the degree of the curing reaction in the SR/C30B was comparable with the control sample. However, in this case SR/C30B exhibited 83% higher enthalpy values when compared to the control. It is believed the extra enthalpy values were produced from the chemical interaction between C30B and the silicone

rubber. This result was observed for SR + C30B mixture as discussed earlier. Such a reaction was assumed to be an induced high extent exfoliation process in the SR/C30B (6 phr) nanocomposite, resulting in increased enthalpy values. In addition the high extent exfoliation was also confirmed by XRD and TEM analyses. When the results from the XRD, TEM, FTIR and DSC analyses were analysed, it was concluded that the exfoliation of the clays in the silicone matrix could not be fully explained using the layer-by-layer mechanism proposed for most rubber nanocomposites [17]. It may therefore be assumed that the exfoliation of the clays occurred via a number of mechanisms that can be explained based on thermodynamic point of view.

According to Vaia and Giannelis [22], once a polymer chain enters between the two clay platelets, there will be a substantial loss of entropy due to a formation of new confined chains. Thus, the organoclays platelet tends to separate from each other if the interaction between the polymer chain and the clay platelet is favourable. This will result enthalpy to increase [23-24]. A variation of enthalpy and entropy interactions is associated to the change of free energy which is lead to a formation of immiscible, intercalated or exfoliated nanocomposite [23].

For example, if the internal interactions between polymer and polymer or particle and particle are strong therefore intercalation and exfoliation is prevented. In the other case, if the polymer and particle interaction is stronger than internal interactions it will drive to intercalation rather than exfoliation [24]. This is because the strong interaction between rubber and plates surface contributes to intercalation as it attach the clay plates together thus prevents the clay from exfoliation. Gary and Clois [24] suggested that the interaction of particle-polymer should be at least slightly stronger than the internal energies to form exfoliation. In addition, the ideal situation to form high yield exfoliation could be achieved by controlling the number of strongly active sites of clay through surface modification in order to prevent further bonding to a second plate of clay [24].

4.7 Cure characteristics of the SR/clay nanocomposites

Table 4.3 summarises the cure characteristics of the SR/clay nanocomposites. Effect of clay type and clay loading on the scorch time, t_{s2}, optimum cure time, t_{95}, cure rate index (CRI: $100/t_{95}-t_{s2}$), the maximum and minimum torques (M_H and M_L, respectively), and Δtorque (Δtorque = M_H − M_L) was investigated. For the SR/C30B and SR/C20A nanocomposites, the scorch and optimum cure times changed noticeably in comparison with the neat SR. For example, the SR/C30B nanocomposite showed a decreased in scorch time by approximately 21% at 12 phr filler loading. Similarly, for the SR/C20A nanocomposite, there was a reduction of 18% in the scorch time at the same filler loading.

On the other hand, the optimum cure time increased gradually as the filler loading was raised. For instance, the largest increase was recorded for the SR/C20A nanocomposite with 12 phr filler. These changes were attributed to the ability of the peroxide radicals to react with the functional groups of the organic surfactants in the C30B and C20A organoclays that consequently affected the vulcanisation times. This result was consistent with the cure rate index (CRI) values which had steadily decreased as the amount of filler increased. Note that low CRI value indicated low rate of cure. Thus it was suggested that the addition of organo modified MMT reduced the peroxide vulcanisation efficiency.

However, this phenomenon was not seen when untreated clay Na^+MMT was used in the rubber. In fact the cure time for SR/Na^+MMT was almost consistent with the pure SR. The CRI values of SR/Na^+MMT were less affected as the amount of filler increased. A similar observation was also reported regarding the effect of organic modified clays on the vulcanization process of SR/clay nanocomposites, but with a different curing system. Voulomenou and Tarantili [4] claimed that there was a possible interaction between the curing agent and the organic moiety on the organoclay surface, instead of interaction between the curing agent and the rubber chains, which resulted in an increase in the vulcanisation time.

Table 4.3: Cure characteristics of neat SR and SR/clay nanocomposites

Sample	Cure characteristics @ 160°C					
	Cure time T_{95} (min)	**Scorch time T_{S2} (min)**	**CRI $100/T_{95}-T_{S2}$ (min^{-1})**	**Max Torque M_H (dNm)**	**Min Torque M_L (dNm)**	**Delta Torque ΔM (dNm)**
neat SR	7.24	3.13	24.33	23.19	1.90	21.29
SR/Na^+ - 4 phr	7.49	3.28	23.75	24.81	2.00	22.81
SR/ Na^+ - 6 phr	7.23	3.32	25.58	25.42	2.02	23.40
SR/ Na^+ - 8 phr	7. 54	3.25	23.31	25.77	2.25	23.52
SR/ Na^+ - 10 phr	7.33	3.14	23.87	26.42	2.36	24.06
SR/Na^+ - 12 phr	8.30	3.24	19.76	26.08	2.29	23.79
SR/C30B - 4 phr	12.03	3.04	11.12	23.41	1.98	21.43
SR/C30B - 6 phr	10.14	2.57	13.21	22.52	1.91	20.61
SR/C 30B - 8 phr	10.29	2.41	12.69	21.83	2.40	19.43
SR/C 30B - 10 phr	10.54	2.48	12.41	21.76	2.41	19.35
SR/C 30B - 12 phr	12.06	2.48	10.44	20.64	2.21	18.43
SR/C20A - 4 phr	7.51	2.59	20.33	22.18	1.89	20.29
SR/C20A - 6 phr	9.28	2.58	14.93	21.16	1.94	19.22
SR/C20A - 8 phr	10.49	2.60	12.67	19.81	2.70	17.11
SR/C 20A - 10 phr	10.21	2.53	13.02	20.51	2.41	18.10
SR/C20A - 12 phr	12.27	2.54	10.28	19.21	2.48	16.73

The minimum torque (M_L), maximum torque (M_H) and Δ torque of the nanocomposites and pure SR were also compared. In all cases inclusion of the fillers in the rubber increased the M_L, which related to increased viscosity. Note that both the maximum torque (M_H) and Δ torque are indication of crosslink density changes in the rubber. The incorporation of Na^+MMT into the rubber increased the M_H and Δ torque by about 13% and 12%, respectively when the filler loading reached 12 phr. The increase of M_H and Δ torque with the clay loading suggested that the pristine MMT increased the crosslink density of the rubber and consequently raised the stiffness and modulus of the nanocomposite.

The inclusion of C30B and C20A had an adverse effect on the M_H and Δ torque of the rubber. It can be seen that both M_H and Δ torque values of these nanocomposites steadily declined as a function of the filler loading. As mentioned earlier, there is a possibility that the

reactive functional groups in the organoclays interfered with the curing process by reacting with the free radicals of peroxide. As a result, there was less peroxide left to react with the rubber chains to form crosslinks reducing the extent of the cure in the rubber.

Similar results with regard to the effect of unmodified clay (MT) and organically modified clay (OMMT) fillers on the curing properties of a silicone rubber were reported by Kaneko and Yoshida [10]. They proposed that the increase of crosslink density in PDMS/MT was attributed to a nucleation reaction between Si-OH groups on the MT clay and the Si atoms of the silicone rubber chains. They concluded that the silanol-terminated PDMS fragments and silicone rubber chain scission were formed from this reaction. The chain fragments then interacted with other hydroxyl groups from other silicone chains, or even with the hydroxyls on the MT clay surface, resulting in an increase in the crosslink density of the rubber.

4.8 Conclusions

SR/clay nanocomposites have been successfully produced via melt-mixing, based on a variety of montmorilonite filler and with regard to chemical functionality. It has been shown, in systems based on silicone rubber (PDMS) and montmorillonite fillers, that compatibility between rubber and filler, and the size of *d* spacing of the nanoclays, are insufficient to produce exfoliated or intercalated nanocomposite.

The experimental results show that there are two key factors which determine the ultimate structure of the SR/clay nanocompsites. The first is the level of filler concentration, regardless of the chemical functionality on the filler. For organo modified MMT (i.e C30B and C20A), formation of highly exfoliated and intercalated nanocomposites was achieved at low filler loading (<8 phr). In addition a mixture of intercalated/exfoliated clay structures was observed in the nanocomposite containing unmodified Na^{+}MMT when the filler was added, up to 6 phr.

The second factor is the presence of favourable interactions between the silicone rubber backbone and the functional group on the filler surface. It has been suggested that the

establishment of an interaction, such as hydrogen bonding, facilitates the exfoliation process in the SR/C30B nanocomposite. This result is consistent with FTIR and DSC analysis. It was evident that the formation of an exfoliated structure in the SR/clay nanocomposites was a spontaneous process that happened during vulcanisation and not during the mixing stage.

In spite of the fact that excellent clay dispersion was achieved in the nanocomposites containing C30B and C20A at the optimum level of filler concentration, they exhibited some adverse effects on the curing process. The interference of organo modifier delayed the onset of curing, reducing cure efficiency. In addition a decrease in the torque value, related to the reduction of crosslink density, was observed in both the SR/C30B and SR/C20A nanocomposites. However the use of Na^+MMT in silicone rubber had no negative effect to peroxide curing efficiency. In fact, the Na^+MMT displayed increased crosslink density of the nannocomposites, as indicated by the delta torque value.

4.9 References

1. Simon MW, Stafford KT, Duan LO. Nanoclay Reinforcement of Liquid Silicone Rubber. *Journal Inorganic Organometealic Polym*er 2008; 18: 364-373.

2. Roy N, Bhowmick AK. Novel in situ polydimethylsiloxane-sepiolite nanocomposites: Structure-property relationship. *Polymer* 2010; 51: 5172-5185.

3. Schmidt DF, Clément F, Giannelis, EP, On the Origins of Silicate Dispersion in Polysiloxane/Layered-Silicate Nanocomposites. *Advenced Functional Matererials* 2006; 16: 417–425.

4. Voulomenou A, Tarantili P A. Preparation, characterization, and property testing of condensation-type silicone/montmorillonite nanocomposites. *Journal of Applied Polymer Science* 2010; 118: 2521–2529.

5. Lebaron PC, Pinnavaia TJ. Clay Nanolayer Reinforcement of a Silicone Elastomer. *Chemistry Material* 2011; 13: 3760–3765.

6. Kim ES, Kim EJ, Lee TH. Yoon, JS. Clay modification and its effect on the physical properties of silicone rubber/clay composites. *Journal of Applied Polymer Science* 2012; 125: E298–E304.

7. Jincheng W, Wenli H. Effect of organic modification on structure and properties of room-temperature vulcanized silicone rubber/montmorillonite nanocomposites. *Journal of Applied Polymer Science* 2013; 129: 1852–1860.

8. Mishra S. Shimpi N. Mali AD. Surface modification of montmorillonite (MMT) using column chromatography technique and its application in silicone rubber nanocomposites. *Macromolecule Res*earch 2012; 20 (1): 44-50

9. Pradhan B, Srivastava SK, Ananthakrishnan, R. Saxena, A. Preparation and characterization of exfoliated layered double hydroxide/silicone rubber nanocomposites. *Journal of Applied Polymer Science* 2011; 119: 343–351.

10. Schmidt DF, Giannelis EP, Silicate Dispersion and Mechanical Reinforcement in Polysiloxane/Layered Silicate Nano composites. *Chemistry Material* 2010; 22(1) : 167–174

11. Kaneko MLQA, Yoshida IVP. Effect of Natural and Organically Modified Montmorillonite Clays on the Properties of Polydimethylsiloxane Rubber. *Journal of Applied Polymer Science* 2008; 108: 2587-2596.

12. Vaulot C, Ziegler P, Haidar B, Physicochemical driving forces behind exfoliation process of a synthetic montmorillonite in PDMS polymers. *Polymer* 2011; 52: 700-707.

13. Madejova J. FTIR techniques in clay mineral studies. *Vibrational Spectroscopy* 2003; 31(1): 1-10

14. Vazquez A, López M, Kortaberria G, Martín L, Mondragon I. Modification of montmorillonite with cationic surfactants. Thermal and chemical analysis including CEC determination. *Applied Clay Science* 2008; 41: 24–36.

15. Kaneko MLQA, Romero RB, Goncalves MC, Yoshida IVP. High molar mass silicone

rubber reinforced with montmorillonite clay masterbatches: Morphology and mechanical properties.*European Polymer Journal* 2010; 46 (5): 881-890.

16. Jia C, Zhang LQ, Zhang H, Lu YL. Preparation, microstructure, and property of silicon rubber/organically modified montmorillonite nanocomposites and silicon rubber/OMMT/fumed silica ternary nanocomposites. *Polymer Composite* 2011; 32: 1245–1253.

17. Paul DR, Robeson LM. Polymer nanotechnology: Nanocomposites. *Polymer* 2008; 49(15): 3187–3204.

18. Southern clay. Product bulletin Cloisite. http://www.scprod.com/product_bulletins. (accessed on 10 Dec 2013)

19. Pavlidou S, Papaspyrides CD. A review on polymer–layered silicate nanocomposites. *Proggress Polymer Science* 2008; 33(12): 1119-1198.

20. Pradhan B, Srivastava SK, Ananthakrishnan R, Saxena A. Preparation and characterization of exfoliated layered double hydroxide/silicone rubber nanocomposites. *Journal of Appied Polymer Sci*ence 2011; 119: 343–351.

21. Wu YP, Ma Y, Wang YQ, Zhang LQ. Effects of Characteristics of Rubber, Mixing and Vulcanization on the Structure and Properties of Rubber/Clay Nanocomposites by Melt Blending. *Macromolecule Material Engineering.* 2004; 289(10): 890-894.

22. Vaia RA, Giannelis, EP. Lattice Model of Polymer Melt Intercalation in Organically-Modified Layered Silicates. *Macromolecules.* 1997; 30 (25): 7990–7999.

23. Ginzburg VV, Weinhold JD, Jog PK, Srivastava R. Thermodynamics of Polymer−Clay Nanocomposites Revisited: Compressible Self-Consistent Field Theory Modeling of Melt-Intercalated Organoclays. *Macromolecules* 2009; 42(22): 9089–9095.

24. Garry WB, Clois EP. Thermodynamics and kinetics of polymer-clay nanocomposites. In. *Fundamentals of Polymer/clay nanocomposites*. Cambridge, UK: University Press; 2011. 17-20

CHAPTER 5: Mechanical properties of silicone rubber/clay nanocomposites

5.1 Introduction

Silicone rubber/clay nancomposites were prepared and cured at 160°C, then the interlayer spacing, *d*, of the clay particles in the rubber matrix was measured by X-ray diffraction spectroscopy (as explained in the Chapter 4). A range of mechanical tests were used to evaluate the mechanical properties of the nanocomposites, such as tensile strength, Young's modulus, elongation-at-break, hardness, tensile hysteresis and abrasion resistance.

In this chapter the effect of the filler loading on the mechanical properties of the rubber vulcanizate is investigated. In addition, for a better understanding of the reinforcing mechanism of the clays, fresh insight into the way intercalated and exfoliated morphologies change the mechanical properties of the rubber nanocomposites is also discussed. The term exfoliated in this chapter is referring to high extent of exfoliation.

5.2 Tensile properties of SR/clay nanocomposite as a function of the clay loading

Fig.5.1 displays the tensile strength of unfilled SR and SR/clay nanocomposites as a function of filler loading. As expected, the pure SR possessed very poor mechanical properties and this was attributed to the structure of the rubber, which could not readily crystallise on stretching and has low intermolecular force [1]. It can be seen that tensile

strength was increased by increasing the Na^+MMT clay loading. For example, the addition of Na^+ MMT even at very low loading (4phr) improved the tensile strength from 0.40 to 0.59 MPa. Interestingly, the tensile strength value is almost similar to the SR filled with 30 phr of natural montmorillonite prepared by Kaneko and Yoshida [2]. In addition, the maximum tensile strength (0.83 MPa) was obtained when the loading of Na^+MMT reached 12 phr, two times as high as that of pure SR.

In contrast, the tensile strength for nanocomposites reinforced by C30B and C20A increased as a function of clay content, but slightly declined when reaching 12 phr. However a limited improvement was achieved by incorporating C30B and C20A organoclays, when compared to the SR filled with Na^+MMT. The result suggests that Na^+MMT seems to be the most effective layered silicate in improving the tensile strength of silicone rubber/clay nanocomposites.

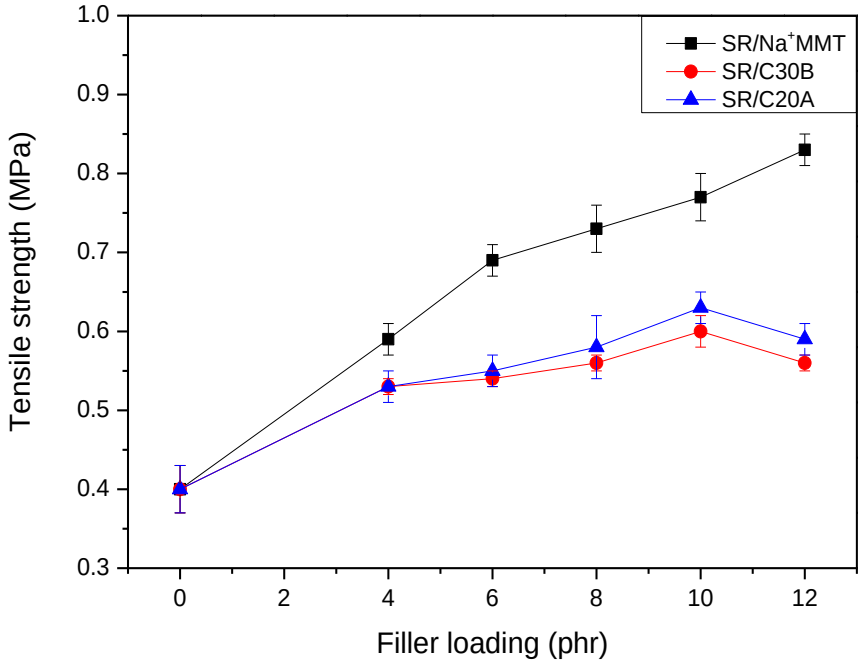

Fig.5.1: Tensile strength of neat SR and SR/clay nanocomposites

Fig. 5.2 presents the Young's modulus of neat SR and SR/clay nanocomposites as a function of clay content. The trend of Young's modulus was similar to the tensile strength. As

Fig. 5.2 shows, the Young's modulus of the SR/Na^+MMT nanocomposite was higher than that of the SR/C30B and SR/C20A nanocomposites with increased filler loading. For example, the addition of up to 12 phr Na^+MMT improved the Young's modulus to 0.45 MPa from 0.28 MPa (pure SR), an improvement of about 60% (Fig.5.2).

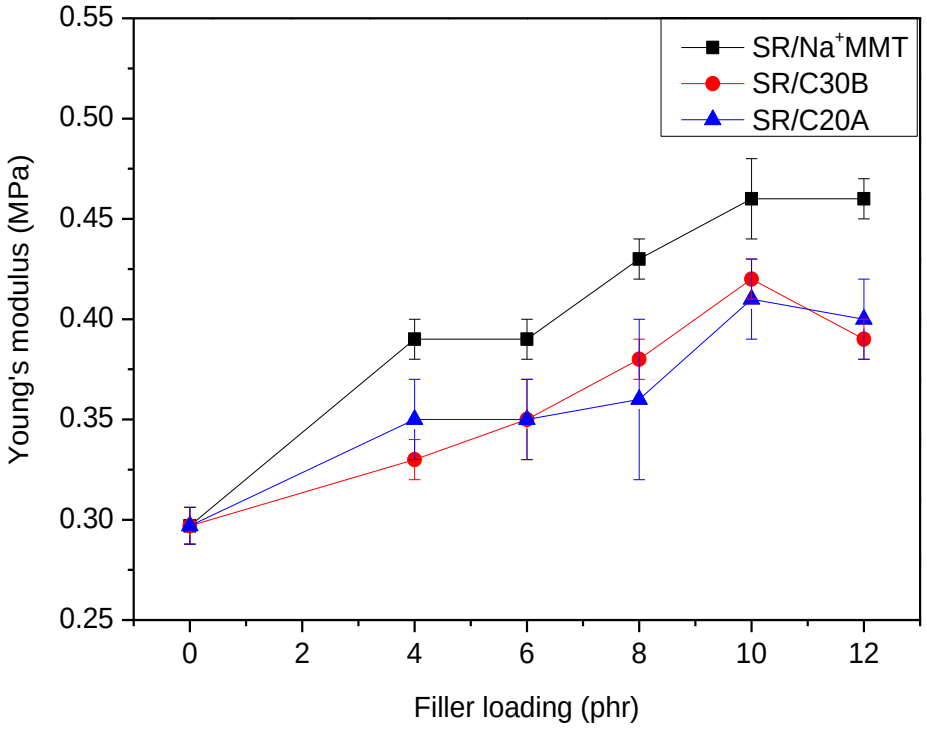

Fig.5.2: Young's modulus of neat SR and SR/clay nanocomposites

What is surprising is that the exfoliated SR/C30B and SR/C20A nanocomposites did not possess particularly high tensile strength or Young's modulus, even though excellent filler dispersion was seen in the rubber. A major improvement in tensile strength and Young's modulus was still seen in the SR/Na^+MMT nanocomposites. However, Na^+MMT had a higher tendency to produce a mixture of intercalated/exfoliated microstructures compared to the other fillers. Therefore the results of this study suggest that intercalated and exfoliated nanostructures in SR/C20A and SR/C30B do not provide a major contribution to the reinforcement in SR.

As discussed in section 4.6, the SR/Na^+MMT possessed higher crosslink density than most of the SR/C30B and SR/C20A nanocomposites. It can therefore be assumed that the enhancement of the tensile strength and Young's modulus in this particular nanocomposite was dominated by the degree of crosslink density instead of filler dispersion. This suggested that the physical and chemical crosslink play a more important role in determining the tensile strength of the nanocomposite.

The present findings seem to be consistent with other research which also found that dispersion state of the montmorrilonite does not affect the strength of the nanocomposite [3]. Schmidt and Giannelis [3] speculated that the level of reinforcement in SR/clay nanocomposite was determined by interfacial strength, derived from interactions between siloxane bonds in the silicone rubber chains and the silanols presents at the edges of the natural montmorillonite platelets. This hypothesis was supported by the sum of the equilibrium solvent uptake and mechanical properties measured [3].

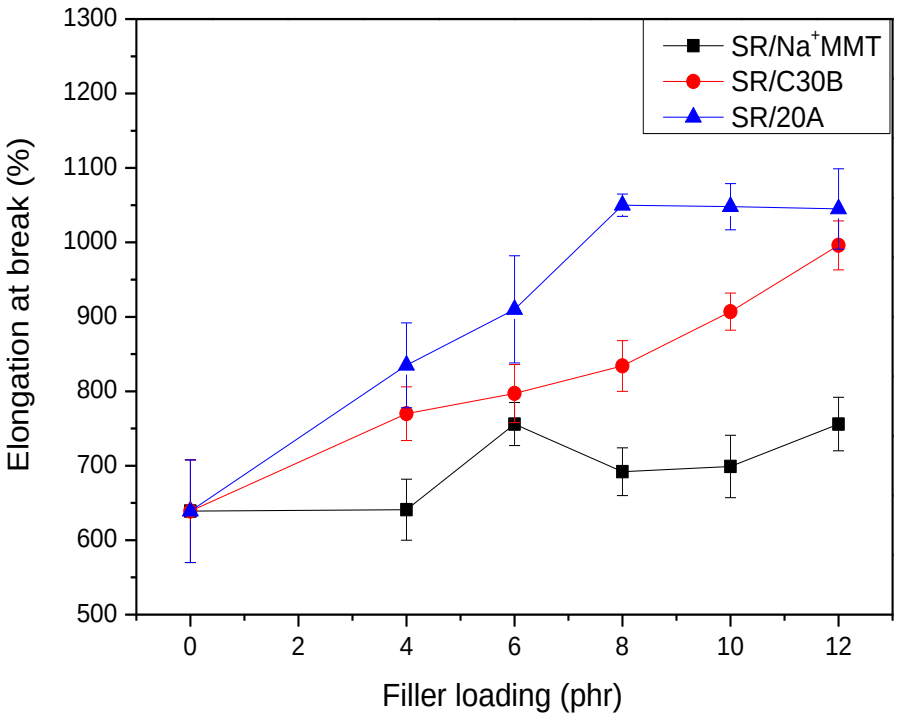

Fig.5.3: Elongation at break of neat SR and SR/clay nanocomposites

Fig. 5.3 exhibits elongation-at-break of the neat SR and SR/MMT nanocomposites. From the graph above it can be seen that elongation-at-break of improved significantly with progressive increases in the loading of the clays, irrespective of the type of the clay used. It is also worth pointing out that the opposite trend regarding effect of clay loading on elongation-at break-was highlighted in the previous study [2]. Kaneko and Yoshida [2] reported that elongation-at-break of SR filled with natural or modified montmorillonite was reduced significantly with increasing the filler loading (from 0 phr up to 30 phr). However, in this case, there was a large improvement in the elongation-at-break of the SR/C20A nanocomposite, particularly at high filler loadings. For example, elongation-at-break improved by 64% when 8 phr of the filler was incorporated into the rubber. Notably there was no further improvement in this property when the loading of the filler reached 12 phr.

The SR/C30B and SR/Na^+MMT nanocomposites exhibited a similar trend but the values were lower for the latter. These results indicated that elongation-at-break was largely influenced by the dispersion of the clays in the rubber matrix. On this basis, intercalated C20A improved the elasticity of the elastomeric matrix more significantly than the exfoliated C30B and intercalated/exfoliated Na^+MMT did.

SR filled with Na^+MMT nanocomposites have a high crosslink density, followed by SR/C30B nanocomposites. This suggested that inferior elongation-at-break of the SR/Na^+MMT nanocomposite was due to restricted deformation during the stretching process, as a result of high crosslink density in the SR/Na^+MMT nanocomposite It was concluded that elongation-at-break was dependent on the state of dispersion of the clays, as well as the crosslink density of the rubber. However, the crosslink density had an even a bigger influence on the rubber properties.

5.3 Hardness

Fig. 5.4 shows hardness of neat SR and SR/MMT nanocomposites at various filler loadings. A significant improvement in the hardness from 18 Shore A (pure SR) to

22 Shore A was measured for the SR/Na^+MMT nanocomposite, as a function of the clay loading. It was found that the increase in hardness was consistent with increases in the Young's modulus of the nanocomposites. By contrast the hardness of the SR/C30B and SR/C20A nanocomposites did not improve any more above the 4 phr loading of the fillers, and remained essentially unchanged with further increases in loading.

However, the inclusion of these fillers did improve the hardness when the results were compared with that of the pure SR (18 Shore A). Since hardness is influenced also by crosslink density, the lower hardness of these two nanocomposites was attributed to a lower crosslink density, as indicated by the Δ torque values as discussed in the Chapter 4.

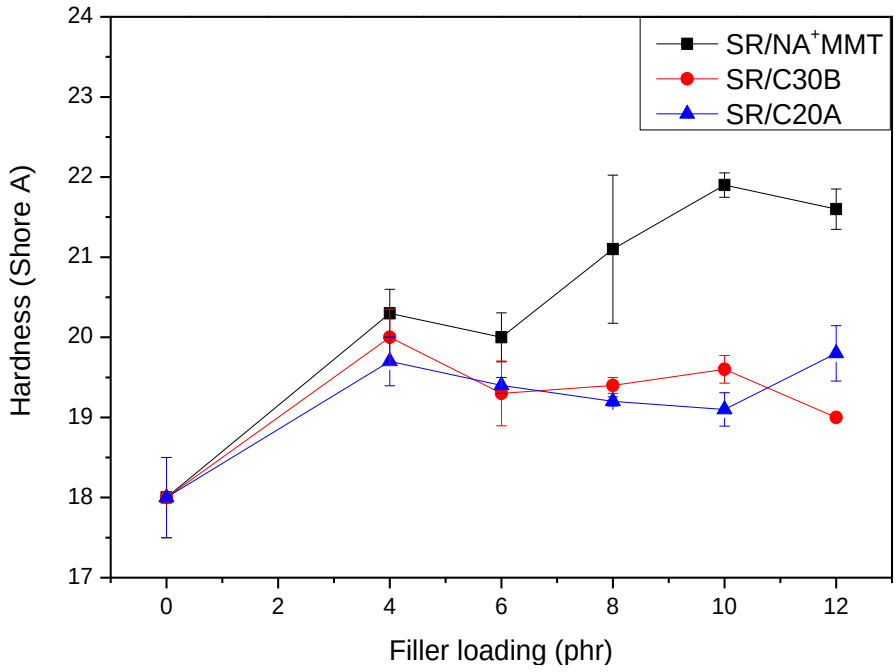

Fig.5.4: Hardness of neat SR and SR/clay nanocomposites

5.4 Store energy density at break (toughness)

Fig. 5.5 is a schematic representation of store energy density at break from a typical stress-strain curve. Stored energy density at break is a measure of the energy stored per unit volume in the rubber before the sample finally breaks. This property indicates the resistance of the rubber to crack initiation and growth. The stored energy density at break

was calculated from the area under the stress-strain curve (Fig. 5.5) using the trapezium rule as described in section 3.6.2.

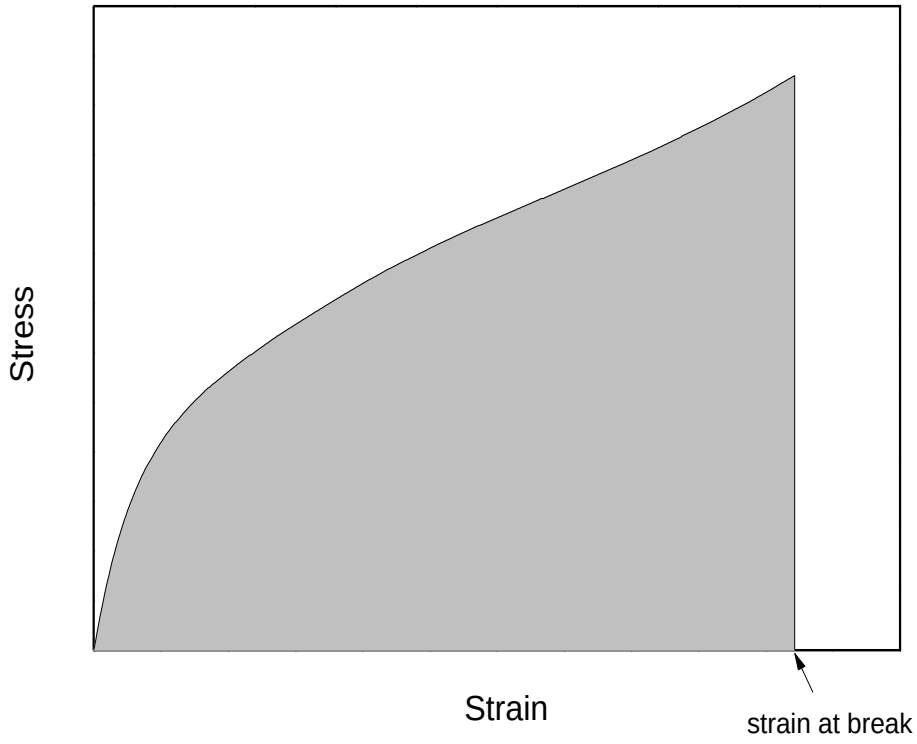

Fig. 5.5: Schematic representation of store energy density at break

Fig. 5.6 shows store energy density of the pure SR and SR/MMT nanocomposites as a function of clay content. As shown, addition of the fillers improved the stored energy density at break of the rubber substantially. But this property only marginally improved for the SR/C20A and SR/C30B nancomposites when the loading of the fillers was increased from 4 to 6 phr in the rubbers. The stored energy density at break continued increasing in the following order, SR/C20A nanocomposite > SR/C30B nanocomposite > SR/Na^+MMT nanocomposite, as the loading of the fillers was raised further from 8 to 10 phr. There was no additional improvement in the stored energy density at break of the SR/C20A nancomposite when the loading of the filler was increased to 12 phr. With regard to the dispersion state of the nanocomposites prepared, the trend suggests that intercalated

SR/C20A nanocomposite give more beneficial to the store energy density. This indicates that the C20A nanocomposites would have good tear resistance.

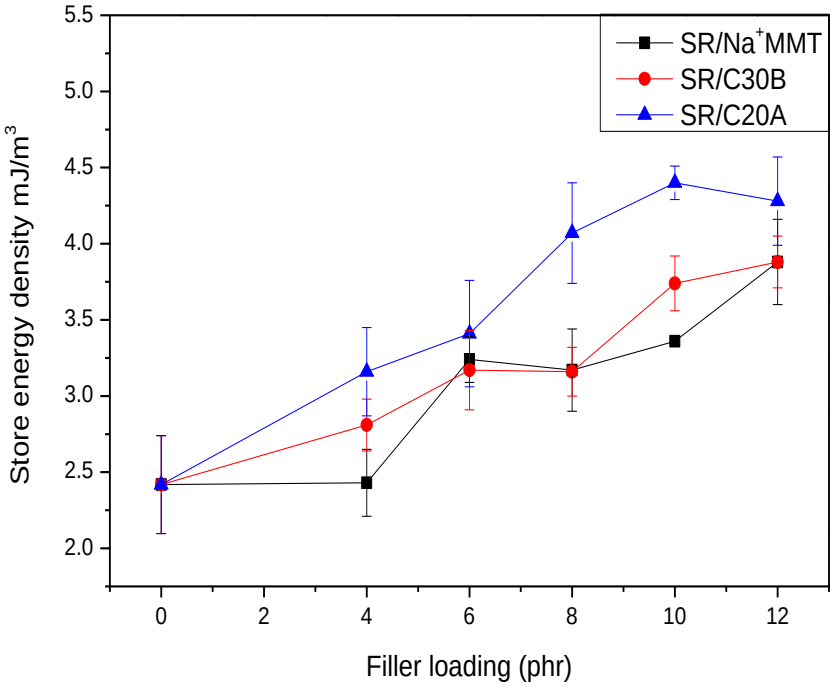

Fig.5.6: Store energy density of neat SR and SR/clay Nano composites

5.5 Hysteresis in the pure SR and clay/SR nanocomposites

When rubber is deformed, it stores energy. However because it is a viscoelastic material some of the energy is dissipated as heat in the rubber. This is termed hysteresis. Hysteresis is measured from the area under a stress versus strain graph produced during a single stress-strain cycle. To measure hysteresis in the rubbers, standard dumbbell test pieces were cycled repeatedly, up to 10 cycles at different strain amplitudes, reaching 400% to generate stress-strain traces. For this experiment, hysteresis was measured among the SR/Na^+MMT, SR/C30B and SR/C20A containing 6 phr of filler. The result was compared with unfilled rubber as a control.

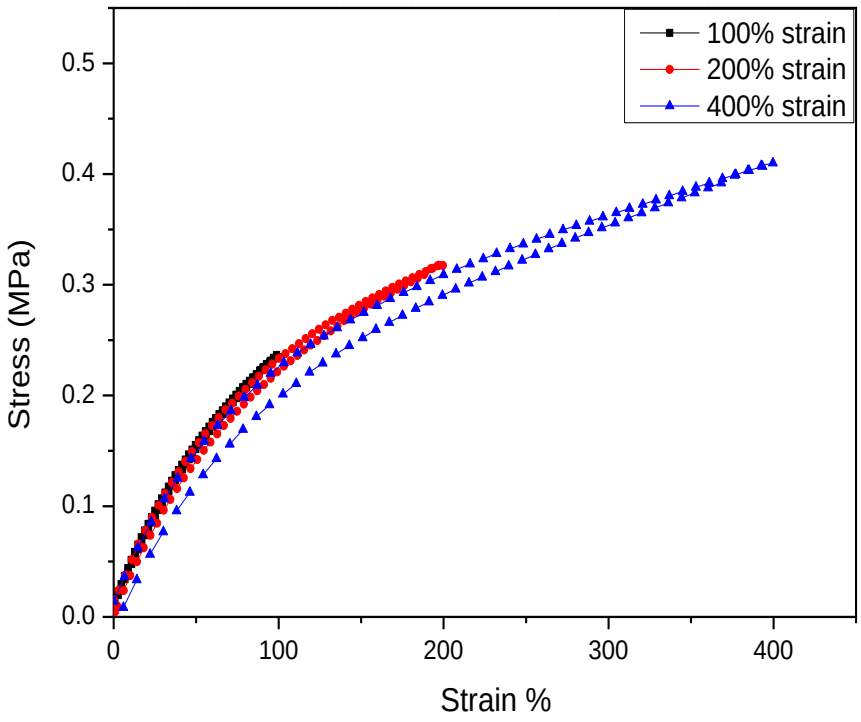

Fig. 5.7: Typical hysteresis curves after the first stress versus strain cycle.

Fig. 5.7 shows typical stress-strain curves for the unfilled rubber after the 1st cycle at different strain amplitudes and the hysteresis loops from which the energy loss in the rubber was calculated. It can be seen that the hysteresis loop enlarged as the level of the applied strain amplitude on the rubber was raised. This indicates that the energy dissipated in the rubber depends on the level of the applied strain amplitude.

Fig 5.8 displays stress-strain curves in deformation of 400% for loading and unloading cycle for the neat SR and SR/MMT nanocomposites (1st cycle and 10th cycles). At a given strain amplitude the hysteresis loop after the 1st cycle was significantly larger in magnitude than that in the 10th cycle as seen in Fig. 5.8.

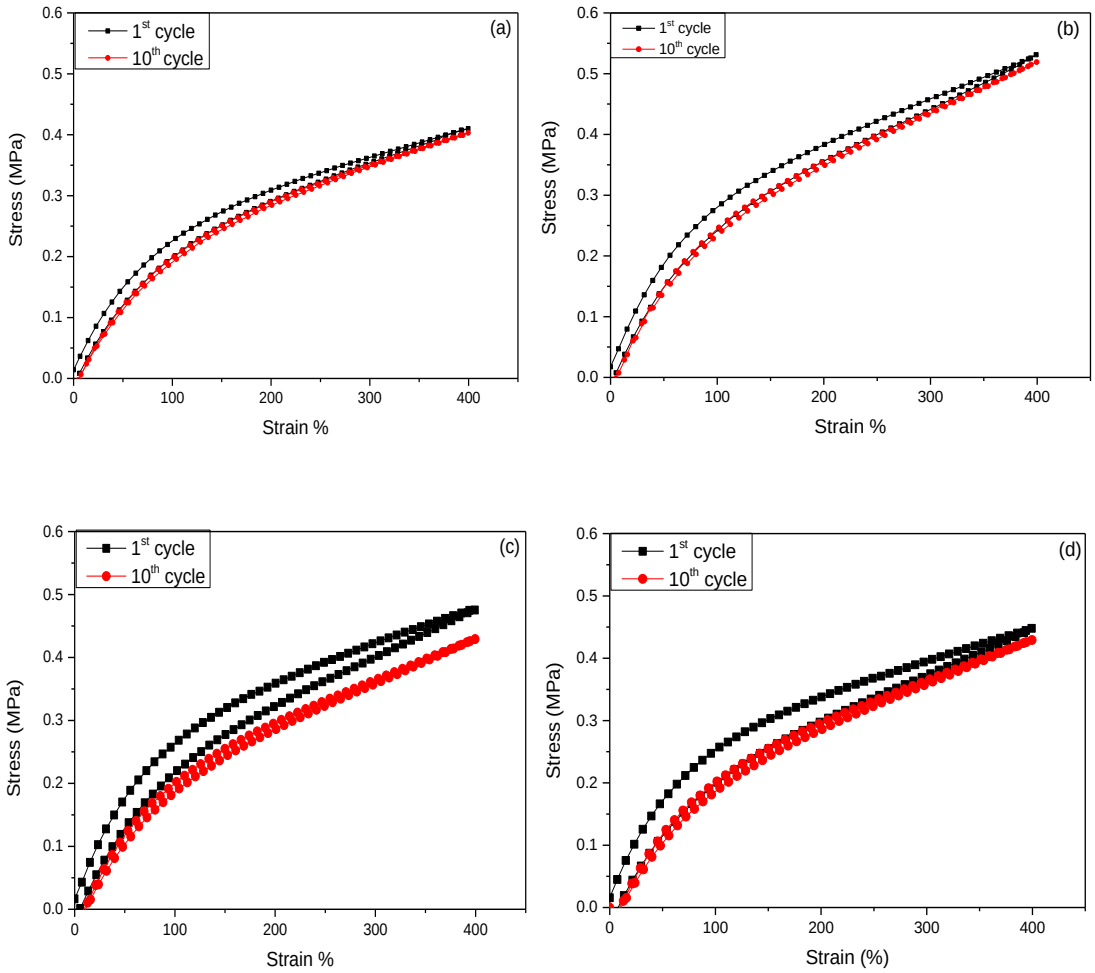

Fig. 5.8: Stress-strain curves in deformation of 400% for loading and unloading cycle (1^{st} cycle and 10^{th} cycles) for the (a) neat SR (b) SR/Na^{+}MMT (c) SR/C30B and (d) SR/C20A nanocomposites.

Table 5.1 compares the dissipated energy of neat SR and SR/MMT nanocomposites measured from the loop area in Fig. 5.8.We can see that the energy loss of the neat SR reduced from 97 to 39 mJ/m^3 at 400% strain amplitude approximately a 60% difference. A similar trend was also observed for the SR/MMT nanocomposites, irrespective of clay type. For example, after the 10th cycle at 400 % strain amplitude, the energy loss in the SR/C20A, SR/C30b and SR/Na^{+}MMT nanocomposite decreased by up to 67 %, 66% and 64% respectively.

Generally, fillers cause energy dissipation or hysteresis in rubber. Clearly in this case the inclusion of the clays induced more energy dissipation compared to the pure SR.

However highly exfoliated SR/C30B and intercalated/exfoliated SR/Na^+MMT nanocomposites displayed lower energy loss when compared with the intercalated SR/C20A nanocomposite (as shown in Table 5.1). For example, in the 1st cycle at 400% strain amplitude, the intercalated SR/C20A nanocomposite had energy loss of about 174 mJ/m^3 whereas the exfoliated SR/Na^+MMT and SR/30B nancomposites had energy losses of 139 and 161 mJ/m3, respectively.

Table 5.1: Hysteresis or energy losses in neat SR and SR/clay nanocomposites

Strain amplitude %	**Dissipated energy, ΔE (mJ/m^3)**							
	Neat SR		**SR/Na^+MMT**		**SR/C30B**		**SR/C20A**	
	1st cycle	**10th cycle**	**1st cycle**	**10th cycle**	**1st cycle**	**10th Cycle**	**1st cycle**	**10th cycle**
100	7	3	7	3	10	3	12	8
200	28	12	36	12	44	16	48	17
400	97	39	139	49	161	55	174	57

Two possible mechanisms explain this phenomenon. In a nanocomposite the energy loss is caused by internal friction between macromolecular chains and the friction between rubber chains and layered clay. For an exfoliated nancomposite high surface area of a single clay platelet generates stronger interaction with the rubber chains. This contributes to less frictional movement between the two during the deformation process. As a result only a small amount of energy is dissipated as heat in the exfoliated nanocomposite. However in an intercalated morphology there is much less interaction between the rubber chains and the clay platelets, and therefore the rubber chains are free to move when deformation is applied. This free movement will generate more frictional heating or hysteresis in the rubber.

From the results it can be seen that hysteresis in the nanocomposites depends strongly on the state and dispersion of the clay fillers in the rubber. The nanocomposites containing exfoliated clays exhibited low hysteresis compared with the one containing intercalated clays (Table 5.1). This finding is in line with the previous works reported for polyurethane (PU)/clay nanocomposite [4, 5]. The authors proposed that the energy dissipation in the PU/clay nanocomposite was determined by the viscoelastic nature of the pure PU chains and also the orientation of the silicate layer platelets [4, 5]. A similar trend was also seen in some silicone rubbers filled with precipitated silica, suggesting that a strong interaction between the filler particles and rubber chains contributed to low hysteresis, as shown in the dynamic properties [6].

5.6 Abrasion resistance

Generally, abrasion resistance testing is carried out to determine the ability of a material to resist processes of mechanical wear (such as rubbing, scraping, or erosion) that have a tendency to gradually remove material from its surface. Most engineering applications require rubber material which has high abrasion resistance in order to retain its original shape under friction. The addition of filler particles in the rubber matrix has a large influence on the abrasive wear of rubbers [7].

In this work an attempt was made to investigate effect of montmorillonite nanoclay on abrasion resistance of silicone rubber/clay nanocomposites. The abrasion resistance of the pure SR and filled silicone rubber was measured in terms of the percentage of material lost by weight. The procedure regarding the abrasion test is discussed in section 3.6.5. The weight of tested rubber was noted between the start and end of the test. The results were compared between unfilled SR and the SR/Na^+MMT, SR/C30B and SR/C20A nanocomposites, at various filler loadings ranging from 4 phr to 12 phr.

Fig. 5.9 displays the effect of various loadings on percentage weight loss of the SR/MMT nanocomposites. Generally a lower weight loss indicates better abrasion

resistance, and vice-versa. As Fig. 5.9 shows, the percentage of weight loss for the unfilled SR was 25%. After the addition of 4 phr to 6 phr of filler, the percentage weight loss of SR/Na^+MMT, SR/C30B and SR/C20A was found to decrease sharply. For instance SR nanocomposite, containing 6 phr Na^+MMT, exhibited the lowest percentage weight loss (7.5%) followed by SR/C20A (11%) and SR/C30B (13%). However the percentage weight loss progressively increased when the filler amount increased from 8 phr to 12 phr, particularly for SR/C30B and SR/C20A. Note that all fillers exhibited a similar trend where 6 phr filler loading appeared as critical filler loading for all curves.

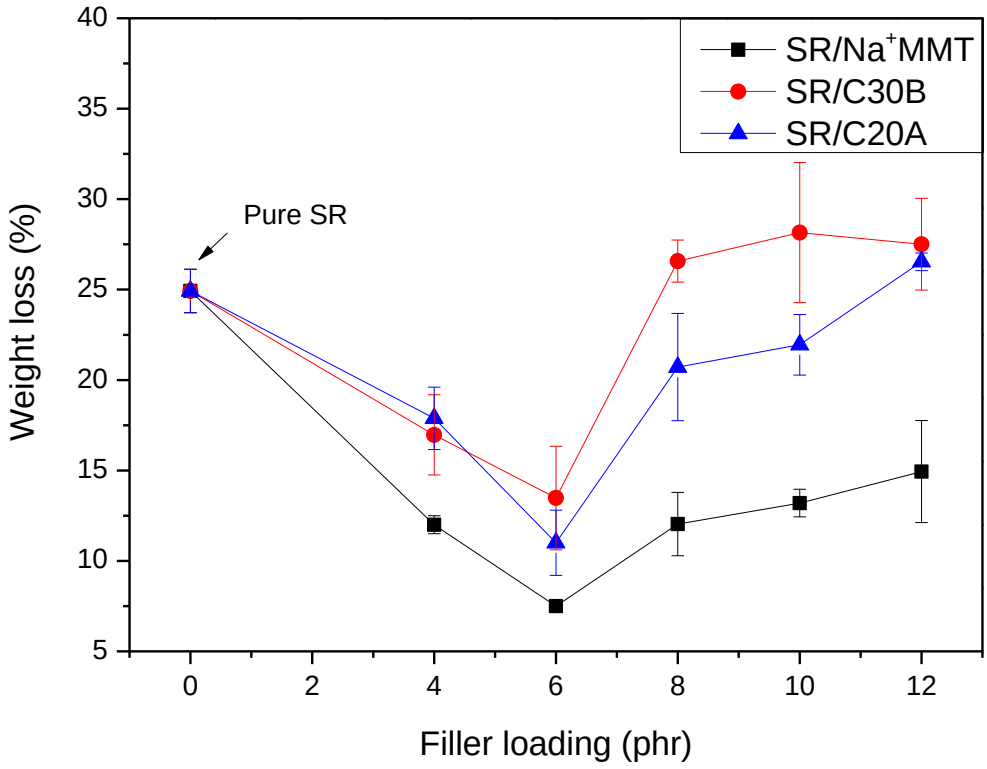

Fig.5.9: Percentage weight loss of SR/MMT nanocomposites at various filler loading.

The result strongly suggests that the abrasion loss reduces slowly until the filler content reaches a break point, known as critical filler loading, after which the abrasion loss starts to increase very quickly with increasing filler loading. However this phenomenon is more pronounced for SR/C30B and SR/C20A. For instance, at the maximum filler loading of

12 phr, the percentage weight loss of SR/C30B and SR/C20A was 28% and 27% respectively, comparable to the pure SR (25%). This phenomenon can be related to filler dispersion in the silicone matrix.

As discussed in section 4.3, C30B and C20A dispersed in nanoscale range at low filler concentration ranging from 4 phr to 6 phr. In principle the smaller particles in the rubber matrix provide a greater surface area. Therefore this result suggests that the enhancement of abrasion resistance for the tested rubber at low filler loadings was probably due to uniform dispersion and better filler-rubber interfacial adhesion. However, fillers tend to agglomerate as concentration increases from 8 phr to 12 phr. This could be the reason why at high filler loadings the rubber shows greater weight loss, indicating poorer abrasion resistance. It is believed that large particles induce more local stress in the rubber matrix due to lack of interfacial bonding. As a result, it is easier to develop crack growth during friction, leading to material loss.

A similar trend was also observed for SR/Na^+MMT nanocomposites, although the weight loss of SR/Na^+MMT was less aggressive with increasing filler loading compared to the other two fillers. The SR/Na^+MMT also exhibited the lowest weight loss (15%) among the other nanocomposites as the filler loading reached 12 phr. It is believed that high covalent bonds are dominant in the SR filled with Na^+MMT, preventing material loss during abrasion tests. The present findings are consistent with previous research which found the degree of wear-loss due to rigid filler particles in the case of silicone rubber is subjected to critical volume fraction [7].

This critical volume fraction divides the wear mechanisms into two regimes [7]. In the first regime, the wear rates of the filled silicone rubbers increase slowly with filler concentration until a critical volume fraction, V_c, is reached, at which point they increase very rapidly with increasing filler concentration. Yang and co-workers [7] speculated that at low filler concentrations, the increase of wear rates was dominated by the neat rubber

properties, except in the cases of effective filler reinforcement. This was because a reduction of wear rate can occur at low filler loading before the critical volume fraction is reached. However in this case effective abrasion resistance was achieved at low filler loading. In the second regime, stress concentration introduced by the rigid particles is favoured, creating a 'damage zone' surrounding the particles that involve micro-cavitation and debonding mechanisms. This explains why weight loss increases with filler loading.

5.6.1 Morphology of worn surface

Further investigation was carried out to observe abraded surfaces of the tested rubber produced during abrasion resistance. Fig. 5.10 (a-d) shows scanning electron microscopy (SEM) images of SR with and without the addition of filler. In this study, a comparison of SR containing different nanoclays was made at a fixed filler loading of 6 phr.

It is apparent that the worn surface of the unfilled SR is rough and the existence of wavy patterns can be seen in Fig. 5.10 a(i-ii). The presence of large holes along the damage zones at the centre of the worn surface of unfiled SR is due to the weakness of unreinforced rubber. One may also observe that the wavy pattern almost disappears for the filled SR, regardless of the filler types, as shown in Fig. 5.10(b-d). This suggests the incorporation of filler in SR changes the basic wear mechanism of the rubber.

By comparing the worn surface of SR/Na^+MMT, SR/C30B and SR/C20A, it can be seen that all the nanocomposites show a similar pattern of wearing, with most of the areas protected from wear damage by embedded particles. Less damaged areas were found on the surface of SR/Na^+MMT (Fig. 5.10b) compared to SR/C30B (Fig. 5.10c) and SR/C20A (Fig. 5.10d). This reflects the lower weight loss measured on SR/Na^+MMT, as discussed earlier.

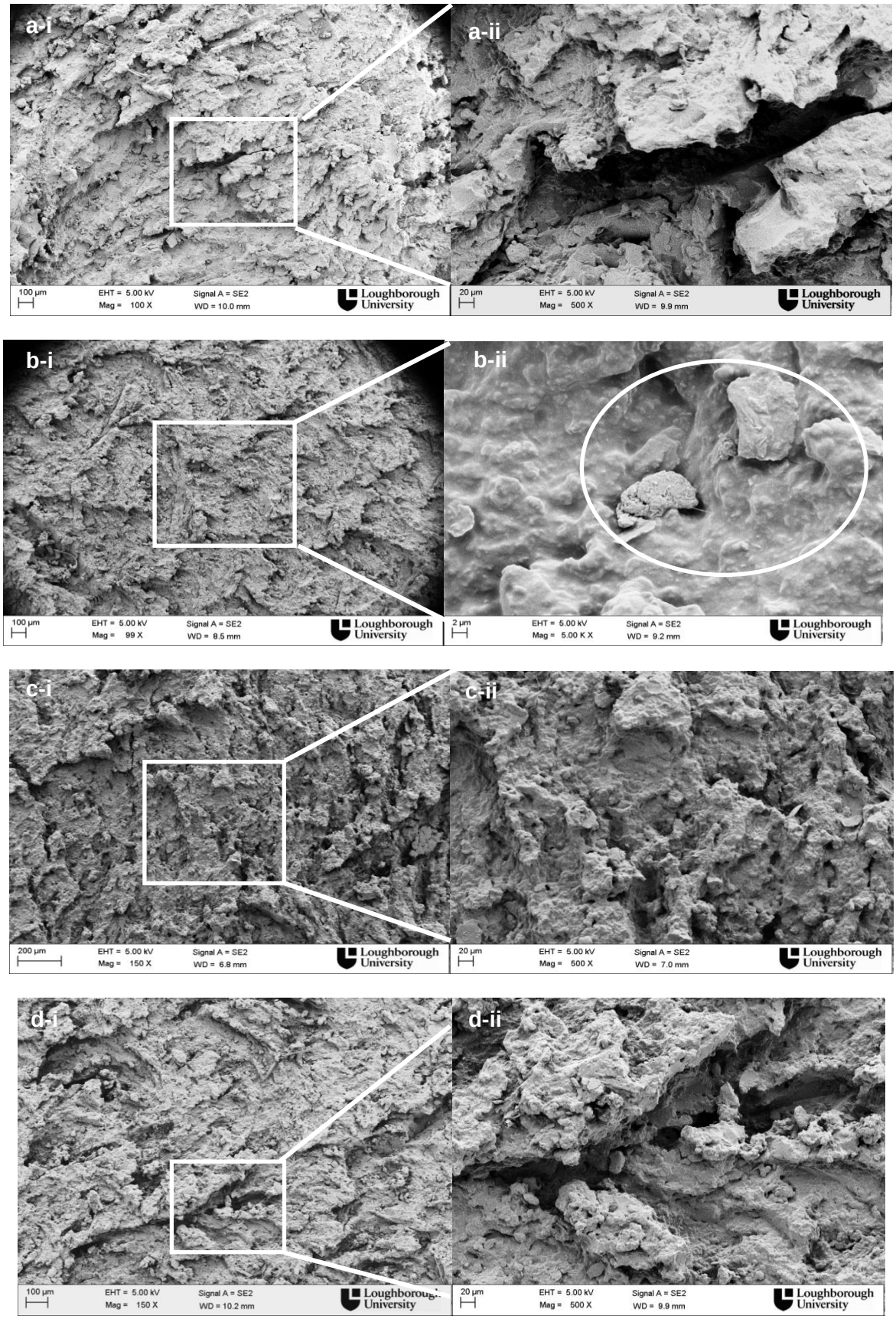

Fig. 5.10(a-d): SEM images of worn surface of (a) neat SR (b) SR/Na^{+}MMT, (c) SR/C30B and (d) SR/C20A after abrasion test.

By contrast the images of SR/C30B and SR/C20A display a few large holes, suggesting the loss of some segments during the test. This corresponds with the higher amount of weight loss measured for both samples after the test (as explained in Fig. 5.8). This was possibly due to a lack of interfacial adhesion in the SR/C20A and SR/C30B nanocomposites.

5.7 Conclusions

Overall, the addition of Cloisite Na^+ (Na^+MMT), Cloisite 30B (C30B) and Closite 20A (C20A) significantly improved the mechanical properties of the silicone rubber. For instance, maximum tensile strength (0.83 MPa) was obtained when the loading of Na^+MMT reached 12 phr, which was two times as high as that of pure SR. This value is comparable with the tensile strength of SR/MMT loaded with higher concentrations of filler (approx. 30 phr) as reported by other researchers [2].

Among the nanoclays, Na^+MMT seems to be the most effective layered silicate in silicone rubber, as suggested by the significant improvement in tensile strength, Young's modulus and hardness, even though the filler had a tendency to produce a mixture intercalated/exfoliated nanostructures in the SR matrix. The results suggest that the tensile strength and Young's modulus in this particular nanocomposite are dominated by the degree of crosslink density instead of filler dispersion.

With regard to the dispersion state of the nanocomposites prepared, the trends suggest that intercalated SR/C20A nanocomposites provide more improvements to elongation-at-break and store energy density properties. Therefore it was concluded that elongation-at-break is dependent on the state of dispersion of the clays, as well as the crosslink density of the rubber. However the crosslink density had even a bigger influence on the strength of the rubber.

Hysteresis in the nanocomposites depended strongly on the state and dispersion of the clay fillers in the rubber. The nanocomposites containing exfoliated clays exhibited low hysteresis compared with the one containing intercalated clays.

Incorporation of the nanoclays in SR altered the wear mechanism of silicone rubber, while addition of fillers minimised the weight loss during abrasion testing, particularly at low filler loading (<6phr). Above this level it was a challenge to control the removal of weight from the rubber. This was probably due to agglomeration issues and low interfacial adhesion between filler and rubber.

5.8 References

1. Sarkar A, Silicone rubber. In: White J, De SK, Naskar K (eds). *Rubber Technologist's Handbook*. Vol 2. United Kingdom, Smithers Rapra Technology Limited; 2009; 387 – 389.

2. Kaneko MLQA, Yoshida IVP. Effect of Natural and Organically Modified Montmorillonite Clays on the Properties of Polydimethylsiloxane Rubber. *Journal of Applied Polymer Science* 2008; 108: 2587-2596.

3. Schmidt DF, Giannelis EP, Silicate Dispersion and Mechanical Reinforcement in Polysiloxane/Layered Silicate nanocomposites. *Chemistry Material* 2010; 22(1):167–174.

4. Jin J, Song M, Yao KJ, Chen L. A study on viscoelasticity of polyurethane–organoclay nanocomposites. *Journal of Applied Polymer Science* 2006; 99:3677–3683.

5. Xia H, Song M. Intercalation and exfoliation behaviour of clay layers in branched polyol and polyurethane/clay nanocomposites. *Polymer International* 2006; 55: 229– 235.

6. Shim SE, Isayev AI. Rheology and Structure of Precipitated Silica a Polydimethylsiloxane System. *Rheology Acta* 2004; 43: 127-136.

7. Yang ACM, Ayala JE, Scott JC, Abrasive wear in filled elastomers. *Journal Material Science* 1991; 26 (21): 5823-5837.

CHAPTER 6: Heat ageing and thermal properties of silicone rubber/clay nanocomposites

6.1 Introduction

Silicone rubbers are commonly used for high temperature applications in many industrial sectors due to their outstanding heat resistance and thermal stability. Since development of SR/clay nanocomposites has gained more interest recently [1-4], it is important to understand the effects of nanoclay on high-temperature mechanical strength and thermal stability of the nanocomposites. There has been relatively little work done to measure the mechanical properties of SR/MMT nanocomposites after ageing at elevated temperatures (e.g. 200°C). Also, there has been little consensus on the effect of clay on the thermal stability of SR/clay nanocomposites. The present study investigated the effects of montmorillonite clay on the heat ageing and thermal stability of some SR/clay nanocomposites.

Recent reviews emphasised the importance of clay dispersion, such as intercalation and exfoliation, on the heat resistance and thermal degradation of rubber nanocomposites [5]. With this in mind, nanocomposites with different level of filler dispersion - namely highly exfoliated Cloisite 30B (SR/C30B), highly intercalated Cloisite 20A (SR/C20A), and intercalated/exfoliated Cloisite Na^+ (SR/Na^+MMT) - were used in this study. The filler concentration in the nanocomposites was fixed at 6 phr. The properties of the unaged and aged nanocomposites such as tensile strength, Young's modulus and elongation-at-break

were compared with the neat SR. In addition the thermal degradation behaviour of the SR/MMT nanocomposites in air and nitrogen was evaluated.

6.2. Thermal ageing properties at low temperature (125°C for 6 hrs and 24 hrs)

Generally silicone rubber is served between 125°C and 200°C [6]. In this chapter the initial study on ageing behaviour of neat SR and SR/MMT nanocomposites was carried out at low temperature 125°C over two different periods (6hrs and 24hrs). Figs. 6.1(a-c) display before and after ageing of tensile strength, Young's modulus and elongation-at-break for pure SR and SR/MMT nanocomposite.

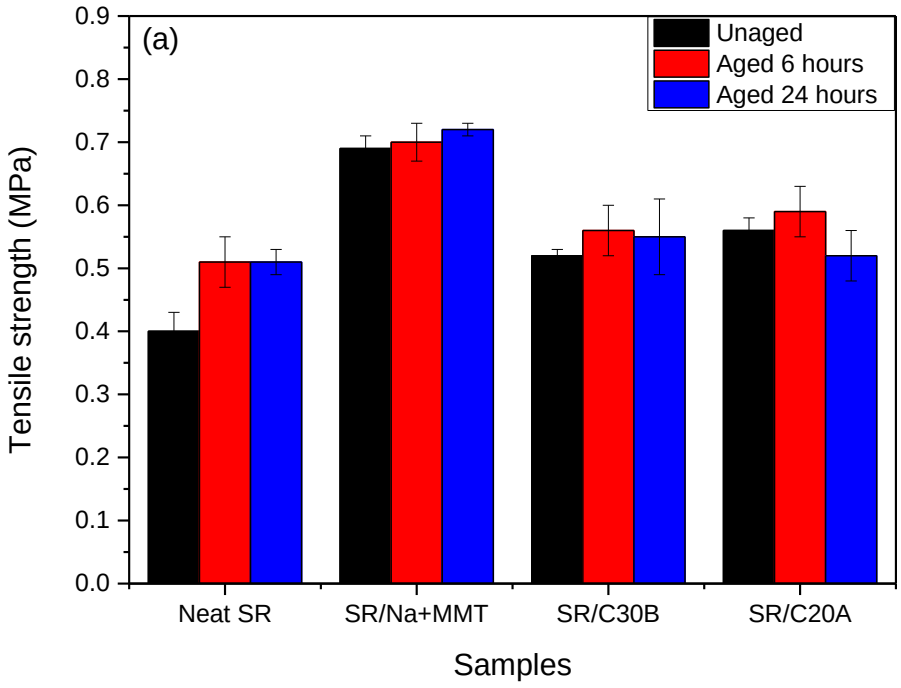

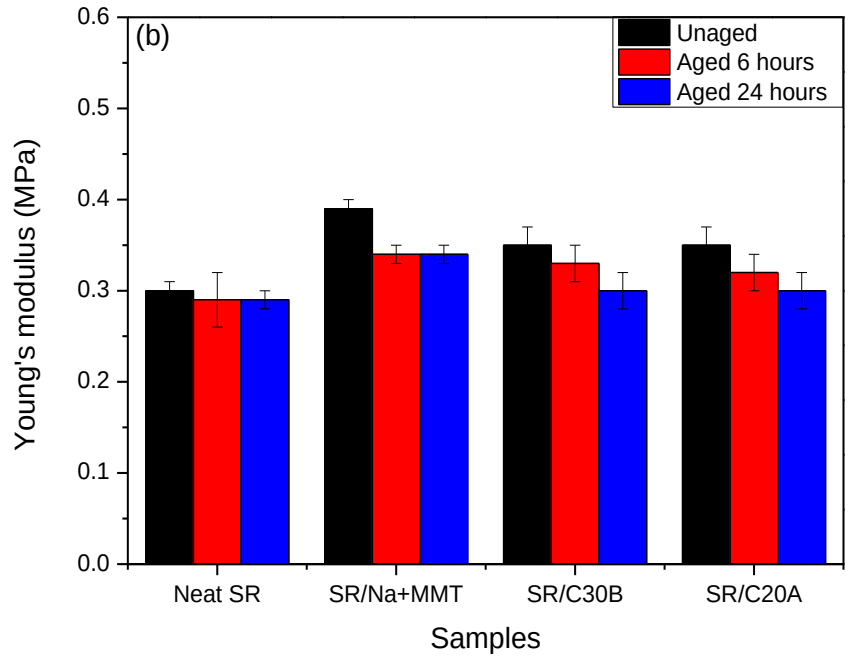

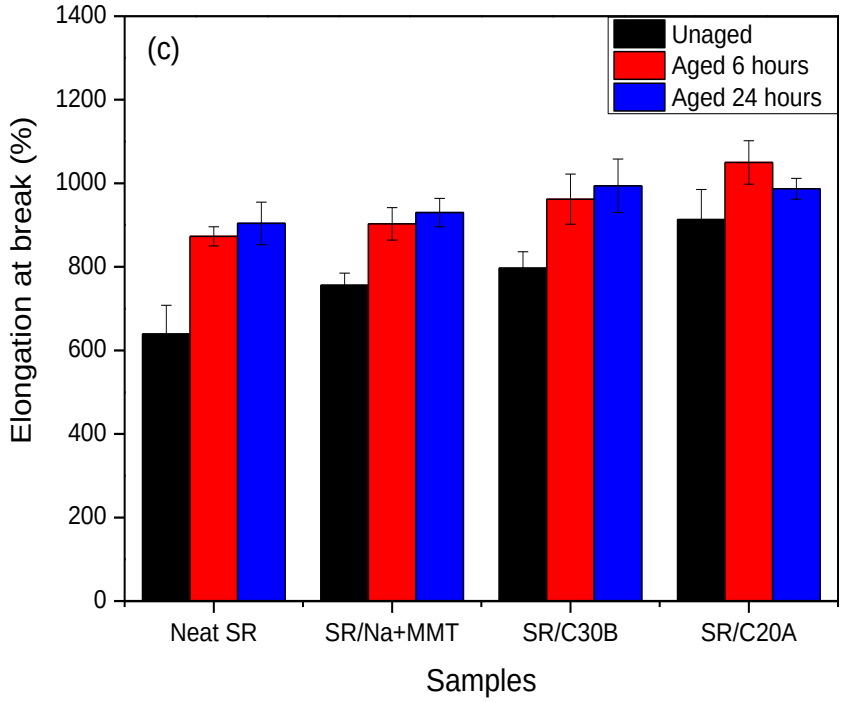

Figs. 6.1(a-c): Unaged and aged (a) tensile strength (b) Young's modulus, (c) elongation-at-break of neat SR and SR/MMT nanocomposites at 125ºC.

It noted no significant change in tensile strength between unaged and aged samples under both ageing conditions, as shown in Fig. 6.1(a), except for neat SR. The tensile strength of neat SR slightly increased from 0.40 MPa to 0.50 MPa. In addition, only a small

drop in Young's modulus (Fig. 6.1(b)) was observed for all samples. The strength reduction was followed by a slight increment in elongation-at-break with the addition of ageing periods as shown in Fig. 6.1(c). This phenomenon was more pronounced for SR filled with C30B and Na^{+}MMT fillers.

The results suggest that the samples start to lose their stiffness and become soft after the ageing treatment. However the change in mechanical property was rather small due to mild aging condition. It seems that little/no major degradation of the pure SR and SR/MMT nanocomposites takes place at low aging temperatures. Hence, the aging behaviour of SR/MMT nanocomposites was further investigated at an elevated temperature (i.e 200°C) over different ageing periods.

6.3 Thermal ageing properties of the rubbers at 200ºC as a function of ageing time

As mentioned earlier, thermal ageing tests were performed at 200°C for 0 h, 10 h, 20 h, 24 h and 30 h durations. The tensile strength, Young's modulus and elongation-at-break of the neat SR and nanocomposites deteriorated when the ageing time was increased (Table 6.1). This was due to a degradation process that occurred at this temperature. An earlier study showed that changes in the mechanical properties of a methyl vinyl SR during ageing was mainly due to network scission or network formation, i.e. crosslinking, or a combination of both [7, 8].

For a clear comparison, thermal ageing properties of the neat SR and nanocomposites were characterized based on percent retention ((aged ÷ unaged) × 100) as displayed in Figs. 6.2(a-c). Fig. 6.2a compares the tensile strength against ageing time for the neat SR and nanocomposites. The tensile strength of the neat SR reduced sharply after 10 h and then continued deteriorating, albeit at a much slower rate, when the rubber was aged for 30 h. A similar trend was also observed for the nanocomposites, but the strength of the rubber was not affected as much by ageing. This suggests that clay helps protect the rubber against ageing, as the nanocomposites performed considerably better than the neat

SR. Overall a large reduction in the tensile strength of both the neat SR and nanocomposites was noticed, but the SR/C30B nanocomposite was the best performing material.

Table 6.1: Aged properties of neat SR and SR/MMT nanocomposites

Ageing time (hours)	**Samples/Tensile properties**			
	Neat SR	**SR/Na^+MMT**	**SR/C30B**	**SR/C20A**
Tensile strength (MPa)				
0	0.40 ± 0.03	0.68 ± 0.03	0.54 ± 0.02	0.52 ± 0.01
10	0.26 ± 0.03	0.52 ± 0.03	0.42 ± 0.02	0.42 ± 0.01
20	0.23 ± 0.02	0.45 ± 0.01	0.42 ± 0.02	0.38 ± 0.03
24	0.19 ± 0.01	0.46 ± 0.01	0.40 ± 0.03	0.40 ± 0.03
30	0.18 ± 0.02	0.40 ± 0.01	0.32 ± 0.01	0.37 ± 0.01
Young's modulus (MPa)				
0	0.30 ± 0.01	0.39 ± 0.01	0.35 ± 0.01	0.35 ± 0.02
10	0.16 ± 0.01	0.25 ± 0.01	0.23 ± 0.01	0.21 ± 0.01
20	0.15 ± 0.01	0.25 ± 0.01	0.21 ± 0.01	0.20 ± 0.01
24	0.17 ± 0.01	0.36 ± 0.01	0.32 ± 0.01	0.21 ± 0.01
30	0.16 ± 0.01	0.29 ± 0.01	0.25 ± 0.01	0.22 ± 0.04
Elongation-at-break (%)				
0	639 ± 69	756 ± 29	797 ± 39	910 ± 72
10	658 ± 118	863 ± 37	867 ± 31	968 ± 73
20	639 ± 73	688 ± 37	969 ± 44	1009 ± 41
24	488 ± 42	477 ± 11	571 ± 35	1006 ± 63
30	463 ± 33	511 ± 27	530 ± 35	640 ± 64

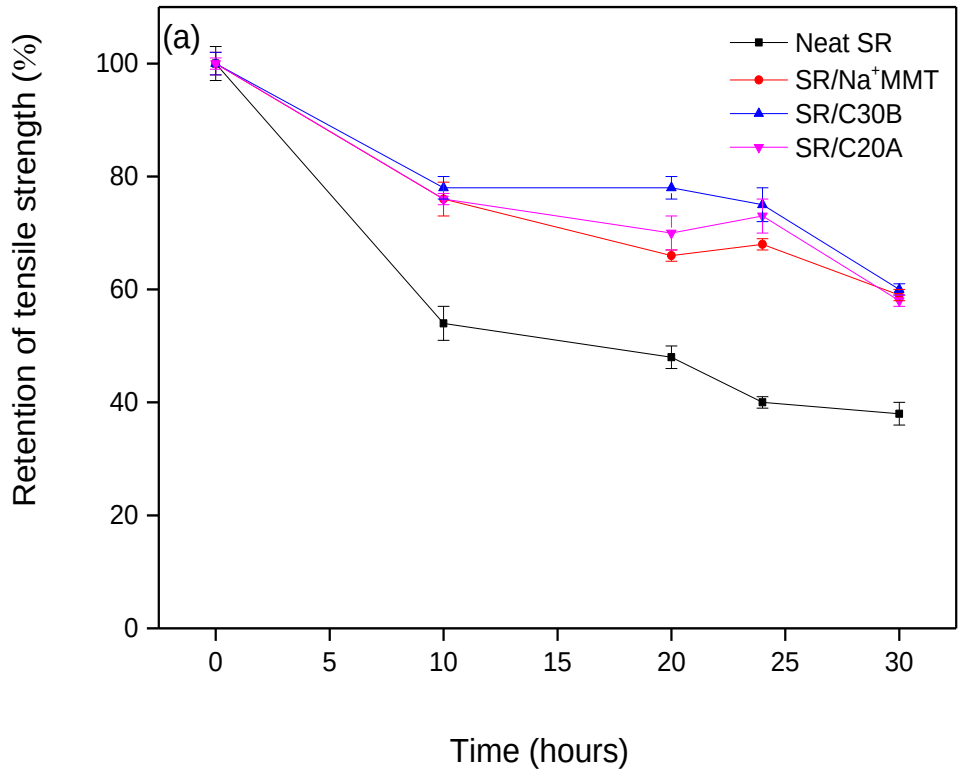

Figs. 6.2a: Percent retention of tensile strength for the neat SR and SR/MMT nanocomposites as a function of ageing time at 200°C.

Fig. 6.2b displays percent retention of the Young's modulus against ageing time for the neat SR and nanocomposites. The Young's modulus of the neat SR decreased noticeably after ageing for 10 h, but this decay slowed after 20 h. Interestingly, there was an improvement in the Young's modulus after 24 h, followed by a modest reduction thereafter. This small increase was due to a rise in crosslink density. It has been reported that chain scission in the SR bonds was largely due to hydrolysis reaction at temperatures below 250°C [7, 8]. Concurrently, the methyl side groups might have gradually oxidized after long term exposure to heat ageing, causing a rise in crosslink density [9]. This potentially explains the modest improvement observed in the modulus of the rubber after 24 h of ageing.

For the nanocomposites the Young's modulus decreased sharply after 10 h, but the decline was less severe when the rubber was aged for another 10 h. Afterward there was a very rapid recovery, particularly for the SR/C30B and SR/Na^+MMT nanocomposites, when

the samples were aged for an extra 4 h. However, the modulus decreased for both nanocomposites after they were aged for 6 h longer. The modulus of the SR/C20A nanocomposite remained inferior over the 30 h ageing test.

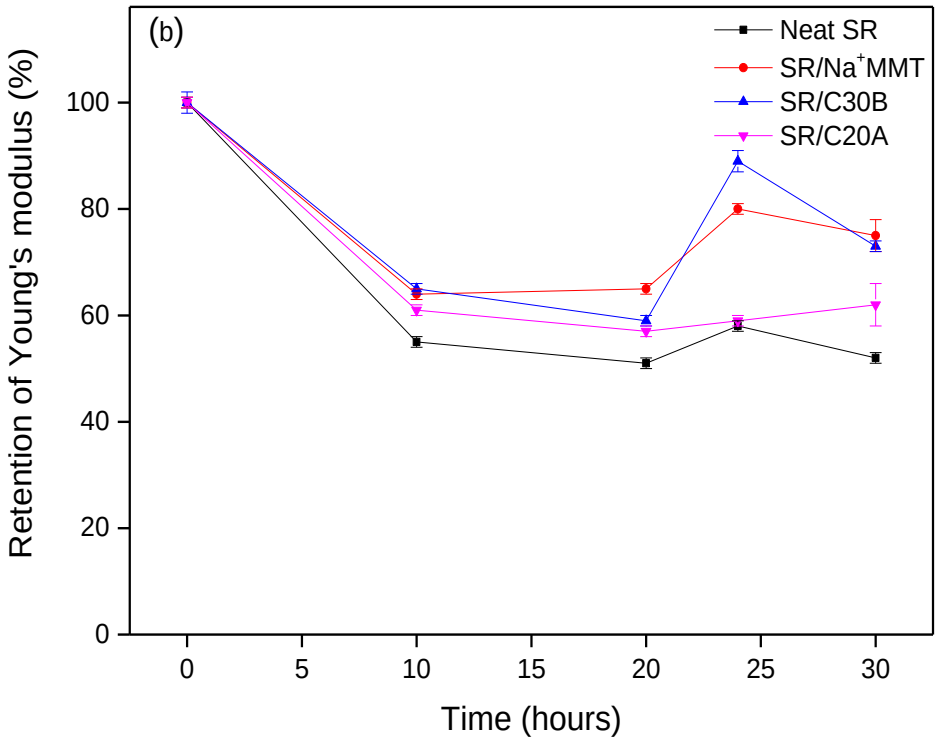

Fig. 6.2b: Percent retention of Young's modulus for the neat SR and SR/MMT nanocomposites as a function of ageing time at 200°C.

Fig. 6.2c demonstrates the elongation-at-break of the neat SR and nanocomposite as a function of ageing time. For the neat SR there was no change in this property for up to 20 h, followed by a steep decrease when the rubber was aged for another 10 h. The nanocomposites showed superior properties, although they performed differently as they were aged. For example, the SR/C30B nanocomposite retained its elongation-at-break better than the other two (which had similar values) after 20 h ageing. Afterwards the elongation-at-break of the neat SR and nanocomposites dropped sharply, indicating a severe deterioration in the elasticity of the rubber.

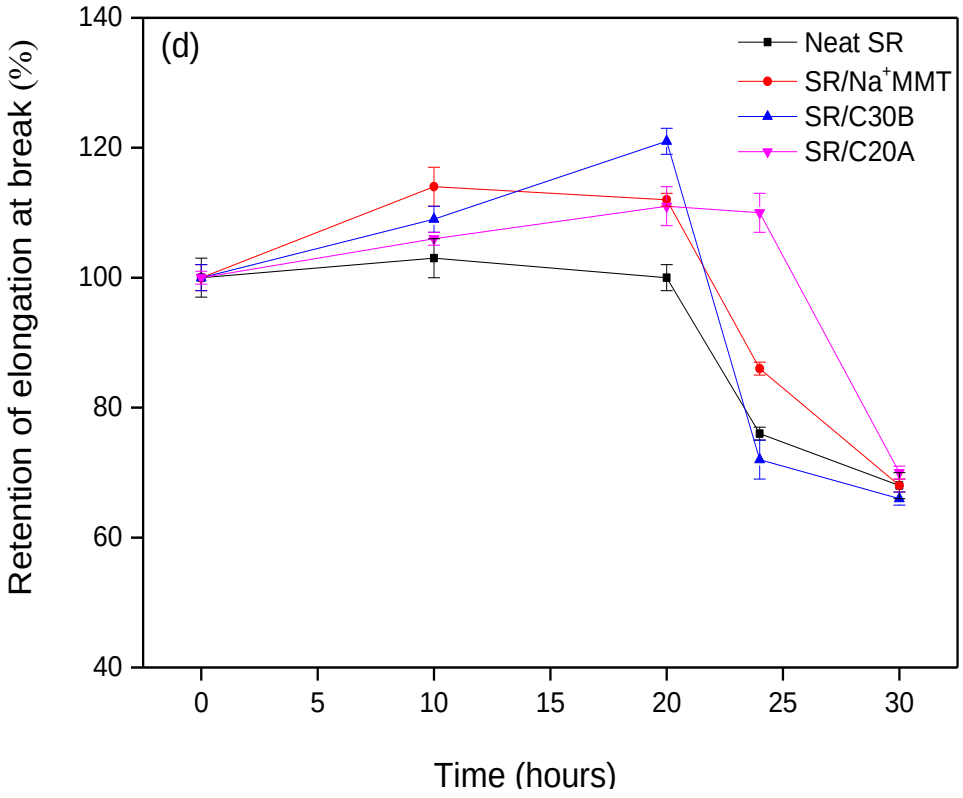

Figs. 6.2c: Percent retention of elongation-at-break for the neat SR and SR/MMT nanocomposites as a function of ageing time at 200°C.

From the results presented in Figs. 6.2a-b, it was evident that the nanocomposites performed differently after they were aged for 24 h. This was probably due to increase in crosslink density, responsible for improvement in the Young's modulus and loss of elongation-at-break of the SR/C30B and SR/Na^+MMT nanocomposites (as shown in Fig. 6.2b and Table 6.1). A similar phenomenon was reported earlier for a silicone rubber filled with silica nanofiller [7], where it was speculated that silanol groups (SiOH) on the silica surface caused cleavage of the rubber chains. The bonding of the cleaved rubber chains to silica resulted in an increase in crosslink density and a loss of mechanical properties [7]. It is likely that the presence of OH groups in the organic modifier (methyl, tallow, bis-2-hydroxyetyl, quaternary ammonium) and the edges of the silicate layers in Cloisite 30B and Cloisite Na^+ clays, were responsible for this increase in crosslink density. However, it is probable that this phenomenon did not occur in the SR/C20A nanocomposite, because Cloisite 20A had no OH groups.

On the other hand, morphology of the clay had a noticeable effect on the heat resistance of the rubber and, in general, the incorporation of clays was beneficial to the thermal properties of the rubber. Based on these results the effect of clay morphology on the thermal resistance of the rubber can be summarized as follows: exfoliated SR/C30B nanocomposite > intercalated/exfoliated SR/Na^+MMT > intercalated SR/C20A nanocomposite.

These findings suggest that, in general, the presence of the clays enhanced the heat resistance of the rubber, reflected by higher retention strength of the nanocomposites with regard to the neat SR. This behaviour has been rarely reported in the case of non-hydrocarbon polymers such as SR. According to Pielichowski and Njuguna [10], besides the chemical nature of SR end-caps, the rate of degradation in SR at high temperatures is increases due to external factors, such as acidic or basic impurities, oxygen, water, fillers and the presence of residual catalyst. However, in this case, the presence of the clays was shown to stabilize the SR structure against thermal degradation.

This phenomenon was observed in all the nanocomposites tested, suggesting that both the unmodified and modified clays had prevented the SR chains from scission during ageing tests. Nevertheless, the inclusion of C30B clay produced the highest resistance to heat ageing among the other corresponding clays. As expected, among the rubbers tested the SR/C30B nanocomposite containing exfoliated clay exhibited the best resistance to ageing. Presumably, the strong rubber-filler interaction offered by the large available surface area of the exfoliated clay platelets reduced chain mobility and helped to minimize chain scission. This was supported by evidence from chemical analysis of the SR/C30B nanocomposite surface, revealed by the ATR-FTIR spectra in Figs. 6.3(a-b).

The results obtained were consistent with the observations made by Choudhury and co-workers [11]. They reported that the addition of Cloisite 30B improved the retention of physico-mechanical properties of a hydrogenated nitrile rubber (HNBR) by disrupting the

oxidative process. The enhancement of thermal stability of the HNBR/C30B nanocomposite was attributed to the interaction between intercalated polymer chains and the clay layers, which formed hydrogen bonding between OH groups on the clay surface and the polar groups (CN) present in the rubber.

6.4 ATR-FTIR analysis of the rubber samples

An attempt was made to measure changes in surface chemistry of the neat SR and SR/30B nanocomposite before and after ageing using a transmission FTIR. IR scans of the unaged and aged samples at 200^{o}C for 20 and 24 h were analyzed as shown in Figs.6.3 (a-b). There were three distinct characteristic peaks on the spectra of the rubber samples. A sharp peak at 1257 cm^{-1} was induced by the deformation of Si-CH_3, and the stretching of Si-C produced a clear band at 785 cm^{-1}. Moreover, the Si-O-Si backbone produced a broad band with two maxima at 1009 and 1078 cm^{-1}. It has been reported that weak bands at 1610, 1561 cm^{-1}, 1460 and 1409 cm^{-1} peaks were evidence of crosslinking networks in SR [12].

Note that no significant change was observed when the IR spectra of the unaged and aged samples of the neat SR were compared in Fig. 6.3a. All the characteristic peaks of the neat SR remained constant in a similar position even after ageing. But intensity ratio of Si-O vibration (1009 cm^{-1} and 1078 cm^{-1}) rapidly decreased with increased ageing time. An obvious reduction of intensity ratio was detected for absorption bands at 783 cm^{-1}, which corresponded to Si-CH_3. It was found that the intensity ratio of Si-CH_3 bands decreased from 1.42 for the unaged to 1.21 for the aged sample, after ageing at 200°C for 24 h. Rapid decrease of the characteristic peaks suggested that the Si-O-Si backbone underwent chain scission at 200°C to form shorter chains. No new peaks were observed in the spectra, which indicated no oxidative product was formed during the ageing process (Fig. 6.3a).

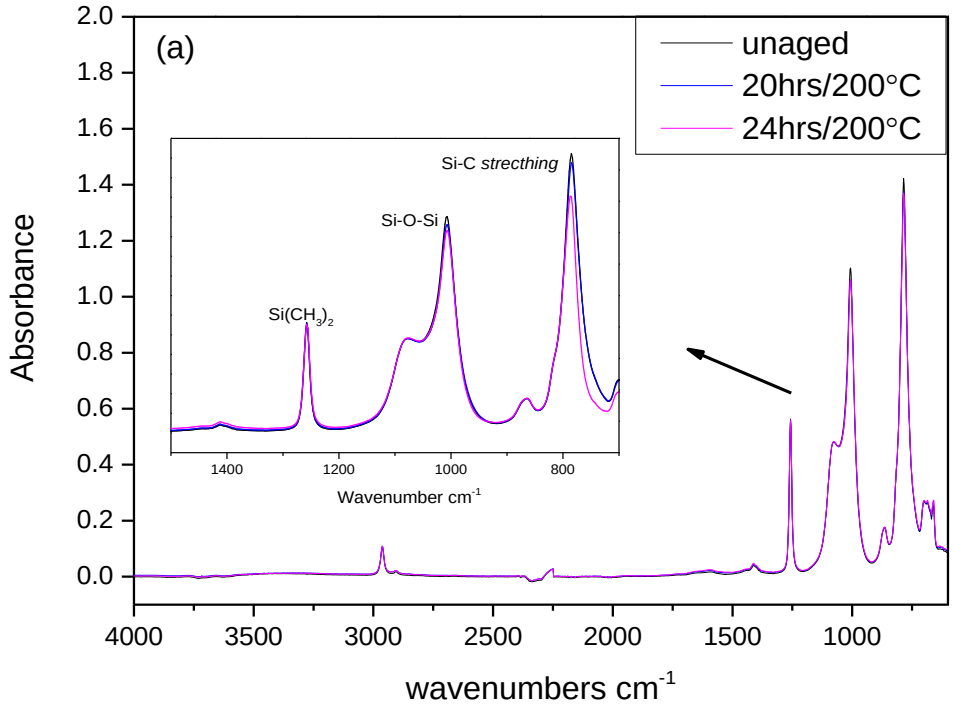

Fig. 6.3a: ATR-FTIR spectra of cured neat SR before and after ageing at 200°C for 20 h and 24 h.

The appearance of small absorption peaks at 1610 and 1561 cm^{-1}, and 1460 and 1409 cm^{-1}, could be attributed mainly to the formation of crosslink networks in SR [12]. It has been reported that the peak near 1411 cm^{-1} corresponds to the rocking vibration of $–CH_2–$ as a part of the rubber cross-linked domain [13]. In this case a sharpening of weak peaks at 1411 and 1593 cm^{-1} was noticeable with increasing ageing time from 20 to 24 h, as shown in Fig. 6.3b. The absorption peak at 1411 cm^{-1} increased from 0.041 to 0.048, and at 1593 cm^{-1} from 0.016 to 0.025. The increase in intensity ratio suggested that more crosslinks were formed in the rubber as a function of ageing time, explaining the improvement in the Young's modulus (Fig. 6.3b). The brittleness of SR after long exposure to air at 200°C was attributed to a mild oxidative crosslinking reaction of the methyl side groups in the main chain of the polymer [7].

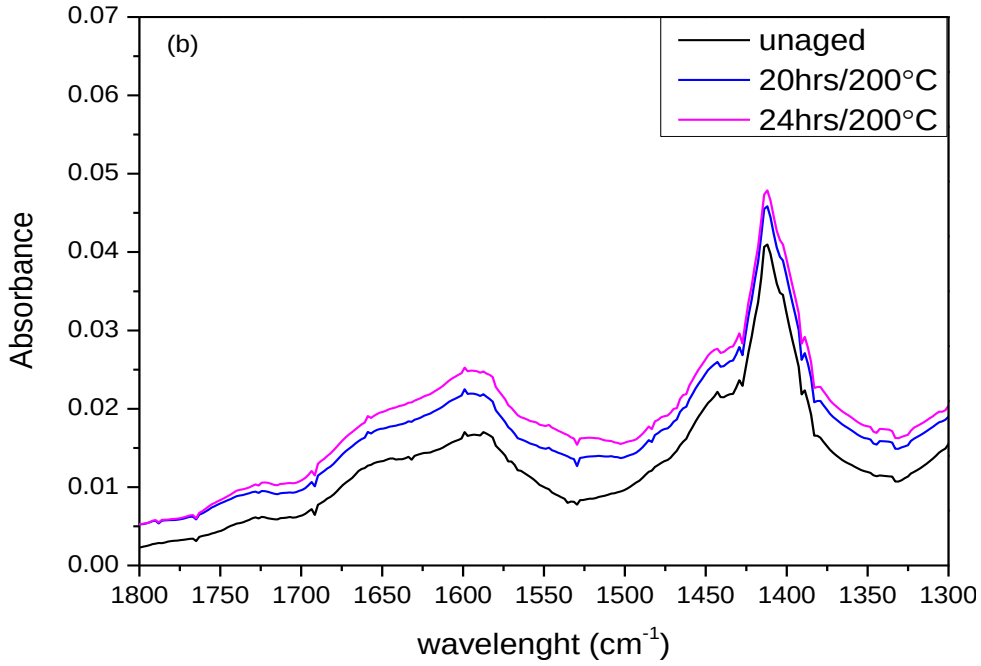

Fig. 6.3b: ATR-FTIR spectra of crosslinking network in the neat SR before and after ageing at 200°C for 20 h and 24 h

Figs. 6.4(a-b) illustrate IR bands for the SR/C30B nanocomposite before and after ageing for 24 and 30 h. Similar to the neat SR, no significant change was observed in the IR spectrum of the rubber. The peak intensity of Si-O and Si-CH_3 bands showed no change during ageing, indicating no serious degradation of the rubber. It appears that the addition of clay protected the rubber from chain scission, direct oxidation, and hence degradation. This might explain why the nanocomposite was more resistant to heat ageing compared to the neat SR, as discussed in the earlier section. Similar to the neat SR, the increase of small peak intensity ratios at 1610 and 1561 cm^{-1}, and 1460 and 1409 cm^{-1} positions showed some evidence of light crosslinking in the rubber with increased the ageing time (Fig. 6.4b).

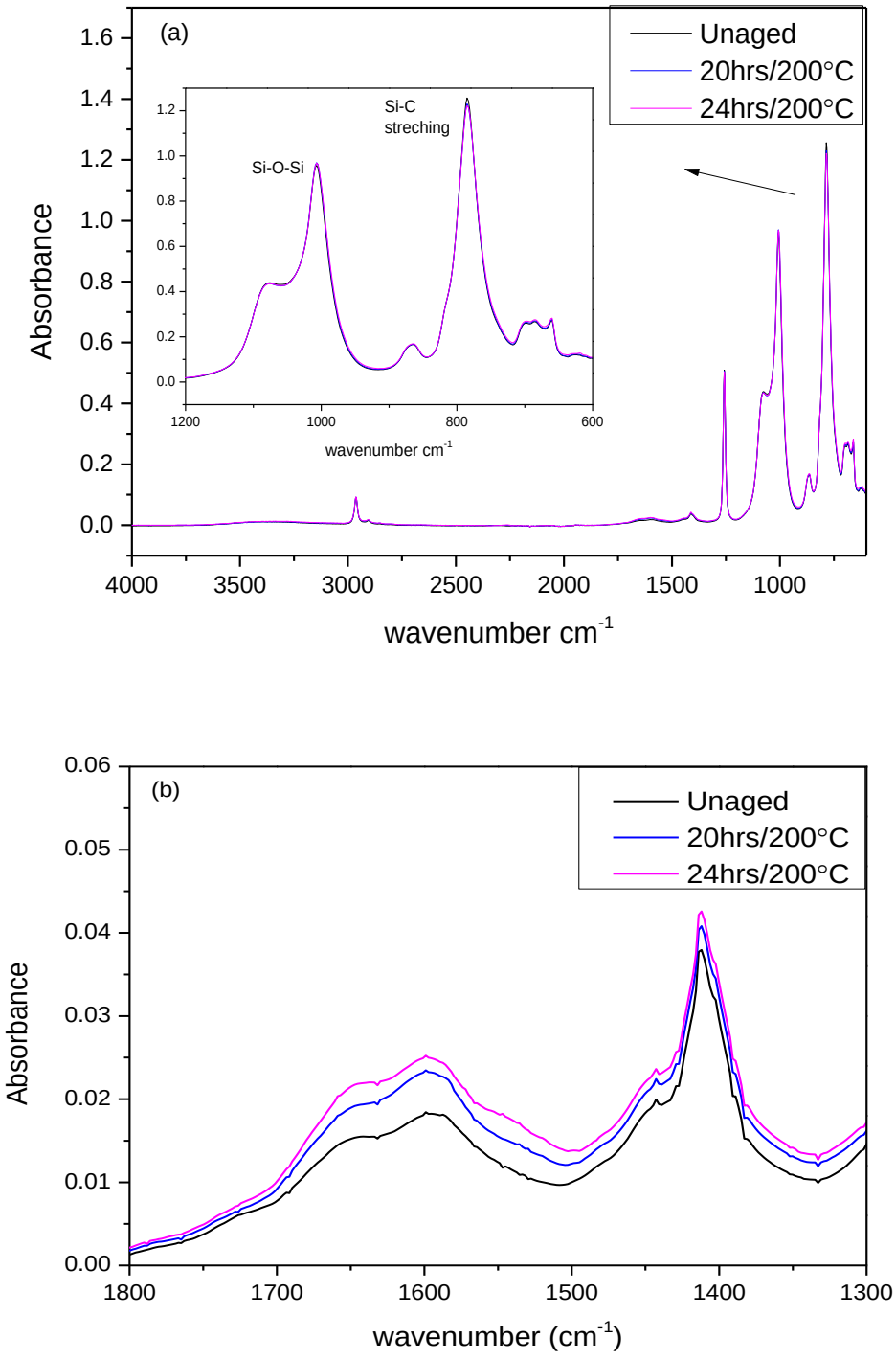

Fig. 6.4(a-b): ATR-FTIR spectra of (a) SR/C30B nanocomposite and (b) crosslinking network in the SR/C30B nanocomposites before and after ageing at 200°C for 20 and 24 h.

6.5 Thermal-oxidative degradation of the SR/MMT nanocomposites

Thermogravimetric analysis (TGA) of the nanocomposites was carried out in air and nitrogen atmospheres. To evaluate improvements in the thermal properties of the rubbers containing the clays the results were compared with the neat SR. Fig. 6.5 displays the TGA curves of the nanocomposites in air. The details of thermal-oxidative degradation in air are also summarized in Table 6.2.

Based on the results shown in Fig. 6.5 and Table 6.2, it was clear that the addition of the clays delayed depolymerisation of the rubber during thermal oxidative degradation. For example, the onset temperatures T_{onset} (the temperature at which 5% of weight loss occurs) of SR/Na^+MMT, SR/C30B and SR/C20A nanocomposites were 340ºC, 340ºC and 342ºC, respectively; 8-10ºC higher than that of the neat SR, whose T_{onset} was 332°C. When a comparison was made among the nanocomposites, the results suggested that T_{onset} was not affected by the intercalation or exfoliation of the clay particles in the rubber.

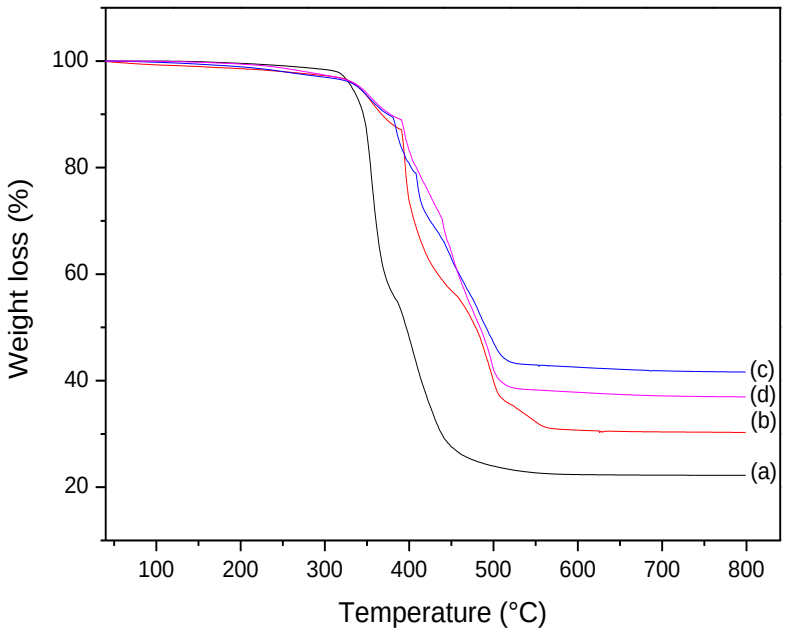

Fig. 6.5: TGA curves of (a) neat SR (b) SR/Na^+MMT (6 phr) (c) SR/C30B (6 phr) and (d) SR/C20A (6 phr) nanocomposites in air.

Table 6.2: TGA results for the thermal oxidative degradation of neat SR and SR/MMT nanocomposites.

Sample	T_{onset} (ºC)	T_{10} (ºC)	T_{50} (ºC)	Final residue at 650°C (%)	Temperature peak of degradation, T_{max} (°C)	Peak height at T_{max} (%/°C)
					T_{01}, T_{02}	T_{01}, T_{02}
Neat SR	332	345	396	22.3	356, 406	1.59, 0.58
SR/Na^+MMT	340	367	478	30.5	390, 468	1.35, 0.53
SR/C30B	340	375	495	42.0	385. 411	0.60, 0.78
SR/C20A	342	378	484	37.4	395, 442	0.65, 0.60

Further analysis revealed that clay morphology did influence the thermal stability of the rubber for T_{10} and T_{50}. With the addition of Na^+MMT, C30B and C20A clays, the T_{10} (the temperature at which 10% of weight loss appears) was shifted to 367°C, 375°C and 378°C, respectivelym as compared to the neat SR, whose T_{10} was 345°C. Interestingly, the T_{50} (as midpoint temperature of the degradation process of rubber) was markedly improved with the inclusion of the clays. With regard to the neat SR, the T_{50} of the SR/Na^+MMT, SR/C30B and SR/C20A nanocomposites were moved from 396ºC (for the neat SR) to 478°C, 495°C and 484°C respectively.

It was evident that the effect of the exfoliated platelets of C30B clay on the thermal degradation was more pronounced at higher temperatures, since the T_{50} of the SR/C30B nanocomposite was about 99°C higher than that of the neat SR. It has been reported that the oxidation reaction of the main SR chains was dominant at temperatures above 250°C [8]. With the presence of exfoliated C30B in the rubber matrix the oxidation reaction was delayed, due to barrier performance of the clay platelets. This result corresponded well to the improvement of the mass residue at 650°C. As described in Table 6.2, the residue for the neat SR was about 22.3%. However, in the presence of the exfoliated C30B clay

platelets in the rubber, the mass residue increased significantly to 42.0%. This was followed by the intercalated C20A and intercalated/exfoliated Na^+MMT clays, where the remaining residue increased to 37.4% and 30.5%, respectively. The exfoliated SR/C30B nanocomposite, had an additional 88% final residue compared to the neat SR. Evidently, enhancement of the final residue in the thermo-oxidative degradation was highly dependent on the dispersion state of the clay particles in the rubber matrix.

6.5.1. Differential thermogravimetry (DTG) curves of the neat SR and SR/MMT nanocomposites in air atmosphere

Degradation rate of the nanocomposites was compared with the neat SR, based on the DTG data shown in Figs. 6.6(a-c) and Table 6.2. Note that Fig.6.6 (a-c) corresponds to the TGA curves presented in Fig. 6.5. The results showed that the neat SR experienced two major thermal-oxidative degradation stages at 356°C and 406°C. Unlike the neat SR, on average the DTG plots of the nanocomposites were more complex and less well defined. This indicated that the use of the clays in the rubber modified the degradation behavior significantly. The SR/Na^+MMT and SR/C30B nanocomposites each exhibited two maxima above 360ºC (Figs. 6.6 a & b). However, the SR/C20A nanocomposite displayed three maxima above this temperature (Fig. 6.6c). In this case, small peaks that appeared at 356°C in the DTG plots (Fig. 6.6c) of the nanocomposites were neglected because they represented low degradation rates.

Based on the T_{max} results in Table 6.2, degradation of the nanocomposites shifted to higher temperatures when compared with the neat SR. The T_{01} (temperature for first step degradation) of the SR/Na^+MMT, SR/C30B and SR/C20A nanocomposites shifted from 356°C (for the neat SR) to 390ºC, 385ºC and 395ºC respectively. This corresponded well with the degradation rate for T_{01} of the SR/Na^+MMT (1.35%/°C), SR/C30B (0.60%/°C) and SR/C20A (0.65%/ºC) nanocomposites, which were lower than the neat SR (1.59%/ºC). Evidently the above changes were more pronounced for the SR/C30B and SR/20A

nanocomposites that contained highly exfoliated and intercalated clay particles, respectively. It appeared that the oxidative reaction in the SR chains that normally occurs at above 250°C [9] was retarded by the presence of the clays which, in turn, reduced the degradation rate of the nanocomposites.

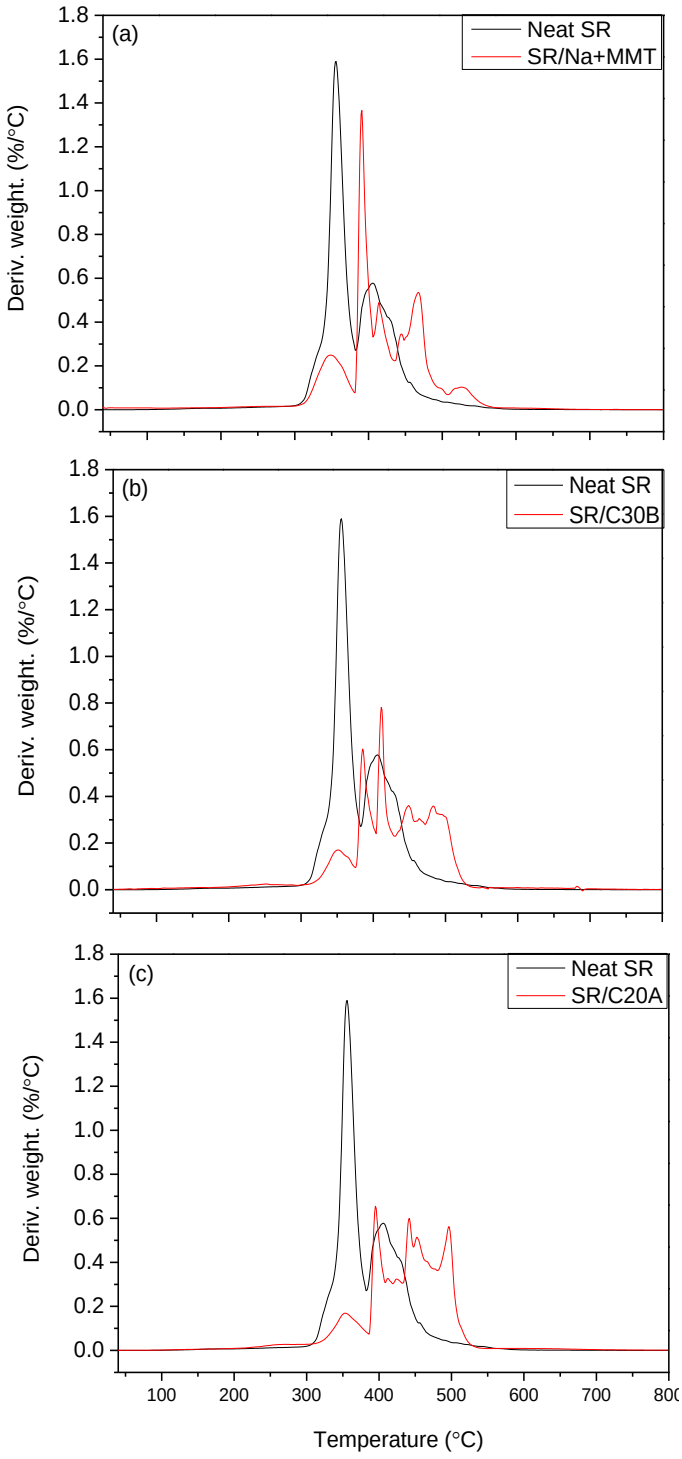

Figs. 6.6 (a-c): DTG plots of the neat SR and SR/MMT nanocomposites in air.

The T_{02} (temperature for second step degradation) of the SR/Na^+MMT (468ºC), SR/C30B (411ºC) and SR/C20A (442ºC) nanocomposites increased to higher values when compared with the neat SR (406ºC). This indicated that the rubber became thermally stable with the addition of the clays. However, the degradation rate T_{02} for the SR/C30B (0.78 %/°C) and SR/C20A (0.60 %/°C) nanocomposites were higher than the neat SR (0.58 %/°C). This showed that the degradation rate of the nanocomposites accelerated towards higher temperatures. In contrast the degradation rate of the nanocomposite containing the intercalated/exfoliated Na^+MMT particles was slightly lower (0.53 %/°C) than the neat SR (0.58 %/°C). This implies that the depolymerisation reaction in this nanocomposite was less aggressive at higher temperatures when compared to the other two nanocomposites. This behavior was probably related to the absence of organic surfactant in the unmodified Na^+MMT clay.

It was clear that the exfoliated C30B clay platelets were the most effective barrier against diffusion of oxygen into the rubber during thermal oxidative degradation, increasing the thermal stability of the nanocomposite. The mechanism of barrier performance in polymer/clay nanocomposites was well explained in a previous study [5], which suggested that exfoliated clay particles acted as a physical barrier preventing oxygen from diffusing into the nanocomposite. In addition, during the thermal degradation process, the depolymerised products were prevented from moving to the combustion interface by the exfoliated clay platelets. This phenomenon potentially explains the better performance of the SR/C30B nanocomposites in the thermal oxidative degradation tests.

6.6 Thermal degradation of the SR/MMT nanocomposites in nitrogen atmosphere

The thermal degradation of the neat SR and nanocomposites was measured in a nitrogen atmosphere. TGA plots of the neat SR and nanocomposites are presented in Fig. 6.7. As expected, the TGA data of the nanocomposites were notably different from those of

the neat SR. Table 6.3 summarizes the thermal properties such as T_{onset}, T_{10}, T_{50}, final residue and T_{max} of the rubbers tested.

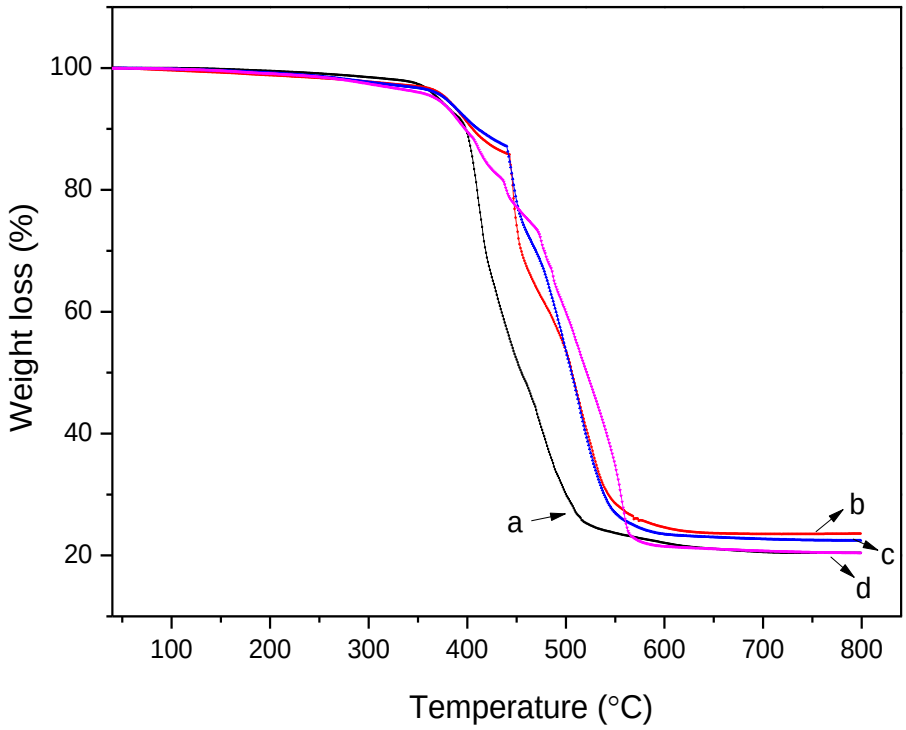

Fig. 6.7: TGA curves of (a) neat SR (b) SR/Na^+MMT (c) SR/C30B and (d) SR/C20A nanocomposites in a nitrogen atmosphere.

The addition of Na^+MMT and C30B clays increased the T_{onset} of the neat SR, which was originally at 370°C, by about 8ºC (to 9ºC). A similar behaviour was also seen for the T10 as shown in Table 6.3. T10 of the SR/Na^+MMT and SR/C30B nanocomposites were shifted to 405°C and 411°C, respectively, whereas the T_{10} of the neat SR was at 399°C. However, the SR/C20A nanocomposite started to degrade slightly earlier than the neat SR. The T_{onset} and T_{10} of this nanocomposite were 368°C and 397°C, respectively. These values were marginally lower than the 370°C and 399°C measured for the neat SR (Table 6.3).

A significant difference in the thermal degradation of the neat SR and nanocomposites was clearly seen when the T_{50} values were compared. This was because

SR is more stable in a nitrogen atmosphere, due to the absence of oxygen (which induces chain scission), although SR usually degrades at higher temperatures [14]. Camino and co-workers [14] reported that the neat SR decomposed to cyclic oligomers at temperatures above 400°C in nitrogen.

Table 6.3: TGA results for the thermal non-oxidative degradation of neat SR and SR/MMT nanocomposites.

Sample	**T_{onset} (ºC)**	**T_{10} (ºC)**	**T_{50} (ºC)**	**Final residue at 650°C**	**Temperature peak of degradation, T_{max} (°C)**	**Peak height at T_{max} (%/°C)**
					T_{01}, T_{02} and T_{03}	***T_{01}, T_{02} and T_{03}***
Neat SR	370	399	455	21.1	412, 474	1.21, 0.53
SR/Na^+MMT	378	405	506	23.5	447, 509	1.57, 0.52
SR/C30B	379	411	506	23.1	445, 514	0.93, 0.73
SR/C20A	368	397	521	21.1	439, 488, 557	0.39, 0.55, 0.89

With regard to the neat SR, the T_{50} of the SR/Na^+MMT, SR/C30B and SR/C20A nanocomposites shifted from 455ºC (for the neat SR) to 506ºC, 506ºC and 521ºC, respectively. An increment change of 66°C in T_{50} value was observed for the SR/C20A nanocomposite. In addition, when the final residues at 650°C were compared, the SR/Na^+MMT and SR/C30B nanocomposites showed about 11% improvement compared with the neat SR. Surprisingly, no such improvement was observed for the SR/C20A nanocomposite where the final residue was similar to that of the neat SR. This behavior may be due to the influence of the organic surfactant in the C20A clay. This will be discussed at a later stage.

6.6.1 DTG curves of the neat SR and SR/MMT nanocomposites in nitrogen atmosphere

Figs. 6.8(a-c) illustrate the DTG data for the neat SR and nanocomposites from the thermal degradation tests in a nitrogen atmosphere. The neat SR underwent two degradation stages in nitrogen, as suggested by the appearance of two characteristic peaks. The SR/Na^+MMT (Fig. 6.8a) and SR/C30B (Fig.6.8b) nanocomposites exhibited three distinct degradation stages, a shoulder followed by two main stages. The T_{max} (T_{01} and T_{02}) of the SR/Na^+MMT and SR/C30B nanocomposites appeared at higher temperatures compared to the neat SR. This indicated that the presence of Na^+MMT and C30B clays significantly delayed the thermal degradation of the rubber.

On the other hand, the SR/C20A nanocomposite showed a more complex degradation behavior, as seen by the appearance of a shoulder and three peaks (T_{01}, T_{02} and T_{03}) at 400°C to 500°C, and also one distinct characteristic peak at higher temperature (Fig. 6.8c). Taking into account this observation, the decomposition of the organic surfactant (dimethyl, dihydrogenated tallow, quaternary ammonium), in C20A clay must be considered in relation to the SR/C20A nanocomposite behavior (even though the amount of the clay used was only 6 phr). Cervantes-Uc and co-workers [16] reported a complex thermal degradation mechanism for the Cloisite 20A clay, in comparison to the unmodified Cloisite Na^+ and 30B clays.

Therefore it may be assumed that the complex behavior of the SR/C20A nanocomposite could be attributed to the decomposition of the organic surfactant in the C20A clay, as reported in a previous study [16]. In this study the SR/C20A nanocomposite showed three Tmax values at 439°C, 488°C and 557°C, corresponding to degradation rates of 0.39%/°C, 0.55%/°C and 0.89%/°C. The trend showed the degradation rate of the SR/C20A nanocomposite accelerating as the temperature was raised from 439 to 557^{o}C (Table 6.3). This explains why low yield residue was obtained at 650°C for this nanocomposite.

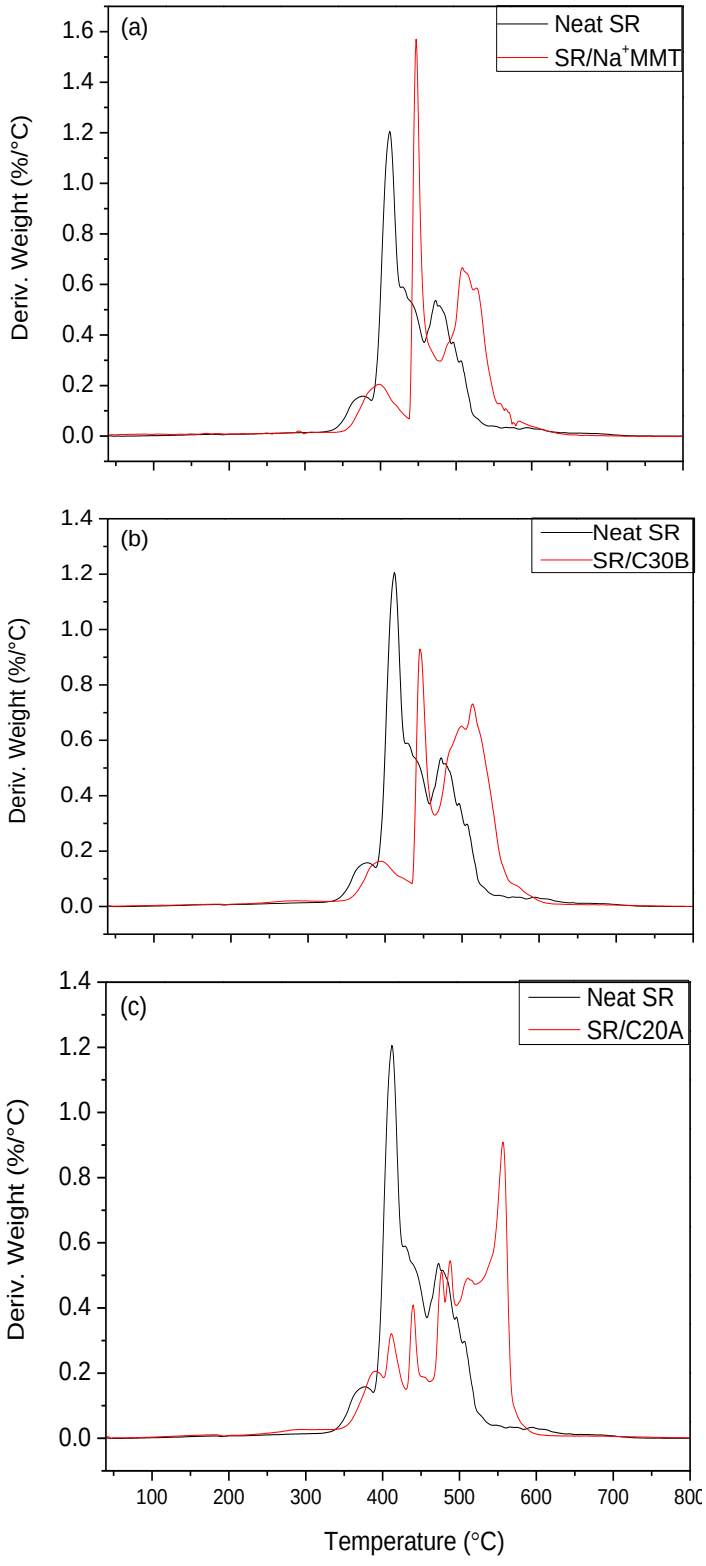

Figs. 6.8 (a-c): DTG plots of the neat SR and SR/MMT nanocomposites in a nitrogen atmosphere.

Overall the SR/C20A nanocomposite had poor thermal stability in nitrogen when compared to the SR/C30B and SR/Na^+MMT nanocomposites. One might expect that the thermal stability of the SR/C20A nanocomposite containing intercalated clay was better than that of the SR/Na^+MMT nanocomposite with intercalated/exfoliated clay, due to the difference in filler morphology. Since the opposite was observed, it was therefore assumed that the organic surfactant in the C20A clay influenced the thermal stability of the rubber. On the other hand, low interfacial interaction in the SR/C20A nanocomposite as reported earlier [18] might have contributed to the poor thermal stability of the rubber.

6.7 Thermal oxidative degradation kinetics of the neat SR and SR/C30B nanocomposite

Referring to the thermal oxidative degradation results discussed in the earlier section (Table 6.2, Fig. 6.5), it was observed that the highly exfoliated C30B clay platelets acted as an effective barrier to the diffusion of oxygen into the rubber, lowering the mass loss decomposition rate of the SR/C30B nanocomposite. Accordingly, the mechanism of thermal oxidative degradation in the neat SR and nanocomposite was investigated using the thermal oxidative degradation kinetics analysis.

In general, when determining the thermal stability of a polymer, measuring the activation energy of decomposition is an important kinetic parameter. Activation energy is defined as the minimum amount of energy required for initiating a particular process, usually in the context of chemical reactions. According to Maiti and co-workers [18], the total activation energy of degradation of clay-filled rubber nanocomposites was attributed to the activation energy of degradation of rubber and energy to break the polymer-filler interaction.

The activation energies against conversion level during the thermal oxidative degradation process of the neat SR and SR/C30B nanocomposite were determined following the procedure described in ASTM E1641-07 [19]. Firstly, a rapid TGA test of the two rubbers was carried out at 5°C/min, 10°C/min and 20°C/min heating rates, as presented

in Figs. 6.9(a-b). By increasing the heating rate to 20ºC/min the weight loss shifted to higher temperatures for both the neat SR (Fig. 6.9a) and nanocomposite (Fig. 6.9b). This indicates that the chemical reactions causing thermal degradation are temperature dependent, as reported previously [14].

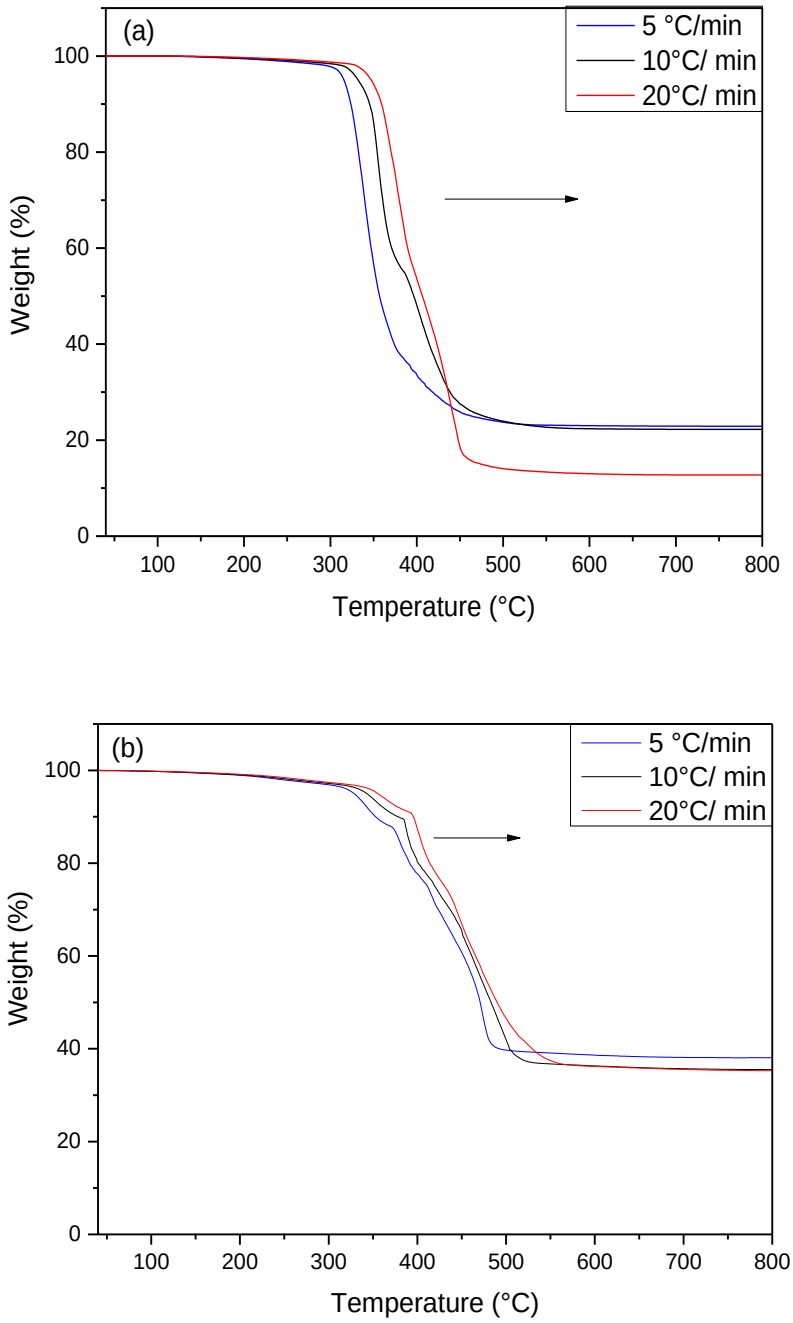

Figs. 6.9(a-b): TGA curves of (a) neat SR and (b) SR/C30B at 5°C/min, 10°C/min and 20°C/min heating rates.

According to the standard method [19], the heating rate β was transformed to log β whereas absolute temperature (K) was converted to 1/T. The logarithms of the heating rates (β) were plotted against absolute temperature (1/T) at any given conversion level to yield a straight line. Table 6.4 presents the parameters of thermal oxidative degradation of neat SR and SR/C30B nanocomposite obtained from the TGA curves in Figs.6.9 (a-b).

Table 6.4: The conversion data at various temperatures for the neat SR and SR/C30B nanocomposite at different heating rate

Sample	**Heating rate (ºC / min)**	**Decomposition at various temperatures in (ºC)**				
		1.0%	**2.5%**	**5.0%**	**10.0%**	**20.0%**
Neat SR	5	224	293	312	321	329
	10	242	313	328	341	351
	20	272	332	347	357	368
SR/C30B nanocomposite	5	158	228	299	335	372
	10	151	227	293	346	383
	20	174	252	329	366	400

Figs. 6.10(a-b), display the Arrhenius plot of log heating rate β (^{o}C/min) against absolute temperature 1000/T (K) of a constant conversion data for the neat SR and SR/C30B nanocomposite respectively (Table 6.4). By fitting the straight lines to the actual data, the slope (*m*) of the lines was measured where *m* was Δ (log β) / Δ (1/*T*). The m and b

values, where b was 0.457/K, were placed in Equation 6.1 to determine the activation energy (*E*).

$$E = -\left(\frac{R}{b}\right) * \Delta(\log \beta)/\Delta\left(1/T\right) \qquad \text{Equation 6.1}$$

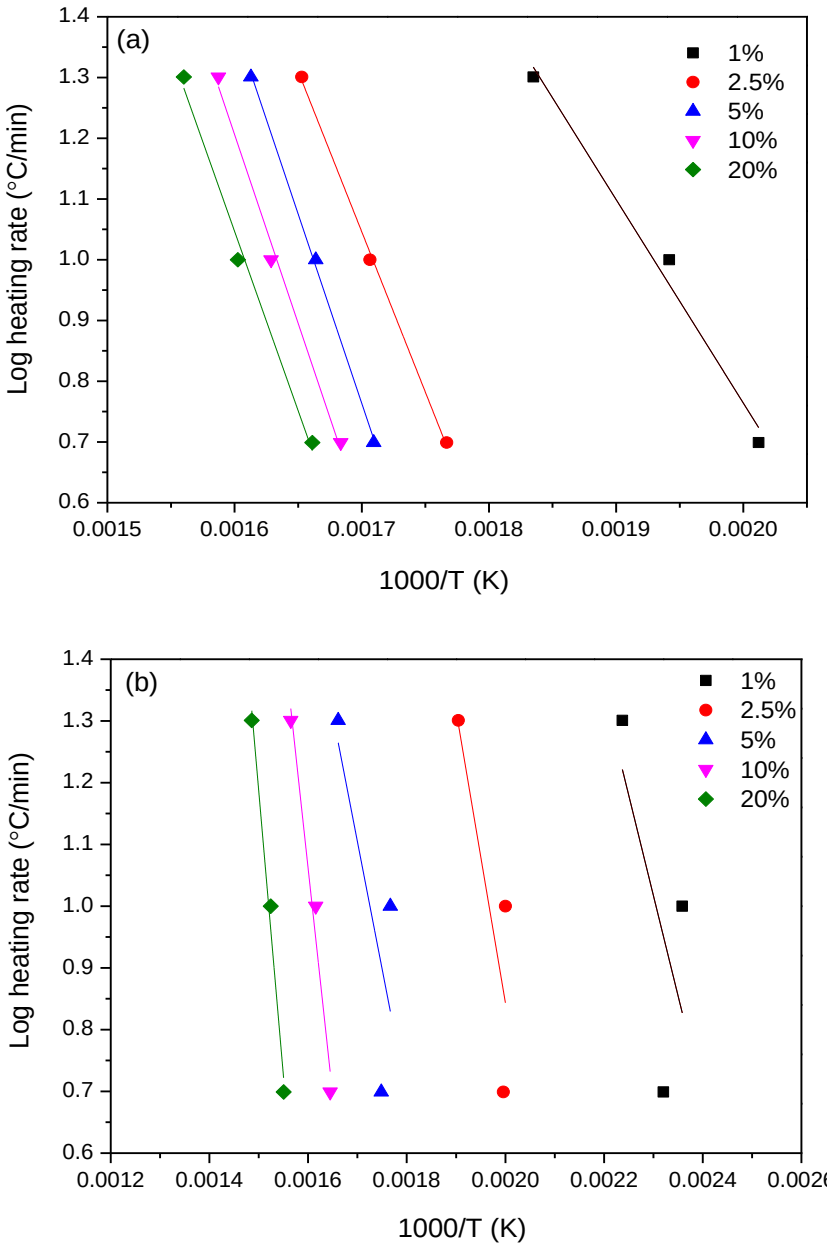

Figs. 6.10(a-b): Arrhenius plots of log heating rate against temperature of constant conversion data for a) neat SR and b) SR/C30B nanocomposite.

Fig. 6.11 displays activation energy (*E*) of the neat SR and SR/C30B nanocomposite, during the thermal oxidative decomposition, against conversion level in air. From this it can be seen that the nanocomposite possessed lower activation energy when compared with the neat SR, at conversion levels less than approximately 10%. However, at the highest conversion level (20%), the activation energy of the nanocomposite was 56% higher, indicating much better thermal stability.

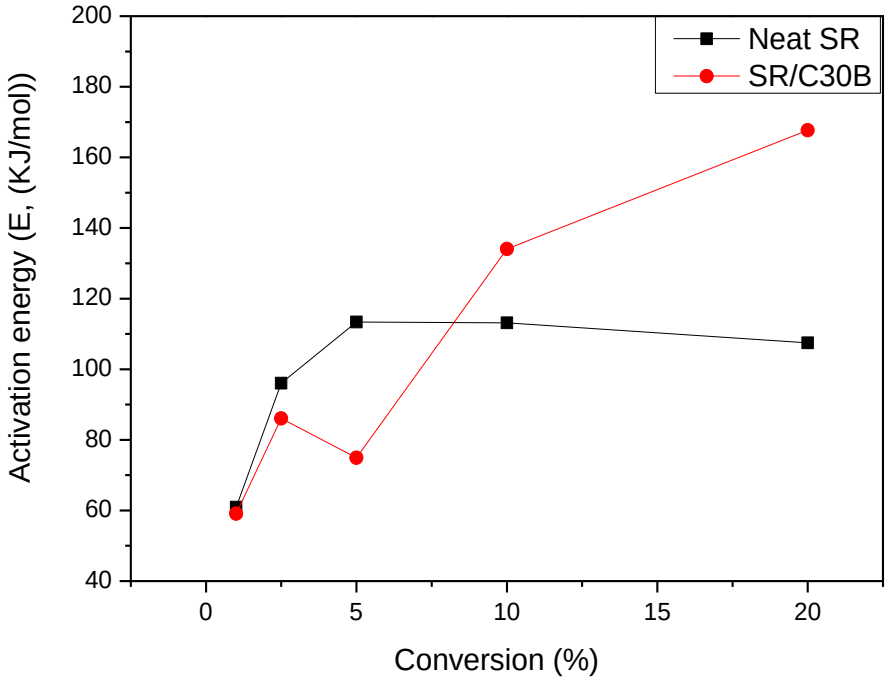

Fig.6.11: Activation energy of the neat SR and SR/C30B nanocomposite during decomposition process against conversion rate in air.

As this study has shown, exfoliated C30B clay has major advantages for the thermal stability and heat resistance of the rubber. Probably the most interesting finding of this study was the fact that the clay morphology did modify the thermal properties of the rubber for the better. This was in addition to the good mechanical properties reported for the aged nanocomposites containing exfoliated C30B clay.

6.8 Conclusions

From this study it can be concluded that addition of the montmorillonite clay enhanced the heat resistance of the rubber, reflected by higher retention strength of the nanocomposites when compared with the neat SR. The presence of exfoliated C30B clay protected the rubber against chain scission and direct oxidation, significantly delaying the degradation process. In addition the FTIR results showed that some crosslinks were formed in the neat SR and SR/C30B nanocomposite with increasing the ageing time to 24 h at 200°C.

Thermal stability in air was strongly dependent on clay morphology, which was found to increase in the following order: highly intercalated/exfoliated SR/Na^+MMT < highly intercalated SR/C20A < highly exfoliated SR/C30B. Moreover, the exfoliated C30B clay platelets prevented oxygen from diffusing into the rubber during degradation, increasing the thermal stability of the nanocomposite. The SR/C30B nanocomposite containing exfoliated clay had a lower thermal degradation rate and better thermal decomposition stability, as well as higher activation energy, in comparison to the neat SR. However, the exact effect of the clay morphology on the thermal degradation of the rubber in nitrogen atmosphere was not clear. It was concluded that, the organic modifier in the C20A clay might have played a role in influencing the thermal stability of the nanocomposite in the inert atmosphere.

6.8 References

1. Voulomenou A, Tarantili PA. Preparation, characterization, and property testing of condensation-type silicone/montmorillonite nanocomposites. *Journal of Applied Polymer Science* 2010; 118: 2521–2529.

2. Vaulot C, Ziegler P, Haidar B. Physicochemical driving forces behind exfoliation process of a synthetic montmorillonite in PDMS polymers. *Polymer* 2011: 52(3); 700-707

3. Kaneko MLQA, Romero RB, Goncalves MC, Yoshida IVP. High molar mass silicone rubber reinforced with montmorillonite clay masterbatches: Morphology and mechanical properties. *European Polymer Journal* 2010: 46 (5); 881-890.

4. Jia C, Zhang LQ, Zhang H, Lu YL. Preparation, microstructure, and property of silicon rubber/organically modified montmorillonite nanocomposites and silicon rubber/OMMT/fumed silica ternary nanocomposites. *Polymer Composite* 2011: 32; 1245–1253.

5. Suneel KS, Himadri A. Aging and Degradation Behavior of Rubber Nanocomposites In: Thomas S, Stephen R (eds). *Rubber Nanocomposites: Preparation, Properties, and Applications.* Chichester, UK: John Wiley & Sons, Ltd; 2010.75-81

6. Doede C, Panagrossi A. Polysiloxane Elastomers. *Industrial Engineering Chemical* 1947: 39(11); 1372–1375.

7. Bruden GJ. High Temperature Properties of Silicone Elastomers. *Journal Industrial Textiles* 1998; 27(4): 294-308.

8. Thomas DK. Stress/strain and swelling properties of a peroxide-cured methylvinyl silicone. *Polymer* 1964; 5: 463–470.

9. Roy N, Bhowmick AK. Novel in situ polydimethylsiloxane-sepiolite nanocomposites: Structure-property relationship. *Polymer* 2010; 51: 5172-5185.

10. Pielichowski K, Njuguna J. *Thermal degradation of polymeric material*. Shropshire, UK: Rapra Technology; 2005.

11. Choudhury A, Bhowmick AK, Soddemann M. Effect of organo-modified clay on accelerated aging resistance of hydrogenated nitrile rubber nanocomposites and their life time prediction. *Polymer Degradradation Stability* 2010: 95 (12); 2555-2562.

12. Chaudhry AN, Billingham NC.Characterisation and oxidative degradation of a room-temperature vulcanised poly(dimethylsiloxane) rubber*. Polymer Degradradation Stability* 2001: 73 (3); 505-510.

13. Pehlivan-Davis S, Clarke J, Armour S. Comparison of accelerated aging of silicone rubber gasket material with aging in a fuel cell environment. *Journal of Applied Polymer Science* 2013: 129 (3); 1446–1454.

14. Camino G, Lomakin S, Lazzari M. Polydimethylsiloxane thermal degradation Part 1. Kinetic aspects*. Polymer* 2001: 42(6); 2395–2402.

15. Lewicki JP, Liggat JJ, Pethrick RA., Patel M, Rhoney I. Investigating the ageing behavior of polysiloxane nanocomposites by degradative thermal analysis*. Polymer Degradation Stability* 2008: 93 (1); 158 – 168.

16. Cervantes-Uc JM, Cauich-Rodríguez JV, Vázquez-Torres H, Garfias-Mesías LF, Paul DR. Thermal degradation of commercially available organoclays studied by TGA–FTIR. *Thermochima. Acta* 2007; 457: 92-102.

17. Nik Ismail NI, Ansarifar A, Song, M, Preparation and characterization of high performance exfoliated montmorillonite/silicone rubber nanocomposites with enhanced mechanical properties. *Polymer Engineering Science* 2013; 53: 2603-2614.

18. Maiti M, Mitra S, Bhowmick AK. Effect of nanoclays on high and low temperature degradation of fluoroelastomers. *Polymer Degradation Stability* 2008; 93(1): 188–200.

19. American Standard Test Method. ASTM E1641-07. *Method for Decomposition Kinetics byThermogravimetry*. New York: ANSI; 2012.

CHAPTER 7: Hybrid filler reinforcement in silicone rubber

7.1 Introduction

Recently, there has been much interest in developing hybrid reinforcement in rubber based on a combination of two different types of nanoparticles, or of nanoparticles with conventional fillers such as CB and silica [1-4] ones. This is because the adverse effects of a single nanofiller can be diluted by adding a second filler which can balance the properties of the filled rubber. More interestingly, hybrid fillers have been shown to give a synergy reinforcing effect to the rubber's properties and, at the same time, the benefits from the individual fillers were still retained [1-4].

Some work was carried out by Jia and co-workers [5] regarding the effect of partial replacement of fumed silica (FS) filler in SR filled with organoclay montmorillonite (OMMT)/FS hybrid filler. In the study, the mechanical and barrier properties were compared between SR/OMMT/FS (100/30/20 phr) ternary nanocomposites and SR/OMMT (100/30 phr) binary nanocomposites. It was found that the ternary nanocomposites displayed better mechanical properties and also decreased the permeability coefficient by about 60%, indicating better gas barrier properties. The inclusion of FS in the rubber before mixing with OMMT increased the viscosity of the compound and mechanical shearing force during mixing with OMMT. As a result, the ternary nanocomposites exhibited better dispersion of OMMT in the rubber matrix.

The final objective of this thesis is to create a hybrid filler reinforcement in silicone rubber based on the combination of two types of nanofillers having different sizes and shapes. In view of the encouraging results reported for the synergistic effects of some hybrid filler systems in rubber [1-4], a hybrid filler system based on MMT and precipitated amorphous white silica filler (PS) was prepared and mixed with silicone rubber (SR).

In this chapter, the amount of PS was increased from 0 to 10 phr whilst the amount of MMT was kept constant at 6 phr in the hybrid filler weight ratio. The idea was to investigate the synergistic effects of this hybrid filler system, if any, on the rubber's properties. For a comparison, it was decided to replace the MMT with fibrous shaped nanofiller, namely multi wall carbon nanotube (MWNT), to form a new hybrid filler system, PS/MWNT. The initial results of the comparative study between a combination of PS/MMT and PS/MWNT are presented in this chapter. Some results on the cure characteristics, tensile testing and hardness of SR/PS/MWNT are discussed.

7.2 Filler dispersion in SR/MMT, SR/PS, and SR/PS/MMT nanocomposites

A series of samples of silicone rubber filled with hybrid fillers was prepared through a melt-mixing route. The details regarding the formulation and preparation of silicone rubber filled with hybrid fillers has been discussed in section 3.2.3. In this chapter, the effect of the filler weight ratio on the filler's dispersion in the SR/PS/MMT nanocomposites was investigated by XRD and TEM techniques.

7.2.1 X-ray diffraction (XRD) analysis of SR/PS/MMT nanocomposites

Fig. 7.1 shows the XRD spectra of the pure MMT and SR/PS/MMT nanocomposites with the hybrid filler (PS/MMT) weight ratios of 0.4, 1.0, 1.3 and 1.7. The spectra of the SR/PS/MMT nanocomposites exhibited distinct diffraction peaks within the range of $2\theta=7.4^{o}$ to 7.5^{o} as shown in Fig. 7.1, which according to Bragg's law correspond to 1.20 to 1.21 nm distance of basal spacing (d_{001}). These values were close to the *d* spacing of the pure Na^{+}MMT which was 1.22 nm (Fig. 7.1a). This suggests that the MMT layers remained

unchanged. It should be remembered that the SR/Na^+MMT nanocomposite contained both intercalated/exfoliated particles as confirmed by the XRD and TEM results in Chapter 4. Therefore, it was strongly believed that the inclusion of PS prevented the MMT particles from delaminating in the rubber.

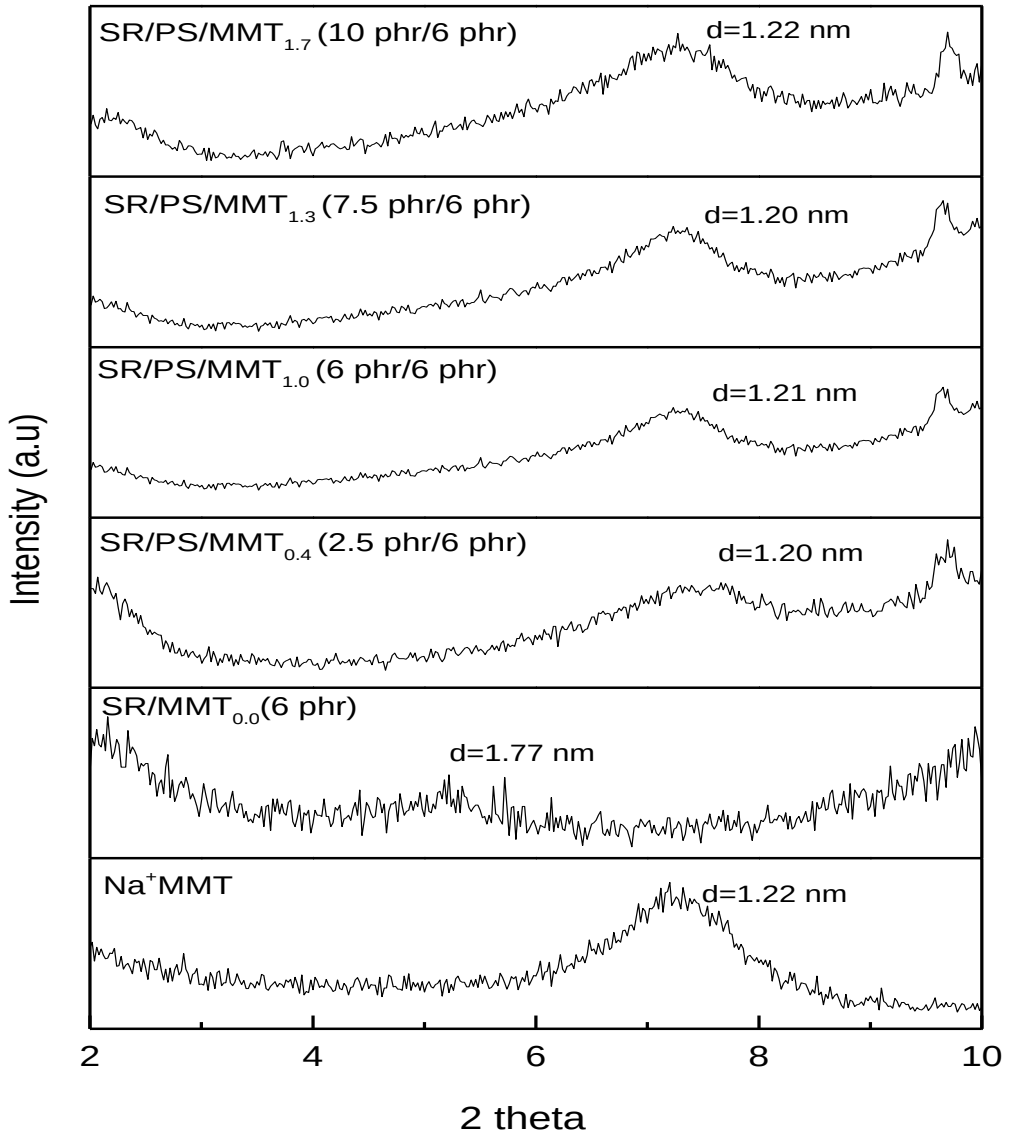

Fig. 7.1: XRD spectra of Na^+MMT clay, SR/MMT-6 phr and SR/PS/MMT nanocomposites with a range of filler weight ratios from 0.4 to 1.7.

7.2.2 Transmission electron microscopy analysis of SR/PS/MMT nanocomposites.

Fig. 7.2(a-d) shows TEM images of MMT and PS fillers dispersed in the SR/PS/MMT nanocomposite with the hybrid filler weight ratio of 1.0. The bright grey area in the images corresponds to the silicone matrix. It was noticed that the MMT (black spots with platy shape) and the PS (black spots with round shape) particles were separately dispersed in the matrix.

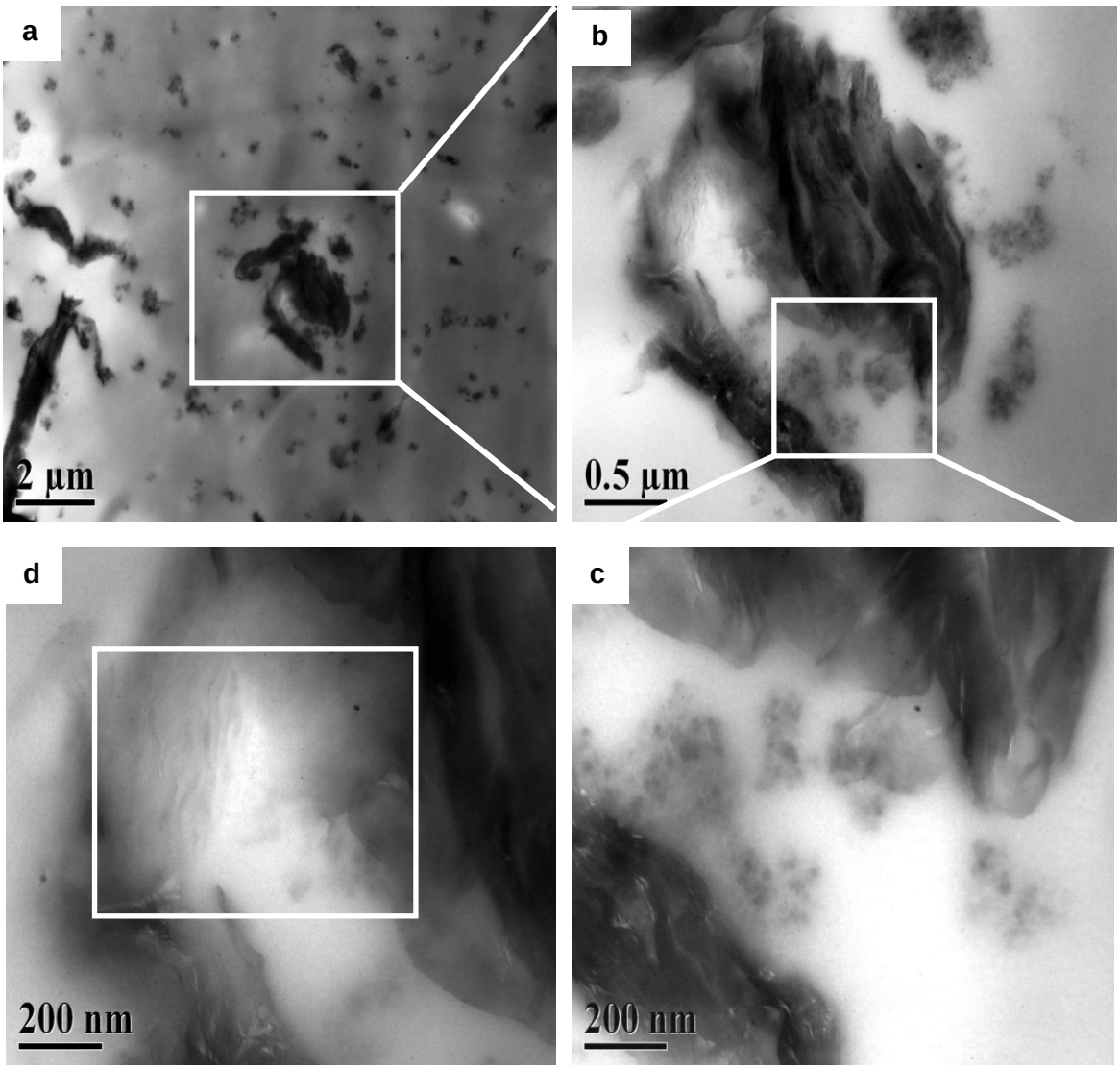

Fig. 7.2 (a-d): TEM micrographs showing dispersion of the (PS/MMT: 1.0) hybrid filler in SR/PS/MMT nanocomposite.

In Fig. 7.2a, it was observed that most of the PS fillers were well dispersed in the silicone matrix and some silicate tactoids were randomly oriented as seen in the images. Evidently, the MMT particles generally consisted of compact face-to-face stacking layers that indicated that the clay layers failed to exfoliate (Fig. 7.2 (b & c)). This was in agreement with the XRD analysis as discussed earlier. In addition, some of the primary PS particles with diameter sizes ranging from 20 to 50 nm formed a network structure as clearly seen in Fig 7.2d. The formation of the silica particles filler-filler network was due to strong hydrogen bonding and van der Waals forces [6]. Remember that no silane treatment was applied to the silica surface to prevent the PS particles from aggregation due to high filler–filler interaction.

TEM images for the SR/PS/MMT nanocomposite with filler weight ratio of 1.7 shown in Fig. 7.3 (a and b) showed a homogenised dispersion of PS particles in the silicone rubber matrix. Obviously, a high density of PS particles' network structure was observed as the filler weight ratios increased to 1.7 which consisted of 10 phr of PS and 6 phr of MMT. In the SR/PS/MMT filled with 1.7 filler weight ratio, some of the compact MMT particles with lateral sizes of about 2µm were surrounded by the silica particles as shown in the TEM images of Fig. 7.3 (a-b).

Similar to the nanocomposite with the low hybrid filler weight ratio of 1.0, most of the MMT layers (black platy shape) were stacked together and no evidence of intercalation and delamination was observed in the high magnification images in Fig. 7.3c-d. This suggested that both PS and MMT fillers were dispersed separately in the rubber matrix and this indicated that there was no internal network formed between the two.

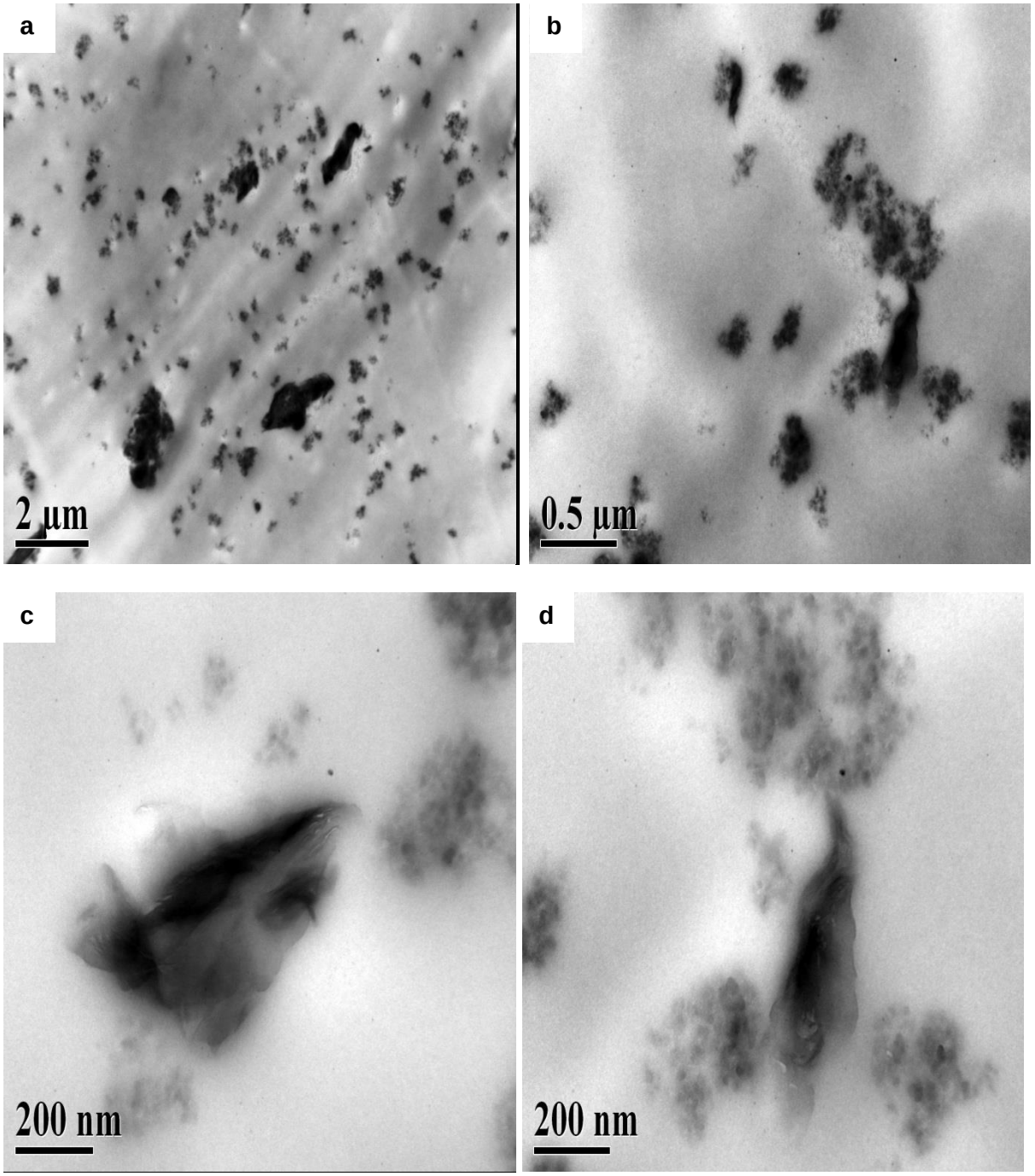

Fig. 7.3 (a-d): TEM micrographs showing dispersion of the (PS/MMT: 1.7) hybrid filler in SR/PS/MMT nanocomposite.

7.2.3 Field Emission Gun Scanning Electron Microscope (FEGSEM) analysis of SR/PS/MMT

The scanning electron micrographs in Fig. 7.4(a–e) show dispersion of the MMT and PS fillers in the SR/PS, SR/MMT, and SR/PS/MMT nanocomposites at low magnification (5000×) and high magnification (10,000×), respectively. Fig. 7.4a (i and ii) represents the overall MMT dispersion in the rubber matrix. Only a few filler aggregates were seen in the rubber and the aggregate size was roughly 1μm in size [Fig. 7.4a (ii)]. The result suggested that good dispersion of the MMT particles in the rubber matrix was achieved.

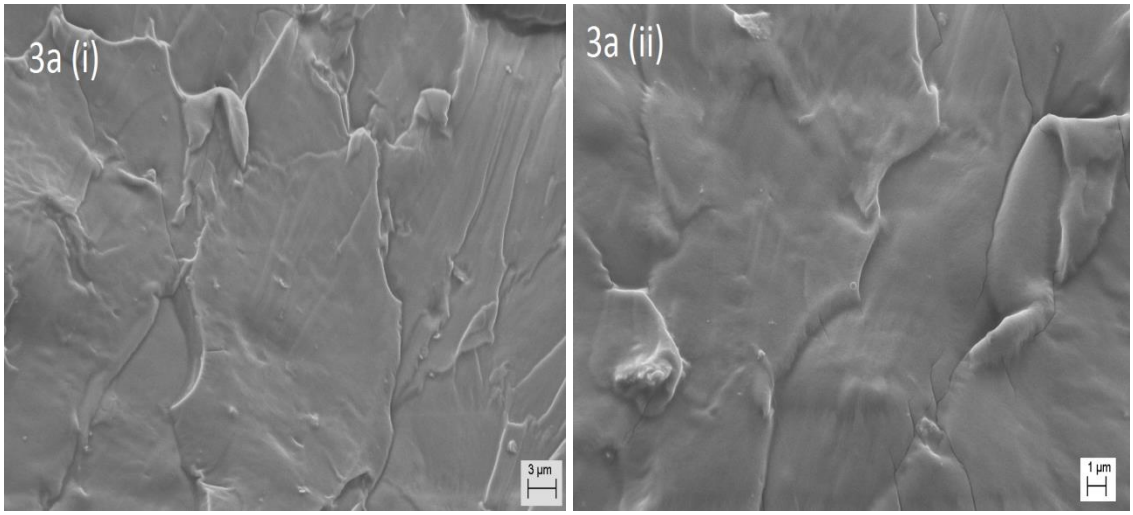

Fig. 7.4a (i-ii): SEM micrograph showing the dispersion of MMT (6 phr) in the rubber (i) 5000x mag and (ii) 10,000x mag.

Fig.7.4b and c, illustrated that most of the PS particles dispersed well in the rubber matrix even at high filler concentrations such as 10 phr [Fig. 7.4c (i and ii)]. Only a few large aggregates roughly 3 μm in size were seen and this was caused by the strong interaction between the PS particles. Normally, the silica surface is treated with bifunctional organosilane to reduce filler–filler interaction and increase dipersibility of the filler particles in

rubber**.** Since no silane was used in this study, filler aggregates were expected to form in the rubber matrix.

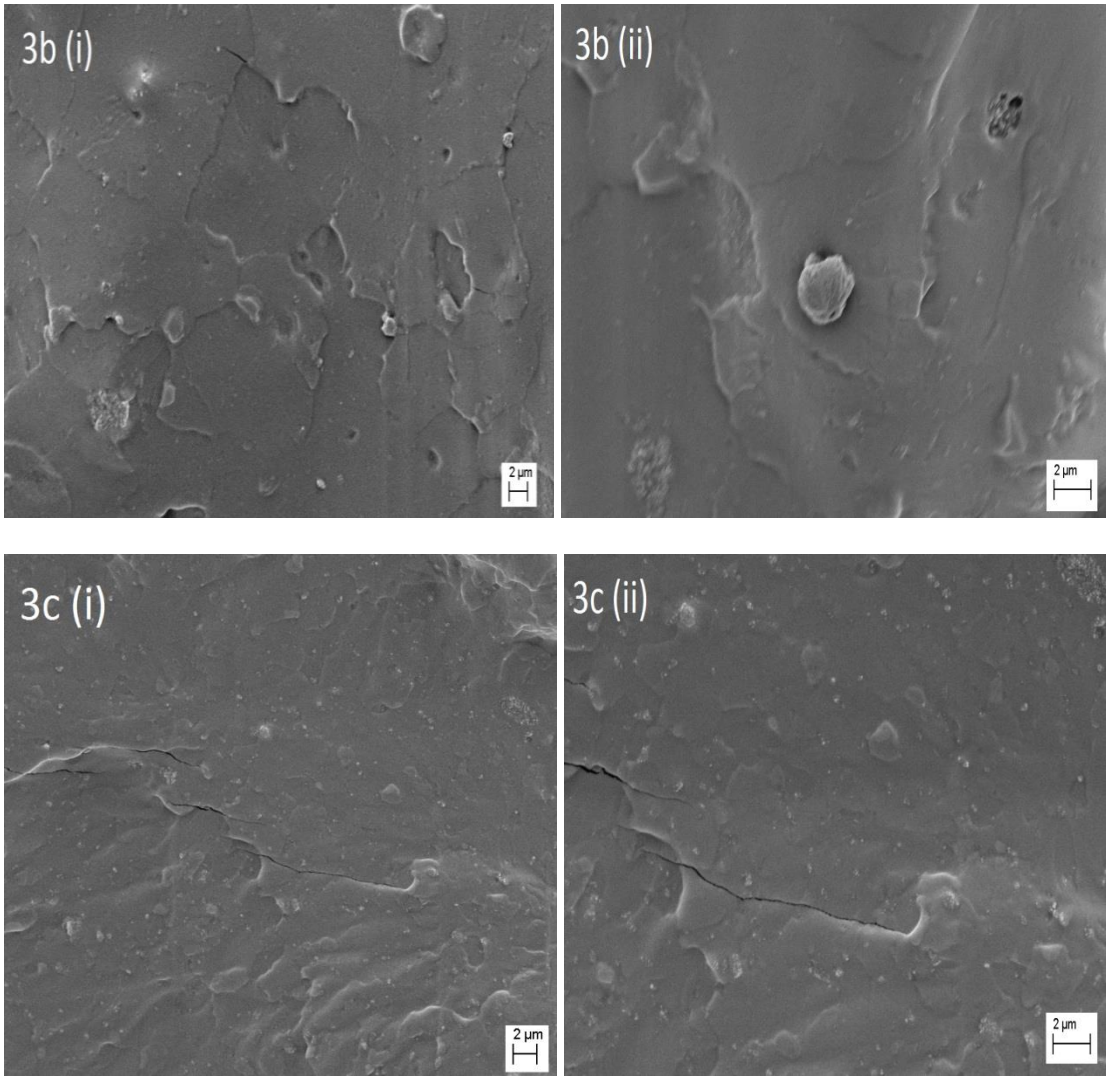

Fig.7. 4(b-c): SEM micrograph showing the dispersion of (b) PS (6 phr) and (c) PS (10 phr) in the rubber [(i) 5000x mag and (ii) 10,000x mag].

Fig. 7.4d(i and ii) shows MMT and PS fillers dispersed in the SR/PS/MMT nanocomposite with the hybrid filler weight ratio of 0.4. It was noticed that the MMT (bright dots with platy shape) and the PS (bright dots with round shape) particles were separately dispersed in the matrix [Fig. 7.4d(i)]. This suggested that there was no PS–MMT network in the nanocomposites. Fig. 7.4d(ii) showed that MMT particles failed to exfoliate in the rubber matrix

and formed aggregates roughly 3 mm in size. However, there was little evidence of the PS aggregates in the SR/PS/MMT nanocomposite with the hybrid filler weight ratio of 0.4, probably because there was small amount of the PS filler in the rubber.

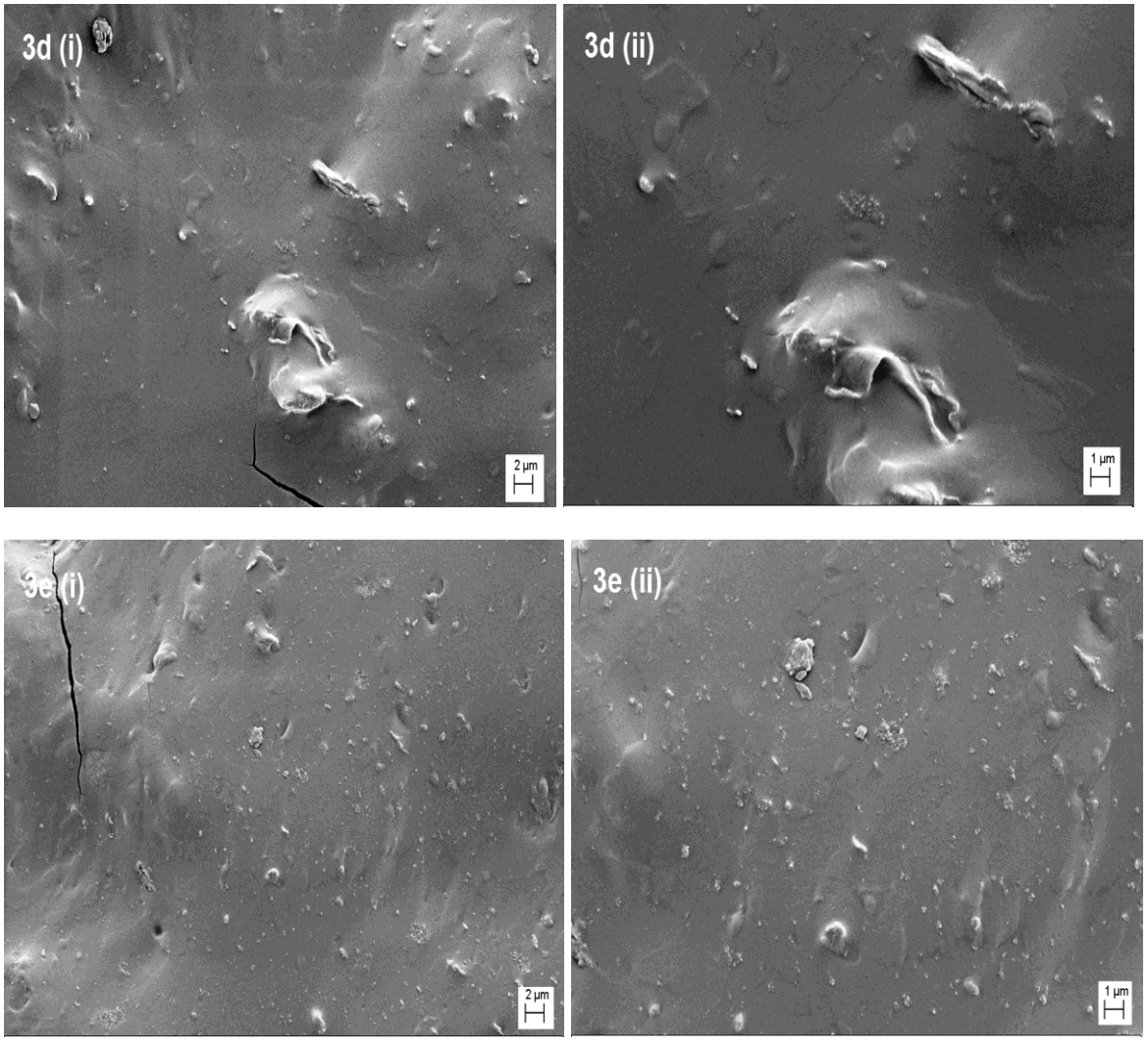

Fig. 7.4(d-e): SEM micrographs showing dispersion of PS/MMT hybrid filler in (d) SR/PS/MMT nanocomposite (0.4) and SR/PS/MMT nanocomposite (1.0) [(i) 5000x mag and (ii) 10,000x mag]

Fig. 7.4 e (i and ii) shows the dispersion of the SR/PS/ MMT nanocomposite with filler weight ratio of 1.7. Obviously, the rubber matrix contained a lot of PS particles as well as aggregates, which were up to 2 µm in size. Remember that no silane treatment was

applied to the silica surface to prevent the PS particles from agglomerating due to high filler–filler interaction. Most of the MMT particles (bright platy shape) formed aggregates in the range of submicron particle size. This suggested that no exfoliation of MMT occurred in the rubber matrix. Both PS and MMT fillers were dispersed separately in the rubber matrix and this indicated that there was no internal network formed between the two.

7.3 Cure characteristics of the unfilled SR, SR/MMT, SR/PS, and SR/PS/MMT nanocomposites

Table 7.1 presents the results from the cure tests. These include optimum cure time (t_{95}), scorch time (t_{s2}), minimum torque (M_L), maximum torque (M_H), and ∆torque (∆M) of the control rubber, SR/MMT nanocomposite containing 6phr MMT, SR/PS nanocomposites containing 6 and 10phr PS, and the SR/PS/MMT nanocomposite where the hybrid filler weight ratio was increased from 0.4 to 1.7.

Overall, the optimum cure time of the SR/PS/MMT nanocomposite was longer than that of the SR/MMT nanocomposite, irrespective of the hybrid filler weight ratio. The scorch times of the nanocomposites were fairly similar at about 3 min, with the exception of the SR/PS nanocomposite with 10 phr PS and the SR/PS/MMT nanocomposite with the hybrid filler weight ratio of 1.7, which had similar scorch times at 2.5 min. The minimum torque, which indicated the rubber viscosity, rose by 70% when the optimum loading of the hybrid filler weight ratio was reached.

This was expected because solid fillers increase rubber viscosity. Also, for these nanocomposites, the maximum torque rose by 33% and ∆torque by 30%, respectively [cf. SR/MMT (MMT: 6 phr) and SR/PS/ MMT (PS/MMT: 1.7)]. As stated earlier, ∆torque indicates crosslink density changes in the rubber and, on this basis, the addition of the hybrid filler was beneficial to the crosslink density of the rubber. Note also that the ∆torque of the SR/PS nanocomposite increased by approximately 12% when the PS loading was raised from 6 to 10 phr. A study demonstrated that when the silica loading was increased, the filler

particles tended to interact between themselves due to the high surface area and the abundance of the OH groups on the silica surface.

Table 7.1: The cure characteristics of the neat SR and nanocomposite

Filler weight ratios (PS/MMT)	**Cure time, T_{95} (min)**	**Scorch time, T_{S2} (min)**	**CRI, $100/T_{95}-T_{S2}$ (min^{-1})**	**Max torque, M_H (dNm)**	**Min torque, M_L (dNm)**	**Delta torque, ΔM (dNm)**
Neat SR (control)	7.24	3.13	24.3	23.19	1.90	21.29
SR/MMT (MMT: 6 phr)	7.23	3.32	25.6	25.42	2.02	23.40
SR/PS (PS: 6 phr)	11.14	3.25	12.7	28.37	2.92	25.45
SR/PS (PS: 10 phr)	15.10	2.55	8.0	31.77	3.15	28.62
SR/PS/MMT (PS/MMT: 0.4) 2.5 phr PS + 6 phr MMT	11.41	3.38	12.5	27.11	2.62	24.49
SR/PS/MMT (PS/MMT: 1.0) 6 phr PS + 6 phr MMT	10.26	3.11	14.0	30.90	2.98	27.92
SR/PS/MMT (PS/MMT: 1.3) 7.5 phr PS + 6 phr MMT	10.45	3.15	13.7	30.76	2.77	27.99
SR/PS/MMT (PS/MMT: 1.7) 10 phr PS + 6 phr MMT	13.42	2.45	9.1	33.79	3.43	30.36

As a result, the viscosity of the compound increased due to high silica–silica interaction [7, 8]. Furthermore, hydrogen bonds were formed between the oxygen atoms in the SR backbone and the silanol groups on the silica surface and this acted as additional crosslinks in the rubber and larger Δ torque values were recorded. It was particularly interesting to note that the crosslink density benefitted so much from the rise in the hybrid filler weight ratio in the rubber as shown by a noticeable improvement in the Δ torque values.

Evidently, the addition and progressive increase in the loading of PS in the SR/PS/MMT nanocomposite was beneficial to the crosslink density and the mechanical properties of the nanocomposite.

For the purpose of clarity, the cure traces of the control rubber, SR/MMT, SR/PS, and SR/PS/MMT nanocomposites with the hybrid filler weight ratios of 0.4, 1.0, and 1.7 were compared in Fig. 7.5. It was obvious that some of the cure properties of the SR/PS/MMT nanocomposites were significantly better than those of the control rubber. For example, ∆torque was 43% higher for the SR/PS/MMT nanocomposite containing the hybrid filler weight ratio of 1.7. However, the optimum cure time and the rate of cure were adversely affected by the addition of the hybrid filler. The optimum cure time increased by 85% and the CRI decreased by 63% when the hybrid filler weight ratio reached 1.7 [cf. SR/PS/MMT (PS/MMT:1.7) and control SR].

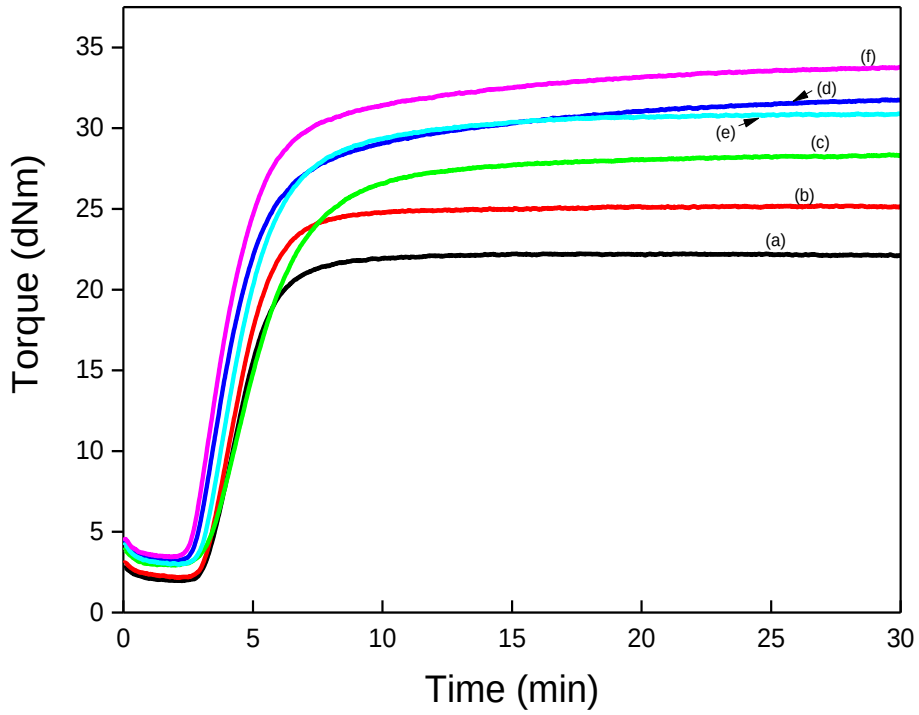

Fig.7.5. Rheometer curves of (a) neat SR, (b) SR/MMT with 6 phr MMT, (c) SR/PS with 6 phr PS, (d) SR/PS with 10 phr PS, (e) SR/PS/ MMT (PS/MMT: 0.4), (f) SR/PS/MMT (PS/MMT: 1.0), and (g) SR/PS/ MMT (PS/MMT:1.7).

Note that the SR/MMT nanocomposite with 6 phr MMT had similar optimum cure and scorch times to the control rubber, but a higher Δ torque value. However, the SR/PS nanocomposite with 6 phr PS had a longer optimum cure time compared with the control rubber though the scorch times were similar. The Δ torque of the SR/PS nanocomposite with 6 phr PS was roughly 20% higher than that of the control rubber, which indicated a higher crosslink density. It was noted that the CRI of the SR/PS nanocomposite with 6 phr PS was 50% lower than that of the SR/MMT nanocomposite with 6 phr MMT, which indicated a lower crosslink density in the rubber. Adverse effects of an increasing loading of PS on the cure time and rate of cure of a DCP cured SR have been reported [9].

7.4 Effect of the PS/MMT hybrid filler weight ratio on the tensile properties of the SR/PS/MMT nanocomposite

The properties of the control rubber were: tensile strength, 0.40 MPa; Young's modulus, 0.30 MPa; M100, 0.20 MPa; elongation at break, 639%; stored energy density at break, 2.42 mJ/m^3; and hardness 18.5 respectively. Fig. 7.6 (a–f) presents the tensile strength, Young's modulus, M100, elongation at break, stored energy density at break and hardness of the SR/PS/MMT nanocomposites as a function of the hybrid filler weight ratio, respectively. Overall, the tensile strength increased by 178% (Fig.7. 6a), Young's modulus by 79% (Fig. 7.6b), M100 by 33% (Fig. 7.6c), elongation at break by 49% (Fig. 7.6d), and stored energy density at break by 202% (Fig. 7.6e) as the hybrid filler weight ratio was increased from 0 to 1.7.

From the results, it was clear that the improvement in both the tensile strength and the modulus was achieved without causing a detrimental effect on the elongation at break of the rubber. In addition, the stored energy density at break is a measure of the energy stored per unit volume in the rubber before the sample finally breaks, hence it was concluded that the increase in the hybrid filler weight ratio enhanced resistance to crack initiation and crack growth in the rubber.

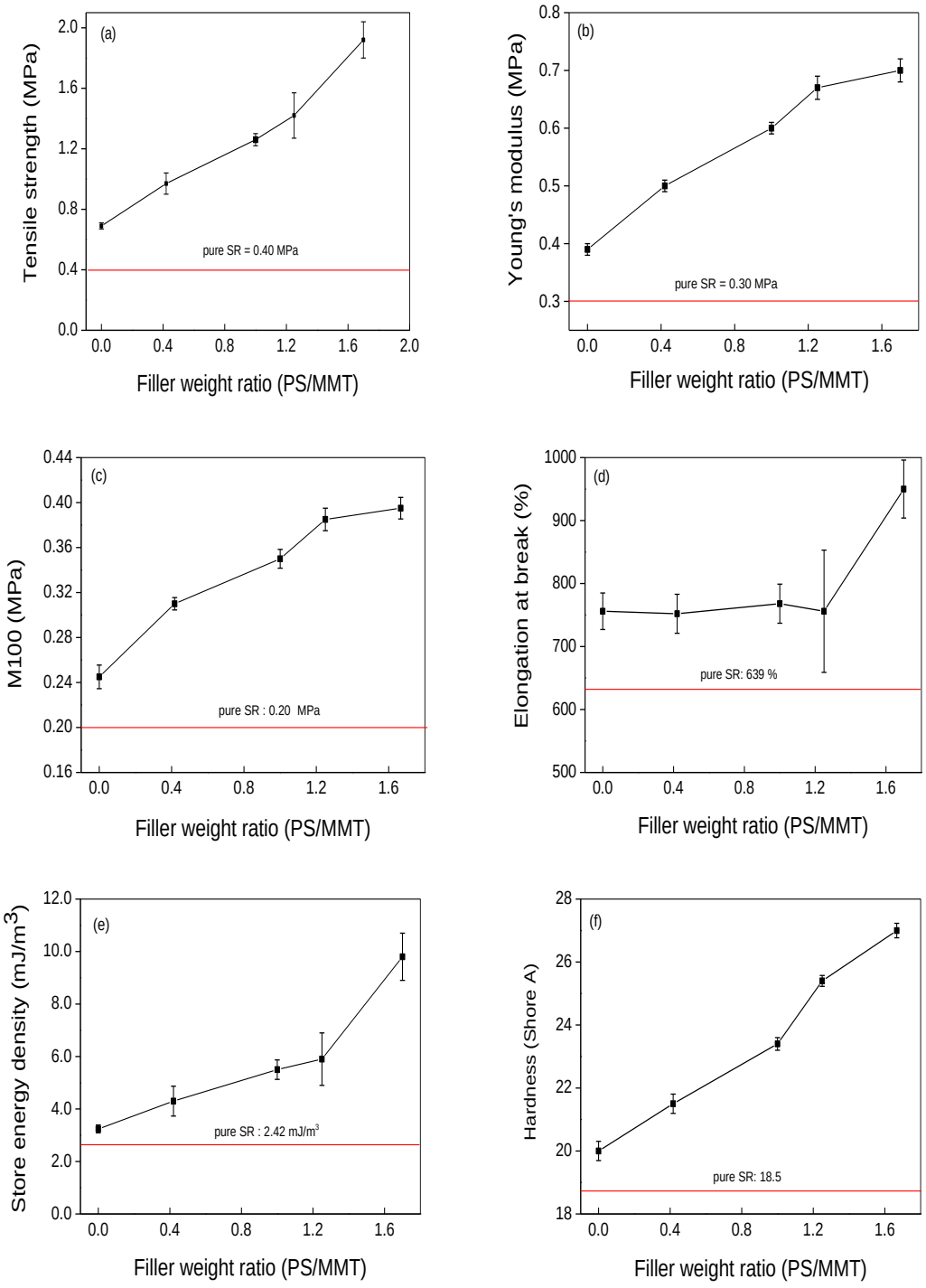

Fig. 7.6: (a) Tensile strength, (b) Young's modulus, (c) M100, (d) elongation at break, (e) store energy density and (f) hardness of the SR/PS/MMT nanocomposites as a function of PS/MMT filler weight ratio.

The rubber properties, such as tensile strength and stored energy density at break, depend on crosslink density [10, 11]. Since the MMT particles did not exfoliate in the SR/PS/MMT nanocomposites to provide optimum reinforcement for the rubber, in this case the improvement seen in the tensile properties was mainly due to the interaction between the active sites on the PS surface and the SR chains which provided additional crosslinks between the SR chains and PS [12]. The hardness benefitted from increases in the hybrid filler weight ratio to 1.7, and rose by 35% (Fig. 7.6f). The rise in the hardness was consistent with the increases recorded for the Young's modulus and M100. This provided additional evidence of the increase in crosslink density in the rubber.

7.5 Effect of PS/MMT hybrid filler on the stress–strain behaviour of the nanocomposites

Fig. 7.6 presents stress–strain curves for the control rubber, SR/MMT with 6 phr MMT and SR/PS nanocomposites containing 6 phr and 10 phr PS. The stress–strain properties of the rubber improved substantially when MMT and PS fillers were added. Interestingly, when the stress–strain properties of the nanocomposites with the same amount of PS and MMT, i.e., 6 phr, were compared with that of the control rubber, the nanocomposite with PS had superior properties. In this case, the maximum stress was 67% higher in favour of the rubber with the PS filler [cf. Fig. 7.7(i) with a(ii) and (iii)] and it continued improving up to 194% when the PS loading was increased to 10 phr [Fig. 7.7a(iv)]. This was due to the additional hydrogen bonding in the SR/PS nanocomposite which stiffened up the rubber [12].

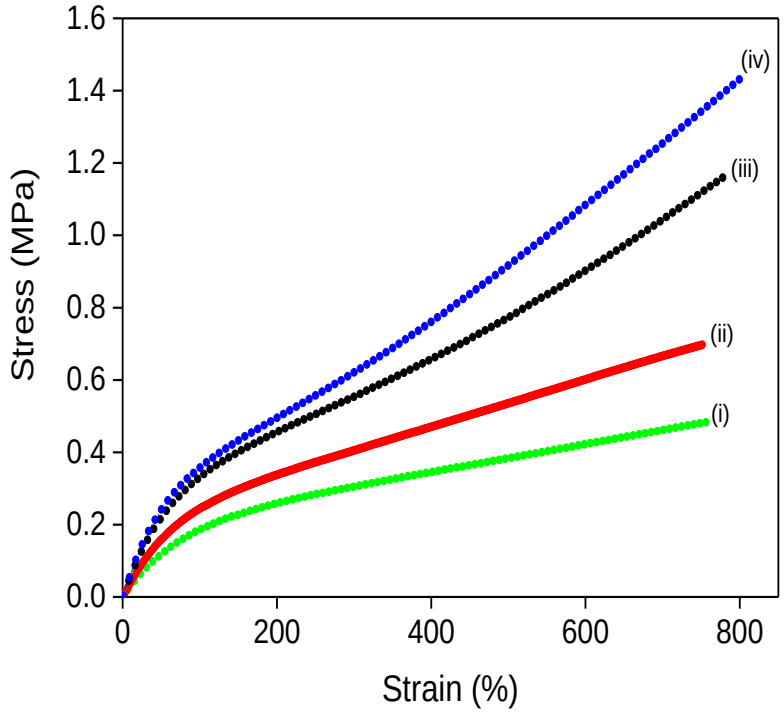

Fig. 7.7a: Stress-strain curves of (i) pure SR and SR filled with (ii) MMT- 6 phr, (iii) PS - 6 phr (iv) PS-10 phr

Fig. 7.7b shows the stress-strain curves of the SR/PS/MMT nanocomposite containing the hybrid filler with different filler weight ratio. The inclusion of the hybrid filler in the rubber showed a similar effect. The maximum stress recorded for the SR/PS/MMT nanocomposite with the hybrid filler weight ratio of 0.4 showed a 98% improvement compared with the control rubber [cf. Fig. 7.7b(i) and (ii)]. As the hybrid filler weight ratio was raised to 1.7, the maximum stress was 308 % higher than that of the control rubber [cf. Fig.7.7b(i) and (iv)]. Clearly, the hybrid filler was very beneficial to the stress–strain properties of the rubber. Interestingly, the stress–strain curves of the SR/PS/MMT nanocomposite exhibited a large increase in the stress level at higher deformation as shown in Fig. 7.7b (iv).

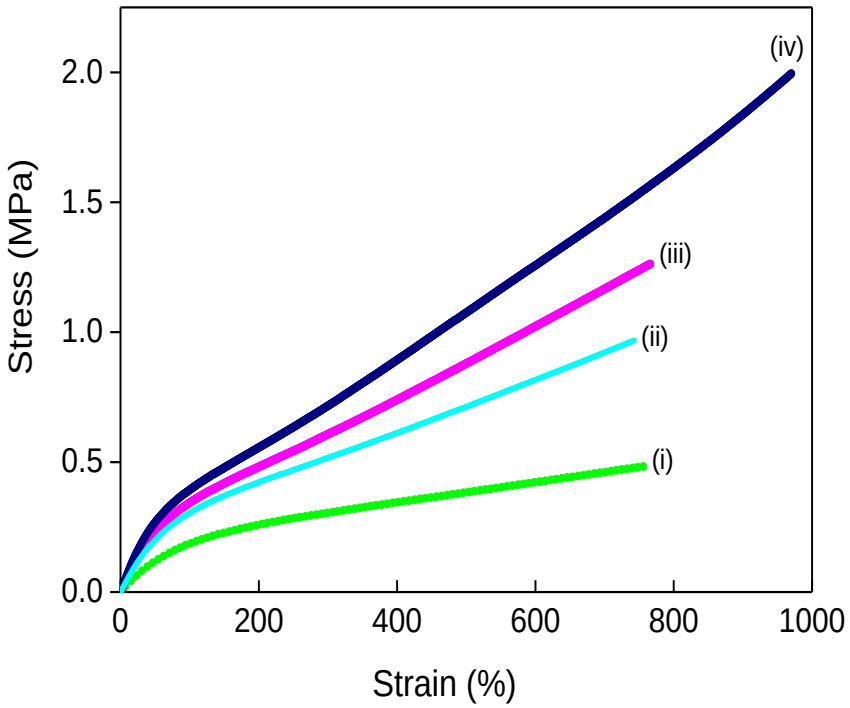

Fig. 7.7b: Stress–strain curves of pure SR and SR/PS/MMT nanocomposites. (i) Pure SR, (ii) SR/PS/MMT (PS/MMT:0.4), (iii) SR/PS/MMT (PS/ MMT:1.0), and (iv) SR/PS/MMT (PS/MMT:1.7).

Normally, this phenomenon is seen in filled NR compounds because the hydrocarbon chains crystallise on stretching at high strains, increasing the strength of the rubber. However, for non-crystallising rubbers such as SR this behaviour does not occur. It was believed that the high surface activity of PS was beneficial to the higher stress level recorded for the SR/PS/MMT nanocomposite. Although, MMT did not exfoliate in the rubber, some contribution from this filler to the rubber properties could not be ruled out. Therefore, it was concluded that the improvement in the stress–strain properties of the SR/PS/ MMT nanocomposite was mainly due to the contribution from the individual filler rather than a synergistic effect of the hybrid filler.

7.6 Hysteresis in the control rubber, SR/PS, SR/MMT, and SR/PS/MMT nanocomposites

Generally, the inclusion of solid fillers such as PS and MMT, causes energy dissipation or hysteresis in rubber. Hysteresis is measured from the area under a stress-strain graph which is produced in a single cycle. To measure hysteresis in the rubbers, standard dumbbell test pieces were cycled repeatedly up to 10 cycles at 200 and 400% elongation to generate stress-strain traces. The energy loss or energy dissipation in the rubber was calculated from the area between the extension–retraction curves produced after the first cycle at 200% and 400% elongation.

Typical stress–strain curves for the control rubber and nanocomposites with PS and MMT at 400% strain amplitude are shown in Fig. 7.8a. The results are summarised in Table 7.2. The energy loss of an unfilled cured rubber is entirely due to the frictional movement of the rubber chains. However, in the nanocomposites, there are a few additional factors that cause hysteresis, which are: filler–filler interaction [13], rubber–filler interaction [14], detachment from the filler surface or slippage on the filler surface of chains having reached their limit of extensibility [15–17], as well as the frictional movement of the rubber chains. When untreated PS is added to rubber, some of the PS particles do not disperse well in the rubber matrix and filler aggregates are formed because of the high surface energy of PS.

At the same time, PS can interact with the rubber chains, though to a lesser extent than well dispersed PS particles do, to form hydrogen bonds. Hydrogen bonds increase the rubber stiffness and modulus [18]. The filler network is composed of hard regions, where a high volume fraction of filler exists, and soft regions, where a low volume fraction of filler is present. Hard regions convert into soft regions when stress is applied to the rubber, and as a result this mechanism will generate energy loss [19].

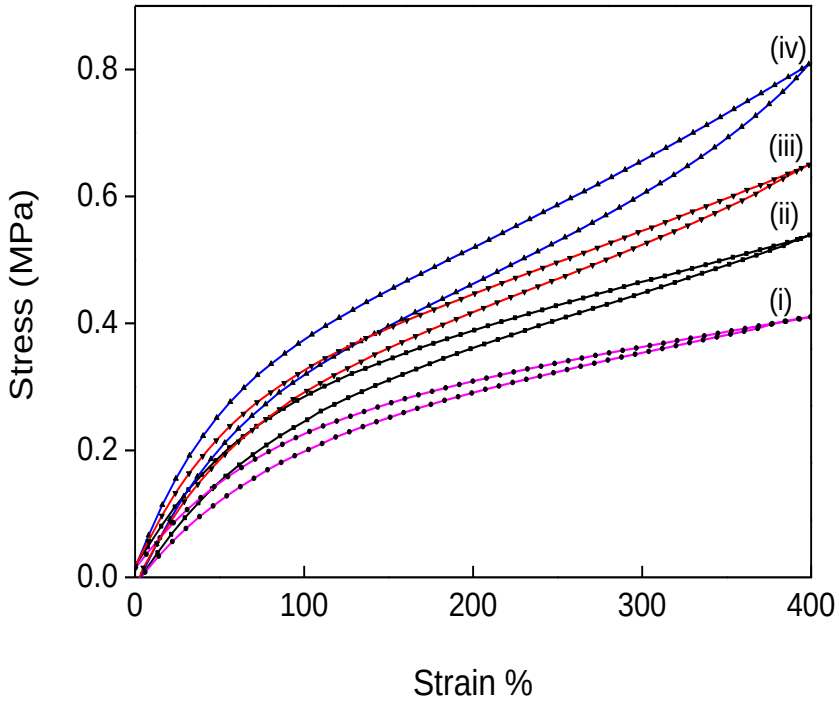

Fig. 7.8a: Stress-strain curves of the (i) pure SR and SR filled with (ii) MMT-6 phr, (iii) PS-6 phr (iv) PS -10 phr.

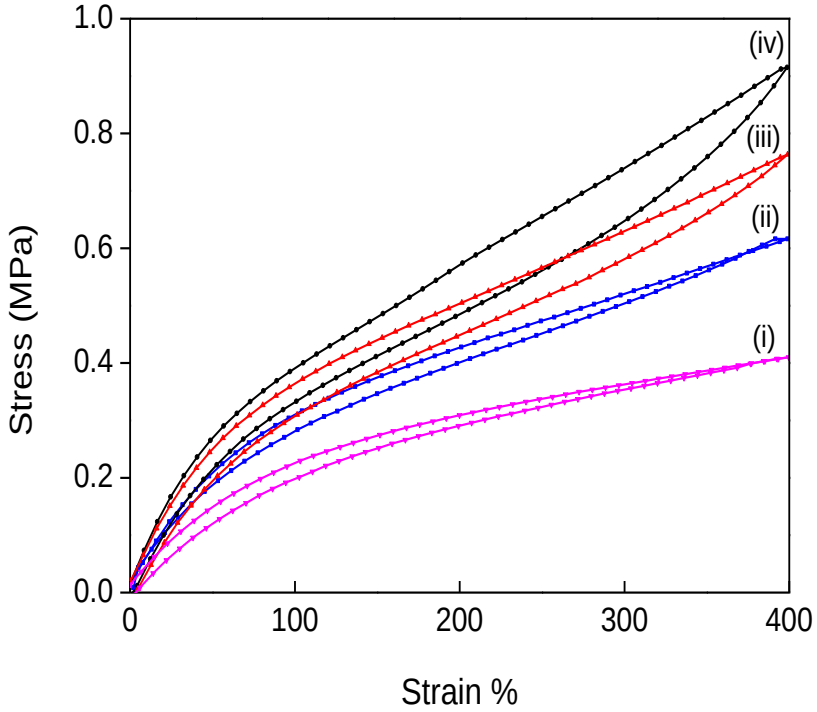

Fig. 7.8b: Stress-strain curves of the (i) pure SR and SR filled with (ii) MMT- 6 phr (iii) PS/MMT (1.0), (iv) PS/MMT(1.7) .

In the case of rubber–filler interactions, there are two kinds of interactions, namely weak Van der Waals bonds resulting from physical adsorption of rubber chains on the filler surface, and strong links which cannot be broken during deformation [20]. Rubber chains which are attached between filler particles break or detach under strain [19]. In fact, filler aggregates are bound together by a distribution of chains of different lengths. The shortest chains will reach their limit of extensibility and then break when the rubber is deformed. There is also a chain slippage process onto the filler surface [21, 22].

Table 7.2: Dissipated energy of the control and nanocomposites at different deformation (first cycle)

Compound	**Energy dissipation (mJ/m^3)**	
	200% strain	**400% strain**
Control rubber	26	97
SR/MMT- 6 phr	36	139
SR/PS - 6 phr	28	105
SR/PS - 10 phr	41	199
$SR/PS/MMT_{(1.0)}$	41	194
$SR/PS/MMT_{(1.7)}$	60	275

As seen in Table 7.2, both the SR/MMT and SR/PS nanocomposites exhibited higher energy losses than the control rubber at both elongations. This was because in the filled rubbers, the level of energy loss was influenced by the dispersion of the fillers. For 200% strain amplitude, the energy loss increased by 38 and 8%, respectively, when 6 phr Na^+MMT and 6 phr PS were added. A similar trend was also observed at 400% strain amplitude, where the energy loss was at 43 and 8%, respectively, for the two nanocomposites. The results clearly showed that the inclusion of MMT contributed to more energy loss in the

rubber than the silica did. There are at least three possible mechanisms to explain the energy loss in these nanocomposites.

It should be remembered that the SR/Na^+MMT nanocomposite contained a mixture of intercalated and exfoliated particles as discussed in Chapter 4. The rubber chains physically adsorbed on the surface of the platelets by weak attractive Van der Waals forces and when the rubber was deformed, the chains detached from the platelets. There was also energy loss due to the internal friction between the macromolecular chains. Ideally, in a filled rubber, low hysteresis will be realised if the interaction between the filler particles and the rubber chains is strong. Since the physical interaction between the platelets and the rubber chains was not strong enough to restrict the chain mobility too much, the chains detached and slid over each other, causing energy dissipation in the rubber.

Since the untreated silica produced a strong interaction with the SR chains and a greater number of links, it was assumed that there was a strong PS–rubber interaction and little detachment from the PS surface or slippage on the PS surface of chains having reached their limit of extensibility. Therefore, the large energy loss measured for the SR/PS/MMT nanocomposites was due to PS–PS interaction, which lead to the formation of hard regions which converted to soft regions (Fig. 7.4d), the breaking up of short rubber chains binding the PS particles together, and the frictional movement of the rubber chains. These processes were exasperated when the PS loading was increased progressively in the hybrid filler system.

Obviously, the hybrid filler weight ratio was an important factor in controlling the energy loss in the nanocomposites. Moreover, the energy loss depended strongly on the interaction of the PS and MMT fillers with the SR chains as well as the dispersion of the fillers in the rubber matrix. Finally, there was no evidence of a synergistic effect of the MMT and PS fillers on the rubber properties under the present mixing and curing conditions.

7.7 Ageing properties of SR/PS/MMT nanocomposites

Table 7.3 compares the tensile properties of neat SR, SR/MMT and SR/PS/MMT nanocomposites before and after aging. The thermal ageing tests were performed at 200°C for 24 hours. The test procedure has been described in the Chapter 3. The tensile strength and Young's modulus of SR/PS/MMT nanocomposites after ageing were generally reduced, regardless of the weight ratios of the PS/MMT hybrid fillers as shown in Table 7.4. In contrast, elongation at break showed an inconsistent trend, where a little increment was observed for the SR nanocomposite filled with 1.0 and 1.3 PS/MMT respectively. Overall, the values of all the aged properties of SR/PS/MMT nanocomposites remained higher than the neat SR and single filler nanocomposite SR/MMT.

Table: 7.3: Unaged and aged properties of neat SR, SR/MMT and SR/PS/MMT nanocomposites.

Samples	**Tensile strength (MPa)**		**Young's modulus (MPa)**		**Elongation at break (%)**	
	Unaged	**Aged**	**Unaged**	**Aged**	**Unaged**	**Aged**
Neat SR	0.40	0.19	0.30	0.17	756	488
SR/MMT (MMT 6 phr) (PS/MMT:0.0)	0.57	0.42	0.36	0.30	695	566
SR/PS/MMT (2.5 phr PS + 6 phr MMT (PS/MMT: 0.4)	0.97	0.61	0.50	0.36	752	718
SR/PS/MMT (6 phr PS + 6 phr MMT) (PS/MMT: 1.0)	1.26	0.96	0.60	0.46	768	819
SR/PS/MMT (7.5 phr PS + 6 phr MMT) (PS/MMT: 1.3)	1.42	1.16	0.67	0.53	756	804
SR/PS/MMT (10 phr PS + 6 phr MMT) (PS/MMT: 1.7)	1.52	1.30	0.70	0.57	950	769

To understand the effect of hybrid filler weight ratios on the thermal aging properties of the silicone rubber nanocomposites, the properties were characterised based on percent retention ((aged÷unaged) × 100). Principally, percent retention measures the sustainability of a sample to thermal treatment. In this case, a higher percent retention obtained in a sample indicates more resistance to heat aging.

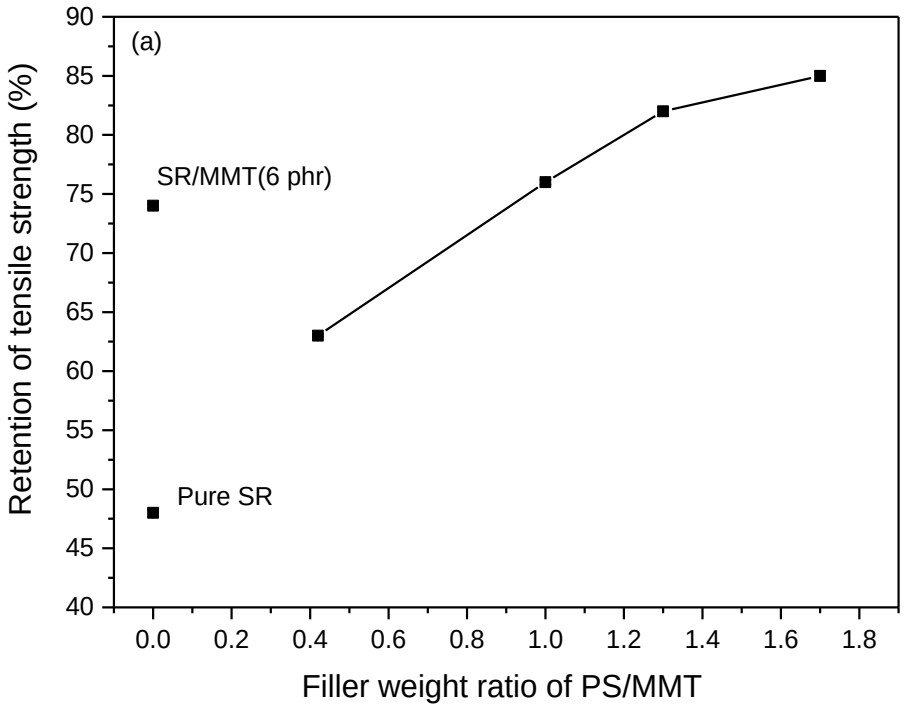

Fig. 7.9a: Percent retention of tensile strength of SR/PS/MMT against filler weight ratios.

Fig. 7.9a displays the percent retention of tensile strength of SR/PS/MMT against filler weight ratios. The result suggested that the resistance to aging of SR/PS/MMT was improved by gradually adding the amount of PS filler in the PS/MMT hybrid filler system. For example, the SR nanocomposite filled with 1.7 PS/MMT weight ratio maintained about 86% of its tensile strength after aging, which was greater than SR/MMT which had a 74% tensile strength retention. Similarly, the retention of Young's modulus steadily increased with the increase of the hybrid filler PS/MMT weight ratio as presented in Fig. 7.9b. This was

probably due to the formation of a strong interfacial interaction between the filler and the silicone matrix as the amount of the PS filler in the PS/MMT hybrid filler increased.

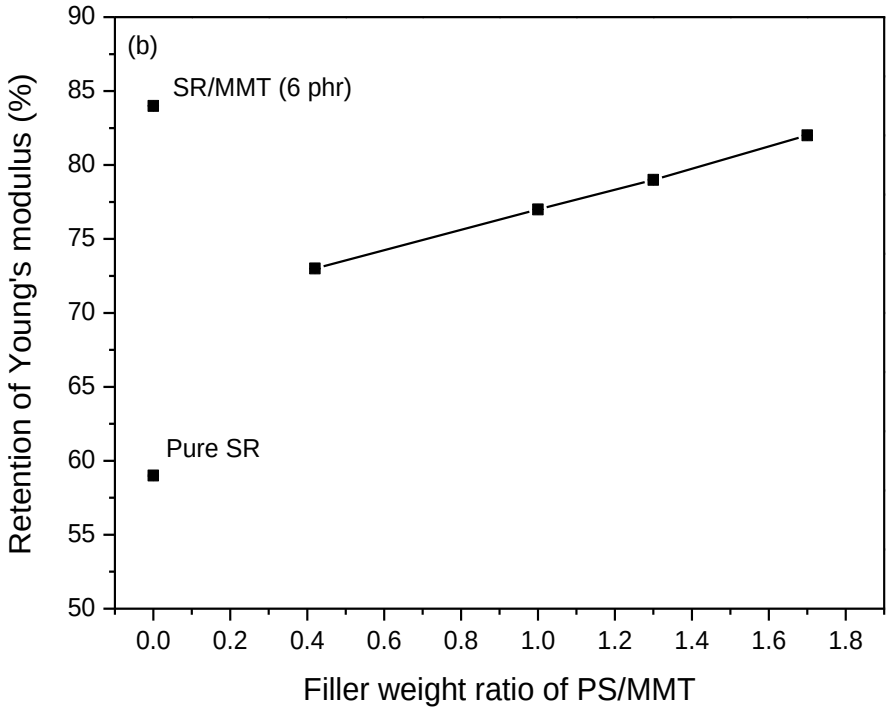

Fig.7.9b: Percent retention of Young's modulus of SR/PS/MMT against filler weight ratios.

On the other hand, the retention of elongation at break of the SR/PS/MMT showed an inconsistent trend against the hybrid filler weight ratio (Fig. 7.9c). It was found that the retention of elongation at break increased significantly as the PS/MMT filler weight ratio reached 1.3, but it dropped dramatically afterwards as shown in Fig. 7.9c. For instance, the elongation at break retention was reduced from 106% to 81% when the rubber was filled with 1.7 filler weight ratio. This was expected since the SR/PS/MMT became stiffer when loaded with a high filler weight ratio as discussed earlier.

Interestingly, all the SR/PS/MMT nanocomposites presented less retention in modulus with regard to the single filler nanocomposite SR/MMT. This was accompanied with the high retention of elongation at break of SR/PS/MMT as shown in Fig. 7.9c. This observation indicated that the SR containing the PS/MMT hybrid filler was less rigid than the

SR containing the single filler MMT after the aging treatment. It was probable that the PS/MMT filler induced minor additional crosslinking during aging, thus most of the SR/PS/MMT nanocomposites could retain their rubbery property during aging. This behaviour was rarely reported for a filled rubber compound as an additional crosslinking always took place during aging, hence the increased rigidity of aged rubber.

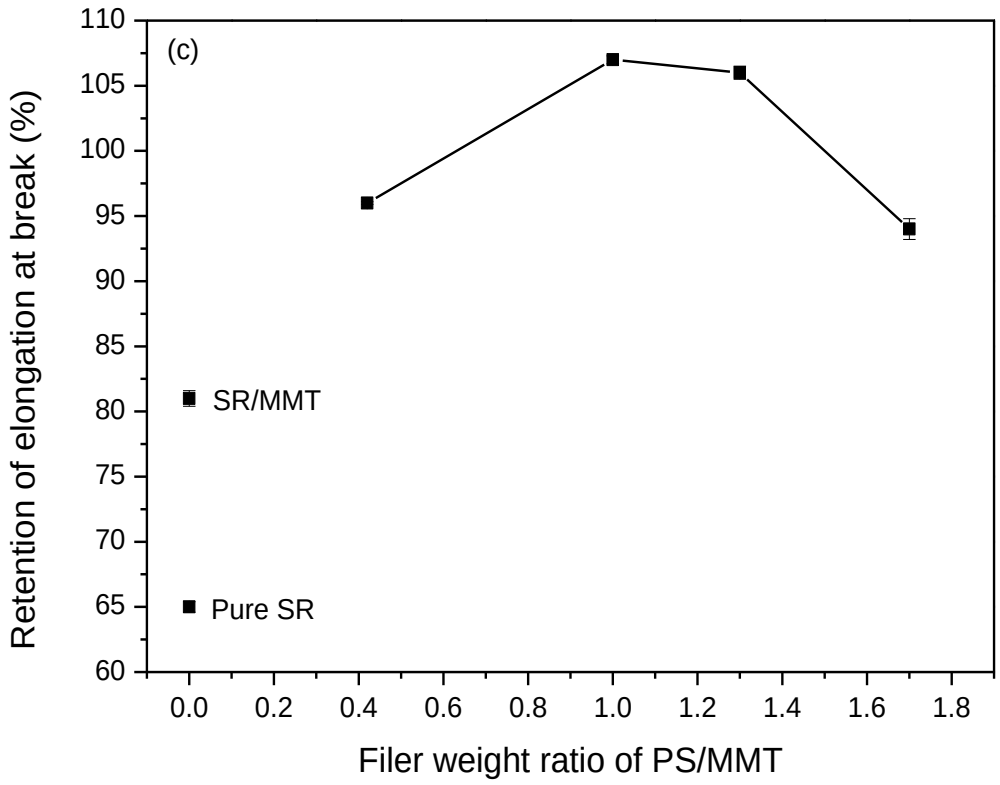

Fig.7.9c: Percent retention of elongation at break of SR/PS/MMT against PS/MMT weight ratio.

7.8 A comparative study between PS/MMT and PS/MWNT hybrid fillers

For comparison, it was decided to replace the MMT with a fibrous shaped nanofiller, namely multi wall carbon nanotube (MWNT), to form a new hybrid filler system, PS/MWNT. The filler's characteristics and the recipes for both the PS/MMT and PS/MWNT hybrid fillers filled with SR nanocomposite were described in Chapter 3. The performance of both hybrid

filler systems were compared based on the curing characteristics, tensile properties and hardness.

7.8.1 Cure characteristics

Table 7.4 compares the cure characteristics of the SR/PS/MMT and SR/PS/MWNT nanocomposites, respectively, at equal filler weight ratio. Overall, the trend shows that the cure time of the compounds became longer as the amount of hybrid filler increased. This result can be attributed to the increased amount of PS as the hybrid filler ratio increased. As stated earlier, the PS particles generated an acidic environment in the rubber compounds, and this usually incurs a longer cure time [23]. In this case, the delay in the cure time was more pronounced for the SR containing the PS/MWNT hybrid filler. This suggests that the use of a PS/MWNT hybrid filler system is less practical from a processing point of view.

In Table 7.4, the scorch time (t_{s2}) displays a small drop through increasing the filler weight ratio of PS/MMT and PS/MWNT respectively in the nanocomposites. This indicated that the safety processing time of the compounds became shorter with the addition of both hybrid filler systems in SR. On the other hand, the cure rate (CRI) values were reduced significantly as the hybrid filler weight ratio increased from 0 to the maximum 1.7, as shown in Table 4.3. The CRI essentially measures the rate of crosslinking in a rubber compound.

It was noted that both hybrid filler systems showed a decreasing trend of CRI as the loading of the hybrid filler weight ratio increased. However, when compared at the equal hybrid filler weight ratio, the SR/PS/MWNT nanocomposites exhibited a lower CRI with regard to the SR/PS/MMT. For example, the CRI values of SR/PS/MMT and SR/PS/MWNT nanocomposites were 9.10 and 6.60 cm^{-1}, respectively, when compared at a 1.7 hybrid filler weight ratio. The results suggested that the addition of PS/MWNT gave an adverse effect to the cure efficiency of the SR compounds.

Table 7.4: Cure characteristics of neat SR and SR/clay nanocomposites

Sample	Cure characteristics					
	Cure Time, T_{95} (min)	**Scorch Time, T_{S2} (min)**	**CRI, $100/_{T95}-T_{S2}$ (min^{-1})**	**Max torque M_H (dNm)**	**Min torque, M_L (dNm)**	**Delta torque, ΔM (dNm)**
SR/PS/MMT SR + 6 phr MMT (PS/MMT:0.0)	7.23	3.32	25.60	25.42	2.02	23.40
SR/PS/MMT(PS:MMT:0.4) 2.5 phr PS + 6 phr MMT	11.41	3.38	12.50	27.11	2.62	24.49
SR/PS/MMT(PS:MMT:1.0) 6 phr PS + 6 phr MMT	10.26	3.11	14.00	30.90	2.98	27.92
SR/PS/MMT(PS:MMT:1.7) 10 phr PS + 6 phr MMT	13.42	2.45	9.10	33.79	3.43	30.36
SR/PS/MWNT SR + 6 phr MWNT (PS/MWNT:0.0)	12.53	3.25	10.80	31.79	4.12	27.67
SR/PS/MWNT(PS:MWNT: 0.4) 2.5 phr PS + 6 phr MWNT	17.06	3.21	7.20	33.98	4.70	29.28
SR/PS/MWNT(PS:MWNT: 1.0) 6.0 phr PS + 6 phr MWNT	16.49	3.11	7.50	38.72	5.57	33.15
SR/PS/MMT(PS:MMT:1.7) 10.0 phr PS + 6 phr MMT	18.32	3.16	6.60	37.69	6.69	31.00

(PS/MMT: _._) refers to hybrid filler weight ratio.

Table 7.4 shows the increasing trend of maximum torque (M_H), minimum torque (M_L) and delta torque (ΔM) with the increase of the hybrid filler weight ratio of PS/MMT and PS/MWNT respectively. In all cases, the torque values of SR/PS/MWNT were higher than the SR/PS/MMT. According to Hanafi [24], the addition of MWNTs in rubber tends to impose extra resistance to flow, thus increasing the torque value. This was attributed to the smaller particle size of MWNT particles with a high aspect ratio, which had a high tendency to agglomerate in a rubber compound.

It was noted that the SR containing the single filler MWNT exhibited a higher torque than the SR filled with the single filler MMT, when compared at a similar filler loading 6 phr. In this case, it was assumed that agglomeration became more dominant in the SR containing the PS/MWNT hybrid filler than the SR/MMT due to the smaller particle size and high aspect ratio of MWNT particles. The filler agglomerations restricted the movement of the rubber chain and caused the maximum torque to increase. This could be the reason why a high maximum torque value was obtained from all SR/PS/MWNT compounds. Apart from this, the high aspect ratio of MWNTs could generate an extra source of entanglement or physical crosslink in a rubber matrix [25]. This also caused the delta torque to increase.

7.8.2 Tensile properties

Fig. 7.9(a-d) compares the tensile strength, Young's modulus, elongation at break and hardness properties of SR/PS/MMT and SR/PS/MWNT against different filler weight ratios. In this case, the single filler composite containing 6 phr of MMT or MWNT fillers, respectively, are compared to the 0 filler weight ratio as shown in the Fig. 7.9(a-d). Overall, the SR containing both of the hybrid fillers respectively exhibited a large improvement in the tensile strength, Young's modulus, elongation at break and hardness as compared to any composite filled with a single filler.

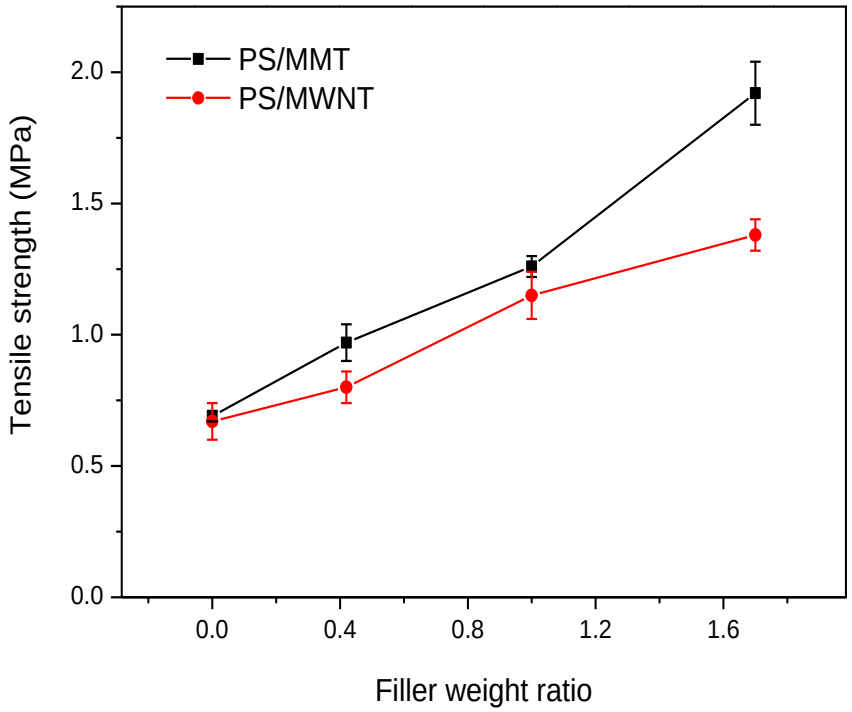

Fig. 7.10(a): Effect of the hybrid filler weight ratio on the tensile strength of the SR/PS/MMT and SR/PS/MWNT respectively.

The variation of tensile strength with increasing PS/MMT and PS/MWNT hybrid filler weight ratio loading in silicone rubber has been shown in Fig. 7.10a. As can be seen, both of the hybrid filler systems present an increasing trend with increasing filler weight ratio. It was noted that the SR filled with PS/MMT exhibited a higher tensile strength in any given filler weight ratio as compared to the SR/PS/MWNT. For example, as the hybrid filler weight ratio reached 1.7, the SR/PS/MMT and SR/PS/MWNT nanocomposites exhibited the maximum tensile strength, which was 1.92 MPa and 1.38 MPa, respectively. This suggested that the SR/PS/MMT nanocomposites had superior tensile strength, which was 30% higher than the SR/PS/MWNT.

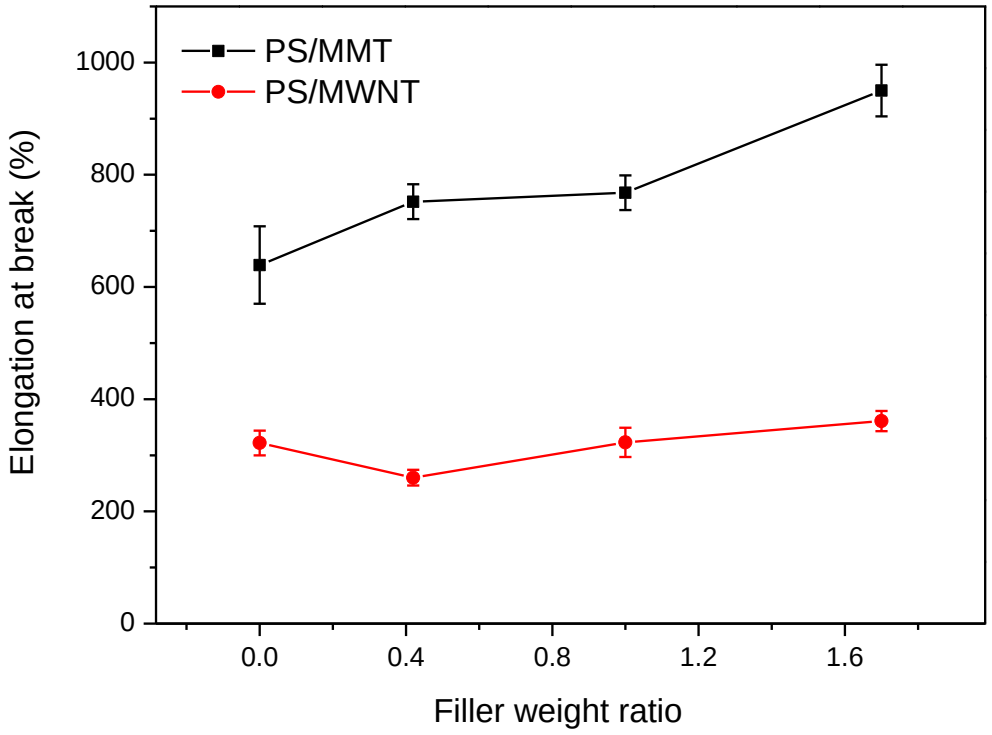

Fig. 7.10(b): Effect of hybrid filler weight ratio on the elongation at break of the SR/PS/MMT and SR/PS/MWNT respectively.

A similar trend was observed for elongation at break in Fig. 7.9b. It was found that the SR/PS/MMT nanocomposites showed higher elongation at break as compared to the SR/PS/MWNT, in all cases. The SR/PS/MMT loaded with a 1.7 PS/MMT hybrid filler ratio gave the highest elongation at break which was 950%. On the other hand, the SR/PS/MWNT exhibited poor elongation at break as the hybrid filler ratio reached the maximum 1.7, which was 361%.

Figs. 7.9c and d compare the Young's modulus and hardness of the SR/PS/MMT and SR/PS/MWNT, respectively, with the variation in filler weight ratio. Both figures show that the Young's modulus and the hardness increased steadily as the hybrid filler weight ratio of PS/MMT and PS/MWNT increased. Notably, the SR/PS/MWNT nanocomposites exhibited a higher Young's modulus as compared to the SR/PS/MMT. This result indicated that the addition of the PS/MWNT hybrid filler improved the stiffness of the nanocomposites,

which was consistent with the hardness properties as presented in Fig. 7.9d. It was noted that the SR containing PS/MWNT displayed higher hardness with regard to the SR/PS/MMT nanocomposites. As mentioned earlier, it was assumed that agglomeration became more dominant in the SR/PS/MWNT due to the smaller particle size of both the PS and MWNT nanofillers. The filler agglomeration could restrict the SR movement. As a result, the SR/PS/MWNT nanocomposites become more rigid than the SR/PS/MMT.

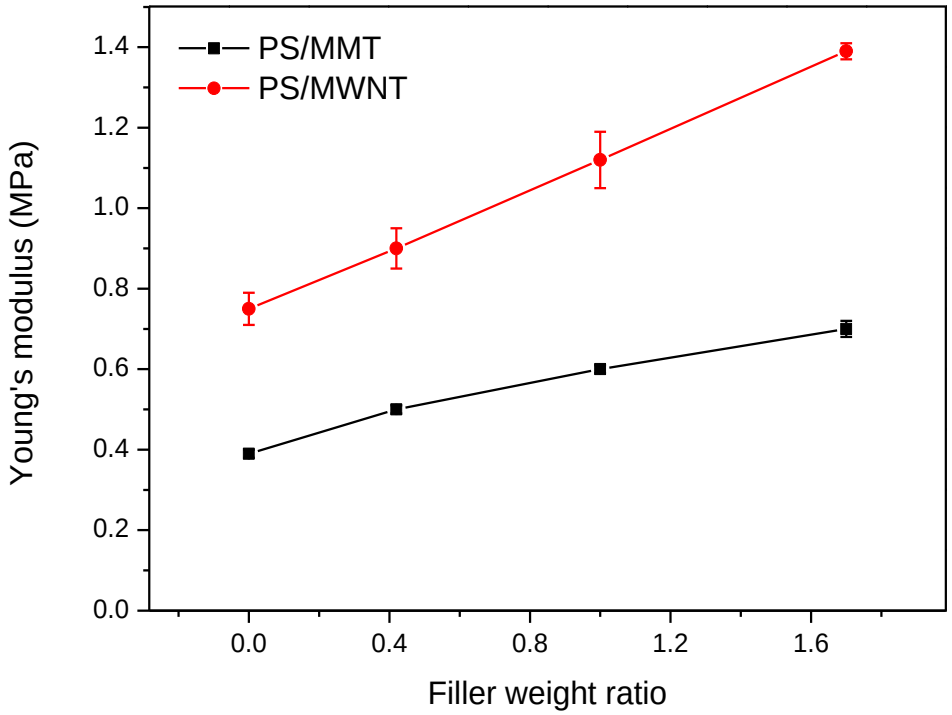

Fig. 7.10(c): Effect of hybrid filler weight ratio on the Young's modulus of the SR/PS/MMT and the SR/PS/MWNT respectively.

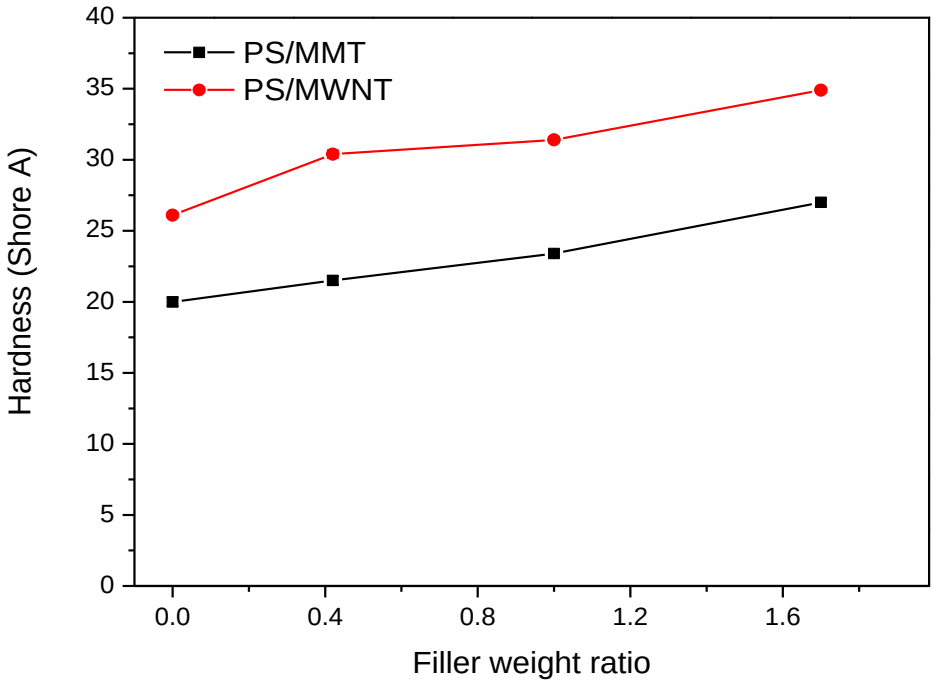

Fig. 7.10(d): Effect of hybrid filler weight ratio on the hardness of the SR/PS/MMT and SR/PS/MWNT respectively.

The addition of the fillers into the soft matrix of rubber involves a different mechanism for enhancement due to several interactions of many different length scales of filler. For example, the improvement in the tensile properties involved a few mechanisms that were related to the catastrophic tearing of cracks, initiated from accidental flaws, microvoids, dewetting or cavitation from the filler surface [26]. Since the hybrid fillers contain different dimensions and lengths of fillers, there is no clear mechanism for the enhancement of the tensile properties in the hybrid filler system which can be explained by one simple theory.

Principally, the load transfer in tension testing is more effective if the chemical link is formed in a composite. In this case, the combination of PS and MMT could provide excellent rubber-filler interaction since both these nanofillers contained some active group (such as silanol) which formed hydrogen bonding, thus strengthening the rubber-filler interface. It was strongly believed that the improvement in the tensile strength of SR/PS/MMT was caused by

the strong physico-chemical interactions provided by the addition of PS/MMT. On the other hand, the lack of chemical interaction between PS/MWNT and the rubber interface could be part of the reason why SR/PS/MWNT nanocomposites had a lower tensile strength than the SR/PS/MMT nanocomposites.

A similar trend of increasing Young's modulus values with increasing hybrid filler weight ratio of PS/MMT and PS/MWNT loadings was observed in Fig. 7.9c. This was due to the stress-transfer mechanism of reinforced elastomers. It was expected that when the functional filler (such as silica) was added into the hybrid filler system, the applied stress would be transferred from the elastomer matrix to the strong and stiff mineral filler. In this case, the increase in Young's modulus was obviously seen in the composites filled with PS/MWNT. It is well known that the MWNT has smaller particle sizes, which provide greater surface areas to facilitate effective contact with the SR chains. As stated earlier, it was proven that the MMT in the PS/MMT system failed to exfoliate in the matrix. If the non-exfoliated MMT particle size was considered, it was thus assumed that the MMT provided a relatively lower surface area than the MWNT did. This could be a possible reason why the SR/PS/MMT presented a low Young's modulus.

Additionally, the stress field in a reinforced composite also contributes to the increase in modulus. Pham and colleagues [26] explained that the stress field near a particle was independent of the size of the particle. But the volume of the polymer, that experienced a given value of stress concentration, increases with the particle size, thus inducing a large flaw within this volume. In principle, if a large flaw exists within this area of stress concentration, the tensile strength is greatly reduced. Therefore, this can partly explain why the SR/PS/MWNT exhibited greater Young's modulus but lower tensile strength as compared the SR/PS/MMT.

7.9 Conclusions

From this study, it was concluded that:

1. By increasing hybrid filler weight ratio, tensile strength, Young's modulus, M100, M300, elongation at break, stored energy density at break, and hardness of the SR/PS/MMT nanocomposite improved, compared with the values for the control rubber, and SR/PS and SR/MMT nanocomposites.

2. The stress–strain properties of the nanocomposites with the hybrid fillers showed a large improvement at high deformation in comparison with the properties of those nanocomposites containing the PS and MMT fillers. The MMT filler exfoliated in the SR/MMT nanocomposite, but did not in the nanocomposite containing the hybrid filler. Therefore, PS was detrimental to the MMT dispersion in the rubber. As expected, the untreated PS formed aggregates in the rubber matrix.

3. The results showed a positive contribution to the crosslink density of the rubber from the hybrid filler, which was caused by the PS–rubber network formation in the rubber. There was no evidence of a synergistic effect of the hybrid filler on the rubber properties. The rate of cure retarded when the hybrid filler weight ratio was raised in the rubber. This indicated that the hybrid filler slowed down the rate of the peroxide curing reaction in the rubber.

4. The energy loss in the SR/PS/MMT nanocomposite increased as the hybrid filler weight ratio was raised from 0.4 to 1.7. A similar effect was recorded for the nanocomposites containing 6 phr PS and 6 phr MMT fillers, although the energy loss in these rubbers was not as high as that measured for the SR/PS/MMT nanocomposites.

5. The SR containing PS/MMT hybrid fillers exhibits excellent resistant to heat ageing as compared to the single filler system SR/MMT. The resistance to aging of SR/PS/MMT was improved by gradually adding amounts of PS filler into the PS/MMT hybrid filler system.

6. The PS/MWNT hybrid filler system gave adverse effects on the cure time and rate of cure in the peroxide cured SR compounds. The comparative study demonstrated that the SR containing PS/MWMT exhibited higher Young's modulus and hardness in comparison to the SR/PS/MMT nanocomposites, but with little increment in the tensile strength and elongation at break as the hybrid filler ratio increased.

7.10 References

1. Bokobza L, Rahmani M, Belin C, Bruneel JL, Bounia NE. Blends of carbon blacks and multiwall carbon nanotubes as reinforcing fillers for hydrocarbon rubbers. *Journal of Polymer Science.Part B:Polymer Physics* 2008; 46: 1939–1951.

2. Qu L, Huang, G, Zhang P, Nie Y, Weng G, Wu J. Synergistic reinforcement of nanoclay and carbon black in natural rubber. *Polymer International* 2010; 59: 1397–1402.

3. Liu YB, Li L, Wang Q. Reinforcement of natural rubber with carbon black/nanoclay hybrid filler. *Plastic Rubber Composite* 2010; 39(8): 370-376

4. Zhao G, Shi L, Zhang D, Feng X, Yuan S, Zhuo J. Synergistic effect of nanobarite and carbon black fillers in natural rubber matrix. *Material Design* 2012; 35: 847-853

5. Jia C, Zhang LQ, Zhang H, Lu YL. Preparation, microstructure, and property of silicon rubber/organically modified montmorillonite nanocomposites and silicon rubber/OMMT/fumed silica ternary nanocomposites. *Polymer Compos*ite 2011; 32: 1245–1253.

6. Donnet ED. Reinforcement of Elastomer by particulate fillers. In: James E, Mark, BE, Frederick RE (eds.) *The Science and Technology of Rubber*. 3rd ed. United Kingdom: Elsevier Academic Press; 2005. 367-401.

7. Aranguren M, Mora E, Macosko CW. Compounding Fumed Silicas into Polydimethylsiloxane: Bound Rubber and Final Aggregate Size. *Journal Colloid Interface Science* 1997; 195(2): 329–337.

8. Levresse P, Feke DL, Manas ZI. Analysis of the Formation of Bound Poly(dimethylsiloxane) on Silica. *Polymer* 1998; 39(17): 3919-3924

9. Ansarifar A and Lim BY. Reinforcement of silicone rubber with precipitated amorphous white silica nanofiller - effect of silica aggregates on the rubber properties. *Journal of Rubber Research* 2006; 9(3): 140-158.

10. Bristow GM, Tiller RF. Correlation of structure and properties of natural rubber vulcanisates. *Kautschuk Und Gummi Kunststoffe* 1970; 23(2): 55 – 59.

11. Wolff S. Chemical aspect of rubber reinforcement by fillers. *Rubber Chemistry Technology* 1996; 69: 325-345.

12. Shim SE, Isayev AI. Rheology and Structure of Precipitated Silica and. Polydimethylsiloxane System. *Rheological Acta* 2004; 43: 127-136.

13. Fröhlich J, Niedermeier W, Luginsland HD. The effect of filler-filler and filler-elastomer interaction on rubber reinforcement. *Composite A* 2005; 36(4): 449–460.

14. Ewe HT, Wolff S, Haddeman M, Grewetta HP, Wang MJ. Filler—Elastomer Interactions. Part IX. Performance of Silicas in Polar Elastomers. *Rubber Chemistry Technol*ogy 1993; 66: 594-604

15. Danmenberg EM, Molecular slippage mechanism of reinforcement. *Rubber Industrial 1996; 42: 26-42.*

16. Boonstra BB. Reinforcement of Elastomer. In Kraus G. (ed). *Reinforcement of Elastomers*, NewYork: Interscience; 1965: 100.

17. Kraus G. Childers CW, Rollman KW. Stress softening in carbon black-reinforced vulcanizates. Strain rate and temperature effects. *Journal of Applied Polymer Science* 1966; 10: 229-244.

18. Clement F, Bokobza L, Monnerie L, On the Mullins Effect in Silica-Filled Polydimethylsiloxane Networks. *Rubber Chemistry Technology* 2001; 74: 847-870

19. Mullins L and Tobin NR. Theoretical Model for the Elastic Behavior of Filler-Reinforced Vulcanized Rubbers. *Rubber Chemistry Technol*ogy 1957; 30: 555-571.

20. Blanchard AF, Parkinson D. Breakage of carbon-rubber networks by applied stress. *Industrial Engineering Chemical* 1952; 44: 799-812.

21. Bueche F. Molecular basis for the mullins effect. *Journal of Applied Polymer Science* 1960; 4: 107–114

22. Bueche F. Mullins effect and rubber–filler interaction. *Journal of Applied Polymer Sci*ence 1961; 5: 271–281.

23. Carli LN, Roncato CR, Zanchet A, Mauler RS, Giovanela M, Brandalise RN, Crespo, JS. Characterization of natural rubber nanocomposites filled with organoclay as a substitute for silica obtained by the conventional two-roll mill method. *Applied Clay Science* 2011; 52 (1-2): 56-61.

24. Ismail H, Ramly AF, Othman N. Effects of silica/multiwall carbon nanotube hybrid fillers on the properties of natural rubber nanocomposites. *Journal of Applied Polymer Science* 2013; 128: 2433–2438.

25. Shanmugharaj AM, Bae JH, Lee KY, Noh WH, Lee SH, Ryu SH. Physical and chemical characteristics of multiwalled carbon nanotubes functionalized with aminosilane and its influence on the properties of natural rubber composites. *Composite Science Technol*ogy 2007; 67: 1813–1822.

26. Pham TT, Sridhar V, Kim JK. Fluoroelastomer-MWNT nanocomposites-1: Dispersion, morphology, physico-mechanical, and thermal properties. *Polymer Composite* 2009; 30: 121–130.

CHAPTER 8: Conclusions and future works

8.1 Introduction

This thesis covers some fundamental aspects of the preparation and characterisation of silicone rubber (SR) / clay nanocomposites. Highly exfoliated and intercalated silicone rubber (SR) nanocomposites based on natural montmorillonite (Cloisite Na^+) and organically modified montmorillonite (Cloisite 30B and Cloisite 20A) were successfully prepared by melt-mixing technique, involving high shearing and followed by vulcanisation at high temperature. A fresh insight on the formation of nanostructure in silicone matrix was presented in this work, based on XRD, TEM, FTIR and DSC studies. The performance of the nanocomposites was evaluated based on their cure characteristics and mechanical properties, and the results compared with the pure rubber. Further understanding with regard to the effect of intercalated and exfoliated nanostructured on the heat ageing properties and thermal stability of the rubber was discussed.

In order to enhance the mechanical properties of silicone rubber/clay nanocomposites a new filler system in silicone rubber, based on the combination between Cloisite Na+ (MMT) and precipitated silica (PS),referred to as PS/MMT hybrid filler, was successfully developed in the present work. Cloisite Na^+ was chosen since it offers benefits to the cure and mechanical properties of the rubber. For a comparison, a new hybrid filler system was created based on PS filler and fibrous shaped nanofiller, namely multi wall carbon nanotube (MWNT). Finally the performances of PS/MMT and PS/MWNT in silicone

rubber were compared in terms of cure characteristics and tensile properties. From the experimental results obtained the following conclusions can be drawn.

8.2 Conclusions

The dispersion state of the clays in the SR/clay nanocomposites prepared via melt-mixing process was highly dependent on the level of the clay concentration. As confirmed by XRD and TEM analysis, formation of highly exfoliated and intercalated nanocomposites was achieved at low filler loading, i.e. <8 phr by weight. Moreover, it was evident that the degree of intercalation/exfoliation in the rubber was unaffected by increasing the mixing time. During mixing the clusters of silicate platelets break into smaller tactoids due to high shear rate. It was proposed that the exfoliation of the clays in silicone matrix could not be reasonably described using the layer-by-layer mechanism but rather was a spontaneous process that happened during the vulcanisation stage, as suggested by the XRD, TEM, FTIR and DSC results. It was concluded that favourable interactions between the silicone chain and OH group on the C30B surface facilitated the exfoliation process of the silicate layers in the silicone rubber.

From the rheology point of view, the presence of organic surfactant on the modified clay caused some adverse effects during the peroxide curing process. The study showed that the interference of organo modifier such as methyl, tallow, bis-2-hydroxyetyl, quaternary ammonium (MT2EtOH) and dimethyl, dehydrogenated tallow, quaternary ammonium (2M2HT) during crosslinking delayed the onset of curing, reducing the cure efficiency of the SR/C30B and SR/C20A nanocomposites. Subsequently the crosslink density of the nanocomposites was also reduced. Unlike in the SR/Na^+MMT, the peroxide curing efficiency and crosslink density of the rubber both improved since there was no interruption from organic modifier in the unmodified Na^+MMT (Cloisite Na^+).

Overall the use of the nanoclays in silicone rubber improved the Young's modulus, tensile strength, and elongation-at-break, by more than 50% as compared to the control

rubber. This is a great achievement for silicone rubber/clay nanocomposite prepared by melt-mixing in light of the published literature discussed in Chapter 2. Among the nanofillers, Cloisite Na^+ appears as the most effective clay for use in silicone rubber, as shown by a subsequent increase in the Young's modulus, tensile strength hardness, and abrasion resistance. In addition, the intercalated or exfoliated nanostructure of C20A and C30B resulted in some small contribution to the strength of the silicone rubber. Therefore in this particular composite the crosslink density had an even a bigger influence on the strength of the rubber.

On the other hand, the intercalated morphology provided greater benefits to the elongation-at-break and store energy density of the rubber. The hysteresis behaviour of the silicone rubber/clay nanocomposites was highly dependent on the formation of nanostructures in the matrix. It was concluded that the highly exfoliated SR/C30B and intercalated/exfoliated SR/Na^+MMT nanocomposites displayed lower energy loss when compared with the intercalated SR/C20A nanocomposite.

As this study has shown, exfoliated C30B clay provided major advantages for the thermal stability and heat resistance of the rubber. The most interesting finding of this study was the fact that the clay morphology modified the thermal properties of the rubber for the better. This was in addition to reports of improved mechanical properties in the aged nanocomposites containing exfoliated C30B clay. However the effect of MMT morphology on thermal degradation of the rubber in a nitrogen atmosphere was inconclusive. It emerged that the influence of organic surfactant present in the modified MMT played a key role in determining the thermal stability of nanocomposites in an inert atmosphere.

In the SR/PS/MMT nanocomposites, the hybrid filler slowed the rate of the peroxide curing reaction in the rubber. In addition, the PS filler was detrimental to the MMT dispersion in the rubber, since there was no evidence of partially exfoliated nanostructure revealed by the XRD and TEM. Nevertheless the main benefit of the dual characteristics of PS/MMT

hybrid filler comes from overcoming the compromises involved in using the MMT single filler system. The PS/MMT hybrid filler can improve strength/stiffness without scarifying toughness and at the same time enhance heat resistance. Finally, the comparative study demonstrated that the SR containing PS/MWMT significantly improved stiffness of the rubber but simultaneously reduced its elasticity. Therefore, it was concluded that the PS/MMT hybrid filler system improved the mechanical properties of silicone rubber more than the PS/MWNT hybrid filler system.

8.3 Future works and recommendations

Findings from this study have helped advance our understanding of the way clays affect the processing of silicone rubber, improving its mechanical properties and thermal stability, which will assist future work on this fascinating subject.

From the processing point of view, it was proven that highly intercalated and exfoliated silicone rubber/clay nanocomposites can be prepared using simple methods, such as melt-blending techniques. However to the preparation of nanocomposites with high filler loading (> 8 phr) is still considered a challenge. In term of characterisation, a direct method to measure exfoliation and intercalation of layered silicates in silicone rubber should be developed to support the present techniques, which rely on XRD and TEM.

The addition of modified MMT (e.g. Cloisite 30B and Cloisite 20A) did improve dispersion in silicone rubber. However certain issues of curing efficiency, due to the interference of organic surfactant during the curing process, need to be minimized. Ideally, the energy consumed during the processing and vulcanisation of rubber should directly influence the final mechanical properties and cost of the end product. Therefore, a study of cure kinetics is essential to provide a clear insight into the actual mechanisms of curing and its effect on the mechanical properties of SR/clay nanocomposites.

Finally, attempts are already being made to develop hybrid filler systems based on layered silicates. Some positive achievements in terms of mechanical properties and heat

ageing, based on PS/MMT hybrid filler, have been revealed during this study. However, we strongly advise that some chemical modifications/alterations of the processing techniques are needed to improve the dispersion of hybrid filler in the nanocomposite. For example, we recommend the incorporation of dispersing or coupling agents to improve PS/MMT hybrid filler dispersion in the silicone matrix. Besides, research have to be focused on how to control the orientation of layered particle in a soft matrix as it may improve the permeation properties of the nanocomposite as well as mechanical properties.

Since, the hybrid filler development in silicone rubber is still in the embryonic stage a lot of scope exists for the creation of a novel silicone rubber product, based on the combination of two different fillers, if a considerable advantage from the fillers can be gained. Promising developments are expected in the formation of synergies effect attributed from the combination of two different fillers. However, this should involve further systematic studies on exploring the synergisms created by the hybrid fillers.

APPENDIX

List of publications

Journals

1. **Ismail, N.I. N**., Ansarifar, A. and Song, M. Preparation and characterization of high performance exfoliated montmorillonite/silicone rubber nanocomposites with enhanced mechanical properties*. Polymer Engineering Science* 2013; 53: 2603–2614.DOI: 10.1002/pen.23528

2. **Nik Ismail, N.I**., Ansarifar, A. and Song, M. Effect of hybrid reinforcement based on precipitated silica and montmorillonite nanofillers on the mechanical properties of a silicone rubber. *Polymer Engineering Science* 2013 (Early view) DOI: 10.1002/pen.23734

3. **Nik Ismail, N.I**., Ansarifar, A. and Song, M. Improving heat ageing and thermal properties of silicone rubber using montmorillonite clay. *Journal of Applied Polymer Science* 2014 (In press) DOI: 10.1002/app.41061

Online publication

1. A Ansarifar, **N I Nik Ismail** and M Song, Hybrid reinforcement of silicone rubber. Plastic research online, Society of plastics Engineers, 8 Nov 2013, DOI: 10.2417/spepro.005164 http://www.4spepro.org/view.php?source=005164-2013-10-30

Conferences

1. **N I Nik Ismail**, A Ansarifar and M Song, Silicone rubber based nanocomposite (Poster) *Rubber Reinforcement by Fillers, Fibres and Textiles: Latest Developments seminar 17-18 December 2012: Queen Mary, University of London, UK*

2. **N I Nik Ismail**, A Ansarifar and M Song**,** Nanometarial as reinforcing filler in rubber (Poster) *Research that Matter Conference,*

   7 March 2013, Loughborough University,UK

3. **N I Nik Ismail,** A Ansarifar and M Song , Preparation and characterization of silicone rubber based nanocomposite (Oral)

   25 – 29 August 2013, Eurofiller 2013, Bratislava Slovakia,